Coordination Chemistry Reviews 474 (2023) 214860

Contents lists available at ScienceDirect

Coordination Chemistry Reviews

journal homepage: www.elsevier.com/locate/ccr

Review

Recent advances on organelle specific Ru(II)/Ir(III)/Re(I) based complexes for photodynamic therapy

Binoy Kar, Utpal Das, Nilmadhab Roy, Priyankar Paira

Department of Chemistry, School of Advanced Sciences, Vellore Institute of Technology, Vellore 632014, Tamilnadu, India

ARTICLE INFO

Article history:
Received 17 June 2022
Accepted 17 September 2022
Available online 7 October 2022

Keywords:
Organelle specificity, Ru(II)
Ir(III)
Re(I) complexes, photodynamic therapy

ABSTRACT

Organelle specificity is an important facet of more efficient and highly selective drugs with reduced side effects which have now been the great challenge to the scientists. In eradication of lethality of cancer, the appropriate anticancer therapeutics should render less toxicity towards the normal healthy cells. Therefore, in present scenario the application of photodynamic therapy (PDT) in healing cancer has brought about a renaissance in the field of anticancer research as PDT is very selective treatment procedure under irradiation of localized light at a particular portion of the body without creating any phototoxic damage to the normal cells. Metal complexes, especially ruthenium (II), iridium (III) and rhenium (I) complexes have been seen to be highly apt for PDT. Hence, a bucket of Ru (II), Ir (III) and Re (I) based various types of complexes have been showcased here mentioning their capability to target specific organelle along with the detailed discussion on pathway of photodynamic therapy.

Contents

1. Introduction . . . 2
2. Importance of different organelles and target specific cancer Therapy . . . 3
   2.1. Extracellular target . . . 3
      2.1.1. Cell membrane . . . 3
   2.2. Cellular receptor . . . 4
   2.3. Intracellular target . . . 4
      2.3.1. Nucleus . . . 4
   2.4. Mitochondria . . . 4
      2.4.1. Lysosome . . . 5
3. Property of a good PDT agent . . . 5
   3.1. Photosensitizers . . . 5
   3.2. Single photon excitation and two photon excitations . . . 5
4. Advantages and challenges of PDT . . . 7
5. Enhancement of PDT . . . 7
6. Organelles targeted ruthenium complexes for photodynamic therapy . . . 9
   6.1. Ruthenium based polypyridyl complexes . . . 9
   6.2. Organelles targeted Ru-Peptide conjugates as PDT agent . . . 29
   6.3. Mixed metallic Ru-complex as a PDT agent . . . 35
   6.4. Ru-based nanoparticle: . . . 38
   6.5. Some other miscllenious Ru-based complexes as PDT agent . . . 40
7. Iridium based complex as a PDT agent . . . 45
   7.1. Iridium based nano complex act as PDT in cancer therapy: . . . 60
8. Rhenium based complexes as a PDT agent . . . 68
   8.1. Tricarbonyl rhenium complexes with different conjugates: . . . 68
   8.2. Tri-carbonyl rhenium complex with N—N chelating ligand: . . . 69

E-mail address: priyankar.paira@vit.ac.in (P. Paira)

https://doi.org/10.1016/j.ccr.2022.214860
0010-8545/

8.3. Di-nuclear rhenium complex . . . 70
8.4. Carbonic anhydrase IX (CAIX)-Anchored Rhenium(I) photosensitizer . . . 71
9. Conclusion . . . 71
Declaration of Competing Interest . . . 72
Acknowledgements . . . 72
References . . . 72

1. Introduction

One of the most perilous diseases known to living world is cancer which is termed to be the second leading risk factor for death after cardiovascular disorders. The uncontrolled growth and metastasis of malignant tumors can be considered as the major cause of cancer [1]. From the report of world cancer research fund we observed that in 2020, 18.1 million cancers cased found around all over the world. In case of man, it was 9.3 million and in case of women it was 8.8 millions. In 2022 1,918,030 new cancer cases and 609,360 cancer deaths were found in the United States from the report of American Cancer Society [2]. Invasive surgery, radiation and chemotherapy are the most prevailing cancer treatments being administered in clinical practice. Cancer metastasis may be aided by invasive surgery. Chemotherapy can produce severe systemic toxicity because of poor selectivity while radiotherapy can cause radiation poisoning and leads to the formation of secondary neoplasia. These sobering realities have driven current efforts towards the development of novel therapeutic platforms which will convey nominal invasive techniques, excellent selectivity as well as low malicious side effects in order to eradicate aforementioned disadvantages. Therefore, main objective of drug development and commercialization involves in design of a molecule affluent with most therapeutic effects in the target tissue while meager with negative side effects in other tissues. In this context, photodynamic therapy (PDT) affords an appropriate therapeutic approach where the photosensitizers (PSs), the light-sensitive compounds are 'switched on' to the target region upon irradiation of localized light. In absence of light, the PSs should be non-toxic and thus PDT offers an opportunity for highly targeted therapy with fewer adverse effects [3–5]. PDT is a two-step treatment that begins with the introduction of a photosensitizing agent and ends with the emission of non-thermal light of a particular wavelength activating the drug [6–9]. The biological effect of PDT is well-accepted because it renders the affects to the specific portion of tissue exposed under light. Moreover, PDT activates the systemic immune responses that are directed towards the tumors [10–12]. Depending upon the situation, the patient can be treated topically, systemically or else intravesically with non-active PSs. Then, PSs may accumulate in both healthy and impaired cells but it is activated by localized light irradiation with suitable wavelength [13,14] (See Fig. 1).

Photodynamic therapy can be classified as Type-I and Type-II depending on the mechanism of action. Type-I mechanism entails the photoinduced electron transfer which leads to the formation of a superoxide or a hydroperoxyl radical ($HO_2^{\bullet}$). Type-II mechanism involves energy transfer from the photosensitizer to ground-state triplet oxygen ($^3O_2$) which is ultimately converted to highly reactive singlet oxygen ($^1O_2$). This singlet oxygen facilitates the cancer cell annihilation. As a result of light irradiation, the photosensitizer excited from ground state (S_0) to the excited singlet state (S_1), and then it swings to the triplet state (T_1) through non-radiative inter-system crossing process (ISC). (Fig. 2) Then and there it transfers the electron or energy to the ground state oxygen which leads to

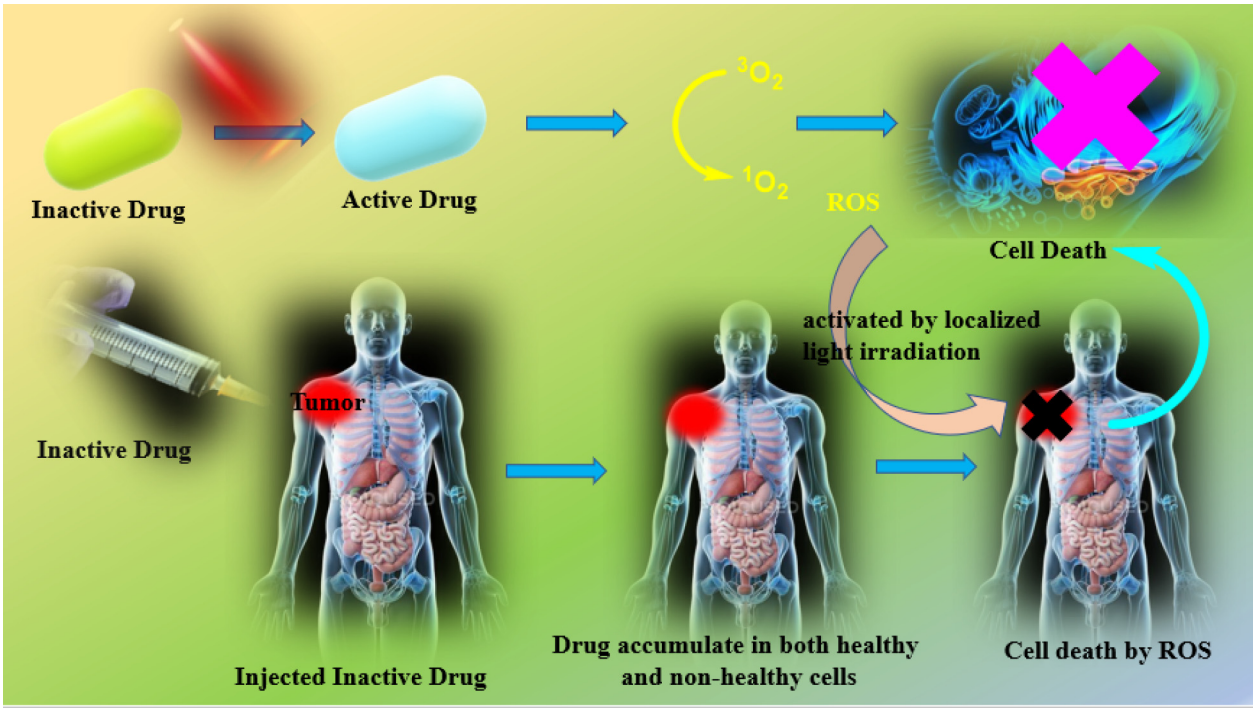

Fig. 1. A pictorial representation of PDT treatment for cancer.

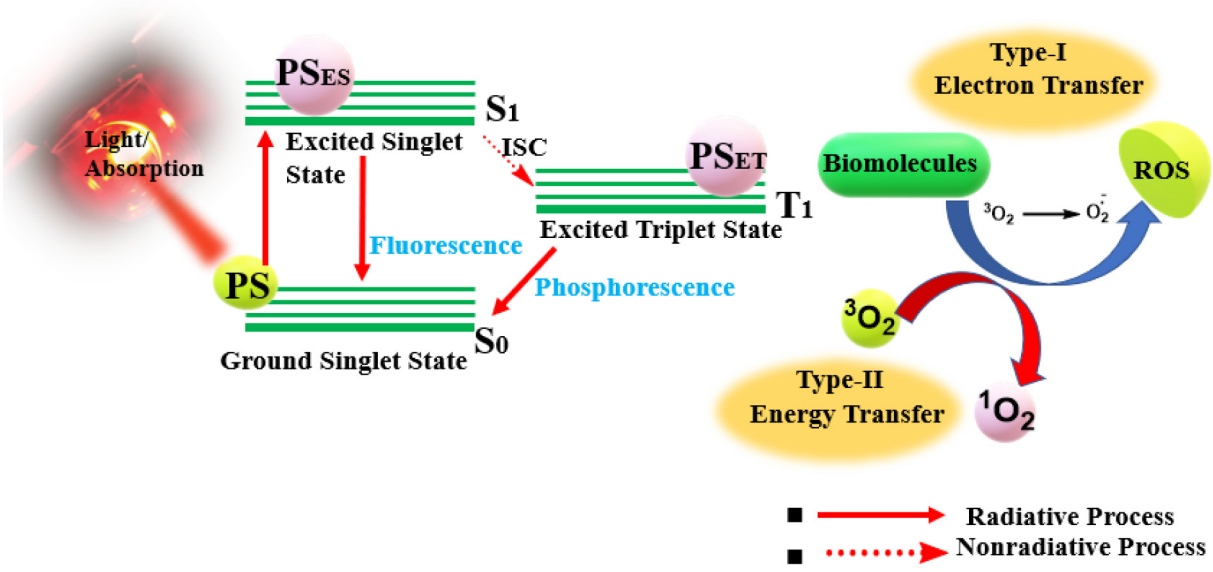

Fig. 2. Mechanistic pathway of PDT.

the formation of reactive oxygen species which actually damages the cancer cells [15–17]. In this process PSs remains unaltered by itself, rather it just works as an "energy relay" to absorb light or transport energy. Owing to this kind of advantages and being beneficial over traditional cancer therapies, it was first established as a treatment method over 100 years ago. The interest in PDT was reignited only in the 1990 s, when FDA approved the first clinically trialed PS, stimulating massive investigation in cancer therapies [18,19]. Photofrin was the first PS which was approved for clinical trial in the case of bladder cancer. A good PSs exhibit several important properties like (1) low dark toxicity, (2) proper retention time, (3) anti-bleaching characteristics that are strong, (4) high extinction coefficient within 700 to 900 nm therapeutic window, (5) to maintain efficacy, limited absorption and tumor-specific selectivity which were great challenges to the scientists [20–23]. Therefore, studies on PDT aimed at tackling the above listed challenges in order to augment the PSs capability in PDT. The United States Food and Drug Administration have approved PDT as a treatment for endobronchial and endo esophageal cancer as well as for premalignant and early malignant lesions of the skin, bladder, breast, stomach and oral cavity [24–26]. In the late 19th century, Niels Finsen *et al.* opened the door of modern phototherapy-based research where they used carbon arc-lamp for lupus vulgaris, the result of which brought the Nobel Prize in 1903 in Physiology and Medicine [27]. In 1900 Raab group investigated the light treatment in combination with photosensitizing agents [28]. In 1907 von Trappeiner and Jodlbauer group demonstrated the need of oxygen in dark as well as in light and introduced the term 'photodynamic activation' [29].

In recent time, metal-based drug including ruthenium and iridium complexes are being highly applauded due to their amazing properties for PDT in cancer [30–32a]. Ruthenium complexes possess some extraordinary properties like solubility, cellular uptake and organelle targeting ability, photo-stability, photophysical property and ROS generation. The electronic distribution of ruthenium is [Kr] $4d^7$ $5\ s^1$, so that its arrangement with different ligand can be presumed to be *hexa*-coordinated octahedral and it can be altered for a variety of purposes, such as solubility, cell uptake effectiveness, targeting capacity, charge distribution, electrochemical and photophysical properties, etc [32b]. Their exceptional photosensitizing qualities, paired with the aforementioned properties, have acquired considerable preferences for being used in PDT. McFarland *et al.* introduced TLD1433 (polypyridyl ruthenium complex) in the field of PDT for bladder carcinoma and it reached phase-IB clinical trial. The profound research on ruthenium-based PSs showed the potential to make a significant contribution in the field of PDT (Fig. 3). Like ruthenium complexes, iridium complexes as well as cyclometalated Ir (III) complexes also exhibited outstanding result in PDT based cancer therapy. High quantum yields, substantial Stokes shifts, long-lived phosphorescence, remarkable color-tuning capabilities and good photobleaching resistance are some of the important properties of cyclometalated iridium complexes which make them pertinent for PDT. As a consequence, they are also chosen as bio-imaging probes. Iridium complexes have also shown momentous impact on PDT due to some special biological and photophysical properties along with the ability of facile ligand modification. Tricarbonyl rhenium compounds demonstrated appealing and intriguing characteristics because of their excellent photophysical and photochemical characteristics, reduced heavy metal toxicity, organelle targeting capability, and other factors. Hence, this review article has been embroidered with myriad class of Ru(II)/Ir(III)/Re(I)-based complexes (polypyridyl, cyclometalated, nano, carbohydrate conjugate, peptide conjugate, bimetallic and so on) for organelle specific PDT application.

2. Importance of different organelles and target specific cancer Therapy

2.1. Extracellular target

2.1.1. Cell membrane

The cell membrane is the first important target for any drug molecule during entering into cell as it holds different receptors and regulates signal transmission in association with the controlling of enzymatic activity. It also provides the space for endocytosis and thus helps the drug to enter into cell crossing through it. It is accountable to maintain the interactions in cellular environment. As the cell membrane consists of lipid bilayer, it can also be

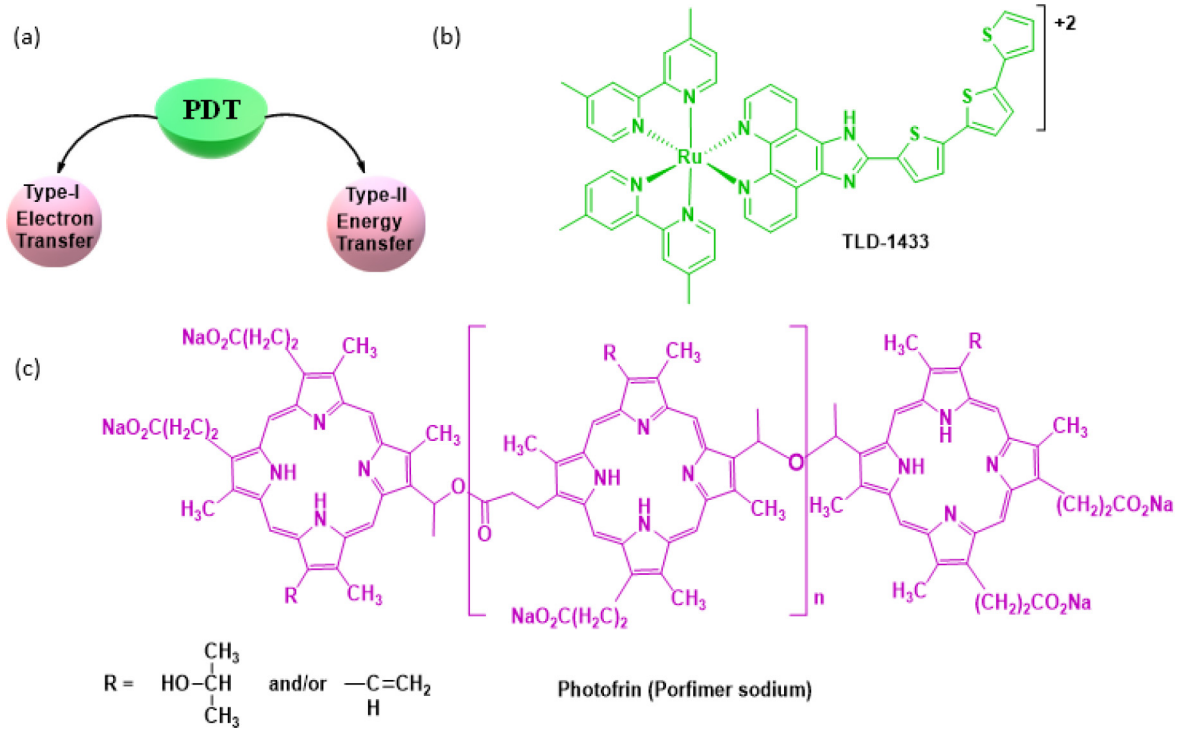

Fig. 3. (a) Types of PDT (b) Structure of TLD-1433 (c) Structure of Photofrin.

mentioned that some specific bilayer activities are seen to be allied to high diversity in lipid composition, its flexibility, some interactions as well as dispersion influencing the role of cell membrane and cell characteristics. Lipid layer contains a lengthy hydrophobic tail along with a polar head. The lipid composition and distribution of cell membrane are not uniform. These constituents expedite the noncovalent interactions with other biomolecules such as proteins and lipids and thereby help to form the membranes of cells and organelles. Therefore, cell membrane can be assumed as a key target for modern chemotherapeutics or small molecules to wrestle with cancer.

2.2. Cellular receptor

Cell receptors remain clinged to the cell's surface to welcome the external molecules such as hormones and nutrients for entering into cells. All the receptors can be classified into two groups: (1) intracellular receptors (found in cytoplasm or nucleus) and cell surface or extracellular receptors (found in plasma membrane). Receptor plays a key role in different physiological as well as pathological processes like growth factor signaling process, extracellular matrix and cell activation during microbial invasion. It is noteworthy that the dissemination of different degenerative diseases such as cancer, neurological disorders and atherosclerosis are mostly reliant on cell surface receptors. The prime aim of cancer diagnosis and treatment is to design the target specific drugs capable of targeting the tumor microenvironment where the role of overexpressed receptors in cancer cell membrane is praiseworthy. A few receptors which are overexpressed in cancer cell's surface can be mentioned as αVβ3 integrin, epidermal growth factor receptor (EGFR), vascular endothelial cell growth factor receptor 2 (VEGFR2), folate receptor (FAR-α) and neuropilin-1 (NRP1) and these receptors are frequently exploited as important targets for healing cancer. The human epidermal receptor 2 (HER2) are seen to be overexpressed in many primary tumors and mainly in breast cancer. In this way cellular receptors provide valuable clues which lead to the knowledge of designing the effective drugs in protection of carcinogenesis.

2.3. Intracellular target

2.3.1. Nucleus

The Nucleus is the most important and largest organelle in the cell. It is also considered to be the "brain" of the cell as it possesses genetic components, chromosomes which consists of DNA and nucleoproteins such as histones that regulate gene expression where transcription from DNA to RNA plays an important role inside the nucleolus. Therefore, DNA in nucleus is the key target for any drug molecules.

It has been noticed that metal complexes are very much efficient candidates to be employed in anticancer therapy owing to their structural variety and interesting properties such as wide range of oxidation states, suitable geometry and large number of ligand coordination to metal centers along with greater extent of adaptability. In addition to this, different functionalization to ligands can modify the cellular accumulation as well as biomolecular targeting ability. The organic ligands regulate the interactions such as electrostatic interaction, hydrophobic groove binding, intercalation, hydrogen bonding, insertion or the mixture of all between metal complexes and DNA. Hence, the metal complexes which are capable of interacting with nucleic acids have been well suggested for cancer therapy.

2.4. Mitochondria

Mitochondrion is highly significant, semi-independent organelle having double membrane that controls cell's metabolism. The inner mitochondrial membrane involves in electron transfer where electrons are moved from NADH to oxygen during redox processes. The energy of these processess helps to thrust H^+ out of the matrix and thereby negative charge is created throughout the mitochondrial membrane. Mitochondria takes part in controlling

the cell metabolism, creation of reactive oxygen species (ROS) as well as cell death. Mitochondria is recognized as the powerhouses of cells and act as energy store which are crucial for cancer metabolism. The Warburg effect or "aerobic glycolysis," takes place in mitochondria explaining the mitochondria's role to hold back carcinogenesis. This is a matter of fact that tumor cells release energy following glycolytic pathway rather than following the tricarboxylic acid (TCA) cycle as a result of mitochondrial malfunction in tumor cells and Warburg suggested that tumor cells had to depend on glycolysis due to the damage of respiratory chain in mitochondria. Consequently, mitochondria targeting drugs find more significance as beneficial anticancer drugs that steadfastly aim to mitochondrial functionality over traditional chemotherapeutic drugs causing mitochondrial dysfunction in an indirect manner with damaged DNAs and thereby trigger the apoptotic signals. A number of mitochondria accumulating transition-metal complexes are seen to be emissive in nature acquiring the capability of both enhanced cellular uptake as well as appreciable organelle-specific distribution. Therefore, mitochondria serves as potential target for designing anticancer metallo drugs.

2.4.1. Lysosome

Lysosomes are condensed granules in cytoplasm bearing hydrolytic enzymes which are mainly accountable to intracellular and extracellular digestion. Lysosome comprises of around 40 different enzymes being classified into five categories: nucleases, proteases, amylase, lipases and monoesters of phosphoric acid. Hydrolases are well known to be the class of enzymes where water molecules are used to cleave the substrates. Therefore, lysosomes being loaded with hydrolases, are liable to destroy the extracellular and intracellular materials. Most of the lysosomal enzymes carry on their function in an acidic environment. The migration of lysosome towards the periphery of the cytoplasm of cancer cell is seen to be indespensible for cancer cell growth, invasion as well as metastasis revealing the noticeable modification for neoplastic disease. It is apparent that during neoplastic transformation, number of lysosomes changes along with the change in shape, luminal pH, hydrolase concentration as well as intracellular distribution. Moreover, at the time of oncogenic transformation, the changes in tumor microenvironment, such as acidity, or changes in gene expression can elicit this type of redistribution. Therefore, lysosomes of cancer cells can be assumed as the prime focus for any anticancer drug.

3. Property of a good PDT agent

A good PDT agent possesses some important properties like (a) good photo stability in aqueous media, (b) long life time in excited state, (c) good solubility, (d) inactivity in dark condition.

3.1. Photosensitizers

The photosensitizer is the most significant component in the production of reactive oxygen species (ROS). The highest absorbance of a good photosensitizer can be found at very long wavelengths. On conversion from singlet to triplet states, it possesses high intersystem crossover (ISC) efficiency. It causes less phototoxic damage to normal cells than it does to cancer cells [33–37a]. A good PSs should meet the criteria like strong absorption should be present in the far-red and near-infrared range (>650 nm), but modest absorption should be present in the shorter wavelength region of visible light (400–600 nm), under physiological conditions the PS ought to produce reactive oxygen species excellently, it must have lower dark toxicity, good degradablity and finally it can be easily removed from the body after treatment [37b]. Porphyrins are pyrrole-based compounds with four subunits and a highly conjugated structure which absorb light in the visible region. However, low selectivity and low absorbance in the IR or NIR regions are downsides of this type of molecule [38]. Three generations of photosensitizers were discovered after that. Hematoporphyrin derivative was considered as first-generation photosensitizer. This moiety absorbs light at roughly 630 nm and has a high quantum yield of 0.64 in methanol, indicating a high efficiency of singlet oxygen generation. This compound is used to treat a variety of cancers including brain, laryngeal, lung, skin, gastric and colorectal cancers. However, the ultimate drawback is that it can penetrate weak tissues only [39]. As cell membrane is one of the most important targets for any anticancer therapeutics, L. Yuan *et al* was tried to develop cell membrane targeted unimolecular prodrug for programmatic photodynamic therapy. They established smart-molecule prodrug **D-bpy** as multifunctional photosensitizer being capable of exhibiting two-photon photodynamic therapy in association with well-disciplined chemotherapy to eradicate the pervasiveness of deep tumour tissues revealing good therapeutic potential.

The main objective to discover the second-generation photosensitizer was to reduce the disadvantages of the first-generation photo.sensitizer. The second-generation photosensitizers included phthalocyanines, chlorins and others. Chlorin e6 (Ce6) was used to treat the breast cancer as well as hypopharyngeal cancer cells. Termoporfin (m-THPC) is a chlorin-based photosensitizer that has been used in clinical trials. Because of their specificity for cancer cells and low skin deposition, this second-generation photosensitizer is crucial. They have a wide range of absorption from 630 to 800 nm and generate reactive oxygen species (ROS). Although all photosensitizers are hydrophobic, they have several disadvantages such as a short circulation half-life and a high rate of self-aggregation. The therapeutic impact was discussed for these two reasons [38]. Afterward some organic and inorganic nano carriers were used as photosensitizers which were considered as third generation photosensitizer. Kono *et al.* designed PEGylated dendrimers to load photoporphyrin IX (PpIX) for PDT [40]. Zhao *et al.* developed folic acid (FA)-conjugated HMSNs to load 5-aminolevulinic acid (5-ALA) for targeted PDT towards B16F10 cancer cells [41]. Some inorganic photosensitizers were vital for the generation of reactive oxygen species (ROS) to damage cancer cells. UV irradiation causes TiO_2 to produce ROS directly [42–44]. Hwang and colleagues examined that photo-excitation of Ag, Pt, and Au NPs created singlet oxygen in 2011 [45]. Semiconductors such as CdSe, ZnO, and others are essential in this regard because they can change their size and composition, allowing absorption spectra to be modified from UV to NIR. At the end of this discussion, we could classify the photosensitizer in two parts, one is organic photosensitizer and another is inorganic photosensitizer. Most of organic photosensitizers involve in Type-II PDT and inorganic photosensitizers involve in Type-I PDT (Fig. 4).

3.2. Single photon excitation and two photon excitations

In fluorescence spectrophotometer, one photon is commonly used for excitation. When a photon with specific wavelength is subjected to a fluorescent molecule (fluorophores), it becomes stimulated and is moved from lower energy, S_0 to higher energy state, S_n. The molecules can be dipped in energy somewhat (to S_1) after shifting to a higher energy state but these fluorophores will eventually drop back to the ground state by releasing the energy as emitted photons which is how fluorescence takes place since the emitted photon is lower in energy as well as larger wavelength due to transfer from S_n to S_1. NIR photon have higher wavelength and lower in energy than visible light photon (700–900 nm) (Fig. 5a).

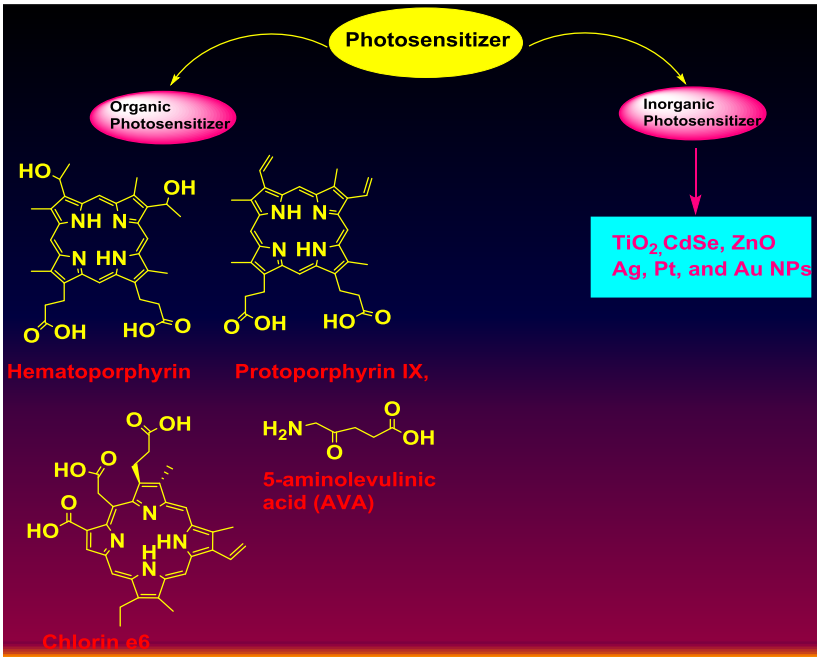

Fig. 4. Classification of some organic and inorganic photosensitizers.

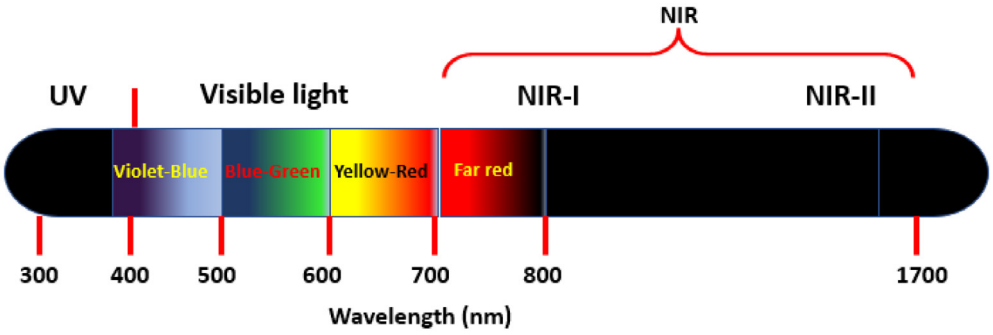

Fig. 5a. The electromagnetic spectrum, ranging from UV to NIR.

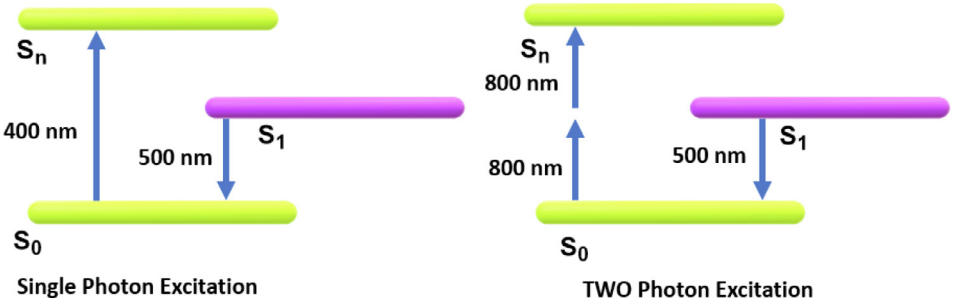

Fig. 5b. Jablonski energy diagrams for single-photon and two-photon excitation. On the left is single-photon excitation, where a single 400 nm photon is enough for fluorescence. On the right is two-photon excitation, where two 800 nm NIR photons are requiredfor fluorescence.

As lower energy NIR photons do not possess satisfactory energy to excite the fluorophore from S_0 to S_n, no fluorescence will be found. In that case two photons excitation takes place. For this, the two NIR photons must arrive in rapid succession; both photons must arrive virtually instantaneously, within one femtosecond (10^{-15} S). Due to this time factor the energy of these two photons are merged and help to excite the fluorophores which is called as two photon excitations. In case of single photon excitation linear relationship was found between excitation light intensity and fluorescence intensity whereas in two photon excitation non-linear (quadratic) relationships was found because the intensity of fluorescence depends on the square of the number of photons received by the fluorophore as multiple photons are involved here (Fig. 5b). In this case, non-linearity gives some advantages as it can localize the excitation [46–48].

4. Advantages and challenges of PDT

PDT offers more advantages than other traditional processes with fewer challenges. Such as: (i) an extensive amount of cells are damaged by the PDT which conveys the immune system to attack the cancer, (ii) PSs has only been activated by the irradiation of light, so there is very minor chance for systemic toxicity, (iii) excellent selectivity, (iv) applicable in nanomaterial for *in vivo* application which can enhance the cell permeability. PDT have also some challenges like (i) the synthesis and purification process of some PSs (chlorin, phthalocyanine derivatives, porphyrin, etc.) are very tough, (ii) poor water solubility, (iii) absence of a tumor target moiety, (iv) ROS have shorter lifetime (<40 ns) and narrow diffusion radii (10 nm), (v) PSs have center of cavity and due to this cavity metal center coordinate in this cavity and leads to metal complex formation. These complexes are very difficult to synthesis as exhibit high cytotoxicity in absence of light irradiation; (vi) PDT is only applicable to that patient who remain in the dark for a long-time. Recently scientist contributed their major efforts to over-come the limitations of PDT. Red or NIR light irradiation can improve the low penetration of light towards the PSs with short wavelength absorption by dint of FRET effect or two-photon excitation PDT etc. Nowadays, scientists have developed innovative photosensitizers (including efficient organic photosensitizers) instead of conventional PSs (Fig. 6) [49].

5. Enhancement of PDT

In general, the PSs can transform molecular O_2 into ROS with the help of irradiation. Therefore, PSs are considered the key entity of this technique and we need to use such kind of PSs which have high ROS transformation efficiency. In order to enhance the absorption efficiency (at visible or NIR wavelength) of the PSs, some mechanism like Förster resonance energy transfer (FRET), fluorescence resonance energy transfer (FRET), resonance energy transfer (RET) and electronic energytransfer (EET) can be successfully employed for transferring the energy from an energy donor to energy acceptor (Fig. 7).

Herein, we have portrayed a few examples regarding the enhancement of PDT. As porphyrin sensitizers have small TPA (two-photon absorption) cross sections, Dichtel *et al.* made some modification to augment the TPA cross sections of porphyrin where TPA efficient donor chromophores were covalently bound to the central porphyrin acceptor (Fig. 8). After TPA, the donors transfer

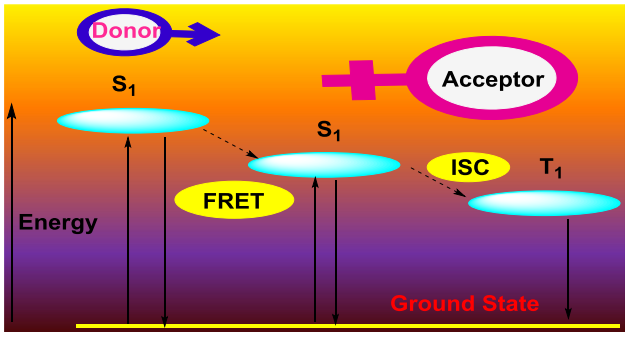

Fig. 7. Mechanism of fluorescence resonance energy transfer.

their excited state energy to the porphyrin moiety through FRET process and thereby generate singlet oxygen species [50].

To enhance the PDT through FRET process Zhu *et al.* also developed two fluorescence resonance energy transfer (FRET) dyads **AceDAN-H_2Por-Lyso** (a) and **AceDAN-ZnPor-Lyso** (b) (Fig. 9). In that case, the donor AceDAN can successfully transfer the excited state energy to the acceptor porphyrin through FRET. As a result of this, generation of deep-red fluorescence and singlet oxygen become useful for cell imaging and PDT [51].

Another FRET application for singlet oxygen generation was developed by Tang and coworkers. They reported donor–acceptor porphyrin PSs comprised of cationic conjugated oligomer (OPV) as a donor unit and porphyrin (TPP) as an acceptor unit (Fig. 10a). The cationic donor had a significant role which improved the water solubility and decreased the accumulation of porphyrin. It promoted the PSs towards the cell membranes and hence these PSs exposed highly efficient PDT treatment with the help of electrostatic interactions [52]. Two-photon-induced PDT was developed by Junbai Li *et al.* with the help of FRET mechanism. In their study Nitrogen-doped graphene quantum dots (***N*-GQD**) was combined with traditional photosensitizers RB and ultimately it was formed as stable photosensitizer being coupled with graphene quantum dots, ***N*-GQD–RB** (Fig. 10b). Hence, following the intramolecular FRET mechanism, the RB could be excited by ***N*-GQD** and upon irradiation with one or two photon laser, ***N*-GQD–RB** displayed high cytotoxicity [53].

Using DPP (Diketopyrrolopyrrole) and BODIPY (Boron dipyrromethene), Zou *et al.* designed and synthesized a novel D-A-D organic photosensitizer DPPBDPI, where DPP and BODIPY were

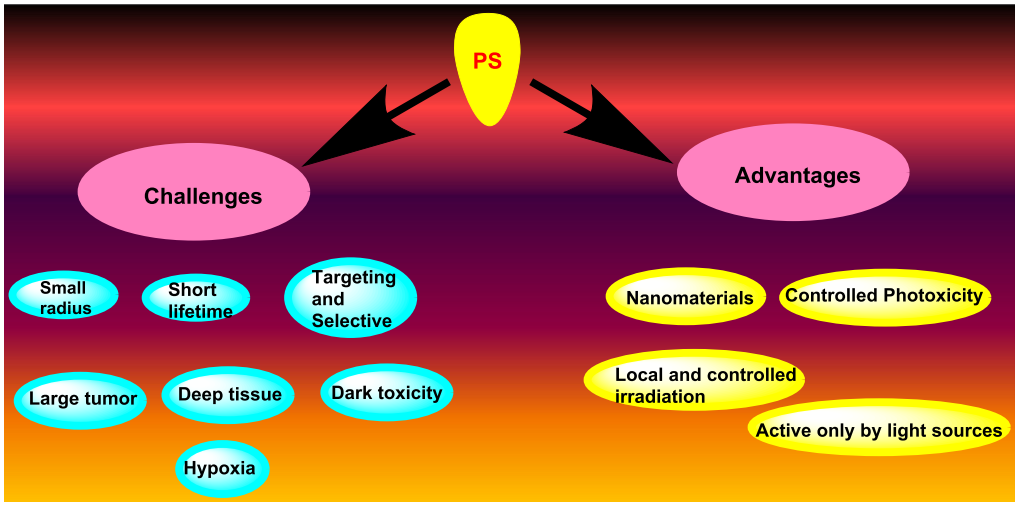

Fig. 6. Generalized shortlist of advantages and challenges of PDT.

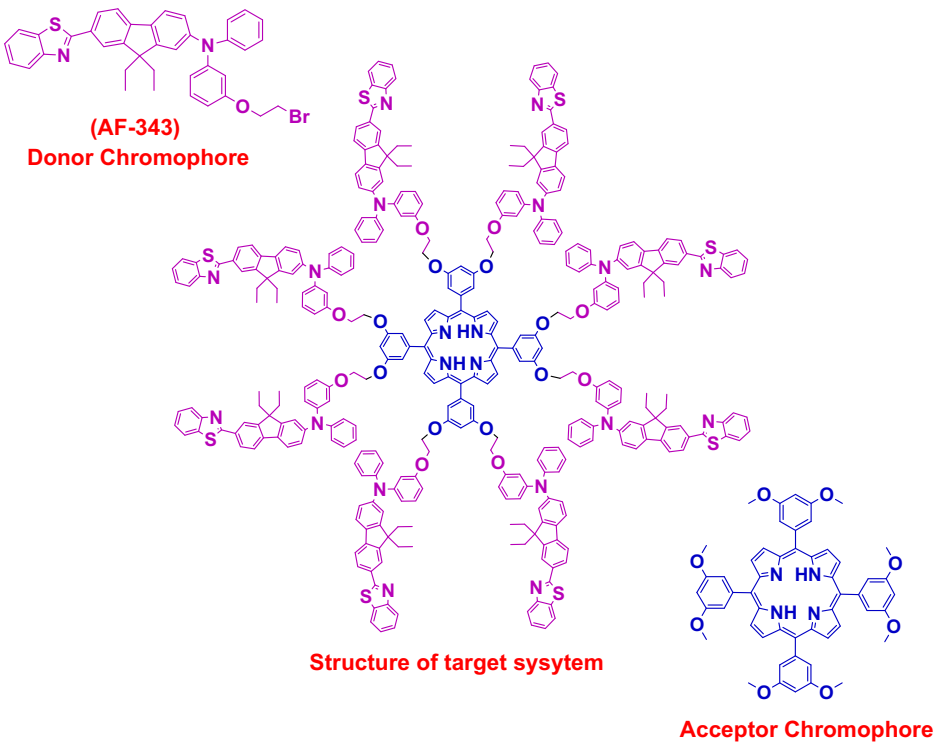

Fig. 8. Structure of target system, Donor Chromophore and Acceptor Chromophore.

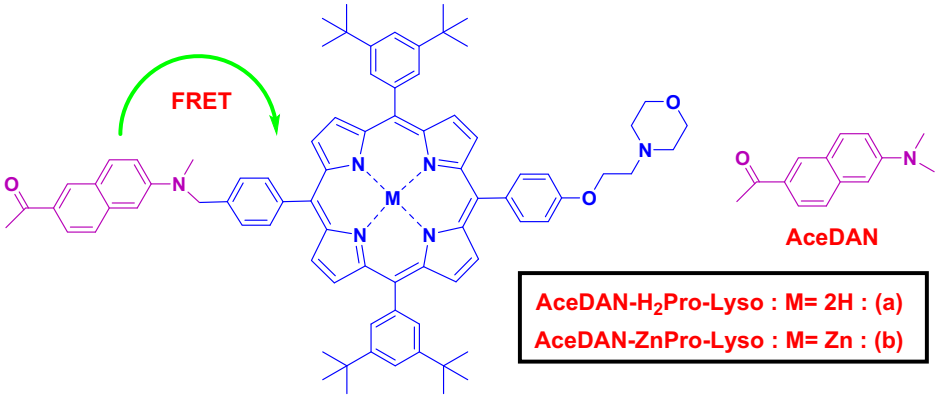

Fig. 9. Structure of dyads **AceDAN-H_2Por-Lyso** (a) and **AceDAN-ZnPor-Lyso** (b).

linked *via* benzene ring as a π-bridge linker (Fig. 11). The DPP part exhibited optical properties and charge carrier mobility. In the end of DPP, BDPI present as π-stacking moieties which facilitate end-to-end π–π interactions followed by the enhancement of charge transport between adjacent molecules. The synergistic effect of the two photosensitizers increases the fluorescence quantum yield 5 % and the singlet oxygen quantum yield up to 80 %. In vitro and *in vivo* experiment of **DPPBDPI** nanoparticles exhibited low dark toxicity and very high phototoxicity towards HeLa cells with IC_{50}-value 0.06 μM. *In vivo* fluorescence imaging experiments indicated that at very low doses **DPPBDPI** can accumulate at the tumor site and inhibits tumor growth without side effects [54].

For the construction of a nano particle platform, Tang *et al.* developed photo-cross-linkable semiconductor polymer dots doped with photosensitizer **Chlorin e6** (Ce6) where photoreactive oxetane groups were present in the side chains of the semiconductor polymer (Fig. 12). After photo-cross-linking reaction, **Ce6-doped** Pdots inhibited the photosensitizer leaching because it demonstrated outstanding stability. In that case efficient energy transfer occurred from the polymer to Ce6 molecules that led to the formation of singlet oxygen molecule. The *in vitro* photodynamic experiments helped them to conclude that under low dose of light irradiation **Ce6-doped** Pdots effectually destroyed the cancer cells. Also, they performed *in vivo* photodynamic experiment with the help of nude mice and they visualised that Pdot photosensitizer repressed the growth of solid tumors [55].

Resonance energy transfer mechanism (RET) is an important process which can dramatically enhance the singlet oxygen generation. This mechanism involves the construction of a novel dyad photosensitizer that is capable of enhancing the intensity of NIR photon and finally increases the formation of singlet oxygen species. Huang *et al.* connected the donor moiety distyryl-BODIPY with photosensitizer diiodo-distyryl-BODIPY to form a dyad molecule RET-BDP (Fig. 13). Finally, they encapsulated this RET-BDP into

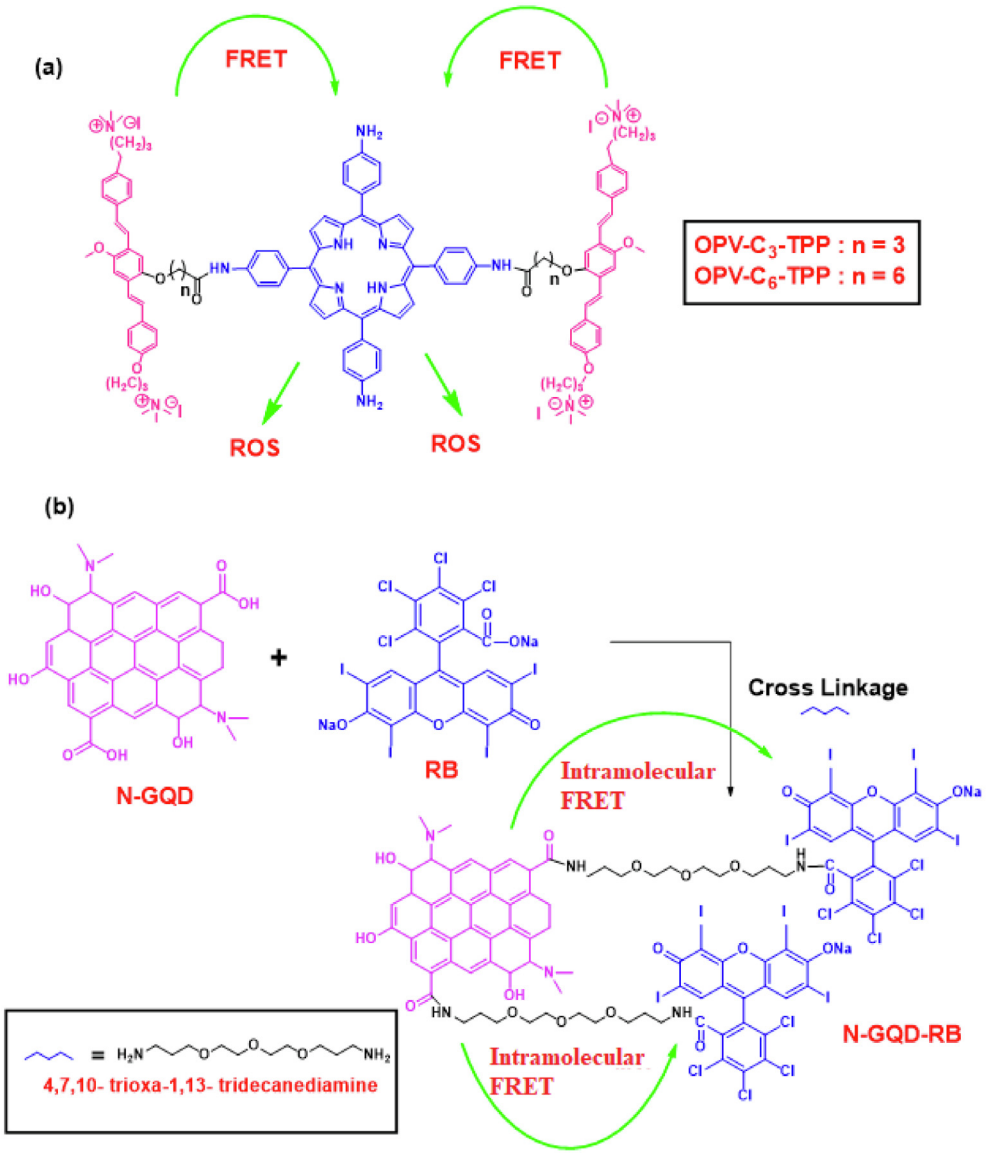

Fig. 10. Structure of **OPV-C_3-TPP** and ***N*-GQD-RB** and FRET process.

biodegradable copolymer Pluronic F-127-folic acid (F-127-FA) which is water soluble and good tumor targeting. The main advantage of this nano particle is its tumor targeting PDT effect in presence of low-power NIR LED light irradiation (10 mW cm^{-2}) both *in vivo* and *in vitro* [56].

6. Organelles targeted ruthenium complexes for photodynamic therapy

6.1. Ruthenium based polypyridyl complexes

Over the last few years, synthesis of Ru (II) polypyridyl complexes and exploration of their key characteristics has become a main focus of research [57–59]. These complexes absorb the visible light and also emit long wavelength light in the red and NIR spectral regions. It has been noted that photochemical and photophysical properties of the complexes can be changed with the nature and the numbers of the polypyridyl ligands attached with the Ru (II) metal center [60,61]. Noncovalent interactions between Ru (II) polypyridyl complexes and biomolecules is ideally suited to the development of novel therapeutic approaches. Polypyridyl based ruthenium complex used in biological system for cellular imaging and diagnostic agents as well as the development of novel classes of therapeutic medicines has received a lot of attention. Here we represented some organelle targeted polypyridyl based ruthenium complexes for various type of cancer therapy.

Six water soluble free-base porphyrin-Ru(II) conjugates, (**1,2,3**) and Zn(II) porphyrin-Ru(II) conjugates (**4,5,6**) with different linkers between the hydrophobic porphyrin moiety and the hydrophilic Ru(II)-polypyridyl complex were synthesized by Zhang *et al.* (Fig. 14). Authors inspected their dual functions, (i) *in vitro* imaging; (ii) photodynamic therapeutic applications. The energy transfer from Ru(II) ^{1}MLCT to porphyrin singlet state was observed at λ 430 nm photoexcitation for the complex **1 to 3** and emissions were observed at λ 659 and 718 nm. In case of complexes **4, 5** and **6**, caused by an increase in the singlet energy level of Zn (II) porphyrin than that of the Ru (II) ^{3}MLCT state, the energy transfer from the Soret-excited porphyrin to the Ru (II) was observed at λ 430 nm of photoexcitation. The emission quantum yield of conjugated complexes **4** to **6** was found to be 10-fold lower than the complexes **1** to **3**. But, the singlet oxygen quantum yield of all

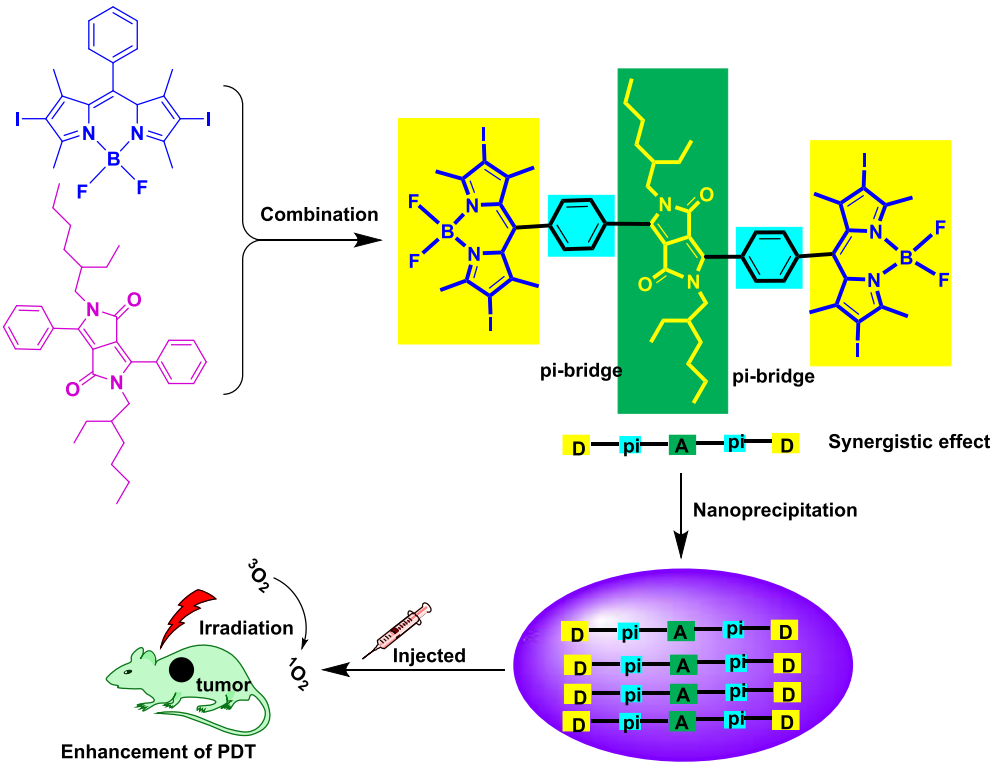

Fig. 11. D–A–D structure of **DPPBDPI** and its enhancement of fluorescence as a theranostic agent for PDT.

the conjugates exhibited no comprehensible difference between conjugates with different linkers [62]. Based on the emission quantum yield and singlet oxygen quantum yield, they further investigated the *in vitro* property of conjugates **1** to **3** against the HeLa cell lines. In dark condition the IC_{50} values were 118, 175, and > 250 μM for conjugates **1**, **2**, and **3** respectively, which was reliable with their cellular uptake properties with **1** ∼ **2** ≫ **3**. From this result, they concluded that conjugate **3** with more hydrophilic poly (ethylene glycol) linkage, was the least efficient in cell penetration. The authors also incubated the complexes **1**, **2** and **3** (5 μM) with HeLa cells for 6 h and simultaneously excited at λ 850 nm. Two photon cross section was found to be 177, 168, and 144 GM for **1**, **2** and **3** respectively. The confocal image of the cell at 0, 8, 16 and 32 min was shown in Fig. 15 after two-photon laser irradiation. The intensities of fluorescence were found to be more in case of complexes **1** and **2** stained cells compared to complex **3** stained cells. Furthermore, the cells were continuously irradiated to understand the efficacy of these conjugates on two photon induced cytotoxicity and upon irradiation the fluorescent images were captured at 8 (Fig. 15, b, f, j), 16 (Fig. 15, c, g, k) and 32 min (Fig. 15, d, h, l). In treated HeLa cells, subcellular localization patterns of Conjugates **1** and **3** were found to be similar to those in control cells after 2PA-PDT (Fig. 15, a, i). From the Fig. 15, f, g, h it was clearly observed the nuclear localization of **2** after 8 to 32 min of irradiation. The light dose- dependant (at 1 μM concentration) photocytotoxicity of these conjugates was found in the following order as **2**>**1**>**3** which was supported with their respective subcellular localizations at the mitochondria, lysosomes and cytoplasm. Eventually, they came to the conclusion that porphyrin-Ru (II) conjugates **(2)** exhibited most promising *in vitro* imaging and PDT activity because of its high emission quantum yield, low dark cytotoxicity along with high phototoxicity [62].

For the amplification of two-photon induced luminescence, singlet oxygen generation, cellular uptake and photocytotoxic properties, Zhang *et al.* synthesized two Ru(II)polypyridyl-porphyrin and Zn(II) porphyrin conjugates (complexes**-7**, **8**, Fig. 18). Complex **7** exhibited emission spectrum in the near-infrared region *via* one and two photon excitation with high quantum efficiency and singlet oxygen quantum yield. Authors also investigated the cellular uptake property of these complexes in HeLa cell with the help of multiphoton laser scanning confocal microscopy. Complex **7** showed 75 % higher cellular uptake ability than complex **8.** After two hours of incubation strong red emission was observed on the cell membrane but not inside the cell (Fig. 16). However after 3 h of incubation, strong red emission from the complex **7** was visualised in the cytoplasm whereas complex **8** exhibited red emission inside the cell membrane after same time of incubation. A very weak emission of **8** was observed in cytoplasm after 4 h of incubation. From this phenomenon they concluded that the cellular uptake property of complex **7** was much higher than complex **8**. Authors also investigated the phototheranostic properties of complex **7** and **8** in presence of TPE against HeLa cells. In presence of 800 nm laser, 70 % of cells (which were incubated with complex **7**) lost (Fig. 17) their morphological integrity. But no significant change was observed in complex **8** under the same condition [63].

Zhang *et al.* reported a noninnocent ligand-based Ru(II) complex (**9**). In this complex they incorporated 5-chloro-8-oxyquinolate-based noninnocent ligand into a merocyanine scaffold Cl-7-IVQ and finally they synthesized new Ru complex of the type, $[Ru(bpy)_2(Cl\text{-}7\text{-}IVQ)]^{2+}$ (Fig. 18). This complex exhibited intense absorption at 600–700 nm and permited an efficient (•OH)-mediated DNA photocleavage. This was the first Ru (II)-complex based DNA photocleaver, that exhibited MLCT absorption at 600 nm and upon red light irradiation the complex selectively inactivated E. coli bacterial cells over HeLa cells [64]. Another Ru (II) polypyridyl complexes (**10**, **11**) were reported by Wachter and co-workers that were activated in the therapeutic window exhibiting photo-activated DNA binding as well as potent cytotoxicity towards cancer cells (Fig. 19). They performed the cytotoxicity study towards human leukemia cell line HL-60 and observed the

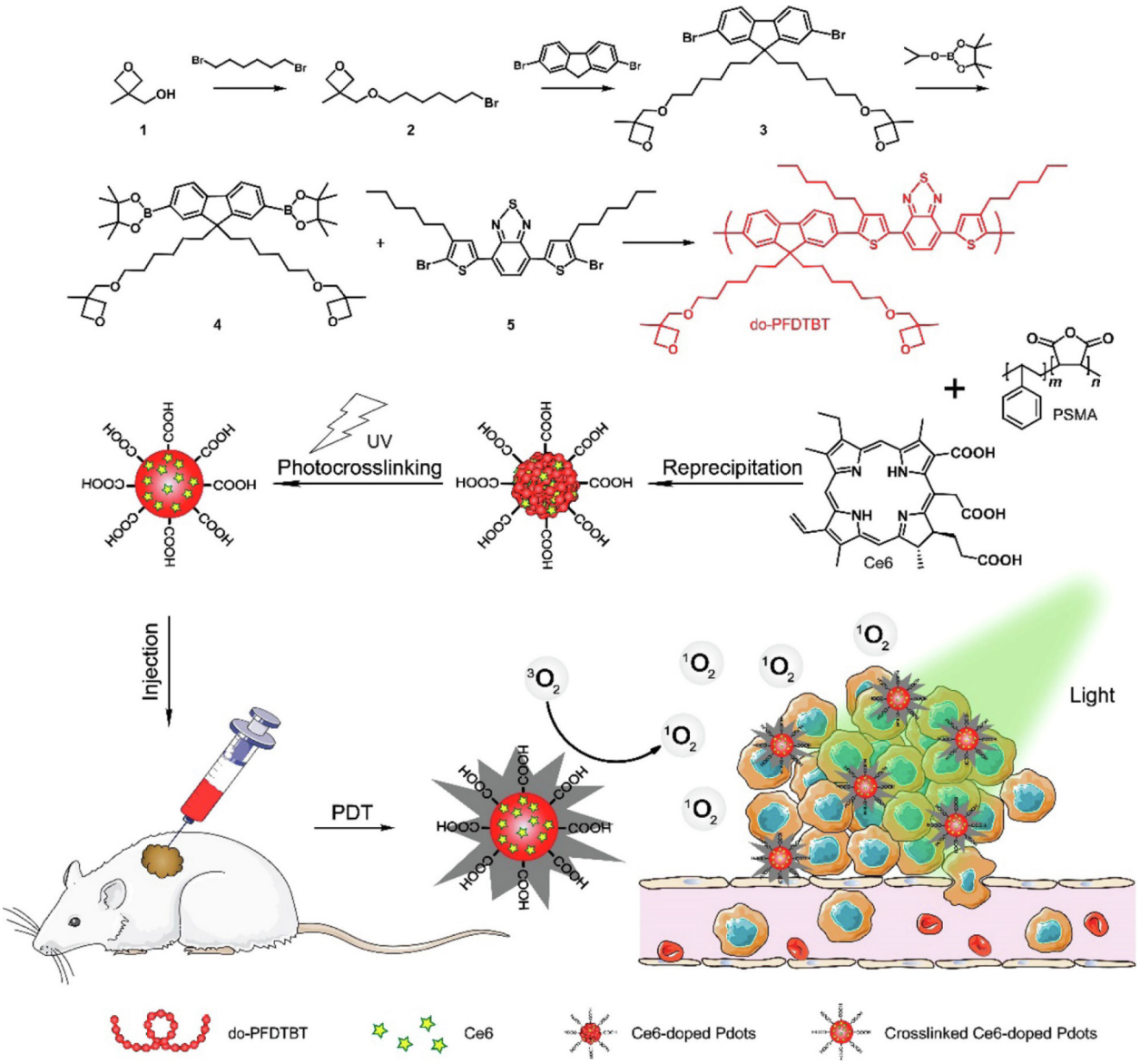

Fig. 12. Synthetic route of **do-PFDTBT** and photodynamic effect of the **Ce6-Doped** Pdots [Adopted from **ref. 55** with permission from American Chemical Society].

activity of these complexes upon light dose dependent manner which indicated that light activation was directly related to the cytotoxicity. In presence of blue light, the IC_{50} value was found to be 1.2 and 2.4 μM for complexes **10** and **11** respectively. Nevertheless, the potency was seen to be deteriorated in presence of red and near-IR light. The potency was further increased with increasing the light dose. In this case the IC_{50} values were observed as 2.3 μM and 5.1 μM in red and near-IR light for complex **11** which demonstrated better activity of complex **11** than complex**10**. The PI (phototoxicity index) values were calculated as 19.7 and 9.2 [(λ_{abs}**(nm)** (**ε (M^{-1} cm^{-1})** 550(4900)] in red and near-IR light for complex **11** whereas for complex **10** the values were observed as 43.8 and 3.32 [(λ_{abs}**(nm)** (**ε (M^{-1} cm^{-1})** 525(8300)] respectively (Table 1). After study, they came in conclusion that complexes exhibited cytotoxicity in cancer cells upon irradiation with red and near-IR light [65].

Tempo-functionalized Ru (II) polypyridyl complexes gave excellent result in case of PDT and anticancer application. *Yang et al.* synthesized tempo functionalized complexes because "Tempo" moiety was known to be redox sensitive and fluorescence enhancer in the intracellular medium. Therefore, TEMPO-functionalized Ru(II) complexes were highly acceptable for photodynamic treatment (Fig. 19). They represented two TEMPO-functionalized Ru(II) complexes[Ru(N—N)$_2L$]PF_6 [Where, N—N = 4, 7-diphenyl-1,10-phenanthroline (**dip-12**), 2,2-bipyridine (**bpy-13**), and (2,2,6,6-tetramethyl-piperidine-1-oxyl free radical) = TEMPO, a nitroxide moiety] along with TEMPO-free analogues (**12-a**, **13-a**). Upon application of PDT induced oxidative stress, it was observed that TEMPO radical moiety was converted to diamagnetic on-radical species in cells. With the help of MTT assay authors investigated the DCF (2,7-dichlorofluorescein) fluorescence assay to observe dark cytotoxicity of **12**, **12-a**. The irradiation of light with complex **12** at 450 nm resulted in a considerable and concentration-dependent increase by means of DCF fluorescence intensity.Under similar conditions, concentration-dependent DCF fluorescence improvement was also detected in **12-a**-treated cells, all but to a considerably lesser amount (up to 4-fold at 0.5–2 M). In presence of light, it was clearly evident (Fig. 20) that complex **12** generated substantially larger intracellular ROS levels than complex **12a** applying the same doses. Under

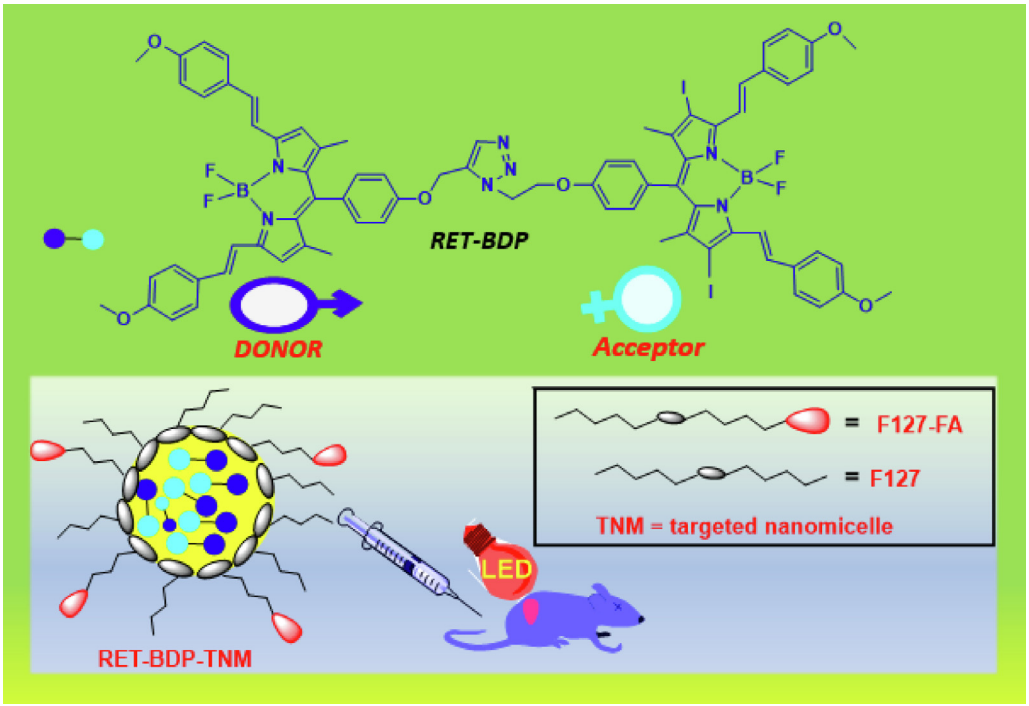

Fig. 13. Schematic representation of RET-photosensitizer-mediated PDT (**RET-BDP- TNM**).

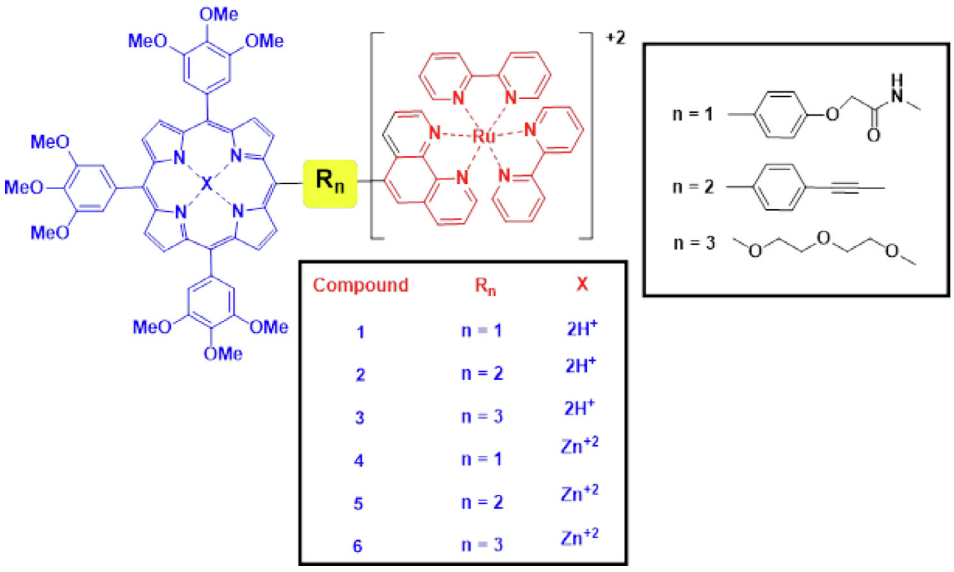

Fig. 14. Structure of ruthenium-porphyrin conjugates (**1**–**6**).

one photon (488 nm), and two photon (800 nm) excitation, it was noticed that **12/ 12-a** penetrated into HeLa cells and localized in cytoplasm but no considerable cellular uptake efficiency was found in case of **13/ 13-a**. In vitro photocytotoxicity was investigated against different cancer cell lines like cervical cancer cell line (**HeLa**), human pulmonary carcinomacell line (**A549**), cisplatin-resistant cell line (**A549R**) and human normal liver cell line (**LO2**) (Table 2). From IC_{50} values of **12/12-a**, moderate cytotoxicity against all cancer cell lines was exhibited in dark but **12** gave 3-times lower dark-cytotoxicity than **12-a**. In presence of light, **12** exhibited 10-times higher phototoxicity than tempo free **12-a** exposing IC_{50} values of 0.24 μM and 2.9 μM for **12** and **12-a** respectively. The PI (phototoxicity index) values were in the following order: **12** in HeLa (280.5) > **12** in LO2 (30.2) > **12-a** in HeLa (6.7) > **12-a** in LO2 (2.8). Actually, the reason of enhanced PDT efficacy of the complexes was due to presence TEMPO moiety which showed effective cellular uptake property and enhanced the intracellular ROS levels [66].

Some other Ru-polypyridyl complexes were synthesized and characterized. Zhou *et al*., Pierroz *et al*. and Liu *et al*., synthesized complexes **14, 15, 16, 17, 18**, and **19** respectively (Fig. 21). **14** with general structure $[Ru(bpy)_2(dpb)]^{2+}$ (Where, bpy = 2,2′-bipyridine, dpb = 2,3-bis(2-pyridyl) benzoquinoxaline) exhibited DNA photocleavage activity in presence of suitable oxidative quenchers in anaerobic conditions and also showed long wavelength ^{1}MLCT absorption with absorption maximum at 550 nm wavelength. In

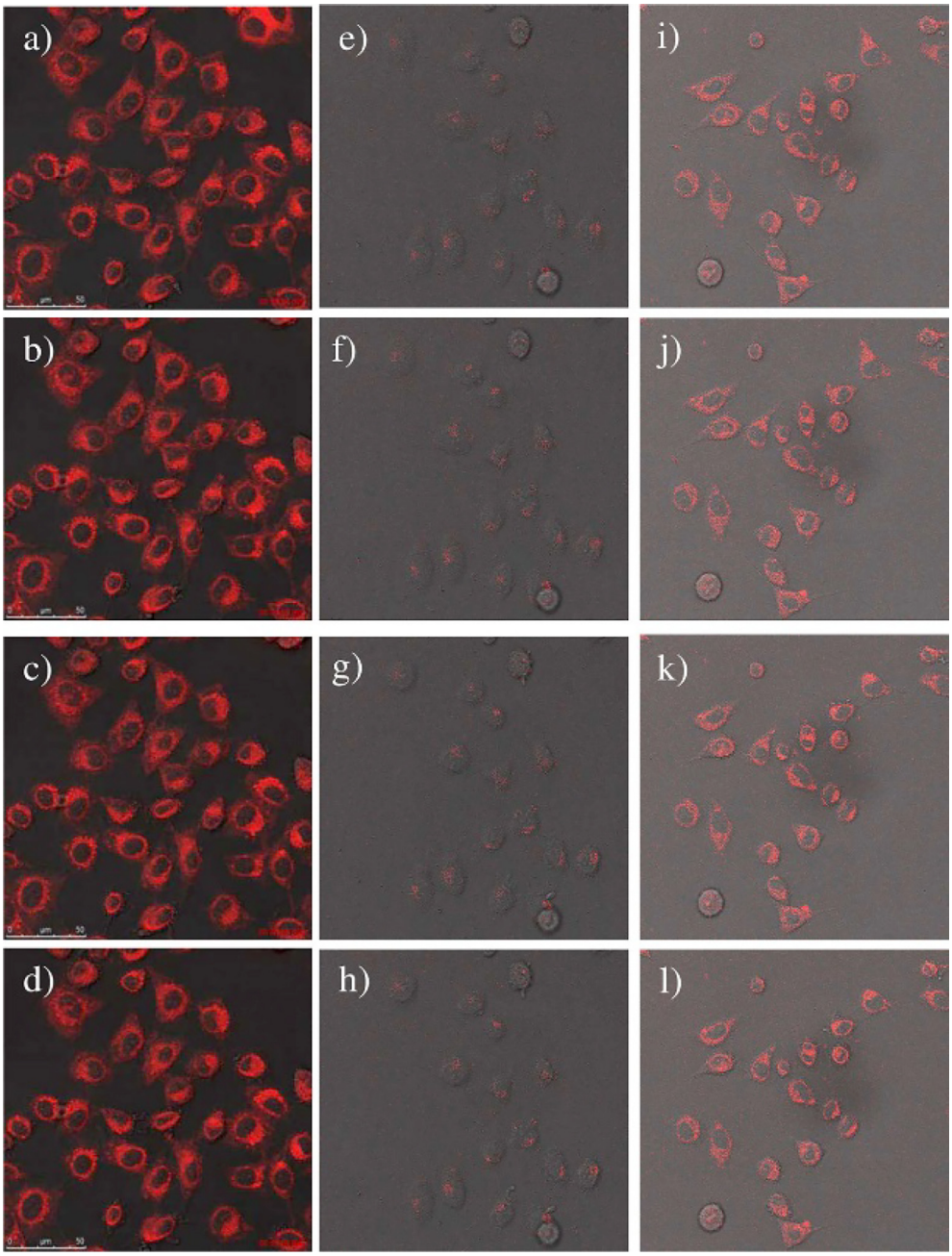

Fig. 15. Confocal microscopic images of HeLa cells treated with 5 μM of 1 (a, b, c, d), 2 (e, f, g, h), and 3 (i, j, k, l) for 6 h. First row- images found for 1 (left), 2 (middle), and 3 (right) treated cells after one snap laser flash (to avoid $^1O_2$ generation) at 860 nm. Second row-images is after 8 min, third row-images is after 16 min, and bottom row-images is after 32 min of laser irradiation. [Adopted from **ref. 62** with permission from American Chemical Society].

case of complex **15** with general structure [Ru(bipy)2-dppz-7-methoxy] $[PF_6]_2$ localized mainly in nucleus of various cancer cells and thereby exhibited cytotoxicity only upon UV-A irradiation. Upon UV-A irradiation, complex was promoted to guanine oxidation and DNA intercalations. Complexes **16** to **19** were mainly mitochondria-targeted two-photon photodynamic anticancer agents. They performed the cytotoxicity experiment with the help of 3D HeLa MCSs. In this work 3D HeLa MCSs was used as the screening model and they exhibited better therapeutic outcome than one-photon PDT when combined with two-photon PDT. In between four complexes, complex **19** showed IC_{50} values 9.6 μM and 1.9 μM in case of one photon and two photon PDT in 3D MCSs. Finally, they came to conclusion that complex **19** demonstrated more attracted PDT potency and it was efficient two-photon PDT candidate [67–69].

In case of two photon photodynamic therapy, Huang *et al.* synthesized tertiaryammonium group's substituted Lysosome targeting Ru (II) Polypyridyl complexes (**20**–**22**). They added tertiary ammonium group with the core structure of the complexes due to increase water solubility and binding affinity with the negatively charged cell membranes (Fig. 24). They examined the lipophilicity or hydrophilicity by analysing octanol/water partition coefficient ($\log P_{o/w}$). The result showed that **20** (-3.54) and **21**(-3.05) exhibited highly hydrophilic with the high positive charge (**+8**). But the complex **22** was found to be most lipophilic (-1.55) with its *N*-butyl chains. When they confirmed that the complexes produced singlet oxygen species upon light irradiation, then they examined cellular localization property of the complexes. Authors investigated cellular localization with the help of confocal laserscanning microscopy on HeLa and HeLa multicellular

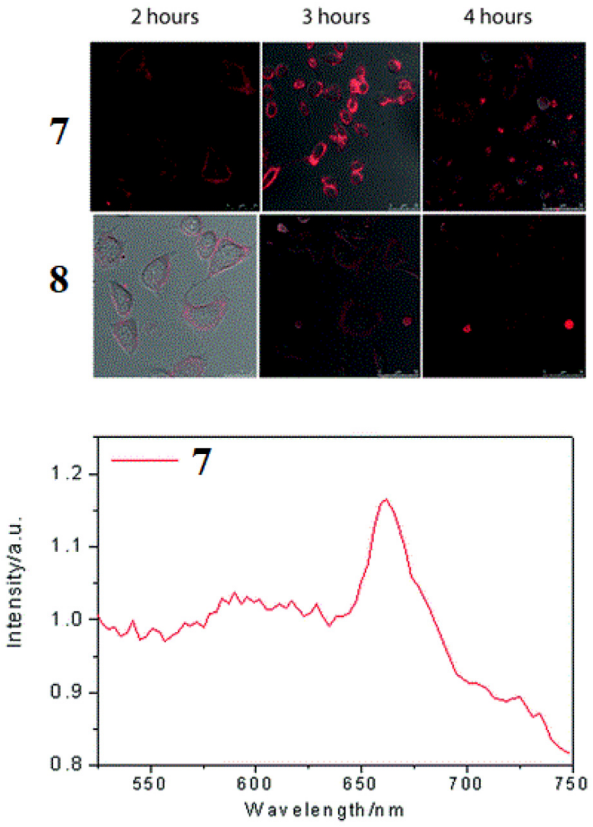

Fig. 16. (a) Confocal microscopic images of **7** (upper row) and **8** (bottom row) towards HeLa cells at different time points (b) In vitro emission spectrum of **7** towards HeLa cells after 4 h of incubation [Adopted from **ref. 63** with permission from Royal Society of Chemistry].

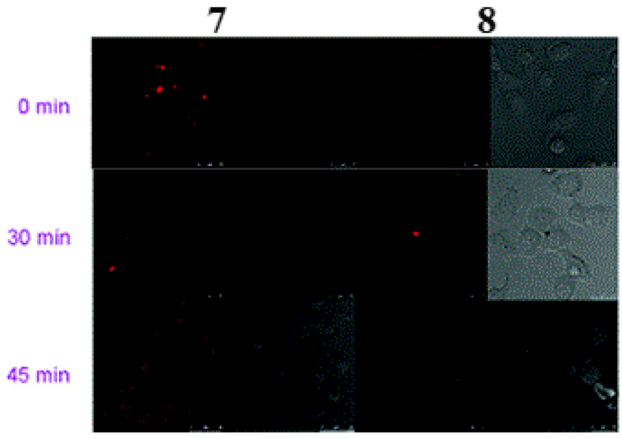

Fig. 17. Confocal microscopic and bright-field images of HeLa cells loaded with **7** (left) and **8** (right). Top row-images for **7** (left) and **8** (right) after 3 h of incubation (to avoid $^1O_2$ generation), middle row-images denoted after 30 min of laser flashes, bottom row-images denoted after 45 min of laser flashes at 800 nm. [Adopted from **ref. 63** with permission from Royal Society of Chemistry].

tumor spheroids (MCTSs). Under OP and TP excitation, spot-like red luminescence (Fig. 22a) of **20** was found in cell. From Fig. 22b it was clearly observed that TP signal of complex **20** demonstrated deep penetration into the MCTSs compared to one photon luminescence signal. They also performed the colocalization assay with some commercial dye like LysoTracker Green (LTG), MitoTracker Green, nuclear targeting dye Hoechst 33342. A good overlapped was found in between the signal of **20** and LysoTracker Green (LTG) (Fig. 22d), but poor overlapped with poor correlation coefficient was found in the case of MitoTracker Green, nuclear targeting dye Hoechst 33,342 (Fig. 22c, e). Then they studied the toxicity of the complexes on HeLa in dark condition. All the complexes exhibited nontoxicity in absence of light towards the cell line with IC_{50} value >300 μM. After that they investigated the phototoxicity of the complexes towards HeLa cells and it was found that complex **20** exhibited highly phototoxicity towards HeLa with IC_{50} value 1.5 μM. In order to investigate the ROS generation ability of complex **20** in cancer cell, authors used the ROS indicator 2, 7-dichlorofluoresceindiacetate (DCFH-DA), which was oxidized to release the green fluorophore DCF. They found a significant overlay between the green signal of DCF and red signal of **20**, indicated singlet oxygen generation in cell under light irradiation. The cellular localization was found to be changed from lysosomes (Fig. 23a) to cytoplasm (**23, b**) and finally the change was observed in nucleus (**23, c**) after increasing the irradiation time. So, they concluded that all the complexes (specially, complex-**20**) generated singlet oxygen species and localized in the lysosomes [70].

Conti *et al.* synthesized two Ru (II) and Ru (II)/ Cu (II) polypyridyl complexes having polyamino-macrocycle unit (a) (Fig. 24). The advantages of protonatable amine groups within the macrocyclic moiety was their high water solubility and strong interaction property with ct-DNA. Furthermore, they investigated that **(a)** and **(a)-Cu(II)** exhibited high tendency to be internalized into human melanoma cellline (A375). They also performed the biological activity towards A375 cells and it was found that both **(a)** and **(a)-Cu(II)** exhibited no toxicity under dark but exhibited cytotoxicity in presence of light. Complex **(a)-Cu(II)** demonstrated dose-dependent photo-induced cytotoxicity. They also disclosed that Fenton-active copper center played a synergetic role with light activation for ROS generation that contributed additional mechanisms for the oxidative damage of biological targets with singlet oxygen generation [71] In case of one photon and two photons photodynamic therapy Karges *et al.* encapsulated Ru(II)polypyridyl complex into polymeric nanoparticles with terminal biotin groups (Fig. 24). It exhibited high selectivity for the cancer cells in comparison with noncancerous cells in a 2D monolayer model as well as 3D multicellular tumor spheroids. *In vivo* study also suggested that the complex was found to be high accumulative inside the tumor cells. Upon one photon (500 nm) and two photon (800 nm) excitation the complex exhibited high phototoxic effect in 2D monolayer cells and 3D multicellular tumor spheroids [72]. To increase the DNA binding property and photocleaving properties, Saonli *et al.* synthesized Ru (II) polypyridyl complexes $[Ru(dppz\text{-}X_2)_3]^{2+}$ (**25, 26, 27, 28, 29**) with dppz ligand and different halogen (X = **H, F, Cl, Br, I**) (Fig. 24). In preparation of complex they used dppz ligand due to its DNA binding and photocleaving property. Lipophilicity is the important property of any complex and in such case lipophilicity varies with the variation of halogen groups. The complex **25** and its ligand dppz with no halogen group exhibited lowest Log*p* value. But, complex **26** with fluoride group increased the Log*p* value. The overall lipophilicity order of the complex with different halogen groups was H < F < Cl < Br < I. Authors also performed the cytotoxicity in dark condition against HeLa (human cervical cancer) and MRC5 (non-cancerous lungepithelial). The respective IC_{50} values have been given in Table 3. All the complexes exhibited moderate cytotoxicity against MRC5 cell with IC_{50} value of 23 to 43 μM where as in HeLa, all the complexes had IC_{50} value >100 μM in dark condition. In presence of light, they performed the same experiment against HeLa cell. Complexes **28** and **29** exhibited no phototoxicity in presence of light but **27** showed moderate toxicity (55 μM). The extra ordinary result was found in case of **25** and **26** which indicated highly phototoxic effect with IC_{50} value 2 μM

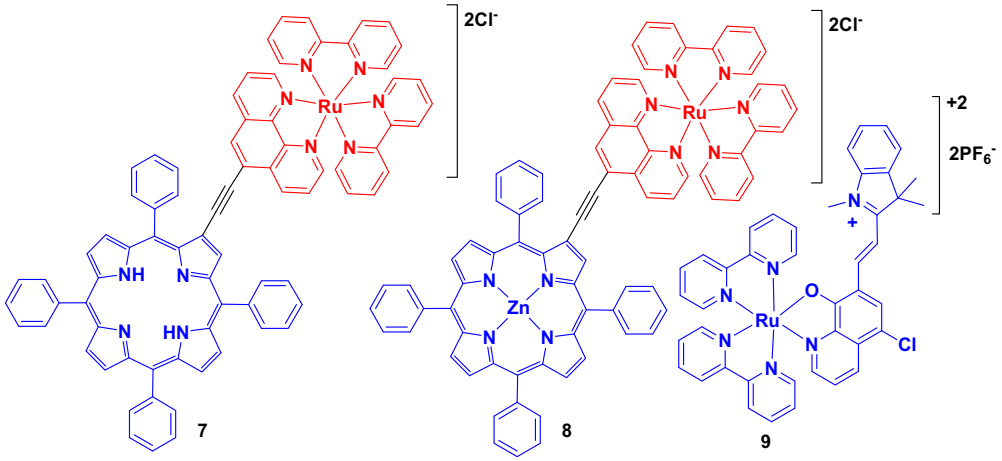

Fig. 18. Structures of porphyrin-based complexes **7, 8** and $[Ru(bpy)_2(Cl\text{-}7\text{-}IVQ)]^{2+}$ (**9**).

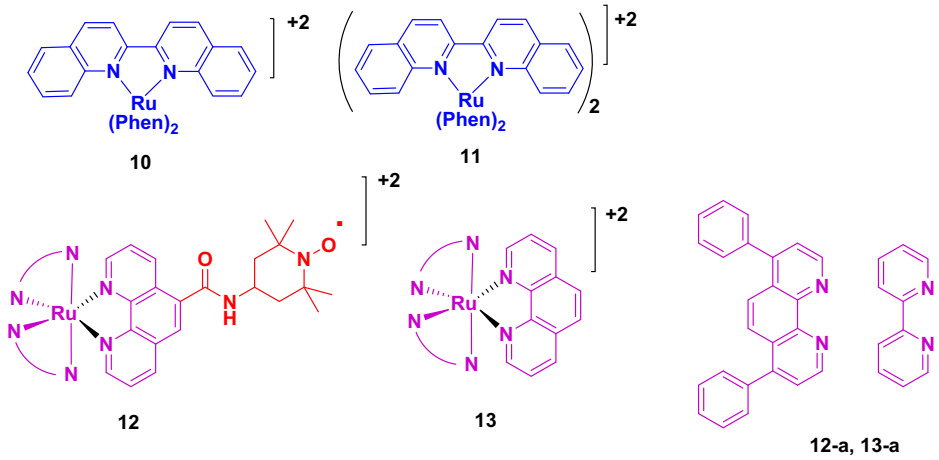

Fig. 19. Structures of complexes **10, 11, 12, 13** and **12-a, 13-a.**

Table 1
Photobiological activity towards HL-60 cells.

IC_{50}							Phototoxicity index	
Complex	λ_{abs}(nm) (ε (M^{-1} cm^{-1}))	Dark	Blue (3 min)	Red (3 min)	Red (6 min)	IR (25 min)	Blue	IR
10	525(8300)	52.5	1.2	13.8	7.6	15.8	43.8	3.32
11	550(4900)	47.3	2.4	4.5	2.3	5.1	19.7	9.2
Cisplatin		3.1	3.1	N.D.	N.D.	N.D.	1	

HL-60 = Human leukemia cell line.

and 5 μM respectively and they also calculated the phototoxic index (PI) for complexes **25** and **26** and the values were >47 and >18 respectively. The overall phototoxicity order of the complexes with different halogen groups was I < Br < Cl < F < H which was not same as that of the lipophilicity order. At the end, they could argue that increased lipophilicity had the positive contribution on PDT potentials but incorporation of a bulky halogen group affected the binding affinity with DNA modifying their activity [73].

Zhao *et al.* synthesized **Ru-tmxf** (Fig. 27) by incorporating tamoxifen ligand which exhibited effectual estrogen receptor-targeting ability to ER + breast cancer cells with Ru (II) polypyridyl moiety having two photon excited singlet oxygen generating property and acting as two-photon fluorescence probe for investigation of cellular uptake and localization. **Ru-tmxf** revealed augmented cellular uptake and PDT effect to estrogen receptor positive breast cancer cells (ER+). Authors investigated cytotoxicity of **Ru-tmxf** and **Ru-OMe** against MCF-7 cell by MTT assay in both light and dark condition. With increasing the concentration of **Ru-OMe** and **Ru-tmxf**, MCF-7 cell viability remained approximately 90 %, revealing their low cytotoxic effect in the dark (Fig. 25a, black and blue bar). But, irradiating the cancer cells cultured with Ru-tmxf for 2.5 h, on the other hand, drastically reduced the cell viability (Fig. 25a, green bar).The same environment was applied for **Ru-OMe** which caused only 17 % cell death (Fig. 25a, red bar). But, it displayed increased phototoxicity in comparison to **Ru-OMe**, **Ru-tmxf**. Authors also compared the phototoxicity against MCF-7 cells, MDA-MB-231 cells along with non-cancerous cells HL-7702 and COS-7 in presence of **Ru-tmxf** upon light irradiation. They found that MCF-7 cells emerged a significant red fluorescence upon PDT treatment which was attributed to PI, without giving

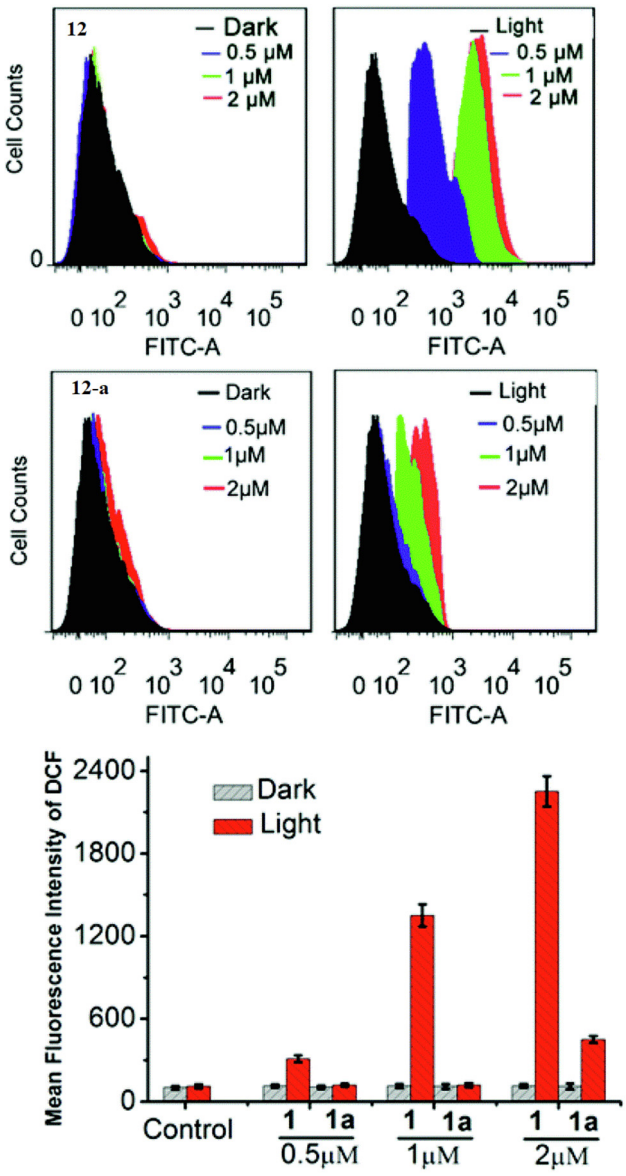

Fig. 20. Analysis of ROS levels with the help of flow cytometry after treating HeLa cells with **12** and **12-a** at the designated concentrations for 24 h and stained with H_2DCFDA [Adopted from **ref. 66** with permission from Royal Society of Chemistry].

away any green fluorescence (Fig. 25c). In case of MDA-MB-231 cells, non-cancerous HL-7702 and COS-7 cells very weak red fluorescent signals were observed. From this result, it was clearly understood that **Ru-tmxf** exhibited PDT effect on ER + cancer cells. By using different organelle specific trackers, they examined possible pattern of action and organelle colocalization. In MCF-7 cell lines the distribution of **Ru-tmxf** was found to be same as that of Lyso Tracker green. This result indicated that the complex localized in lysosomes. Under light irradiation or only treatment of **Ru-tmxf** towards MCF-7 cell, red fluorescence in lysosomes was visualised. The same effect was also observed when the cell was treated with **Ru-OMe** (control molecule) in dark or light irradiation. As a consequence, the undamaged portion was found in lysosomes of MCF-7 cell under this condition. But when the cells were treated with **Ru-tmxf** under light irradiations (12 J/cm^2), red fluorescence was seen to be vanished. The experimental evidences helped them to come to the conclusion that **Ru-tmxf** arbitrated PDT could damage lysosome (Fig. 26a). They further performed fluorescence microscopic imaging study with DCFH-DA (Fig. 26b) to ensure the production of singlet oxygen in MCF-7 cell after two photon irradiation. In live MCF-7 cells treated with **Ru-tmxf**, green fluorescence was also seen following TP irradiation. But, live MCF-7 cells showed only weak fluorescence either being exposed under light or being treated with **Ru-tmxf**, which suggested that **Ru-tmxf** could produce singlet oxygen successfully under TP irradiation. At the end author stained MCF-7 cells with calcein AM and propidium iodide (PI) (Fig. 26c) to confirm the cell death upon TP irradiation. The use of light alone or only **Ru-tmxf** green fluorescence was found indicating no cell death but application of PDT revealed slight green or obvious red fluorescence. As a whole, it was understood that **Ru-tmxf** used as a killer of ER+ breast cancer cells under TP irradiation [74].

Aldehyde functionalised long wavelength absorbing Ru (II) polypyridyl complex (**30**) as a photosensitizers was synthesized by Karges *et al.* They inspected the photophysical property of complex **30** by both experimentally as well as theoretically. They also combined benzylamine with aldehyde groups as a proof of its flexibility and as a synthetic precursor for conjugations (Fig. 28). The synthesized conjugate (**31**) exhibited high toxicity towards cervical cancer cells (HeLa) upon light irradiation (450, 480, 510 and 540 nm). Not only that, no dark cytotoxicity (IC_{50}>100 μM) was found on treatment of conjugate **31**. Upon light irradiation complex **31** demonstrated high phototoxicity in micro molar range with phototoxic index value >10.8 and >7.3 [510 nm (20 min,5.0 J/cm^2)] in HeLa and RPE-1 cell respectively [75].

Another two different types of Ru (II) polypyridyl complexes were synthesized by Karges *et al.* and Swavey *et al.* Karges group encapsulated Ru (II) polypyridyl complex with amphiphilic polymer DSPE-PEG_{2000}-folate and Sandya Rani-Beeram group introduced 5,10-(4-pyridyl)-15,20-(pentafluorophenyl) porphyrin with Ru (II) polypyridyl complex (**32, 33**) (Fig. 29). In aqueous solution the **32** exhibited better photophysical property than the complex itself. In dark condition the complex alone exhibited dark toxicity against the different cell lines where the nanoform was able to solve the problem. Upon light irradiation from 480 nm to 595 nm, the nanoform **32** exhibited cell death against 2D monolayer cells and 3D multicellular tumor spheroids through 3/7caspase pathway in low micromolar range. ICP-MS studied also revealed that the nanoform accumulated in the lysosomes and

Table 2
IC_{50} values and PI values of the complexes against different cell lines in dark and light conditions.

IC_{50} (μM)								
	HeLa		A549		A549R		LO2	
Complex	Dark (Light)	PI	Dark (Light)	PI	Dark (Light)	PI	Dark (Light)	PI
12	67.3 ± 1.5 (0.24 ± 0.09)	280.5	70.0 ± 0.2 (0.39 ± 0.07)	179.6	74.9 ± 1.4 (0.42 ± 0.06)	178.4	87.2 ± 0.9 (2.9 ± 0.6)	30.2
12-a	19.2 ± 0.4 (2.9 ± 0.2)	6.7	27.5 ± 0.3 (3.0 ± 0.2)	9.2	26.9 ± 0.9 (1.9 ± 0.7)	14.07	25.6 ± 2.3 (9.2 ± 0.4)	2.8
13	>100 (90.0 ± 1.6)	1.1	>100 (82.2 ± 1.3)	1.2	N.D. (N.D.)	–	>100 (>100)	1.0
13-a	>100 (>100)	1.1	>100 (86.0 ± 0.2)	1.2	N.D. (N.D.)	–	>100 (>100)	1.0

Irradiation with light at 450 nm for 5 min (7.5 J cm^{-2}).

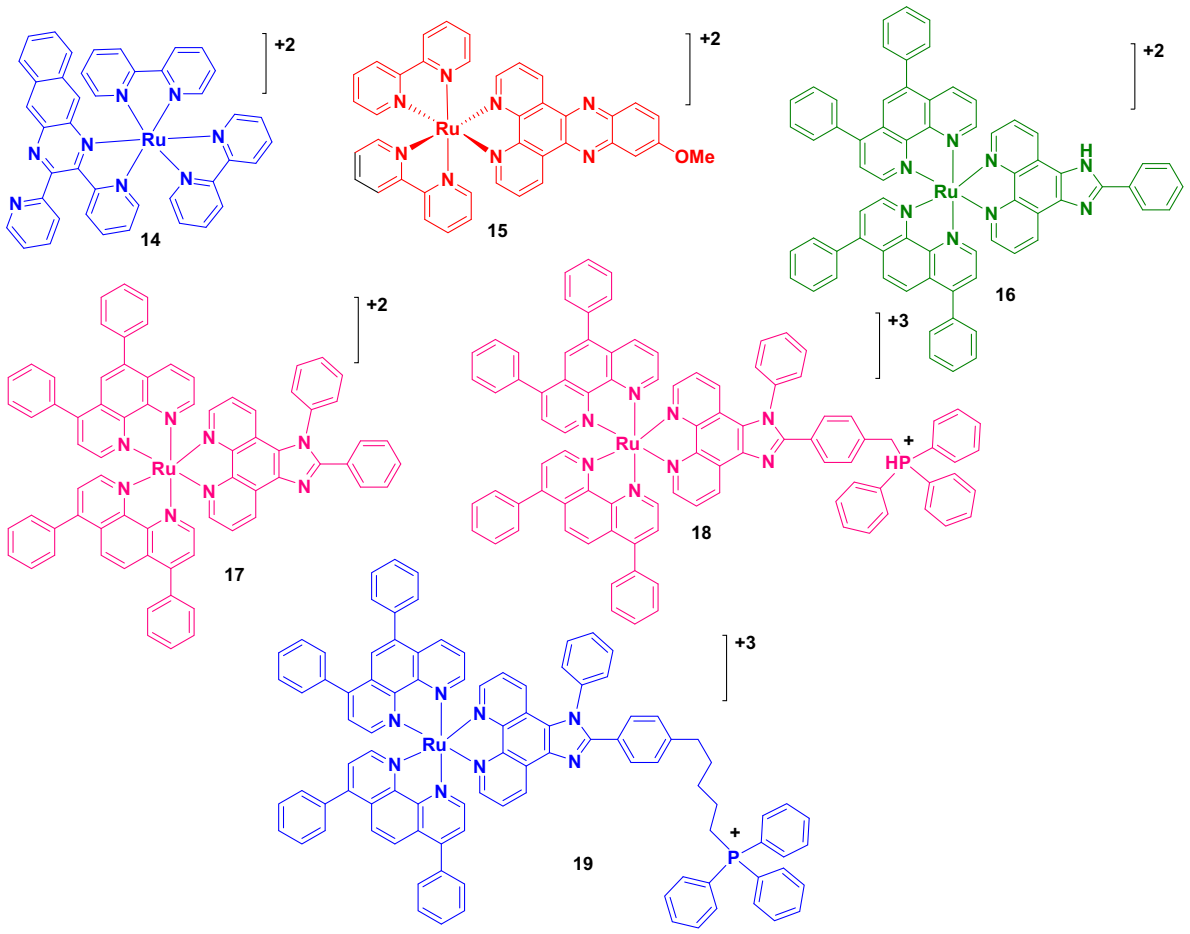

Fig. 21. Structure of complex- **14, 15, 16, 17, 18, 19.**

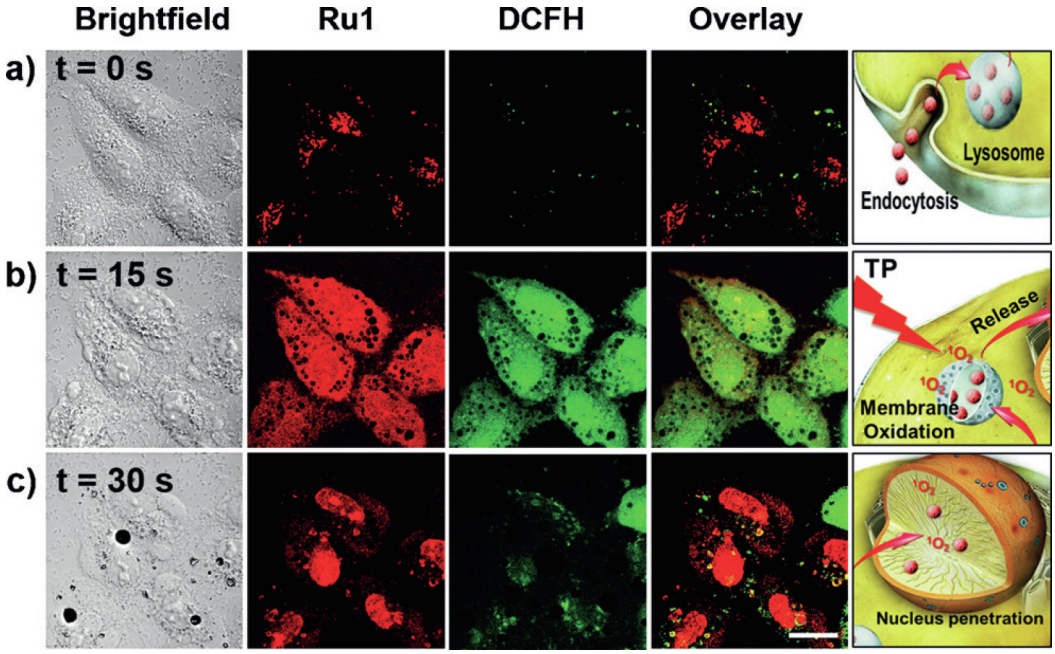

Fig. 22. a) One Photon and Two Photon luminescence images of **20** in a HeLa cell monolayer. b) One Photon and Two Photonluminescence images of **20** MCTSs. c) Colocalization images of **20** with MTG. d) Colocalizationimages of **20** with LTG. e) Colocalization images of **20** with 33342. Scale bar: 30 mm. [Adopted from **ref. 70** with permission from Wiley-VCH].

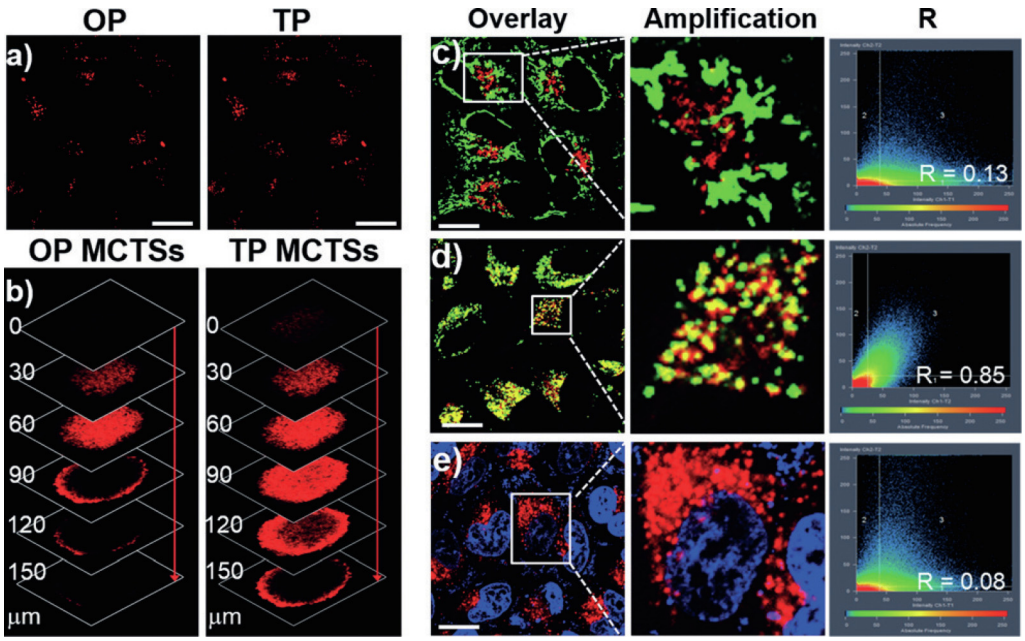

Fig. 23. Micrographs and ROS creation in HeLa cells incubated with **20** (2.0 mm) after irradiation with a two-photon confocal laser (800 nm) at different time, 0 s; 15 s; and 30 s. Scale bar: 15 mm. [Adopted from **ref. 70** with permission from Wiley-VCH].

exerted the cancer targeting effect [76]. In case of, complex **33** electronic absorption and electrochemical studies also revealed that there was an electronic connection between the orbitals of the peripheral ruthenium metal centers and the porphyrin orbitals. From the DNA binding study with complex **33**, Swavey group confirmed that there was an interaction between metal porphyirn complex and double-stranded DNA. They also performed the cellular toxicity study with both melanoma and normal cells and found that complex **33** exhibited low dark toxicity towards both types of cells. But the combination of visible light and **33**, melanoma cell was much affected than the normal cell. This suggested that complex **33** mainly affected the melanoma cells [77]. The use of Ru-polypyridyl complexes in cancer treatment, Goldbach *et al.* introduced a very interesting strategy. Like platinum based anticancer drugs, the thermal decomposition of Ru-Cl bonds were found to be occurred in some complexes followed by coordination with DNA or protein. But the problem was thermal decomposition of Ru-Cl bond might be occurred in aqueous medium anywhere in human body and that's why both antitumor activity and general toxicity were found to take place simultaneously. Hence, poor selectivity was detected towards cancer cells in presence of Ru-Cl bond. Due to this reason, they focused on some protective groups that provided more strong binding property than chloride and also cleaved in a controlled way *in vivo*. In this regard they used thioether ligands because- (1) Ruthenium (II) tends to bind with soft sulfur atom, (2) thioether are slightly basic in water that makes the Ru complex less sensitive with pH change. Finally in presence of visible light irradiation, controlled release of thioether ligands were found. They selected two types of thioether ligand, first one was *N*-acetyl-L-methionine and the second was D-biotin and finally they synthesized two complexes like [Ru(terpy)(bpy)(*N*-acetyl-L-methionine)] Cl_2 and [Ru(terpy)(bpy) (D-biotin)] Cl_2 (**34, 35**). In dark condition the coordination bond between the rutheniumpolypyridyl moiety and thioether ligand was found to be thermally most stable. This protected complex then was used as a prodrug and it was activated by visible light irradiation (Fig. 30) [78].

In previous section, we have already discussed with the **Ru-tmxf** complex as a lysosome targeting agent. Here we have also intended to mention some other Ru-based lysosome targeting complexes. Liu *et al.* synthesized three heteroleptic bis-terpyridine ruthenium (II) complexes with general formula, $[Ru(tpy\text{-}R_1)\ (tpy\text{-}R_2)]^{+2}$ [Where, tpy = 2,2′:6′,2″-terpyridine, R1/R2 = phenyl,4-{2-[2-(2-Methoxyethoxy)ethoxy]ethoxy}phenyl, pyren-1-yl, or4-phenyl-BODIPY(boron dipyrromethene)] as photosensitizers for photodynamic therapy in cancer (**36, 37,38**). They investigated the phototoxicity against human lung cancer cell line (A549) and the CCK-8 cell viability test kit. Both the complexes **37** and **38** exhibited very low dark cytotoxicity but without light irradiation complex **37** was slightly less toxic than complex **38**. In presence of 500 nm light irradiation the toxicity of both the complexes increased. Complex **37** displayed more phototoxicity with EC_{50} value of 1.50 μM (PI- 35.3) whereas the complex **38** with EC_{50} value of 7.41 μM (PI- 4.90). This result suggested that in 500 nm light irradiation complex **37** acted as a better PS and encouraged the cell death more significantly than complex **38** towards A549 cells. To determine the intracellular PDT mechanisms of the complexes, the localization of complex **37** and complex **38** was studied in different organelles by confocal laser scanning microscopy (CLSM). A549 cells were marked with complexes **37** and **38** and examined with different cellular organelle trackers including Hoechst 33,342 (nuclear blue tracker), Lyso-Tracker Red, ER-Tracker Red (endoplasmic reticulum red tracker) and MitoRed (Mitochondria tracker red). With the help of confocal microscopy, they found well overlapped of green emission from complex **37** with red fluorescence from Lysotracker Red (Fig. 31) but no more result was noticed from other trackers. From this result they concluded that complex **37** mainly localized in lysosomes. For the complex **38** no better result was found in that test. With the help of flow cytometric analysis, authors also confirmed photoinduced lysosomal damage upon treatment of the complex **37** (5, 10, 20, and 40 μM). As a result, they stained A549 cell with complex **37** and incubated for 4 h followed by irradiation in presence of 500 nm light. They also employed Lyso-Tracker Red for detection of lysosomal damage. Lyso-Tracker Red fluorescence intensity was correlated with the integrity of the lysosomal membrane which revealed that stronger the lysosomal damage, the lower the Lyso-Tracker Red fluorescence intensity. It was apparent

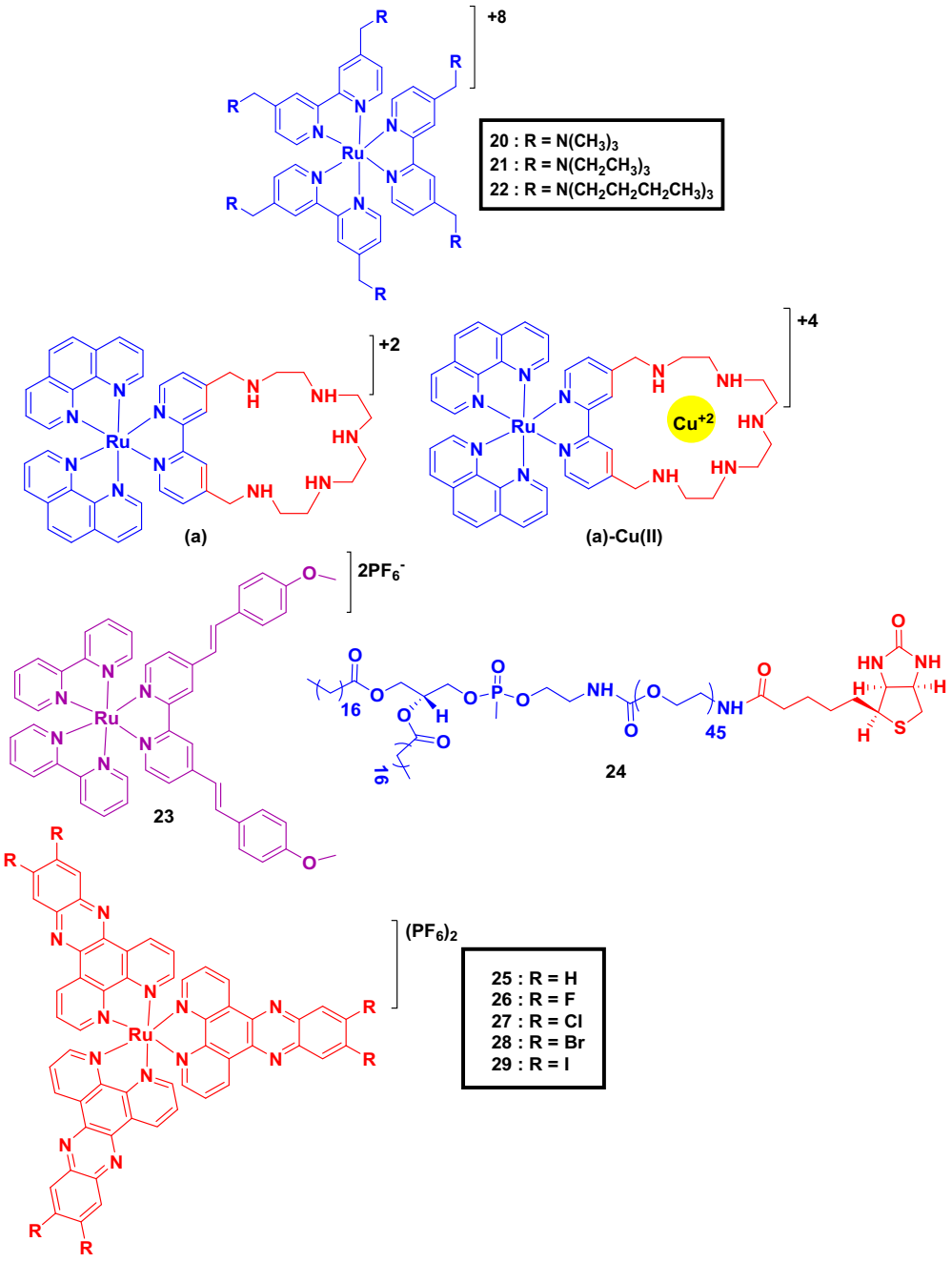

Fig. 24. Structures of complexes from **20** to **29.**

Table 3
IC_{50} values of complexes from 25 to 29 against MRC5 (human non-cancerous lung) and HeLa (human cervical cancer) in dark and in presence of light irradiation.

Complex	IC_{50} value (μM)			
	MRC5 (dark)	HeLa (dark)	HeLa (420 nm)	PI (IC_{50} dark/ IC_{50} light) HeLa
25	42.28 ± 9.6	>100	2.12 ± 0.11	>47
26	41.05 ± 4.4	>100	5.45 ± 0.35	>18
27	34.30 ± 2.5	>100	55.40 ± 8.4	>1.8
28	23 ± 8.9	>100	98.01 ± 1.9	>1.0
29	43.01 ± 6.1	>100	>100	n.d.
Cisplatin	16.8 ± 1.8	4.10 ± 0.20	n.d.	n.d.

Light dose 9.27 $J.cm^{-1}$.

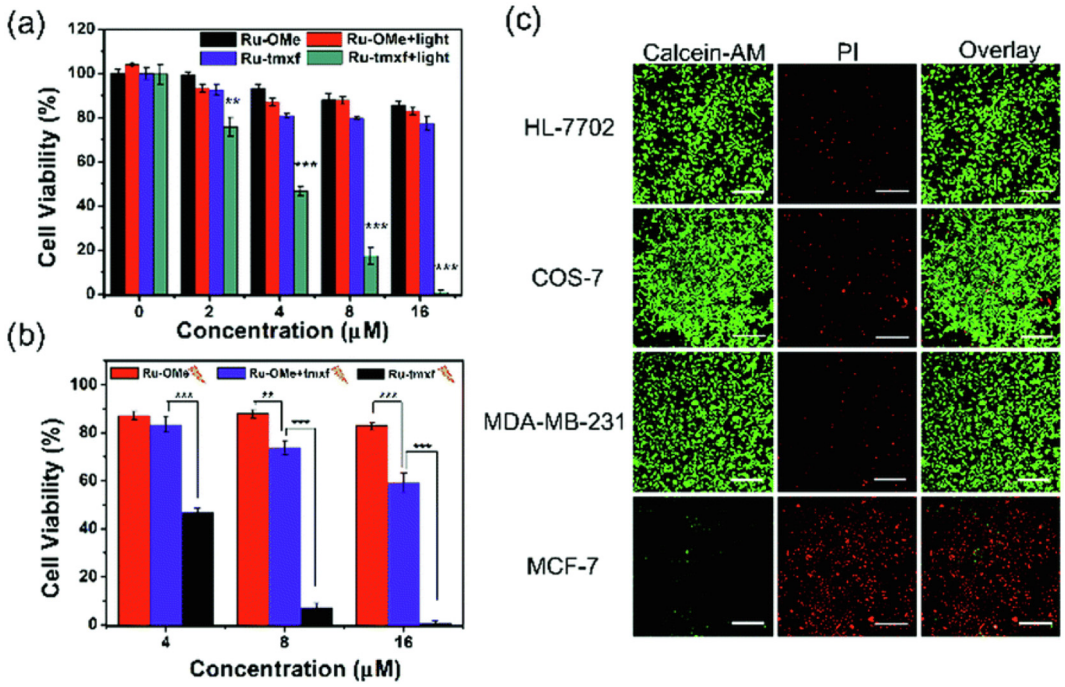

Fig. 25. a) Dose-dependent cytotoxicity of **Ru-OMe** and **Ru-tmxf** towards MCF-7 cells under dark or light conditions (12 J/cm^2); (b) Cytotoxicity of **Ru-OMe**, **Ru-OMe** plustamoxifen (concentration ratio is 1:1) and **Ru-tmxf** to MCF-7 cells in presence of light conditions (12 J/cm^2); (c) Confocal luminescence imaging of calcein-AM and PI labelled HL-7702, COS-7, MDA-MB-231 and MCF-7 cells after PDT treatment. λ_{ex}: 488 nm, λ_{em}: 505–545 nm (calcein-AM); 620–700 nm (PI). Scale bars: 280 μm. [Adopted from **ref. 74** with permission from Royal Society of Chemistry].

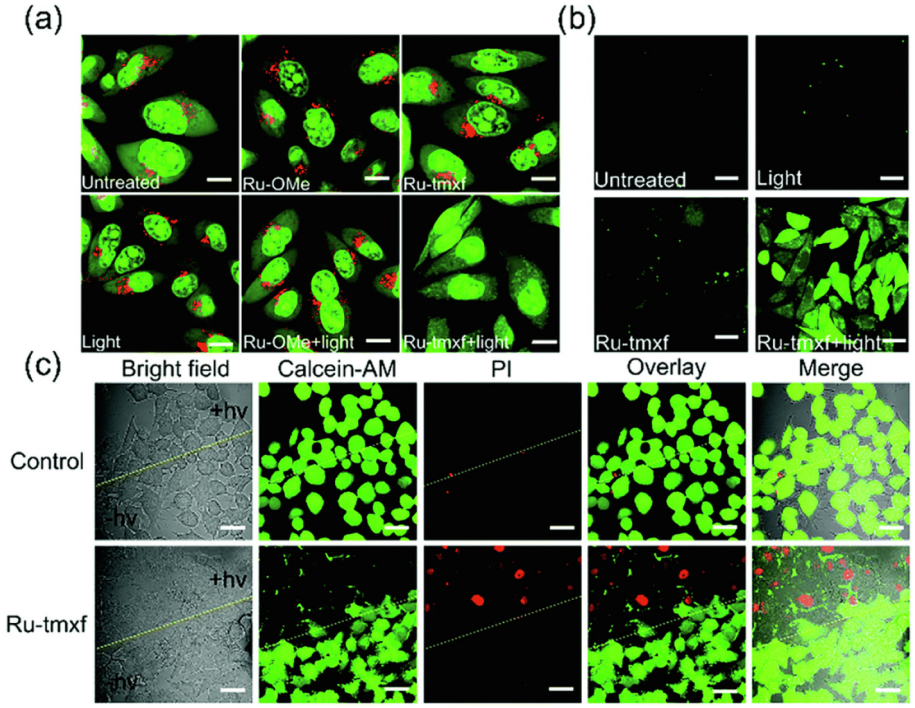

Fig. 26. (a) Confocal luminescence imaging of acridine orange (AO) stained MCF-7 cells after different treatments. (λ_{ex}: 488 nm); λ_{em}: 515–545 nm (greenchannel) and 620–640 nm (red channel). Scale bars: 10 μm; (b) Luminescence images of intracellular $^1O_2$ production by **Ru-tmxf** under TP irradiation. (λ_{ex}: 488 nm); λ_{em}: 480–520 nm (DCF). Scale bars: 30 μm; (c) Cell viabilityassay for MCF-7 cells incubated with **Ru-tmxf** in both absence and presence of TP irradiation by calcein-AM/PI. (λ_{ex}: 488 nm), λ_{em}: 505–545 nm (calcein-AM); 620–700 nm (PI). Scale bars: 30 μm. [Adopted from **ref. 74** with permission from Royal Society of Chemistry].

that 20 μM or 40 μM concentration of complex **37** caused lysosomal damage (Fig. 32) [79] (See Table 4).

Another lysosome targeting polypyridyl ruthenium complex **Rhein-Ru(bpy)$_3$** was synthesized by Chen *et al.* (Where, bpy = 2, 2′-bipyridine, rhein = 4,5-dihydroxy-9,10-dioxoanthracene-2-carboxylic acid) (**39**). They investigated the ROS production of complex **39** in presence of light irradiation with the help of flowcytometry using DCFH-DA as fluorescence probe for ROS detector. The

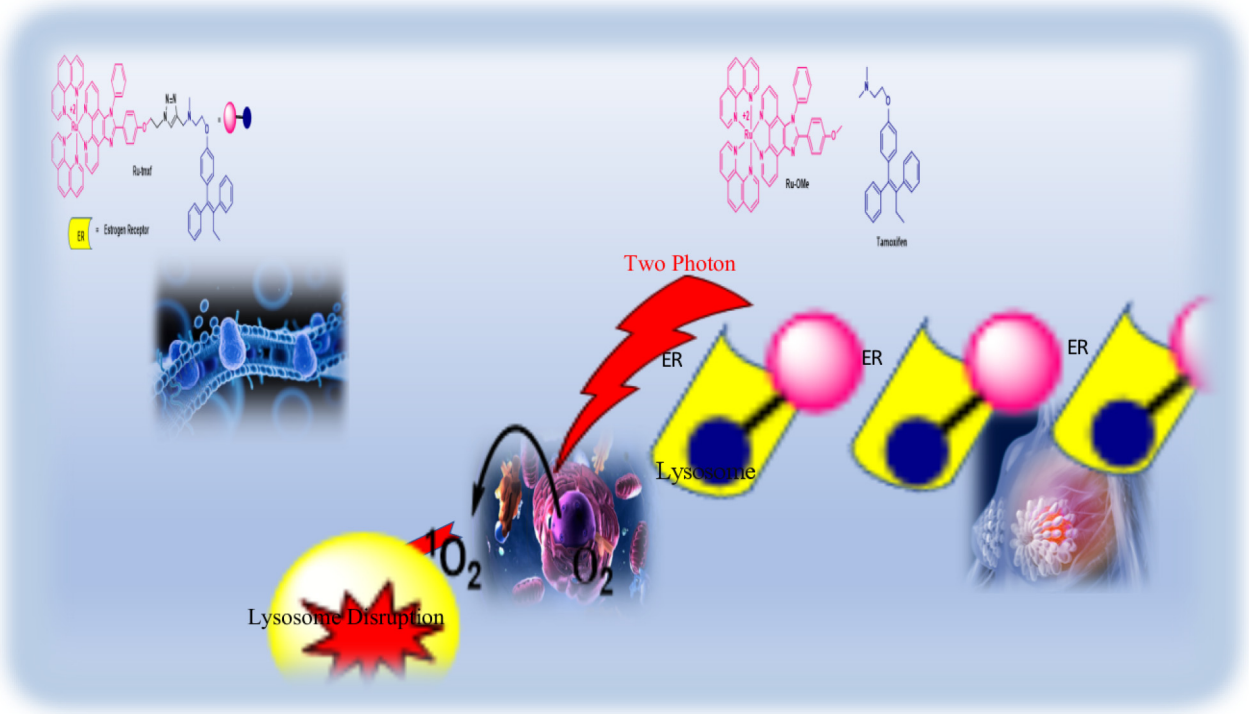

Fig. 27. Lysosome targeted **Ru-tmxf**complex.

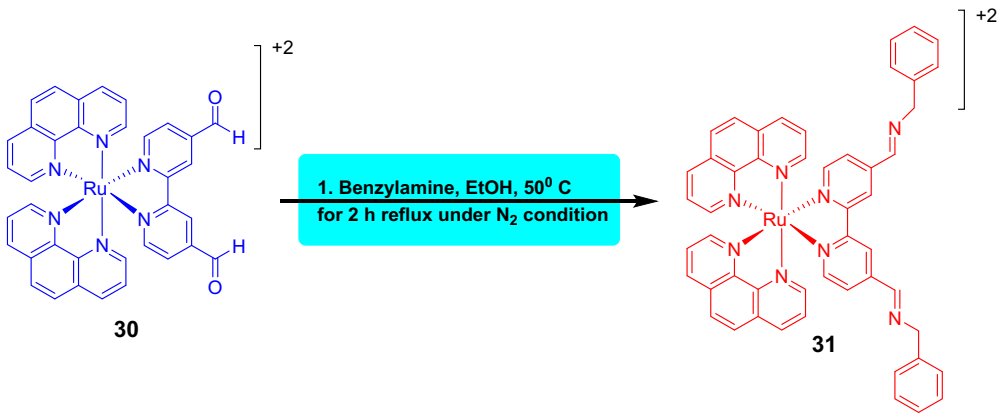

Fig. 28. Ru (II) polypyridyl complex-**30** and synthesis process of conjugate complex-**31.**

fluorescence intensity was found to be very weak (Fig. 33a) in dark as well as with increasing the concentration of complex **39**. But increase in fluorescence intensity (Fig. 33b, c) was observed after 15 min of light irradiation with 0–20 μM of complex **39** concentrations. This result indicated complex **39** produced profuse ROS in cancer cell in presence of light irradiation. They performed the cytotoxicity study against different cells like MCF-7, A549, NB-4, A2780, cisplatinresistant A2780 cells (A2780R) and human normal liver cells (LO2). In dark condition, incubation of complex **39** exhibited poor cytotoxicity against A2780R, A549, MCF-7 and LO2 cells with IC_{50} values of ~ 91.3, ~64.7, ~250.6 and ~ 35.1 μM respectively. But in presence of light irradiation the complex exhibited IC_{50} values ~ 3.2, ~2.4, ~7.6 and ~ 8.7 μM respectively against the concerned cell lines. In case of A2780R cell line, the complex exhibited high efficiency than the cisplatin with PI value of ~ 28.5. From the result they affirmed that this complex overcame the A2780R (cisplatinresistance) cells. Authors also examined cellular localization in A549 cell by CLSM. From this they observed the signal from complex **39** overlapped with the commercial lysosome dye LTG (Fig. 34). So, they came in conclusion that the complex **39** mainly accumulated in lysosomes [80] (See Fig. 35 and 36).

Mitochondria is the essential organelle in cell. Actually, it is the "powerhouse of cell". Therefore, if a drug can cause mitochondrial damage of cancer cells, it can be particularly administered for successful drug in cancer therapy. Zhang *et al.* synthesized Chlorambucil Conjugated Ruthenium (II) Complex and found its accumulation in mitochondria of HeLa cell. Chlorambucil (CHL) is a DNA alkylating agent. But, some serious issues like drug instability, "off-target" binding and in-situ monitoring have limited its further clinical applicability. In this context, they developed **CHL-RuL** (**41**), a novel heteroleptic Ru (II) complex with a **CHL** conjugated pendant that can be used as an image-guided chemo-photodynamic combined theranostic agent. Because of their

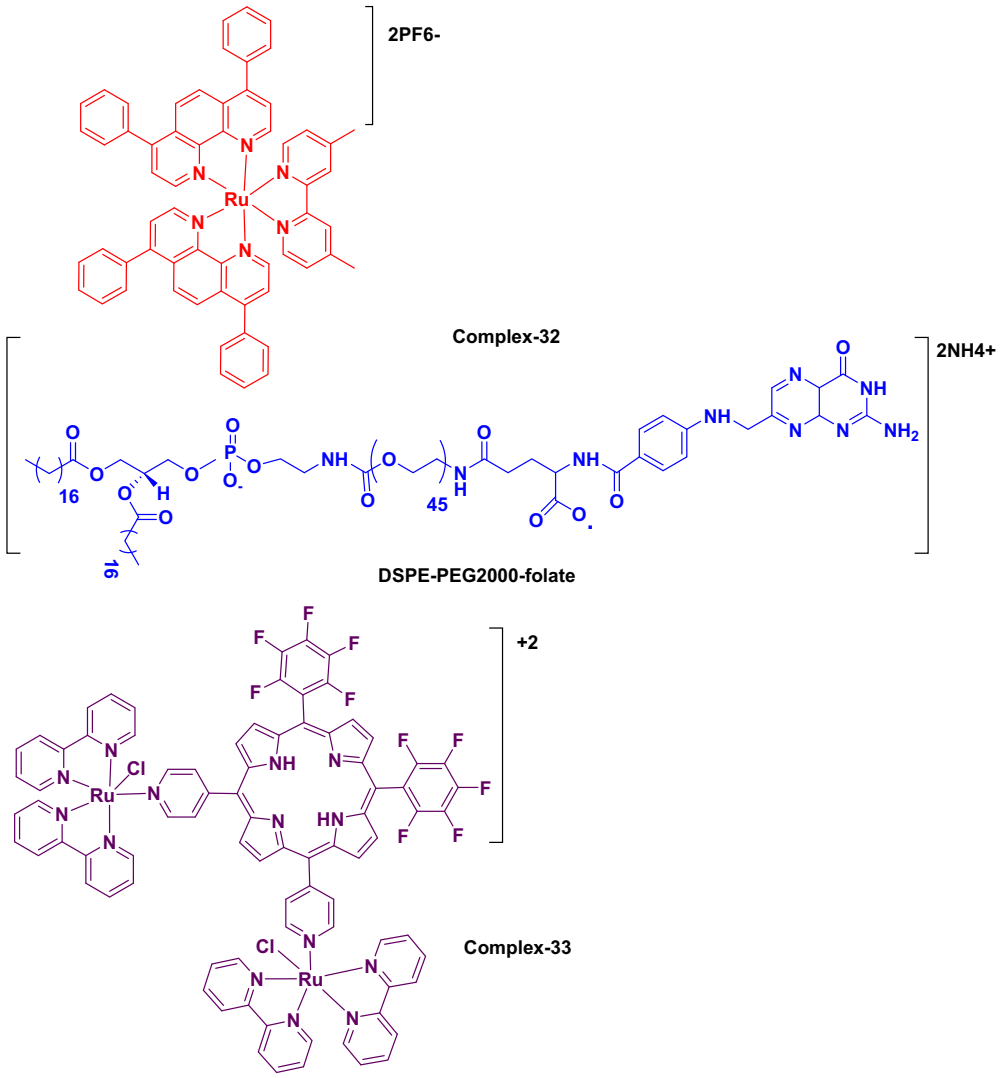

Fig. 29. Structures of complexes **32** and **33.**

favourable water solubility, synthetic tailorability, biological compatibility, long emission lifetime derived from the triplet metal-to-ligand charge-transfer (^{3}MLCT) excited-state and efficient two photon absorption properties, Ru(II)-polypyridyl compounds showed excellent advantages as photosensitizers for TPE-PDT [81–85]. The coumarin functional group is known to be an efficient light-harvesting functional group and the coupling of Ru (II) complexes with coumarin donors can result in an increased visible light-harvesting array which can help to improve optical characteristics. Therefore, complex**40** and **CHL-RuL** (**41**) displayed strong UV–vis absorption bands near about 400 nm as well as strong red emission with long MLCT triplet state lifetimes (1.41 s for **40**, 1.34 s for **41**), moderate singlet oxygen quantum yields in aqueous solution (0.38 for **40**, 0.40 for **41**) and significant two photon absorption (TPA) cross sections (123 GM for **40**, 118 GM for **41**). This is enough for TPE-PDT. To investigate ROS generation ability, authors used flow cytometry assay with DCF-DA. After 2 min of irradiation with visible light, 10 μM of complex **40** treated cells exhibited comparable fluorescence intensity of DCF to 50 μM TBHP-treated cells. But in the same condition complex **41** (10 μM) exhibited 2-fold increased fluorescence intensity (Fig. 37). Therefore, intracellular singlet oxygen generation property was found in complex **41**. HeLa cells were co-stained with **CHL-RuL** (**41**) and 50 μM of commercial organelle-specific trackers for 6 h in order to validate CHL-RuL's subcellular localization (mitochondria and lysosome probes). They found the nice overlapped between the red phosphorescence of **CHL-RuL** (**41**) and the green emission of mitochondria probe (Fig. 38). This result revealed that the **41** localized in mitochondria nicely [86] (See Table 5).

The Golgi apparatus is a phospholipidmembrane-based organelle that acts as a processing centre for proteins, lipids and other big molecules before they are exported to their final destinations outside the cell. Zhao *et al.* synthesized Golgi-apparatus-targeting complex **42** with Ru (II) pyridine succinimidyl ester complex and sphingosine lipid. It unveiled low toxicity, greater targeted selectivity, permitted bright steady imaging even at low doses and was used to treat cancer cells with its vicious photodynamic activity. A confocal fluorescence imaging investigation was carried out to assess the cellular uptake of complex **42**. The target cells in this study were HeLa cells. In this cell line, a visible red fluorescence signal localised in the Golgi apparatus was perceived, which was highly in agreement with the GolgiTracker Green (NBD C_6- ceramide) signal with a similar fluorescence intensity showing that the complex **42** was successfully internalised. HeLa cells were treated with the complex **42** at 4 °C in dark for 2 h in order to further investigate the potential mechanism of cellular uptake of the com-

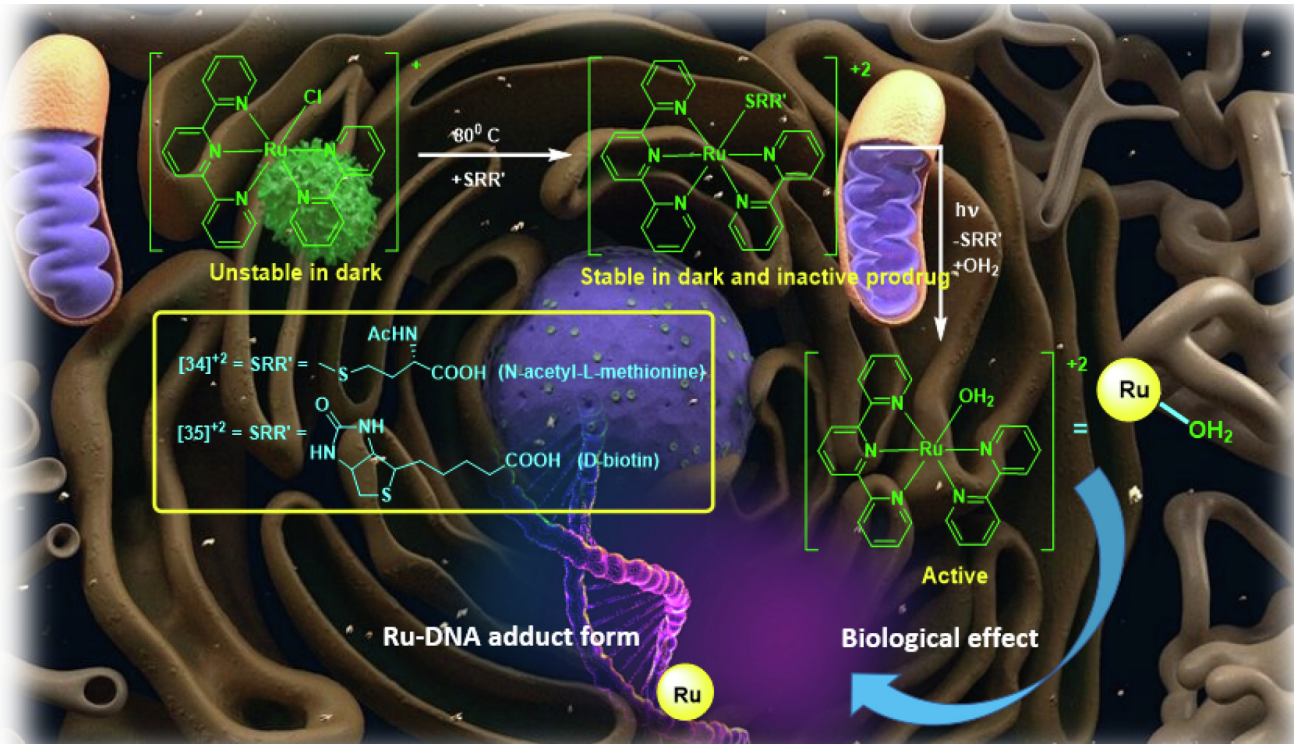

Fig. 30. Structure of complexes **34, 35** and protection-deprotection process by light and adduct form with DNA.

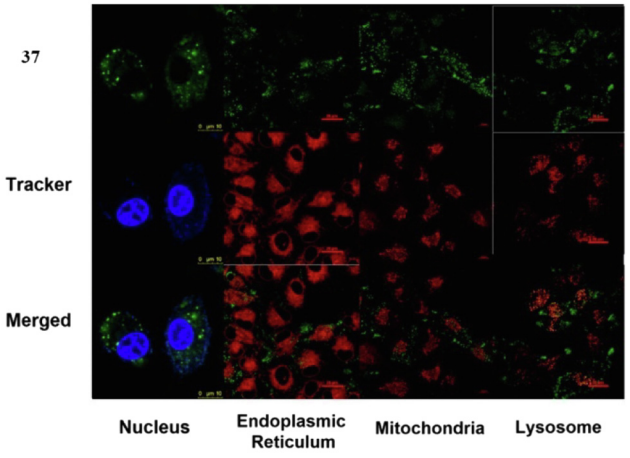

Fig. 31. Fluorescence imaging of live A549 cells stained with complex **37** and different organelles targeting fluorescent dyes. In the cytoplasm complex **37** was detected as bright green.

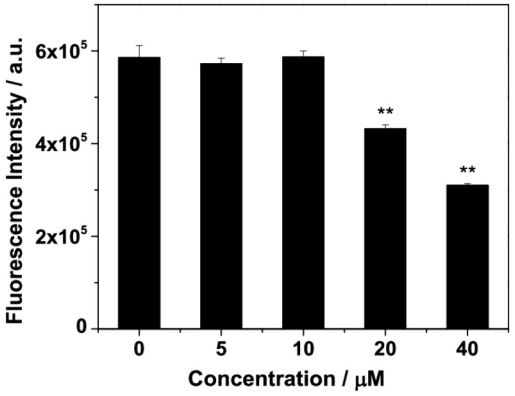

Fig. 32. The flow cytometry plot of lysosomal damage detection. [Adopted from ref. 79 with permission from American Chemical Society].

plex **42**. At lower temperature (4 °C), there was almost little red fluorescence signal inside the cells indicating the internalisation of the complex **42** was blocked. This data revealed that the complex **42** was uptaken via temperature dependent endocytosis mechanism. They used photodynamic treatment to notify whether it had a greater therapeutic effect when it came to destroying HeLa cells or not. MTT assay was employed to assess the cytotoxicity of the complex **42**. To investigate the potential phototoxicity caused by the complex **42**, HeLa cells were cultured with it and then subjected to 488 nm irradiation for varying lengths of time (3, 5, 10, 30, and 60 min). The IC_{50} value of the **42** was > 100 μM before irradiation and it was much lower only after 3 min of irradiation (IC_{50} = 87.48 ± 1.22 μM). After irradiation for 5, 10 and 30 min, the IC_{50} values were observed to be 65.59 ± 3.36, 42.73 ± 3.09, and 22.24 ± 2.35 μM respectively. But more effective cytotoxicity was achieved after 60 min of irradiation and the IC_{50} value was lowered to 3.45 ± 0.54 μM. They eventually came to the conclusion that singlet oxygen was highly cytotoxic and caused DNA damage and the loss of the Golgi apparatus. Therefore, light irradiation could boost cell lethality by stimulating the complex **42** to create $^1O_2$. The loss of the Golgi apparatus was followed by DNA damage as a result of apoptosis or other cell-death-inducing mechanisms, ultimately resulted in cell death [87]. TNBCs are breast tumors that do not express the estrogen receptor (ER), progesterone receptor (PR), and human epidermal growth factor receptor-2 (HER2). TNBC treatment is difficult since the three missing receptors are established therapeutic targets for other breast cancer subtypes, yet there are no specific medicines for TNBCs [88]. Bioorthogonal labeling is a new technology for selectively labelling biomolecules in living cells. The copper-catalyzed azide–alkyne cycloaddition (**CuAAC**) reaction is often used in this direction. This is due to its

Table 4
Summarized the ruthenium-based complexes with their PI value against the particular cell lines with the localization of targeted organelles.

Complex	Cell lines	Localized and targeted organelles	PI	Dose	References
1, 2,3	HeLa	Lysosomes, Mitochondria, Cytoplasm	–	–	[62]
10	HL-60	–	43.8 (red), 3.32 (near IR)	[(λabs(nm) (ε (M^{-1} cm^{-1}) 525(8300)]	[65]
11	HL-60	–	19.7 (red), 9.2 (near IR)	[(λ_{abs}(nm) (ε (M^{-1} cm^{-1}) 550(4900)]	[65]
12/12-a	HeLa, LO2	Cytoplasm	6.7, 2.8	450 nm for 5 min (7.5 J $cm^{-2)}$	[66]
20	HeLa	Lysosomes	313	450 nm, 10 Jcm^{-2}	[70]
25, 26	HeLa	–	>47, >18	9.27 $J.cm^{-1}$	[73]
Ru-tmxf	MCF-7, MDA-MB-231	Lysosomes	–	–	[74]
31	HeLa, RPE-1,	–	>10.8, >7.3	510 nm (20 min,5.0 J/cm^2)	[75]
37	A549	Lysosomes	35.3	0.48 J cm^{-2}	[79]
39	A2780, A2780R, A549, MCF-7, LO2	Lysosomes	9.5, 28.5, 26.9, 20.9, 4.0	450 nm light for 15 min, 3.5 mW cm^{-2}	[80]
49–54	MRC-5, HeLa	–	>150, 42, ND, >5, ND, >5	2.58 J cm^{-2}, and 9.27 J cm^{-2}	[97]
[D-57]$^{+2}$	A549, MCF-7	–	26, 11	5 min at 450 nm with (3.2 ± 0.2) J cm^{-2})	[99]
[L-57]$^{+2}$	A549, MCF-7	–	86, 30	5 min at 450 nm with (3.2 ± 0.2) J cm^{-2})	[99]
60	Bel-7402	Cytoplasm	106	450 nm (10 J cm^{-2})	[100]
64	–	Mitochondria	250	470 nm	[105]
79c	A2780cis	–	206	48 Jcm^{-2}	[114]
85-CDs	A549, LO2	–	20, 6.2	450 nm	[119]

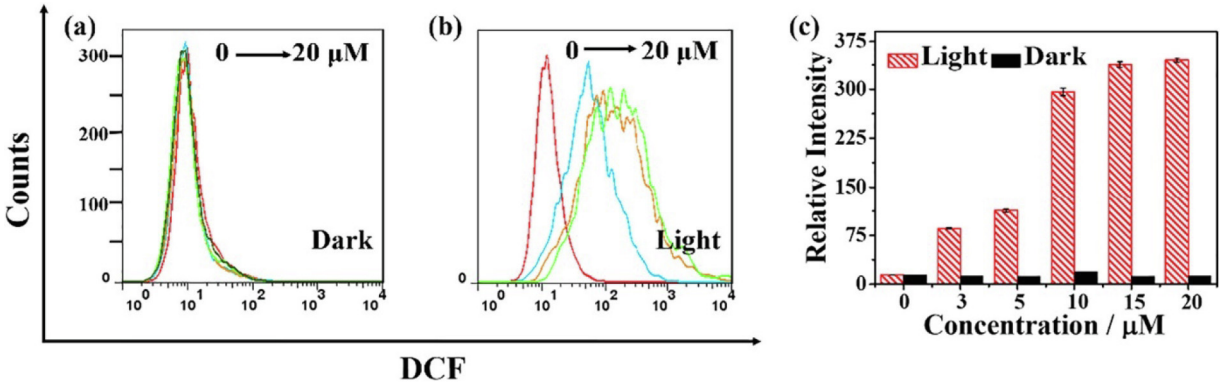

Fig. 33. (a) Cellular ROS detection with the help of DCFH-DAby flow cytometry, incubated with complex **39** for 4 h in the dark. (b) light irradiation for 15 min (c) In dark and light condition relative fluorescence intensity of DCF in A549 cells when treated with complex **39** at different concentrations (0 ∼ 20 μM). In the histogram the level of ROS induction in A549 cancer cells treated with complex **39.** [Adopted from **ref. 80** with permission from Elsevier].

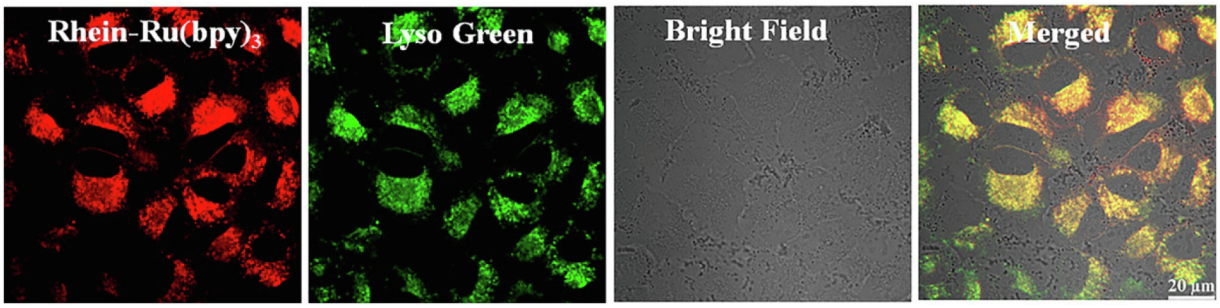

Fig. 34. Confocal images indicated intracellular fluorescence in A549 cells exposed to complex **39** for 24 h, and localized with LysoTracker Green. [Adopted from **ref. 80** with permission from Elsevier].

fast kinetics and the presence of reactive groups such as terminal alkynes or azides that cause minimal disruption. **CuAAC** focuses on the differences in highly expressed proteins between tumour and normal cells, making it simple to identify tumour cells. One of the most common metabolic precursors is *N*-Azidoacetylmanno samine-tetraacylated (**Ac_4Man-NAz**), an azide-modified sugar. Azide groups can be precisely inserted into the plasma membrane of tumour cells via incubation. Photosensitizers with **CuAAC** reaction exhibited efficient tumor selectivity [89–94]. Keeping these in mind, Lin *et al.* synthesized two Ru (II) complexes having analkyne group (**43, 44**). They achieved successful tumor-specific photodynamic treatment against triple-negative breast cancer using bioorthogonal labelling. Both complex (**43** and **44**) was performed the orthogonal reactions with azide but the second-order rate of complex **43** was calculated to be 27.3 ± 3.7 $M^{-1}s^{-1}$ at varied concentrations of **Ac_4Man-NAz**, while that of complex **44** was 37.1 ± 2.1 $M^{-1}s^{-1}$. These values were within the range of **CuAAC** reaction rates that had been recorded. As a result, complex **44** can be chosen

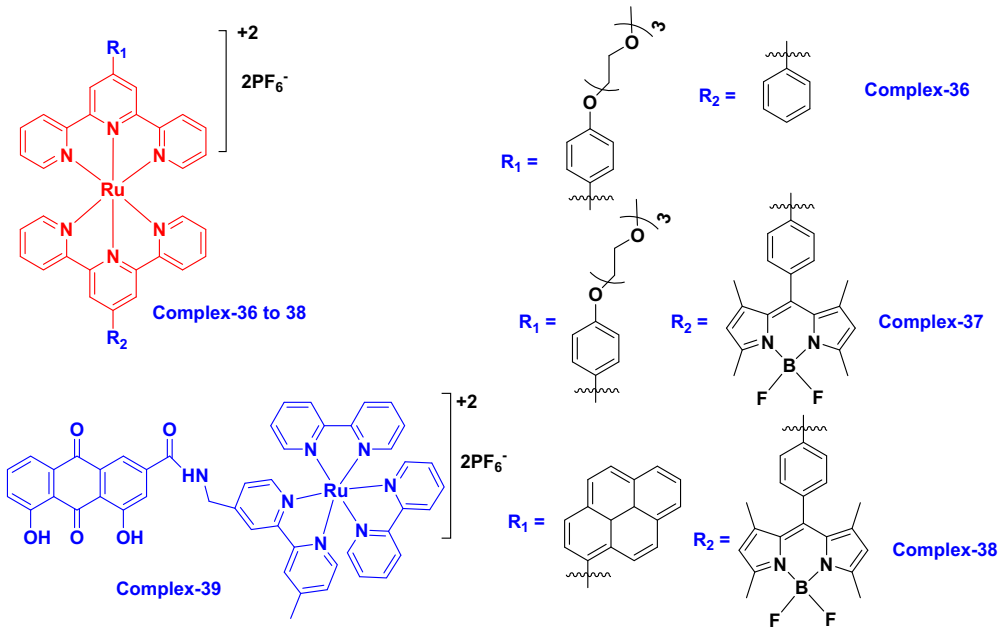

Fig. 35. Structure of lysosome targeting complexes from **36 to 39**.

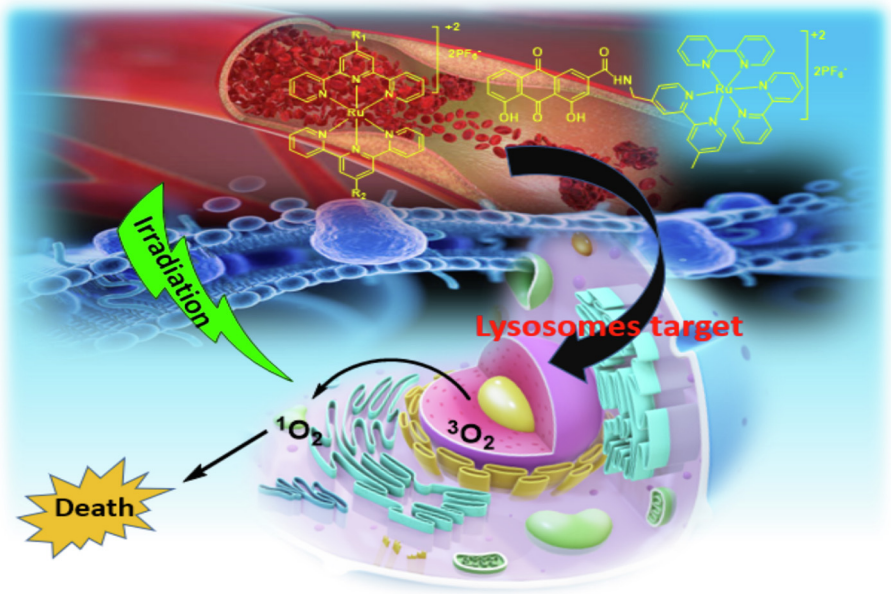

Fig. 36. Simple pictorial representation of lysosome targeted complexes **36**–**39**.

for future study. Therefore, two photon absorption property was investigated with the complex **44**. With a $^1O_2$ quantum yield of 0.80, complex **44** demonstrated exceptional $^1O_2$ generating efficiency. They used the MDA-MB-231, TNBC cell line to confirm the *in vitro* bioorthogonal labelling of complex **44**. To deliver azide-based artificial receptors to the plasma membrane, MDA-MB-231 cells were pre-incubated for 3 days in a medium containing 50 μm **MAc$_4$Man-NAz**.The cells were then incubated in a phosphate buffer containing complex **44**, 25 μM CuSO4, 125 μM THPTA and 2.5 mM sodium ascorbate for another 1 h after the culture media was removed. Complex-**44** bioorthogonally interacted with the azide-based artificial receptors at the membrane, as evidenced by a visible red emission around the cells. After established bioorthogonal labelling capabilities to the MDA-MB-231 cell line's plasma membrane, they investigated phototoxicity following the MTT assay protocol. Complex-**44** had low cytotoxicity towards MDA-MB-231 cells in the dark with or without bioorthogonal labelling (Fig. 39a, b). They discovered that with raising the Ru(II) complex concentration, cell survival was lowered when exposed to a mild light dosage of two-photon irradiation. Moderate photocytotoxicity was found in the absence of bioorthogonal labelling. They observed the bioorthogonal labelling group's cell viability which was<25 % under the same treatment with IC_{50} value of 10. 6 ± 0.87 μM and PI >18.9. But the complex exhibited no significant toxicity towards non-canceroushuman cell line MCF-10A under the same condition. Following **Ac$_4$Man-NAz** pretreatment and irradiation, a considerable number of red dots were observed, which came about as a result of EthD-1 suggesting cell death, as

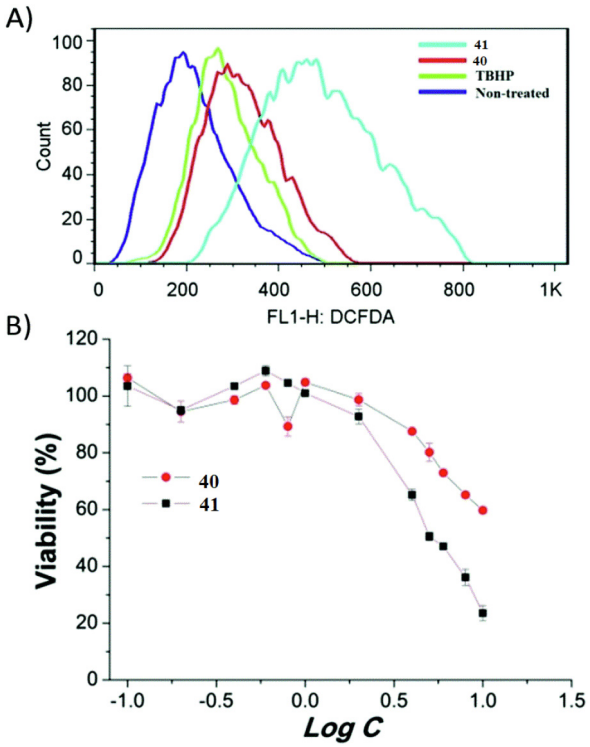

Fig. 37. (a) Flow cytometry assay for visible light-induced ROS generation levels of **40** and **41** in living cells by DCF-DA (b) Viability of HeLa cells under light irradiation, treatment with different concentrations of **40** and **41.** [Adopted from **ref. 86** with permission from Royal Society of Chemistry].

illustrated in (Fig. 39c).The photocytotoxicity was confirmed when the green fluorescence of calcein-AM as a living cell indicator was scarcely visible. **Ac_4Man-NAz**-pretreatment without irradiation, on the other hand, resulted in a strong green fluorescence followed by the removal of red fluorescence. Only green fluorescence could be seen with or without light, when no **Ac_4Man-NAz**-pretreatment was used. The ROS production experiment utilizing (DCFH-DA) as the indicator supported this conclusion. Authors observed only metabolic labelling of **Ac_4Man-NAz** and two-photon irradiation resulted in bright green emission. At the end they came to conclusion that in order to make the photosensitizer tumour selective, bioorthogonal labelling was highly effective [95] (See Figs. 40 and 41).

Chen *et al.* justified the complex **45** on the basis of emission enhancement behavior and photocleavage activity in comparison to complexes **46, 47 and 48**. They found that complex **45** showed fluorescence from singlet excited state of dppn-based ligand-centered and also it produced singlet oxygen from triplet excited state of dppn-based ligand-centered. As a result, complex **45** exhibited both emission enhancement and photocleavage activity towards DNA at the same time. Complex **47** was discovered to be the most traditional DNA light switch, but it had poor DNA photocleavage performance, whereas complex **48** was an excellent DNA photocleaver but could not report DNA binding via luminescence enhancement. Complex **45** showed a 10-fold increase in cytotoxicity against human lung cancer cells A549 after being exposed to visible light. The particular combination of the Ru (II) arene and dppn subunits resulted in these fascinating features [96]. DNA intercalating six Ru (II) polypyridyl complexes (**49** to **54**) was synthesized by Mari *et al.* and employed them in photodynamic therapy (PDT) as potential photosensitizers (PSs). All compounds exposed promising singlet oxygen production quantum yields which were well comparable to PSs currently on the market, as confirmed by DFT calculations. They also intercalated into the DNA double helix efficiently which was very important for understanding the DNA targeting capability of the complexes. Confocal microscopy and high-resolution continuum source atomic absorption spectrometry were used to determine the cellular localization and uptake of complexes **49** to **54**. They examined the toxicity of Ru complexes on cervical cancer (HeLa) and non-cancerous (MRC-5) cell lines after unveiling the fact that all Ru compounds produced a high amount of $^1O_2$ in hydrophobic environments. When both cell lines were cultured for 48 h in the dark, all complexes were found to be noncytotoxic (IC_{50} > 100 μM). By treating the HeLa cells with metal complexes for 4 h and then subjected them to two different light treatments, one for 10 min at 350 nm and another for 20 min at 420 nm, the effect of light irradiation on increasing cytotoxicity was investigated. They discovered that when complexes were exposed to light, they showed a distinct cytotoxic profile which followed the order as 51≈53 < 52 < 54 < 50 < 49. At 350 nm and 420 nm, complexes **51** and **53** were seen to be nonphototoxic. Complexes **52** and **54** showed almost

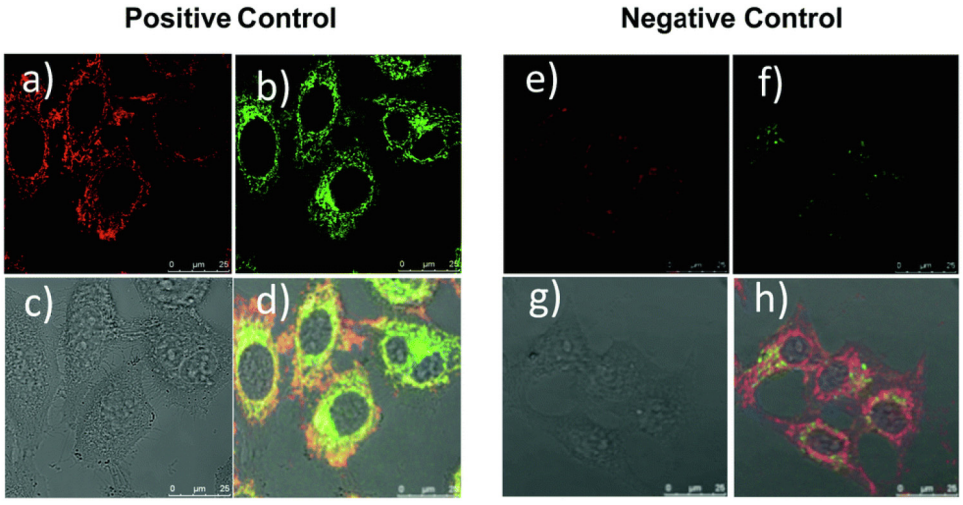

Fig. 38. Positive (mitochondria, a-d) and negative (lysosome, e-h) co-localizationstudy of **41**. (a, e) **41** treated with HeLa cells (b)Treated with Greenmitochondria marker – Invitrogen M7514 (f) Treated with Greenlysosome marker – Invitrogen L7526 (c, g) Bright field images; (d, h) Merged images. Yellow dots denoted the overlapping fluorescent signals from **41** and the organelle probes. [Adopted from **ref. 86** with permission from Royal Society of Chemistry].

Table 5
Summarized iridium-based complexes with their PI value against the particular cell lines with the localization of targeted organelles.

Complex	Cell lines	Localizedand targeted organelles	PI	Dose	References
96, 97	–	Mitochondria, Lysosomes	–	–	[132]
98	A549, A549R, HeLa, U87	Mitochondria	125, 531, 44, 65	450 and 630 nm	[133]
100	HeLa, MCF-7, CNE-2, A549	Mitochondria	177.8, 93.1, 257.8, 164.3	425 nm	[134]
111	HeLa, A549, A549R	Lysosome membrane permeabilization	8.4, 8.0, 4.2	425 nm	[137]
112	HeLa, A549, A549R	Lysosome membrane permeabilization	63, 24, 9.7	425 nm	[137]
113	HeLa, A549, A549R	Lysosome membrane permeabilization	>200, >137, >83	425 nm	[137]
114	HeLa, A549, A549R	Lysosome membrane permeabilization	>476, >322, >139	425 nm	[137]
119	–	Cytoplasm	–	–	[139]
120	–	Mitochondria	–	–	[140]
125	HeLa	Mitochondria	75	12 J cm^{-2})	[142]
132	HeLa	Mitochondria	150	405 nm	[143]
150	A549, A549R	Mitochondria	15.49, 12.29	405 nm (12 J cm^{-2})	[150]

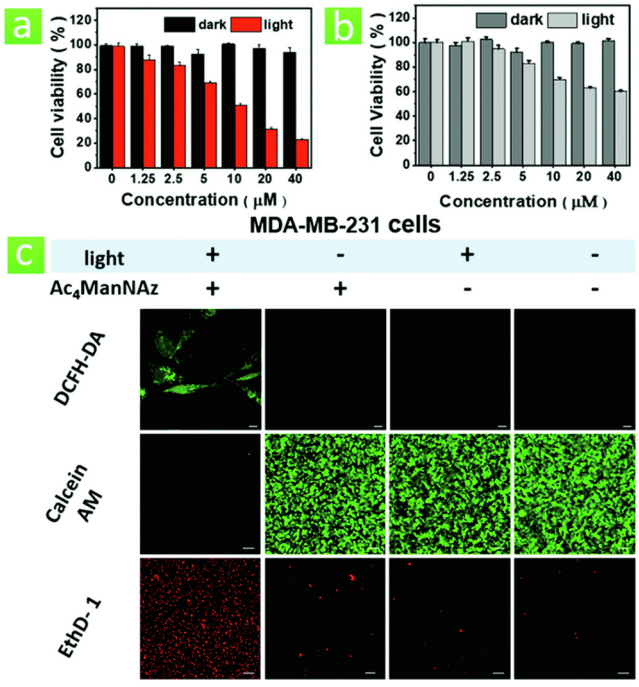

Fig. 39. Photocytotoxicity of **44** (10 mM) towards TNBCs: (a) pretreated with **Ac_4Man-NAz** or (b) Upon two-photon irradiation without **Ac_4Man-NAz** (c) DCFH-DA staining (scale bar: 20 mm) and calcein AM/EthD-1 dual staining (scale bar: 100 mm). [Adopted from **ref. 95** with permission from Royal Society of Chemistry].

negligible or mild activity (47.5 μM) when they were irradiated at 350 nm. Irradiation at 420 nm, on the other hand, resulted in moderate activity for both complexes, with a fivefold increase in cytotoxicity. With IC_{50} values of 2.0 and 5.5 μM respectively, the complexes **49** and **50** displayed a notable phototoxic impact especially when irradiated at 420 nm. Luminescence microscopy and HR-CS AAS were used to investigate cellular localization and uptake in HeLa cells. They also observed that complex **49** and complex **50** displayed a very good cellular absorption comparable to other Ru complexes investigated with these methodologies abiding by AAS analysis. It was obvious that DNA photocleavage investigations supported their theory and demonstrated the critical role of light-mediated DNA damage in total phototoxicity. At the end they concluded that due to the better nuclear accumulation, remarkably good phototoxic index and highly effectual light-induced DNA breakage, complexes **49** and **50** had a lot of potential as novel and revolutionary metal-based PDT agents [97]. The rate of cell death can also be accelerated by targeting the cell's power house, the mitochondria. Remembering this fact, Hanzhong Ke *et al.* synthesized PZn–Ru, (**55**) an amphiphilic compound in which a porphyrin moiety and a polypyridyl Ru(II) moiety were covalently connected together via an ethynyl bridge. PZn–Ru (**55**) had a large two-photon absorption cross-section and could produce $^1O_2$ using both linear as well as two-photon stimulation. It was also cell permeable and could be enthused selectively in cellulo with high spatial control using a laser which resulted in high local concentrations of singlet oxygen and thereby caused enough damage leading to apoptosis. Flow cytometry was used to investigate the cellular absorption of **PZn–Ru** (**55**) by human nasopharyngeal cancer HK-1 cells. The fluorescence intensity of the HK-1 cells after 6 and 24 h of incubation with **PZn–Ru** (**55**) was found to be around 7 and10 times higher than that of the untreated cells respectively. From this result they depicted that **PZn–Ru** (**55**) was rapidly taken up by the HK-1 cells. The amphiphilic structure of **PZn–Ru** (**55**) which had a proper hydrophobic and hydrophilic balance to facilitate cellular uptake, was the main reason for this.They used two photon and linear fluorescence microscopy to investigate the subcellular localisation of **PZn–Ru** (**55**) in HeLa and HK-1 cells. After 40 min of incubation, substantial solid red fluorescence was seen in the mitochondria of HeLa cells when excited at 850 nm. Co-localization of **PZn–Ru** (**55**) (red emission) with a commercial mitochondria tracker (green emission) was observed having confocal pictures of cells co-stained with **PZn–Ru** (**55**) where mitochondria tracker was able to corroborate the observed mitochondrial localisation. They also performed the photocytotoxicity experiment against HK-1 cells by MTT assay and found that **PZn–Ru** (**55**) exhibited noncytotoxicity in absence of light while high phototoxicity in light condition. At last, they concluded that under visible and NIR excitation, the molecule exhibited a significant $^1O_2$ quantum yield. In presence of **PZn–Ru** (**55**), significant cell killing occurred after appropriate photoexcitation, suggesting that **PZn–Ru** (**55**) could be a good choice for TPA photodynamic treatment [98]. Poor water solubility, selectivity, and ill-defined intracellular targets are common problems with light-activated ruthenium polypyridyl anticancer prodrugs. As a result, Lameijer *et al.* synthesized two light-activatable prodrugs, $[\mathbf{D\text{-}57}]^{2+}$ and $[\mathbf{L\text{-}57}]^{2+}$. A thioether ligand was covalently coupled with D- or L-glucose and bonded to ruthenium via a thermally stable Ru-S coordination bond and formed this complex. The lipophilicity of the dppn ligand in the complexes compensated the hydrophilicity of the glucose moiety, allowing passive uptake. A very strong cytotoxic activity was produced after irradiation with a modest dose of visible light, as measured by submicromolar EC_{50} values. These complex's high phototoxic indices could be the result of at least two photochemical processes which was taken place in the mitochondria. As it interacted with plasmid DNA at a high base pair and Ru ratio, mitochondrial DNA appeared to be a plausible target of the achiral photoproduct $[56]^{2+}$.The two enantiomers exhibited no difference in absorption or cellular localisation *in vitro*, and the addition of sodium azide demonstrated energy-independent

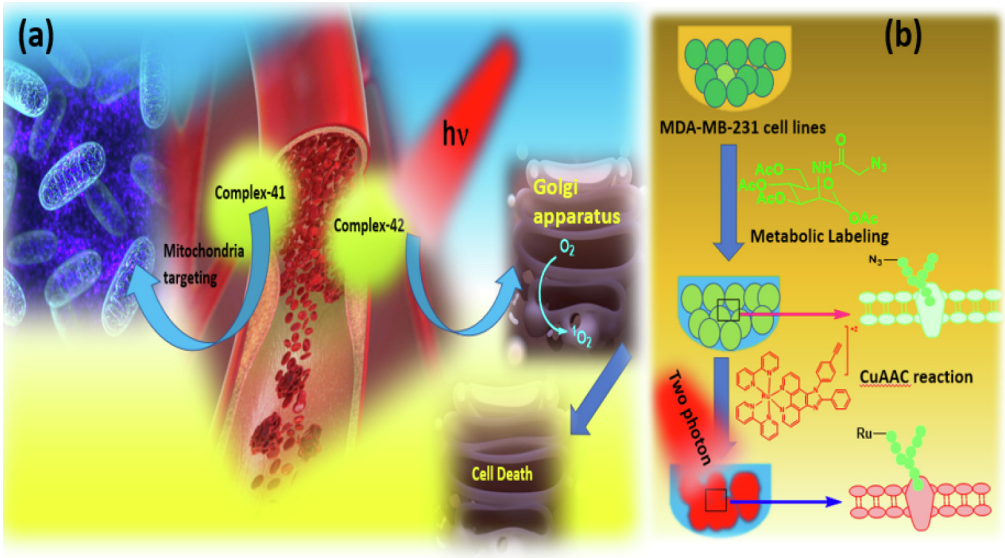

Fig. 40. (a) Graphical representation in which **41** target the mitochondria and **42** target Golgi apparatus, (b) pictorial representation of the bioorthogonal labelled **44** as a two-photon photosensitizer.

drug uptake. These findings showed that neither GLUT nor SGLT were involved in the uptake of these complexes, implying that other enzyme (such as efflux pumpsor glucosidases) in darkwere responsible for the twofold increased cytotoxicity of [**D-57**]$^{+2}$and [**L-57**]$^{+2}$. Although [**D-57**]—the complex conjugated to the natural D-glucose moiety would be expected to be the most intriguing "targeted" enantiomer, [**L-57**]—the complex attached to the non-natural L-glucose moiety showed a higher phototoxic index due to its decreased cytotoxicity in the dark [99]. Simple Ru (II) terpyridyl complexes had low singlet oxygen generation quantum yields and a limited excited-state lifetime, making them unsuitable for PDT. Due to this reason Huang *et al.* synthesized three Ru (II) terpyridyl complexes (**58, 59 and 60**) with mixed ligand for photodynamic therapy (PDT) and studied their anticancer activity. Also, with this complex they investigated dark and photo cytotoxicity, DNA binding and DNA photocleavage activity, cellular localization and finally cellular uptake assay. Having considered the $[Ru(bpy)_3]^{2+}$ as a standard they examined the $^1O_2$ quantum yield of the complexes by quenching the fluorescence intensity of 1,3–dip henylisobenzofuran (DPBF). They found 0.38, 0.41 and 0.45 quantum yields for complexes **58**, **59** and **60** respectively. The non-fluorescent organic compound, Dichlorodihydrofluorescein (DCFH) converted into the fluorescent product, DCF upon oxidation by OH• radical. In absence of Ru (II) complexes, the fluorescence intensity of DCFH was found to be less within 30 min whereas it was increased dramatically when complexes **58** to **60** were present. They found that the intensity of DCFH fluorescence was increased around 35, 45 and 66-fold for treatment of complexes **58, 59** and **60** respectively. As a result, complexes might produce ROS through both type I and type II pathways. Interfering with transcription and translation by interacting with DNA could lead to cell death. They also investigated the DNA transcription inhibiting activity of the complexes. Complex **58** had little effect on DNA transcription even at a high concentration of 10 M which indicated that it had a low DNA binding affinity. But with increasing the area of intercalative ligand, they found decreasing value of C_{50}^{inh} (the concentration of Ru(II) complex required to inhibit DNA transcription by 50 %) and the value was 5.0 μM for complex **59** and 2.0 μM for complex **60**. As a result of the intercalation of complexes **58, 59** and **60** into the template DNA, the DNA transcription process was blocked. They investigated both dark and photo cytotoxicity towards Bel7402 (human hepatocellular carcinoma), HepG2 cells and LO2 (human normal hepatocyte). Complexes **58** and **59** exhibited nontoxicity against the cancer cell lines in dark condition with IC_{50} value >100 μM whereas the complex **60** exhibited slightly toxicity. The cytotoxicity of Ru (II) complexes was increased considerably after being exposed to 450 nm LED light. Complex **60** became extremely toxic to Bel7402 cancer cells with IC_{50} value as low as 0.8 μM (PI 106) [450 nm (10 J/cm^2) for 44 h].Untreated cells were also exposed to the same irradiation process as a PDT control and the light was determined to be harmless for the cells [100] (See Table 6).

A photosensitizer's cellular uptake and cellular localisation into tumour cells is a significant predictor of therapeutic success. They used a confocal laser scanning microscopy (CLSM) and organelle specific probes for this study. They discovered that Ru (II) complexes did not overpower the signal of Hoechst 33,342 after incubation with HepG2 cells (Fig. 42). The lysosome–specific fluorescent probe LysoTracker® Green (LTG) and the mitochondria–specific fluorescent probe MitoTracker® Green (MTG) were partially overlapped with the Ru (II) complexes' signals. They also used ICP–MS to determine the complexes uptake property within HepG2 cells. The majority of Ru (II) complexes appeared to be in the cytoplasm rather than the nucleus. Finally, they came to the conclusion that Ru (II) complexes could penetrate cells but in the dark complexes were unable to reach the nucleus. Furthermore, Ru (II) complexes were non-toxic to cells in the dark and thus the cytoplasm localization of Ru (II) complexes might aid to reduce dark–cytotoxicity [100] (See Figs. 43–45).

Carbohydrate-modified complexes are an intriguing alternative because they have been proven to improve the selectivity of biological probe interactions. Not only that lower toxicity, increased biocompatibility and the use of the targeting properties of sugar-specific receptors or metabolic pathways are some of the other advantages of introducing these groups. As a result, metal complexes containing sugar are being studied more and more. In presence of irradiation the complexes are able to generate singlet oxygen and exhibited anticancer effect [101–103]. Gottschaldt *et al.* synthesized Ru (II)-glycoconjugate $[Ru(bpy)_3]^{2+}$ type of complexes with combination of D-glucose, D-galactose or D-mannose thioglycosides (**61, 62, 63**) and investigated the cellular uptake property towards HepG2 cells. They found that the glycoconjugates had a delayed uptake by cells, requiring 24-hour incubation

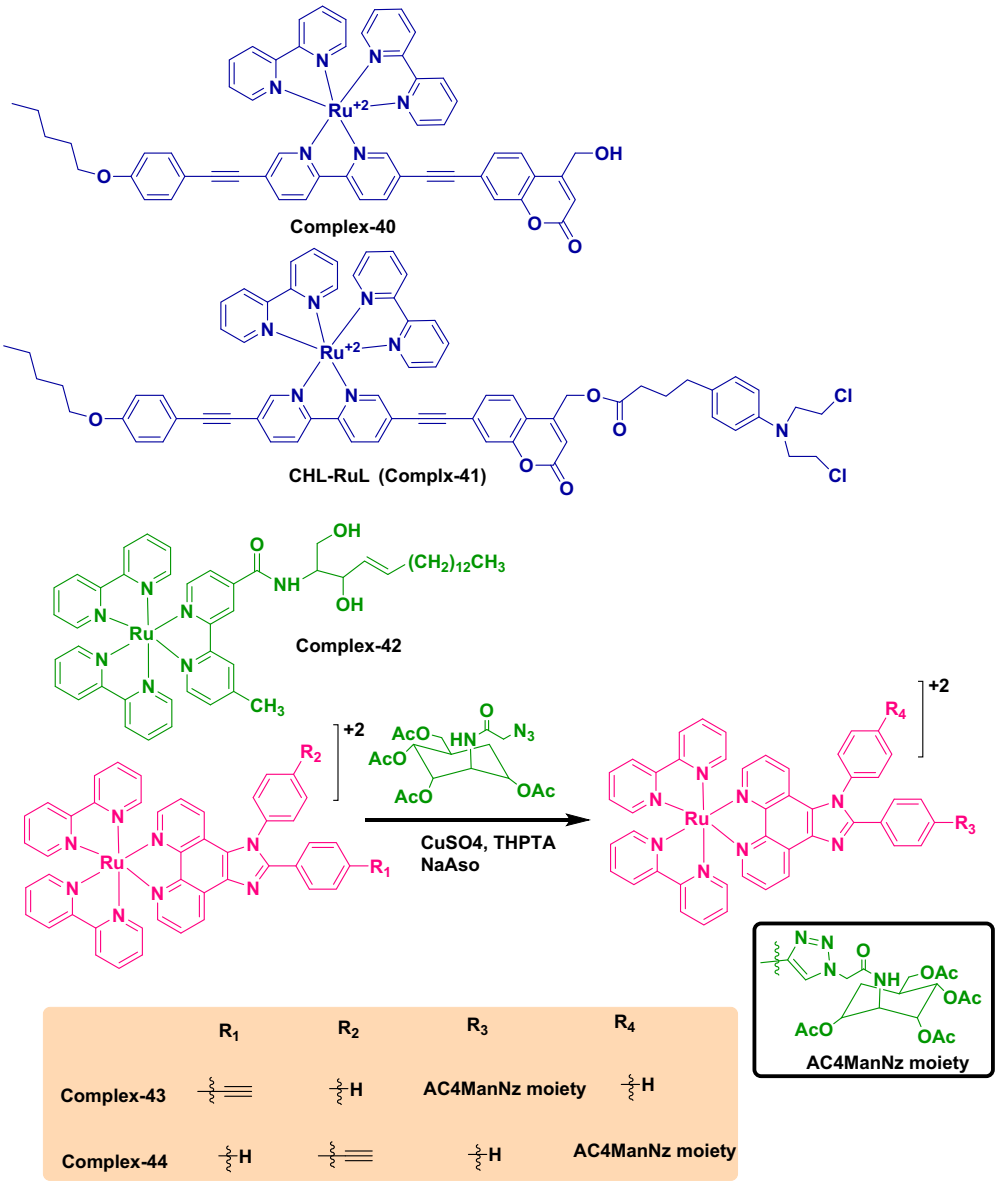

Fig. 41. Structure of complex **40**–**44**.

Table 6
Summarized the rhenium-based complexes with their PI value against the particular cell lines with the localization of targeted organelles.

Complex	Cells lines	Localized and targeted organelles	PI	Dose	References
165	–	Near nuclear membrane	–	–	[181]
171a	HeLa	–	27.8	365 nm	[189]
174, 175	A549	Lysosomes	60.8, 41.8	425 nm, (36 J cm^{-2})	[194]

and the glucose-substituted conjugate had the largest absorption of the sugars tested with galactose- and mannose-conjugates having lesser uptake and a distinct cellular staining pattern in formalin-fixed cells. In vitro research revealed that the kind of connected carbohydrate determined cellular uptake of congeneric substituted ruthenium bipyridyl complexes in terms of size, hydrophilicity and charge. At the end they hypothesized that the conjugates were taken up via an endocytosis process rather than a transporter, but they were unable to conduct studies to establish this [104].

6.2. Organelles targeted Ru-Peptide conjugates as PDT agent

There are so many applications of peptide conjugated Ru complexes in Chemical Biology and drug development. Conjugation can make hydrophobic compounds more water soluble, promote cellular absorption, help in acting as targeting motifs and improve biocompatibility to lower toxicity.When light is employed to irradiate organo-ruthenium complexes with polypyridyl ligands, they can display significant anticancer action. Due to the heavy atom effect, their massive population of the triplet metal-to-ligand

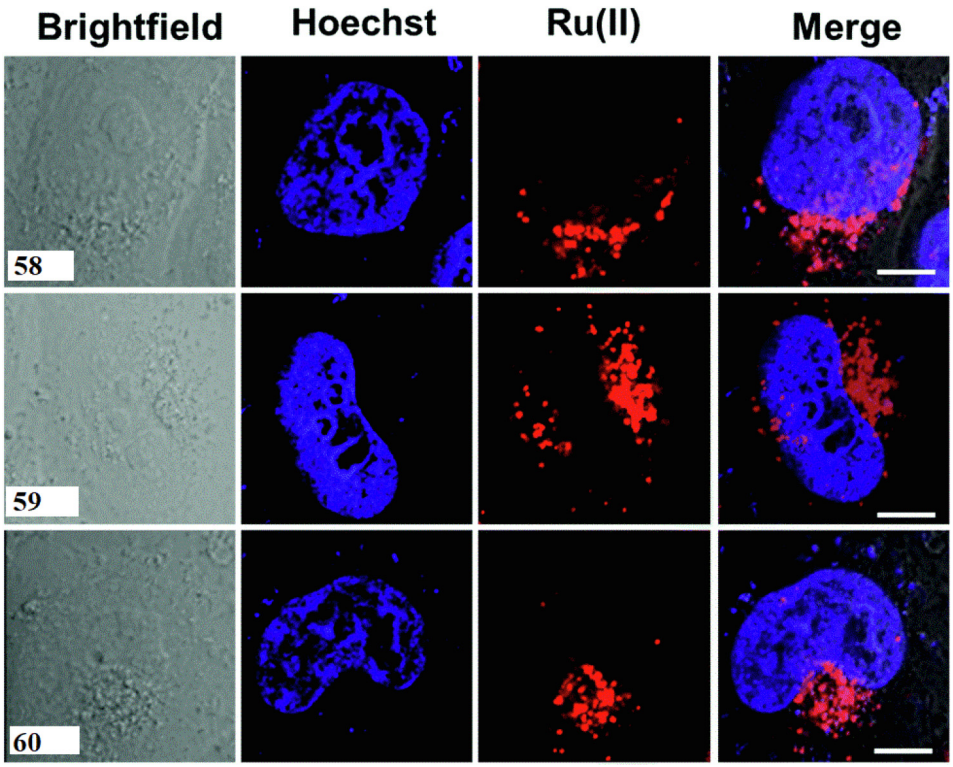

Fig. 42. Colocalization images of complexes **58–60** with nucleus dye Hoechst 33,342 (Scale bars = 5 μm.) [Adopted from **ref. 100** with permission from Royal Society of Chemistry].

charge-transfer state gives substantial $^1O_2$ yields, while the solubility of these complexes can be altered by altering the counter ions. Herein, we have represented some organelle-targeted and cancer cell-targeted PDT active Ru-polypyridyl complexes with peptide conjugation.

By combining Ru-complexes on a protein carrier scaffold adorned with subcellular mitochondria targeting groups, Sabyasachi *et al.* represented a macromolecular strategy to increase phototoxicity and efficacy of the PS (**64**). They investigated a macromolecular PS for targeting the mitochondria, the "power house of the cell" and one of the most important organelles to be attacked by drug molecule for inhibiting effectual tumour growth in an acutemyeloid leukemia cell line (AML).They also presented a bioinspired technique for converting the blood plasma protein serum albumin (HSA) into an effective nanotransporter for phototoxic pharmacological compounds with synergistic properties due to molecular design (Fig. 46).They discovered that as compared to the simple Ru complex, the nanotransporter **cHSA-PEO-TPP-Ru** had dramatically improved photophysical characteristics and increased $^1O_2$ quantum yields as well as superior mitochondria-specific co-localization. It exhibited lowest IC_{50} values in various cancer cell lines and in an AML cell line, effective growth suppression was reported with preferential death of leukemic cells over normal bone marrow cells, implying a therapeutic window for this drug in AML. They also performed the intracellular localization of **cHSA-PEO-TPP-Ru** with the help of laser scanning confocal microscopy into Human Cervical Cancer cell lines (HeLa cells, as model system). The cell was incubated with low concentration of drug for 4 hr. They gave the excitation 458 nm and fixed the emission window at 530–710 nm. Authors also discovered a clear colocalization (Fig. 47) of **cHSA-PEO-TPP-Ru** in mitochondria (Pearson's coefficient 0.88), where they were mostly located outside the nuclear region (Pearson's coefficient 0.07), after staining with various sub-cellular organelle dyes with selectivity for membranes (Cell Mask Deep Red Plasma Membrane Stain), the nucleus (Hoechst 33,342 Solution), mitochondria (Mito Lite Blue FX490. They also confirmed that **cHSA-PEO-TPP-Ru** was rapidly transported across the membrane and accumulated in the cytosol with no evidence of localization in membranes (Pearson's coefficient 0.2) or lysosomes (Pearson's coefficient 0.3) [105].

Wang *et al.* synthesized Ru-SST (**66**) by combining with the exceptional peptide hormone SST and the PS $[Ru(bpy)_3]^{2+}$which had attractive phototoxicity along with tumor cell selectivity (Fig. 48). Complex**-66** exhibited a number of advantages over Ru-complexes in terms of antitumor properties including appealing receptor specific cellular uptake, light-controllable cytotoxicity, powerful anti-proliferative effects and minimal systemic toxicity. They inspected the singlet oxygen generation of complexes **65** and **66**. They also investigated the emission quenching by measuring emission spectra in both oxygen-free and oxygen-saturated MilliQ water. They observed there was a 35 % of emission fall off for complex **66** and 29 % of emission fall off for complex **65**. These quenching values matched with $[Ru(bpy)_3]^{2+}$ which had a quenching value of 41 % in water. This phenomenon was caused by an energy transfer from ^{3}MLCT state of the electronically excited Ruthenium(II) complex to oxygen in its ground state ($^3O_2$), this could lead to the creation of singlet oxygen (ROS). They also employed the singlet oxygen sensor 9,10-anthracenediyl-bi(methylene) dimalonic acid (ABDA) to confirm the formation of $^1O_2$. They mixed complexes **65** and **66** with 20 μM of ABDA in PBS buffer and then irradiated by a 470 nm LED and found that complexes **65** and **66** exhibited >70 % diminished in ABDA absorptionat 380 nm which indicated the formation of effective singlet oxygen. They also investigated the cellular uptake of both the complexes in human non-small-cell lung cancer (NSCLC) A549 cells. In A549 cell, they added both the complexes with same amount and studied by laser scanning confocal microscopy. They took the emission image from 580 to 707 nm. After incubated with complex **65**, only minor

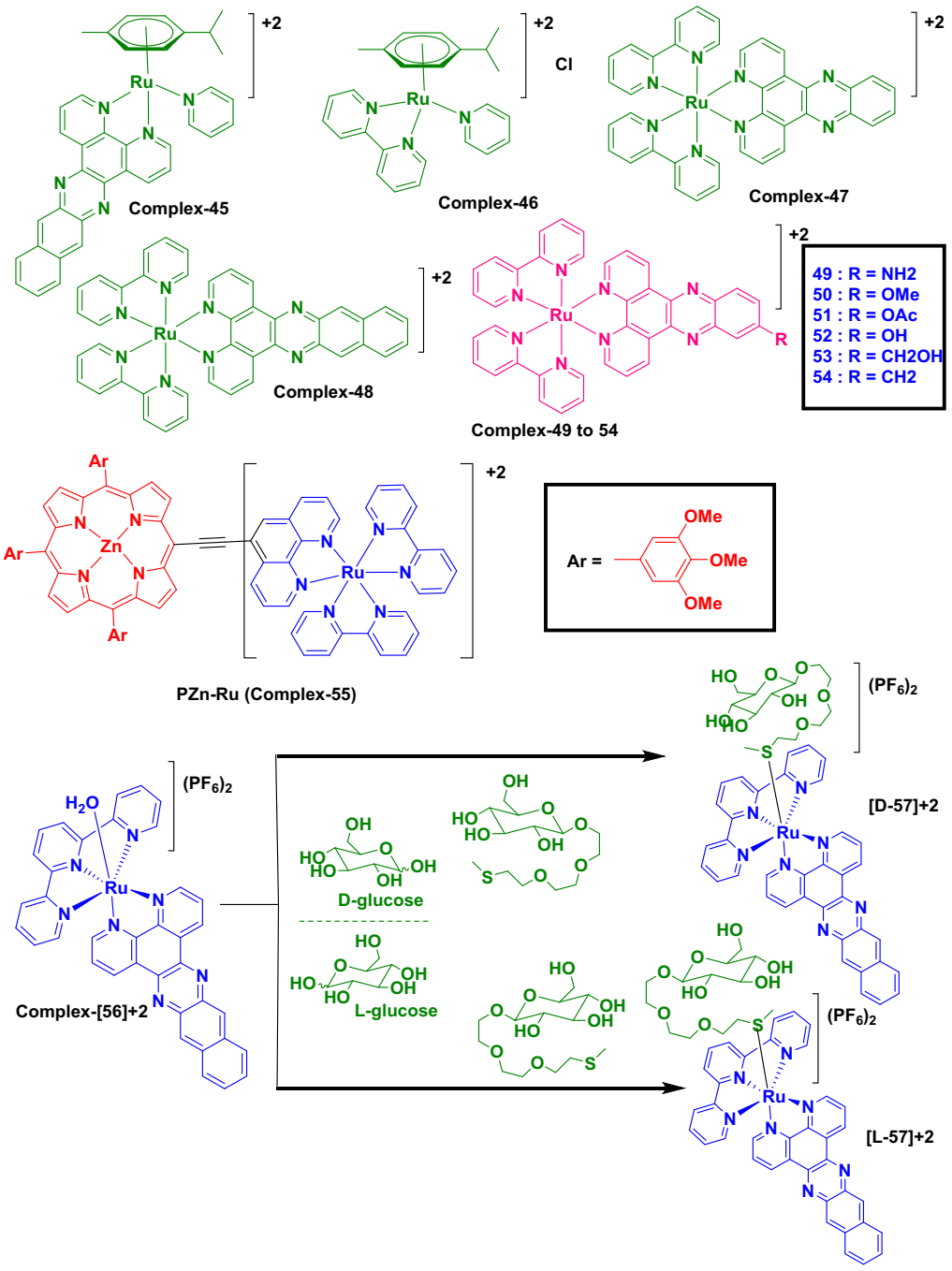

Fig. 43. Structure of complexes **45** to **55** and synthetic pathway of [**D/L-57**] $^{+2}$ from [56] $^{+2}$.

emission was recorded within the cells, whereas complex **66** was immediately and efficiently transferred across the membrane and accumulated inside the cells. When they compared to the control experiment, 100-fold increase in absorption was found which indicated a considerable improvement in cellular transport following conjugation with SST. They also performed the light and dark cytotoxicity in A549 cell with the complexes **65** and **66**. In presence of light irradiation complex **66** exhibited cytotoxic effect with IC_{50} value 13.2 ± 1.1 μM but not toxic effect was found in dark condition whereas the complex **65** showed IC_{50} value 67.5 ± 1.1 μM. From their result we understood that peptide conjugated complexes have great impact in PDT as well as in cancer treatment [106]. In the series of peptide conjugated Ru-polypeptide complexes, Blackmore *et al.* also synthesized two Ru (II) complex (Fig. 50) with formula $[Ru(LL)_2PIC]ClO_4$ (where, PIC = 2-(4-carboxy phenyl)-imidazo-[4,5–f][1,10]-phenanthroline and LL = dpp and bpy) (**67, 68**). Through a β-alanine bridge linked to the probes' terminal carboxy units, the complexes were both conjugated to **VQRKRQKLMP–NH_2**. Here they used nuclear localization Signal (NLS) peptide **VQRKRQKLMP–NH_2**, which was generated from transcription factor NF-kB responsible for internalization of NF-kB in to the nucleus. Authors observed confocal luminescence images of live CHO cells followed by incubation for 16 h (Fig. 49) with the help of both the complexes. The dye undoubtedly infused the cell in both cases. To understand the distribution and localization of the conjugates within cells they used nuclear dye DAPI.

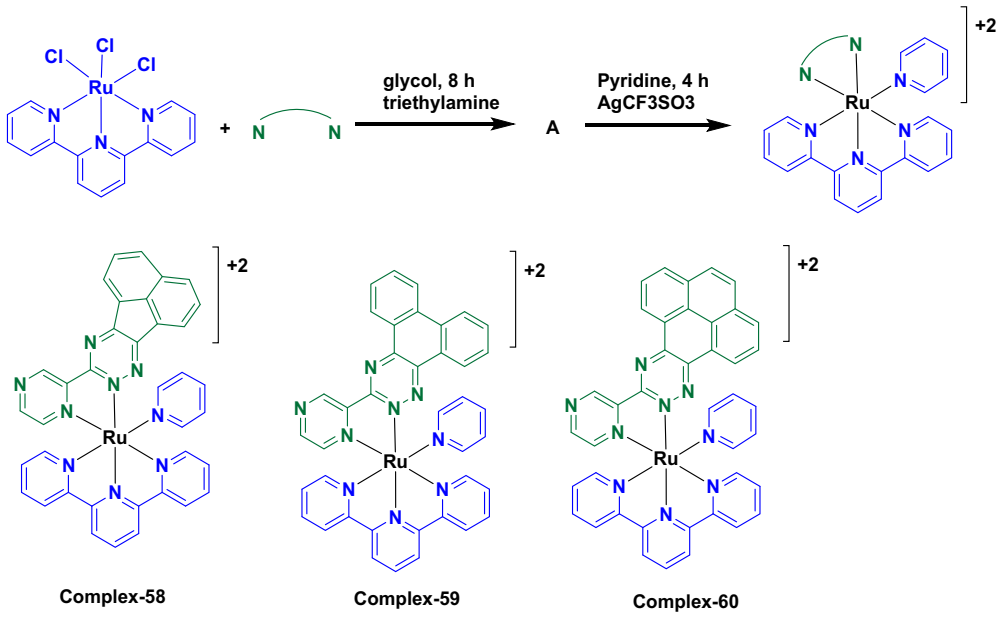

Fig. 44. Synthetic pathway and structures of complexes **58**–**60**.

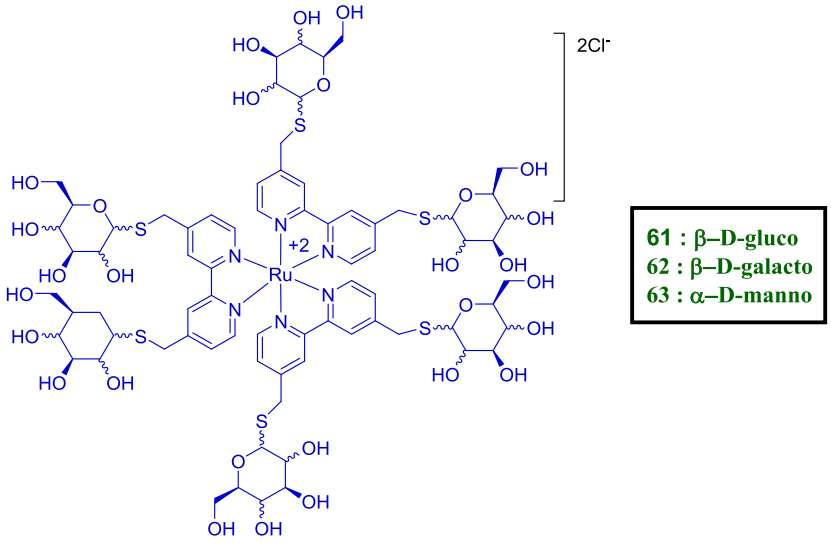

Fig. 45. Structure of complexes from **61** to **63**.

Strong colocalization of both two complexes with DAPI was found. This indicated that the complex–NLS conjugate can pass through the nuclear envelope [107] (See Figs. 51 and 52).

The mechanisms of cell penetrating peptide uptake are still being researched, with reports of both energy-independent and energy-dependent systems. These peptides had previously been used to carry a variety of molecular cargo into cells including imaging agents, nucleic acids, medicines, and nanoparticles which are presently being tested with Ru(II) complexes. In this regard Marcélis *et al.* coupled the TAT peptide with Ru-complexes and found [Ru(TAP)$_2$(phen-TAT)] (**69**) and [Ru(phen)$_2$(phen-TAT)] (**70**) as the TAT peptide might influence the behaviour of the complex at the excited state as well as its photo reactivity with a G-base. They investigated the effect of the TAT attachment to the complex **69** upon blue-light irradiation in presence and absence of 17-mer oligodeoxyribonucleotides (ODNs) with no G-base (**ODN$_0$**) or one G-base (**ODN$_G$**). The calculated average luminous lifetime for complex **69** in absence of ODN was longer than that of the corresponding free complex. Thus, the excited state was modestly shielded by the TAT peptide due to decrease radiationless deactivation by solvent molecules. In presence of **ODN$_0$**, especially double-stranded (**dsODN$_0$**) the span of lifetime was amplified. In presence of **ODN$_G$**, average luminescence lifespan was decreased and this effect was larger with **dsODN$_G$** than with single-stranded (**ssODN$_G$**). These shorter luminescence durations indicated quenching by PET reactions with the G-base of ODN$_G$. From the lifetime measurements they confirmed that **Ru–TAT** conjugate **69** interacted with ODNs and that the complex's photoreactivity was maintained even after it was attached to the TAT peptide. Authors examined the cytotoxicity and phototoxicity of complexes **69, 70** as well as free reference complex with the help of MTT assay. The free complex exhibited very low phototoxicity and cytotoxicity in dark as well

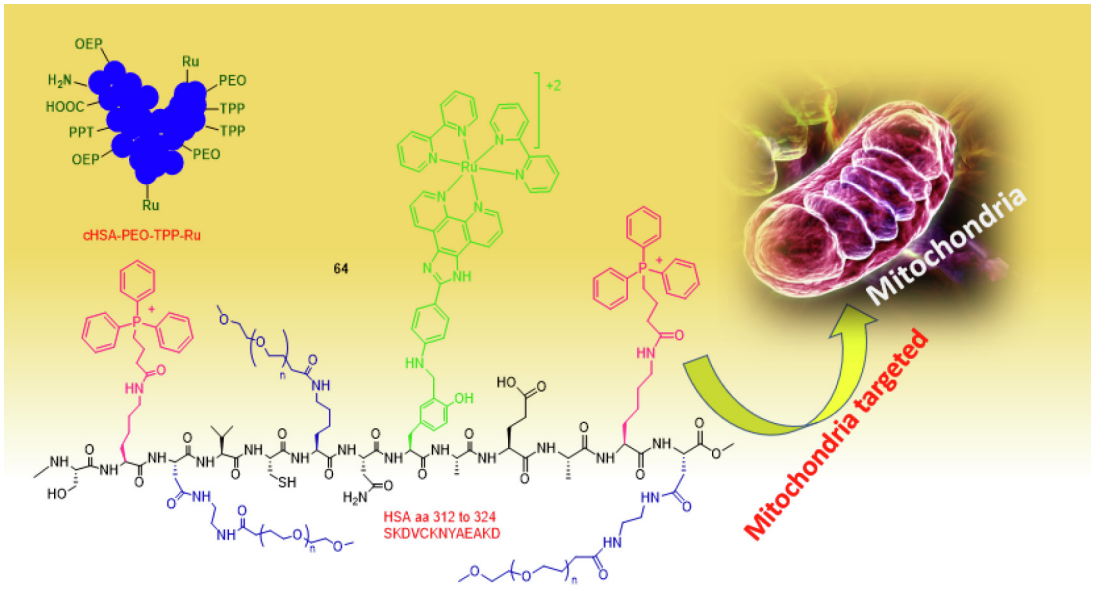

Fig. 46. Mitochondria targeted complex **64**.

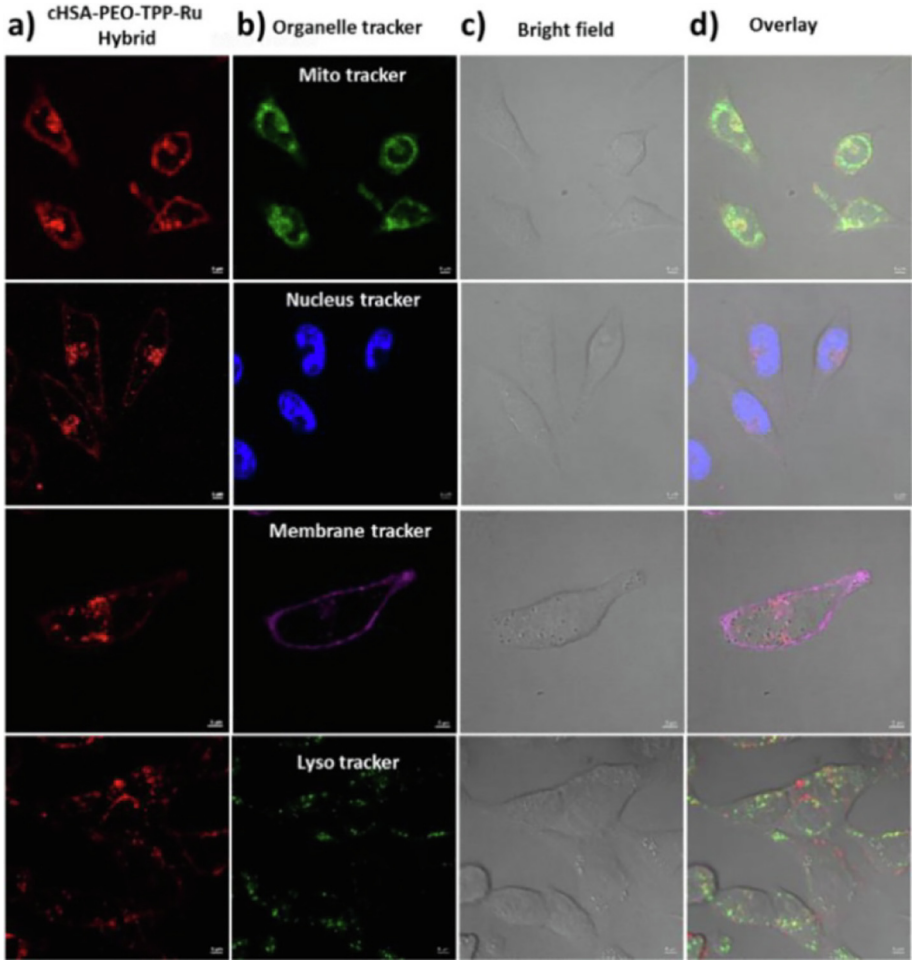

Fig. 47. Confocal microscopic images of HeLa cells incubated with **cHSA-PEO-TPP-Ru** and commercial organelle trackers. Overlay images and colocalization analysis of cells stained with mitochondria (0.88), nucleus (0.07), membrane (0.2) and lysosome (0.3) markers presented that cHSA-PEO-TPP-Ru localized in mitochondria. (a) **cHSAPEO-TPP-Ru** emission, (b) Organelle trackers emission, (c) bright field images (d) overlay of three images. [Adopted from **ref. 105** with permission from American Chemical Society].

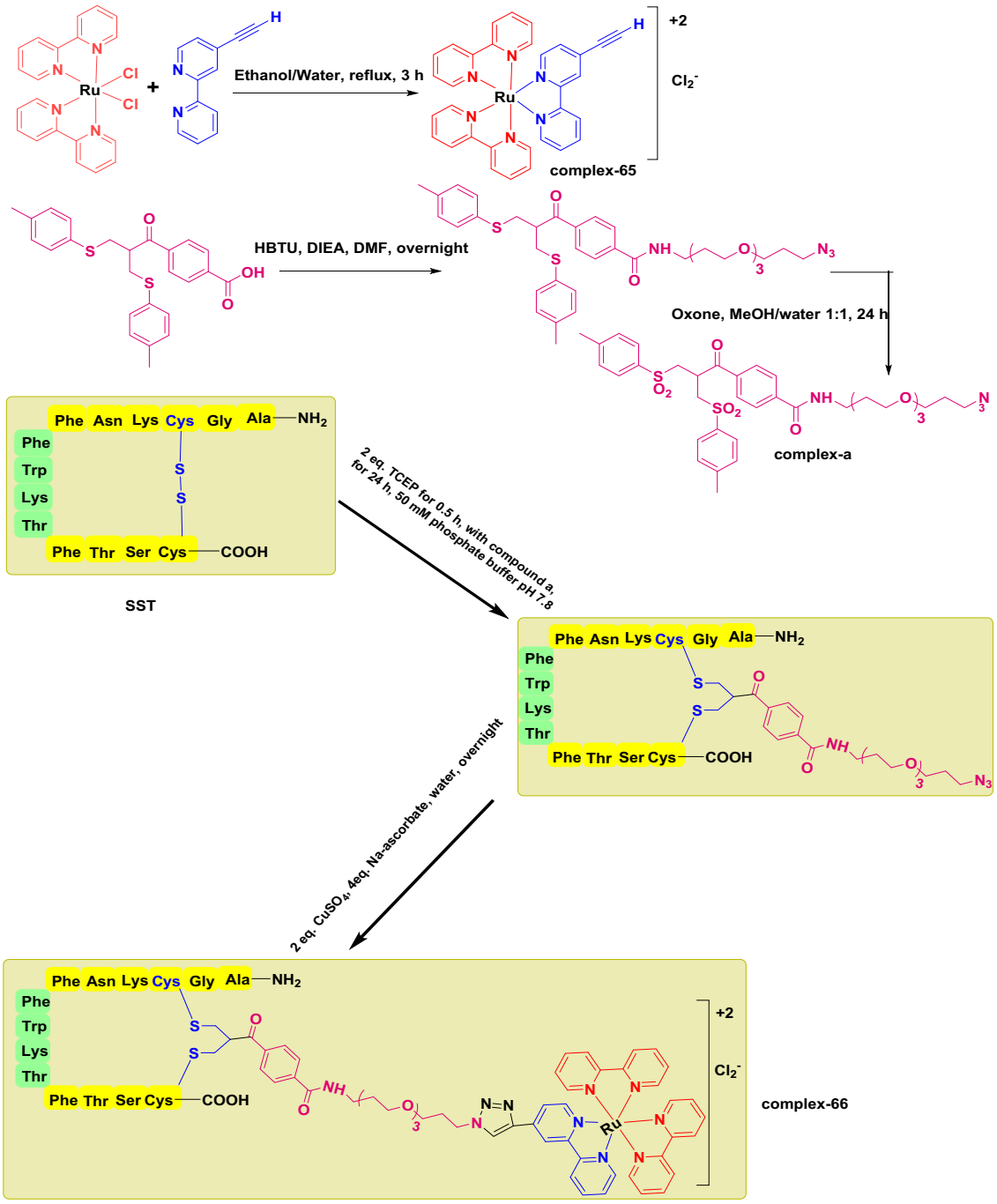

Fig. 48. Synthetic pathway of complex **66**.

as in blue-light irradiation. They used the same intracellular concentration of these two conjugates in MTT experiments with varied external incubation concentrations but the same incubation period. They also found in the dark or under irradiation, both complexes **69** and **70** had essentially negligible toxicity at 1 $ng_{Ru}/mg_{protein}$ intracellular concentration. But, for complex **70**, a higher intracellular concentration of 25 $ng_{Ru}/mg_{protein}$ had an influence on this experiment. Conjugate**70** had considerably stronger photo cytotoxic effect on HeLa cells than conjugate-**69**. This was because of the fact that the complex **69** did not have access to the genetic material preventing photoelectron transfer and the formation of the DNA photo adduct. They also used confocal microscopy on HeLa cells that had been treated with conjugates **69** and **70** to confirm this idea. To gather information on the localization of the tethered complexes inside the cells, they used a particular nuclei marker (Draq5) to stain the cell nuclei. Conjugate **70** showed a diffused staining in the cytoplasm with localization within endosomal and endoplasmic reticulum vesicles indicating its intracellular distribution. Conjugate **69**′s intracellular distribution was substantially comparable to that of **70**′s. Confocal microscopy revealed that both conjugates **69** and **70** were primarily found in vesicles and cytoplasm, but not in the nucleus [108].

Martin *et al.* presented a new ruthenium (II) peptide combination adorned with the ability of monitoring dynamic changes in local O_2 concentrations within living cells. A single mitochondrial penetrating peptide, **FrFKFrFK-CONH$_2$** (r = D-arginine), was

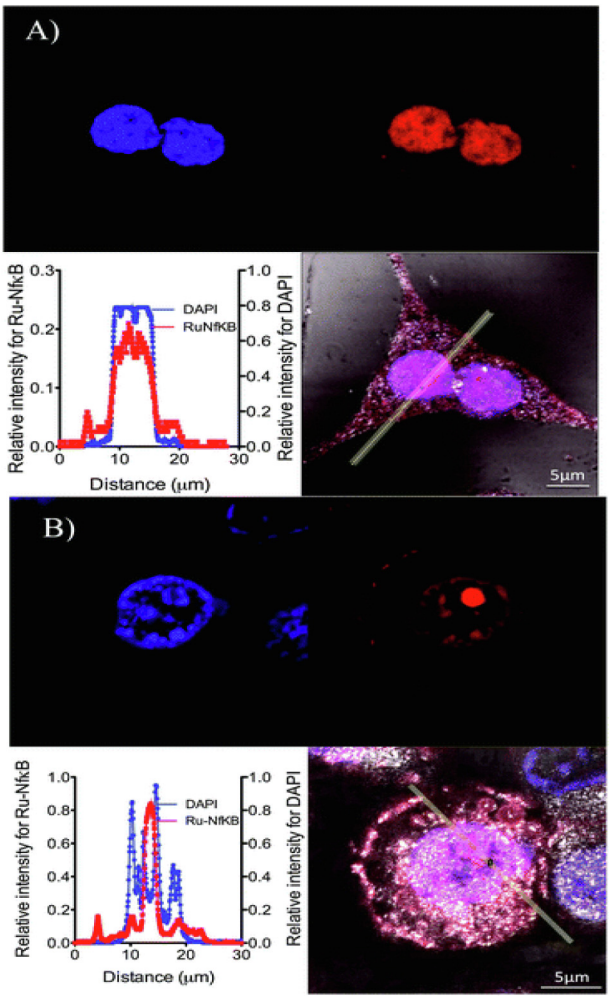

Fig. 49. (A) Nuclear localization of complex **67** and uptake (B) Nuclear localization and uptake of complex **68** into live CHO cells Live cells for 24 h before addition of the ruthenium complexes and DAPI. Merged image of the ruthenium complex, DAPI and the backscatter refection (bottom right), the yellow line denoted the fluorescence intensity profile in the graph on the left generated using ImageJ image analysis software. [Adopted from **ref. 107** with permission from Royal Society of Chemistry].

bridged over a luminous dinuclear ruthenium (II) polypyridyl complex. They also showed that the probe's capacity to respond dynamically to changing O_2 contents within living HeLa cells was demonstrated using Antimycin A. In a concentration dependent manner, $[(Ru(bpy)_2phen\text{-}Ar)_2\text{-}MPP]^{7+}$ (**71**) was taken up by the cell through rapid and irreversible way. In terms of the balance between emission intensity and cytotoxicity, 75 μM in the contacting solution was the best concentration for uptake and imaging. Using confocal laser scanning microscopy, they investigated the detailed uptake and localization of the complex. The conjugate penetrated the cells within 5 min of being added to the contacting solution, which was a quick uptake. It appeared to accumulate inside the cytoplasm after 1 h of incubation, then localized firmly in the mitochondria, and localization was completed at 37 °C after 2 h of incubation, both in the presence and absence of light. Although luminescence imaging demonstrated that some complexes stayed in the cytoplasm, it was clear that the dye highly preconcentrated inside the mitochondria; additionally, the conjugate was nuclear excluding. To confirm the localization of the complex in mitochondria, they used Mito Tracker Deep Red. They found that the conjugate $[(Ru(bpy)_2phen\text{-}Ar)_2\text{-}MPP]^{7+}$demonstrated substantial colocalization with the MitoTracker. MitoTracker was red; the complex was green and the colocalization was found to be yellow. This research emphasized on the significance of combining luminous metal complexes with MPPs' (mitochondrial penetrating peptide) targeting capability in guiding metal complexes to the mitochondria as well as the importance of peptides in metal complex targeted imaging. Authors also investigated the phototoxicity of complex **71** in HeLa cells by measuring the uptake of DRAQ 7 in complex **71** under visible irradiation as shown in (Fig. 53A–D). After 20 min of irradiation on complex **71** loaded cells at 488 nm, the cell death was found. There was consistent of phototoxicity of the complex rather than cytotoxicity. As a control, a section of the same sample that had not been exposed to light was investigated, and no damage to the cells was found (Fig. 53, E, F), suggesting that irradiation did indeed promote DRAQ 7 uptake, that rendered cytotoxicity [109].

6.3. Mixed metallic Ru-complex as a PDT agent

After discussion the PDT activity and organelle targeting ability of some monometallic ruthenium complexes, our focus came

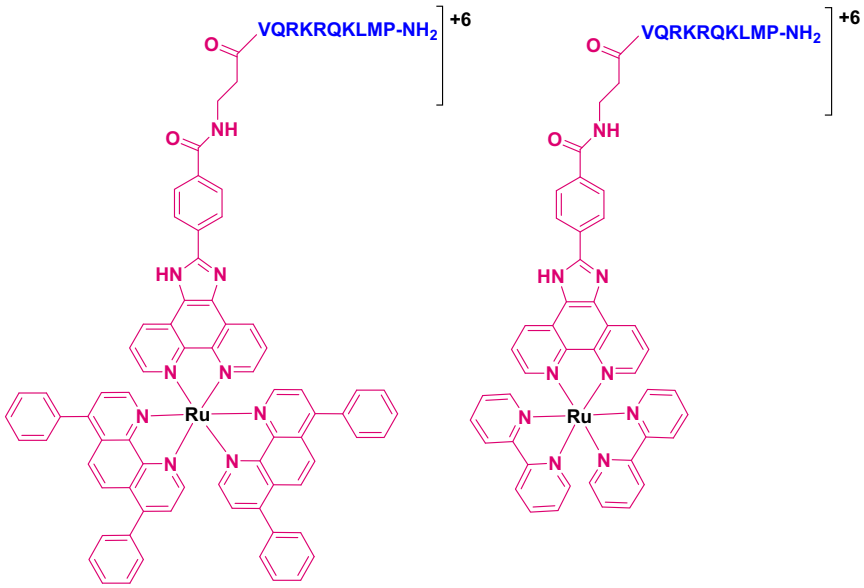

Fig. 50. Structure of complex-**67** and **68**.

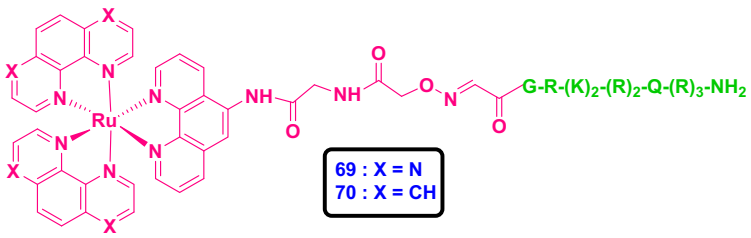

Fig. 51. Structure of complex **69** and **70** with TAT peptide.

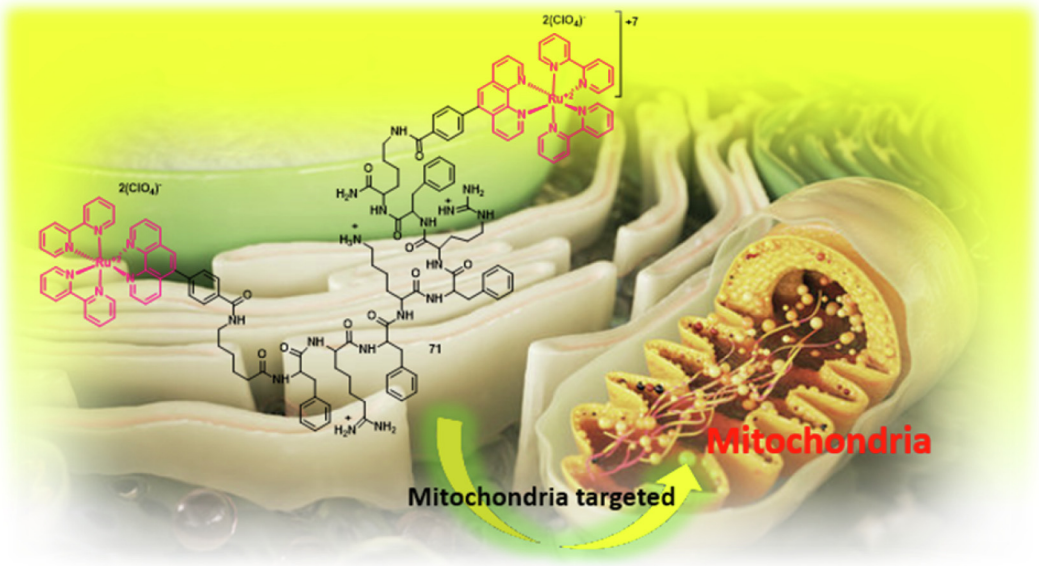

Fig. 52. Pictorial representation of mitochondria targated complex-**71**.

towards the discussion of some bimetallic ruthenium complexes in this field. Here we have represented some examples.

Ru-polipyridyl compound demonstrated specific attributes in one and two photon luminescence. In this regard, Chao *et al.* developed binucler Ru(II) polypyridyl complexes with the formulla, $[(phen)_2Ru(L_{1-7})Ru(phen)_2]^{4+}$ (**72**–**78**) which had greater pi-conjugated systems, good water solubility and pH resistance, high photostability and had been used as single and two-photon luminous cellular imaging probes. For biological applications, high cell viability is necessary. Due to this authors had used MTT assays to conduct cell viability studies using HeLa cells. Over the period of 24-hour incubation, all of the complexes exhibited high cell viability at several concentrations (5 μM to 20 μM). Among all the complexes they selected complex **75** for other study. Authors used two-photon fluorescence microscopy (TPM) imaging (Fig. 54) to determine the benefit of employing complexes **72**–**78** as two-photon luminescence cellular dyes for living cells. TPM images of HeLa cells stained with complex **75** was resembled as OPM (one photon fluorescence microscopy) images, demonstrating that the dye had penetrated into the cytoplasm. They also observed two photon fluorescence microscopic image of HeLa cells co-stained with complex **75** and DAPI or MitoTracker Green independently (Fig. 55) which revealed that complex **75** was localized in the cells similar to, but not identical to that of MitoTracker Green. Author also used ICP-MS analysis to confirm the amount of complex present in either nucleus or in cytoplasm and thus they visualised that>90 % ruthenium was accumulated in cytoplasm of the cells [110] (See Fig. 56).

The increase of cellular uptake of molecules can be made possible by enhancing their lipophilicity. It has also been discovered that it opens up the possibility of binding to various targets, such as hydrophobic nooks in proteins and cell membranes. Gill and coworkers clarified these two significant aspects. Gill *et al.* first reported dinuclear Ruthenium complex $[(Ru(phen)_2)_2(tpphz)]^{4+}$ (**79a**) and later they reported $[(Ru\ (DIP)_2)_2(tpphz)]^{4+}$ (**79b**) (where, DIP = 4,7-diphenyl-1,10-phenanthroline). To make it even easier to produce an MLCT active luminous molecule, the core tpphz bridging ligand was maintained. They incorporated DIP as an ancillary ligand to improve the lipophilicity and they found the calculated octanol–water partition coefficient, logP, for complex **79b** was 1.52 ± 0.13 compared to −0.93 for complex **79a**. For extensive co-localization study in which the overlap of emissions with existing cellular fluorescent labeling techniques were carried out to better investigate intracellular targeting. They incubated MCF-7 cells with complex **79b** and the nuclear dye DAPI at the same time. They found that two luminescence signals had little overlap in cellular co-localization analyses indicating that Ru (II) complex did not significantly co-localize with the DNA dye. From that result they concluded that the bulky DIP ligand of complex **79b** was impeded into cellulo groove binding interactions with DNA. They performed the co-localization studies for two especially lipid-dense organelles, ER and Golgi apparatus for recognizing the nature of the intracellular localization and emission of complex **79b**. They also used immune fluorescent co-staining methods in which MCF-7 cells was stained with complex **79b** were probed with particular antibodies for proteins that located in either the ER or the Golgi apparatus. Author

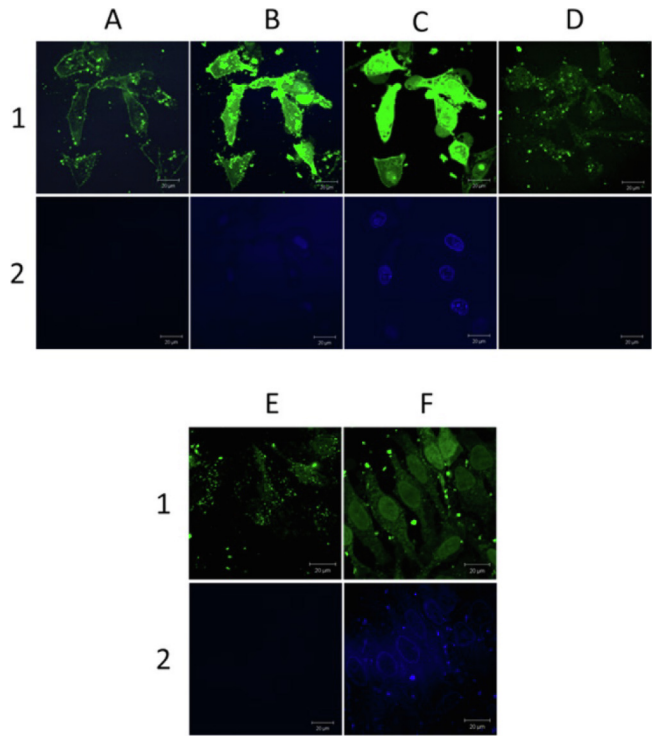

Fig. 53. Phototoxicity of complex in HeLa cells. Row 1 presented both channels for complex and DRAQ 7, and row 2 presented the DRAQ 7 channel only to record toxicity. (A) Immediate uptake of complex evident in images collected after 5 min exposure. (B) No toxicity to cells was observed. After 20 min somewhat toxicity was observed. (C) After 25 min, DRAQ 7 had entered the nucleus of all the cells indicating cell death. (D) After 35 min of exposure to complex in a new location of the same sample that had not been exposed to the laser no entry of DRAQ 7. (E) HeLa cells were incubated with complex for 2 h in dark condition, washed, and DRAQ7 was added. (F) Cells were exposed to continuous irradiation and DRAQ 7 entered the nucleus after 20 min scanning [Adopted from **ref. 109** with permission from American Chemical Society].

used FITC (fluorescein isothiocyanate)- conjugated secondary antibodies to visualize each antibody's cellular location. The complex's imaging compatibility with the commonly used FITC fluorophore was further established by the complex's considerably red-shifted emission wavelength of complex **79b**. Again, immunofluorescent co-stained with complex **79b** and a calcium-binding protein, calnexin found in Er-membrane reveals a clear overlap within MCF-7 cells. From the result at the end, they concluded that a significant amount of complex **79b** localized and targeted the ER-organelles [111].

Metal ion mediated self-assembly had been widely utilized to create a broad range of macrocycles and cages [112,113]. In this regard Thomas *et al.* introduced kinetically inert, water soluble, self-assembled metallomacrocycles (**79c**). These macrocycles contained polypyridyl Ru (II) and Re (I) units which was relevant to PDT sensitizers under investigation. They discovered that complex **79** was efficiently internalised by cells where it acted as a potent photosensitizer by generating reactive oxygen species (ROS) which damaged the plasma membrane. Authors investigated the cellular localization by confocal laser scanning microscopy (Fig. 57) in presence of human breast cancer cells MCF-7 and they found that complex was localized in MCF-7 cell. The cellular reactions were seemed to be typical of oncosis/necrosis processes which was likely to be the result of $^1O_2$ production in cellulo.The alterations had been occurred only when the treated cells were exposed to light indicating a phototoxic response.When cells were exposed with almost the same concentration of complex **79c**, their morphology remained normal under the dark condition. They also investigated the cell viability by MTT assay. Author measured complex **79c**'s photo-cytotoxicity against A2780cis after confirming that it was phototoxic to MCF7 cells and caused damage to biomolecules via singlet oxygen generation. Author picked this second cell line due to its extremely resistant nature to the commonly used Pt (II)-based therapeutic cisplatin. Complex **79c** exhibited significant impact on cell viability under the light condition. The phototoxic index was found to be 206 for the complex **79c** which indicated that complex **79c** exhibited nanomolar cytotoxicity against cisplatin resistant cells [114] (See Fig. 58).

On the basis of disadvantage of Ru-dinuclear complex like $[(Ru(phen)_2)_2(tpphz)]^{4+}$ it was thought that rather high incubation concentrations (>200 mm) was required to get acceptable nuclear staining for confocal laser scanning microscopy. Thomas *et al.* synthesized binuclear Ir (III) Ru(II) complex $[(bhq)_2Ir(tpphz)Ru(phen)_2]^{3+}$ (**80**). Following cell-free investigations they observed that the complex interacted with bovine serum albumin (BSA) with a comparable rise in emission and DNA binding affinity in Sudlow's

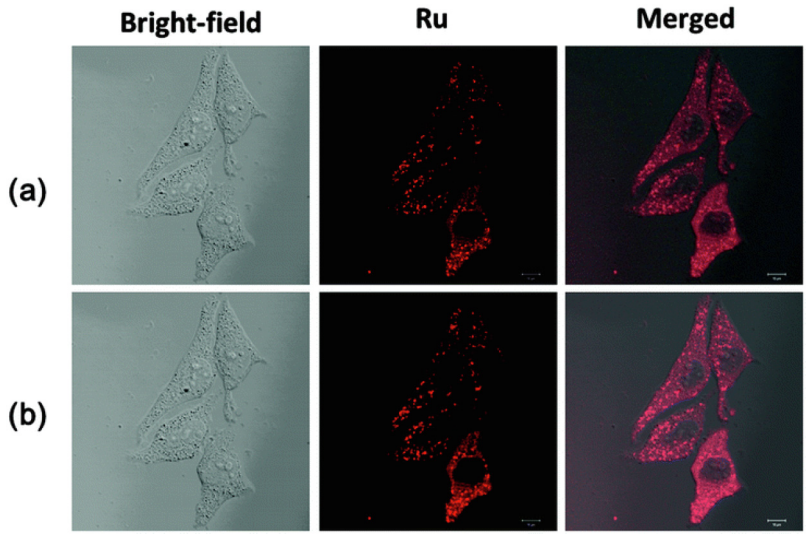

Fig. 54. (a) OPM and (b) TPM images of HeLa cells incubated with complex **75** (10 μM) for 2 h at 37 °C under 458 and 830 nm One- and two-photon excitation. [Adopted from **ref. 110** with permission from Royal Society of Chemistry].

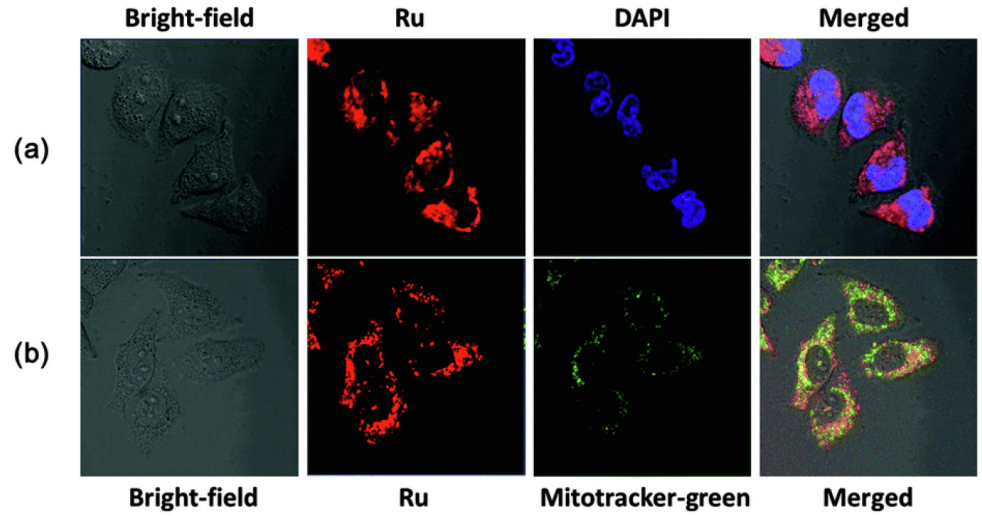

Fig. 55. OPM images of living HeLa cells incubated with 10 μM 75 for 2 hat 37 ^{0}C and also incubated with DAPI (a) and MitoTracker Green (b). [Adopted from **ref. 110** with permission from Royal Society of Chemistry].

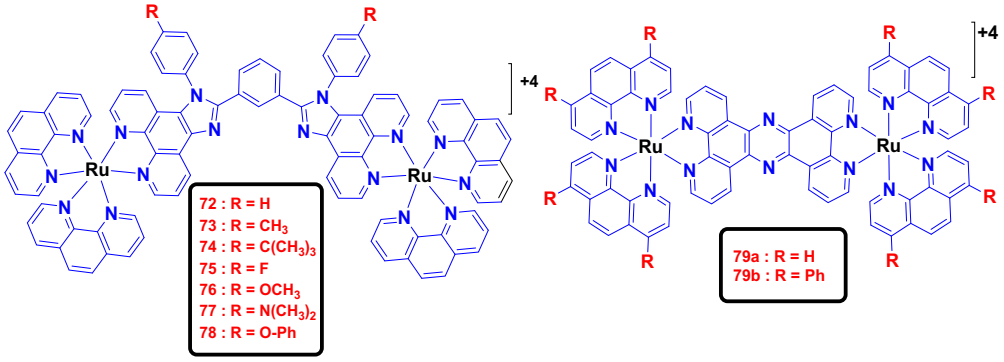

Fig. 56. Structure of complex from **72** to **79b**.

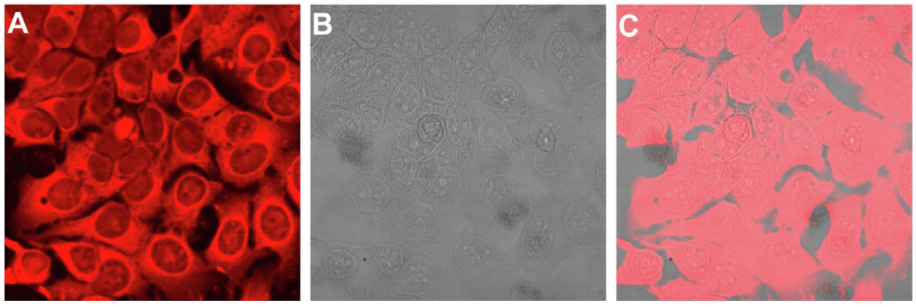

Fig. 57. (A) CLSM images of MCF7 cells stained with complex **79c** at 640–700 nm emission. (B) Phase Contrast image at 485 nm and (C) Merged image. [Adopted from **ref. 114** with permission from Wiley-VCH].

Site I. In contrast, the complex was rapidly absorbed by live cells in serum-free environments where it was bound specifically to cell nuclei and worked as a DNA imaging agent. Author also confirmed that the cytotoxicity of the complex was also significantly changed in the absence of serum proteins. Due to the higher degree of cellular uptake, an elevated amount of oncosis/necrosis was found [115].

6.4. Ru-based nanoparticle:

Nanoparticle research is a rapidly expanding field, with particles ranging in size from ultrafine (1–100 nm) through fine (100–2500 nm) to coarse (2500–10 000 nm). Because of their small size and the leaky vasculature of tumours, ultrafine nanoparticles have long been considered for anti-cancer therapeutics. This leads to an

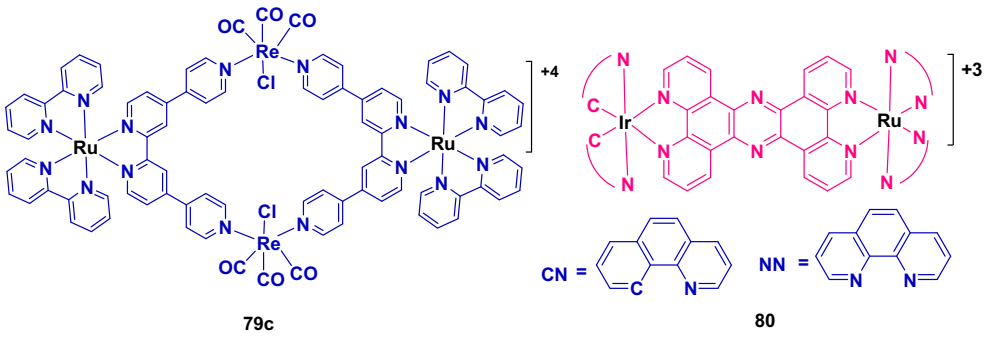

Fig. 58. Structure of complex- **79c** and **80**.

increased permeation and retention rate (EPR) within tumours, resulting in the accumulation of nanomaterials at these sites, allowing for more direct targeting of tumours. Researchers have shown a great deal of interest in conjugating Ru-complexes to nanomaterials of different compositions in order to develop novel types of probes and drugs [116,117]. Here we have represented some nano complexes with their anticancer properties under PDT condition.

Karges *et al.* presented MSNs (mesoporous silica nanoparticles) functionalized Ru (II)-polypyridine complex for cancer-targeted PDT agent. Author involved two tumour targeting methodology, one was MSNs where the nanoparticles were accumulated in tumour tissues due to the EPR effect and the another one was folic acid, most of which absorbed via folate receptors being overexpressed in a number of malignancies. In their report, they derivatized incredibly effective PS [Ru(bphen)2(4,4′-dimethyl-2,2′-bipyridine)]-$[PF_6]_2$ (Fig. 59) with carboxylic acid (**81**) and aldehyde (**82**) and ultimately connected the PS with MSN through amide or imine bond formation. A modified solgel approach was used to prepair mesoporous silica nanoparticles (**G-MSN**) from tetraethyl orthosilicate in presence of CTAB. After that they functionalized the particle on the surface and inside the holes with the help of polyamino linker-**DETATMS** and ultimately, they formed **G-MSN-DETATMS**. Authors created **G-MSN-DETATMS-FA** via covalently attachment of Folic acid (FA). They also connected the complexes **81** and **82** with MSN particle through amine bond and imine bond formation and they obtained G-complex-**81** with FA, G-complex-**83** without FA, G-complex-**82** with FA and G-complex-**84** without FA respectively. The particles were studied with SEM and TEM. In the experiment they found that Ru-functionalized particle exhibited high luminescent property and generated singlet oxygen species upon light irradiation but the particle did not show any toxic effect in dark condition. Upon irradiation at 480 or 540 nm in low nanomolar range the particle without FA demonstrated phototoxic effect but they were unable to differentiate the cancer and non-cancer cells. Upon irradiation particle with FA did not target non-cancerous human normal lung fibroblast cells but cancerous human ovarian carcinoma cells were targeted in low nanomolar range [118]. As another example, complex-**85-**CD_S (Fig. 61**; a**) was synthesized by Mao *et al.* employing CDs modified with a Ru (II) complex (**85**) enabling lysosome-targeted imaging and photodynamic therapy (PDT). The ligand part of the complex had protonated and deprotonated sites. The advantages of the complex **85** was the ability of emission of pH-sensitive light which was required for various lysosome-targeted imaging and photodynamic therapy. They calculated the singlet oxygen species quantum yield of complex **85**, **CD_S**, and complex **85-CD_S** under 450 nm light irradiation with ABDA as the $^1O_2$ indicator and $[Ru(bpy)_3]Cl_2$ as the standard in aerated buffer solutions. From this result they found that complex **85-CD_S** exhibited quantum yield value of 0.18 and 0.48 at pH 7.4 and 5.0 respectively. This result suggested that in acidic condition complex **85-CD_S** generated $^1O_2$ more adequately than in neutral condition. They investigated cellular uptake property of complex **85** and complex **85-CD_S** by confocal laser microscopy in human lung cancer cell A549 (Fig. 60). The increasing nature of time-dependent emission intensity demonstrated that complex **85** and complex **85-CD_S** penetrated the A549 cell and retained in cytoplasm. Colocalization experiment also revealed that they could image lysosomes selectively. Authors also declared that complex **85** and complex **85-CD_S** penetrated into cancer cell with both energy-dependent mechanism and endocytosis pathway. Complexes also exhibited photodamage under one photon at 450 nm and under two photon at 810 nm excitation. Under two photon excitation complex **85-CD_S** exhibited good penetration ability, inhibitory effect against the cancer cell growth [119]. Ghaddar *et al.* also prepared nanoparticles of magnetite-silicon-titanium that were treated with a polypyridyl ruthenium dye (Fig. 61**; b**). In presence of white or green light the dyed-NP_S (**86**) exhibited better ROS generation. The authors investigated the photodynamic effect of the excited NPs against A549 cell. They also proved that under light excitation there was an increased amount of ROS production in A549 NP-loaded cells than the control cell [120] (Fig. 62).

Graphitic-phase carbon nitride (**g-C_3N_4**) nanosheets have gained attention as two-dimensional (2D) semiconductor materials in recent years. This nanosheets have already been constructed as targeted drug delivery carriers and their photochemical as well as electrocatalytic characteristics have been demonstrated. When semiconductor photosensitizers are triggered by light, pairs of electrons and holes are created simultaneously. In this regard Chao *et al.* designed multifunctional photosensitizer, in which they coordinated $[Ru(bpy)_2]^{2+}$ with **g-C_3N_4** nanosheets through Ru–N bonding. In presence of visible light, **Ru-C_3N_4** (**87**) was induced the formation of O_2 from H_2O_2 or H_2O in a hypoxic tumor and at that time it produced ROS (•OH, $•O_2$, and $^1O_2$). Authors investigated the cellular uptake property of this species with the help of confocal laser scanning microscopy (CLSM). They incubated A375 cell with the nano for 24 h and observed red fluorescence during hypoxic conditions. They further investigated intracellular catalase-like activity of **Ru-g-C_3N_4** with the help of peroxide assay kit under 1 % O_2. When they treated with 1 mM H_2O_2 for 30 min they observed significant green fluorescence in A375 cell which indicated high H_2O_2 level in A375 cell. They also confirmed that the nano decomposed the intracellular H_2O_2 levels. Due to the oxidative stress, the cancer cell was imbalanced. Authors also investigated apoptosis through flow cytometry and live-death staining experiment in A375 cell. They observed the apoptosis after PDT. Mitochondrial dysfunction and cell damage was observed to be caused by ROS. The authors also observed the mitochondrial dysfunction and change in mitochondrial membrane potential by this nanomaterial with the help of probe JC-1. At the end the

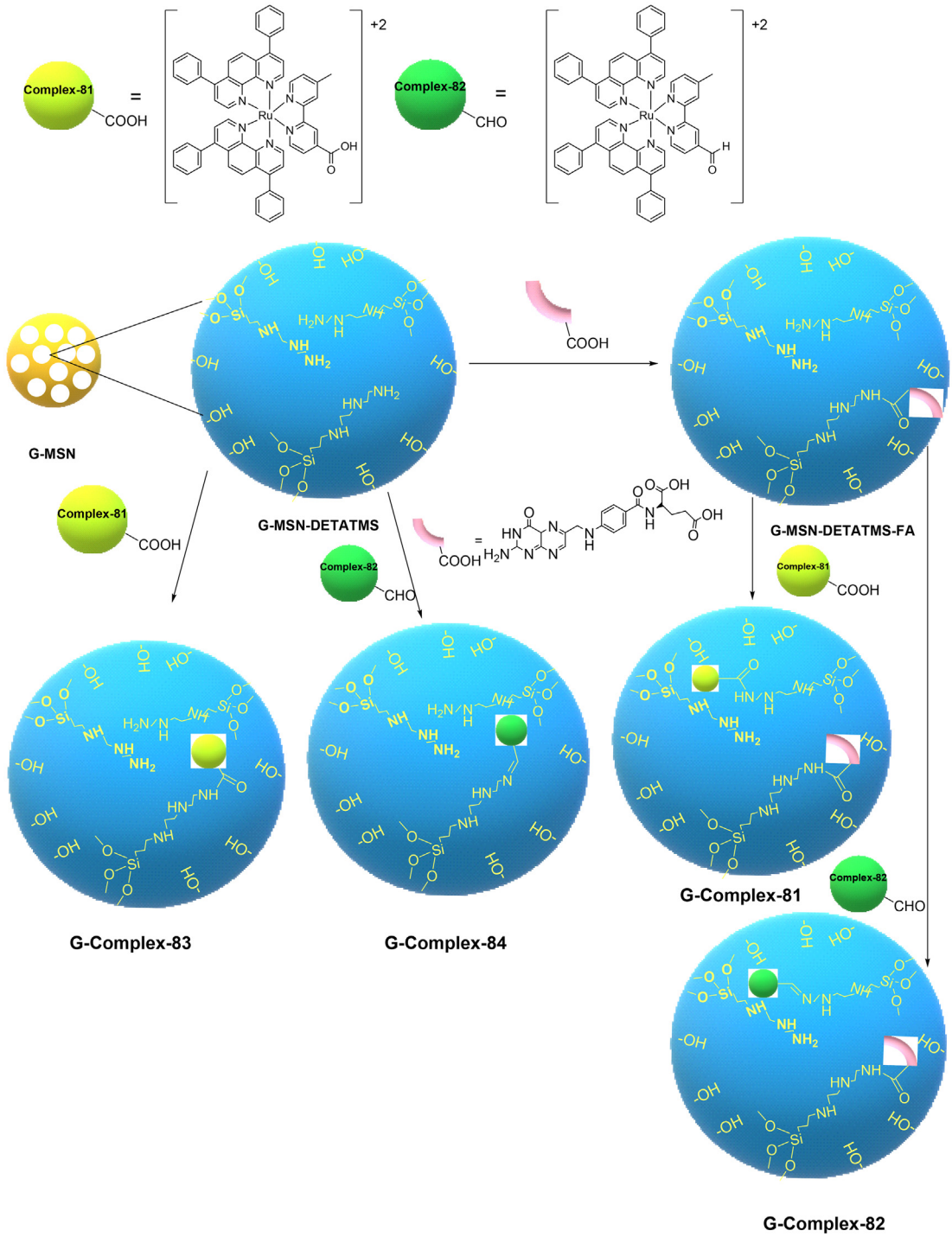

Fig. 59. Karges *et al.* synthesized nano Ru complexes.

authors concluded that numerous ROS generated by **Ru-g-C_3N_4** during irradiation, devastated the mitochondria [121].

6.5. Some other miscllenious Ru-based complexes as PDT agent

After through discussion in the above section, here also we have glued some other polypyridyl complexes which was derivatized by some functional group, amino acid and also cyclometalated ruthenium complex which exhibited PDT effect as well as anticancer property. For example, Hess *et al.* synthesized two $[Ru(phen)_2$-dppz$]^{2+}$ derivatives with different functional groups on the dppz ligand[dppz-7,8-$(OMe)_2$ (**88**), dppz-7,8-$(OH)_2$ (**89**)] and studied as photosensitizers (PSs) for photodynamic therapy (PDT) against different cancer cells. In acetonitrile both the complexes exhibited red phosphorescence and their singlet oxygen quantum yields for (**88**) is 75 % and for (**89**) is 54 % respectively. Cellular uptake andanticancer efficiency are also depended on lipophilicity of a compound and it can be estimated by the determinationof log$P_{o/w}$ value ($P_{o/w}$ is the partition coefficient between octanol and water). From the result they found that complex **89** exhibited high lipophilic nature with log$P_{o/w}$value (-0.20) than the complex **88** with log$P_{o/w}$value (-0.52). In dark condition on HeLa cells monolayer complex **88**

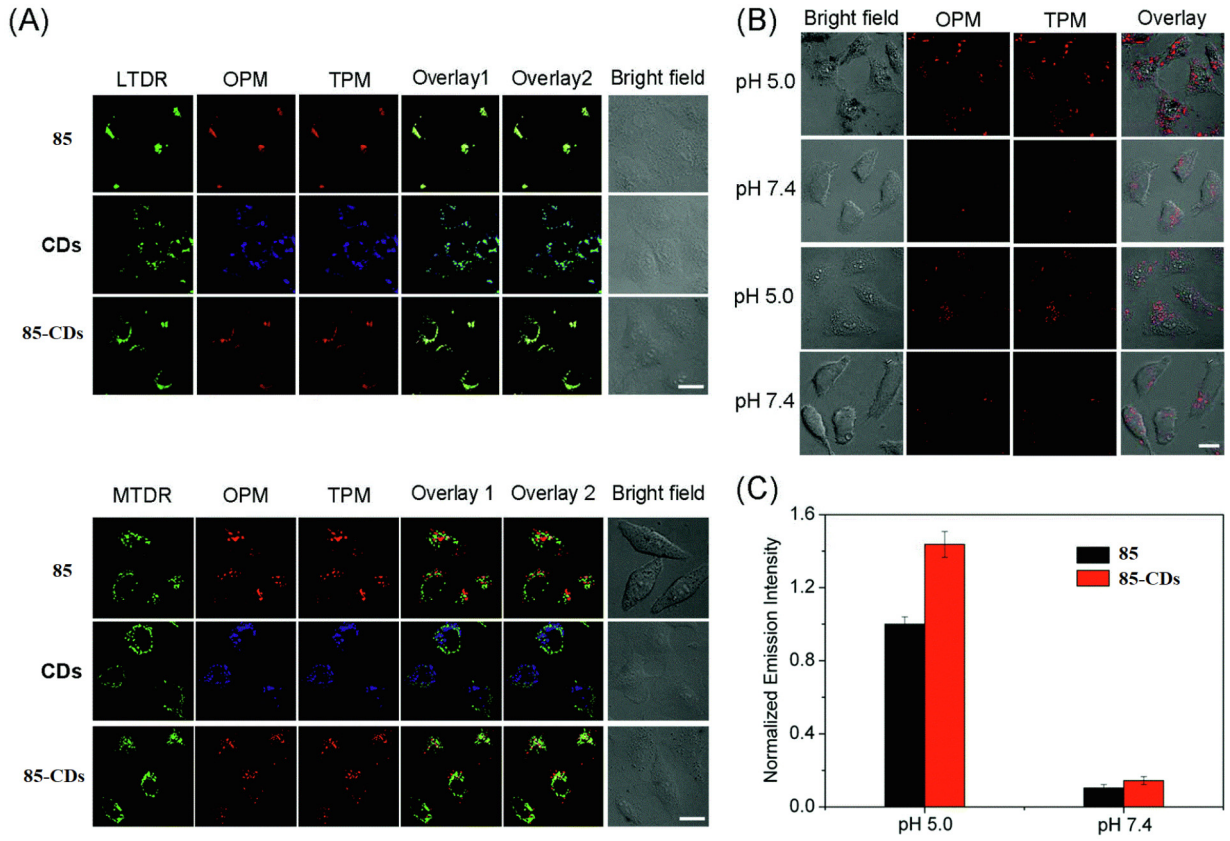

Fig. 60. (A) Confocal microscopy image after A549 cells were incubated with complex **85** (20 μM) for 2 h, **CDs** (200 μg/mL) or complex **85-CDs** (20 μM) for 4 h. (complex **85** and complex **85-CDs**: OPM: λex = 405 nm, TPM: λex = 810 nm, λem = 660 ± 20 nm; CDs: OPM: λex = 405 nm, TPM: λex = 710 nm, λem = 470 ± 30 nm; MTDR and LTDR: λex = 633 nm, λem = 665 ± 20 nm (MTDR) and 668 ± 20 nm (LTDR). (B) pH-dependent phosphorescentimages of complex **85** or complex **85-CDs**-labelled A549 cells. (C) Intracellular phosphorescence intensityof complex **85** or complex **85-CDs** in the attendance of nigericin at different values of pH. Data are expressed as the mean ± standard deviations (SD). Number of cells:10. Scale bars: 10 μm. [Adopted from **ref. 119** with permission from Royal Society of Chemistry].

demonstrated more toxic with IC_{50} value of 36.2 μM than the complex **89** (IC_{50}>100 μM). But both the complexes exhibited non-toxic towards multicellular HeLa spheroids with IC_{50}>100 μM. Upon one-photon irradiation, complex **88** with IC_{50}value of 3.1 μM, exhibited high phototoxicity than complex **89** towards HeLa cell monolayers with IC_{50} value of16.7 μM. Complex **88** was found to be active toward HeLa spheroids with IC_{50} value of 9.5 μM when two-photon irradiation (800 nm) was applied only on complex **88**. Authors also interested to investigate the differences between the OP and TP cell imaging properties of complexes **88** and **89** on cancer cell spheroids. Due to the lower cell penetration property of compounds, the cellular absorption efficiency of cancer cell spheroids and cancer cell monolayers might differ significantly. Under the same experimental conditions, the MCTS penetration ability of complex **88** (50 μM, 12 h) was substantially higher than that of complex **89** (50 μM, 12 h), as shown in (Figs. 63 and 64). As shown in (Fig. 63, B) complex **88** was capable of reaching deep into the core of HeLa spheroids (up to 300 μm). Z-scan images revealed that complex **89** exclusively stained the outer sphere of the HeLa spheroid (Fig. 64, B). There was no signal to be observed from the center of HeLa MCTSs. Because of minimal penetration property of complex **89** into MCTSs and its apparent preferential location on cell membranes, complex **89** was a poor choice for TP-PDT. So, under TP laser excitation, complex **88** showed a greater and clearer phosphorescence in the deeper portions of the spheroids than under OP laser excitation, supporting the deeper tissue penetration and increased PDT efficacy of TP light over OP light. Finally, they concluded that in case of cellular localization and anticancer activity, the functional group on the intercalative ligand had a great impact [122] (Fig. 65).

Two Ru (II)-polypyridyl complexes with two different amino acids viz. tyrosine and tryptophan were synthesized by Ramu *et al.* (**90, 91,**). From isothermal titrationcalorimetry (ITC) studies, they found that these complexes were bound with ct-DNA through an entropically driven process. Viscosity studies also revealed that complexes **90** and **91** bound with ct-DNA through groove binding. The most important character of the complexes was at lower exposure time and they exhibited photo-induced cytotoxic activity in presence of visible light [123].

Zhuang Lv *et al.* synthesized type-I PS based on cyclometalated Ru(II) complexes (**92, 93**) (Where,2,4-difluophenylpyridine was used ascyclometalated ligand). A coumarin moiety which had an excellent chromophore due to its electron-donating and light-harvestingabilities was introduced into cyclometalated ligand to enhance the light-absorption ability and modulated the energy level of cyclometalated Ru (II) complex. Actually, they developed effective PS that exhibited excellent therapeutic effect under hypoxia condition. In visible region complex **93** exhibited lower oxidation potential and stronger absorption than the coumarin-free counter part. Authors investigated the phototoxicity of complexes **92** and **93** to HeLa cell by MTT assay under hypoxia condition. As in (Fig. 66, a) the ratio of PDT cell viability to dark cell viability was found to be 0.94 for complex **92** and 0.22 for complex **93**. The findings suggested that complex **93** demonstrated signifi-

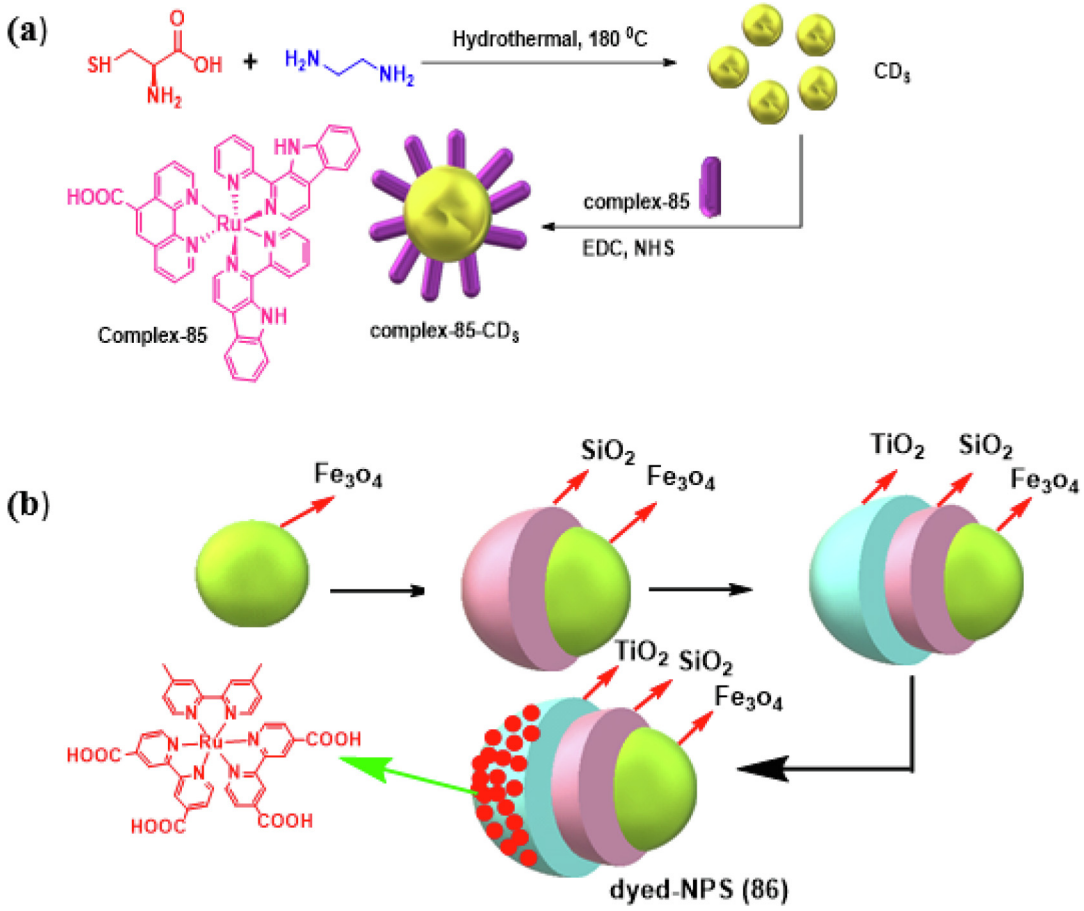

Fig. 61. (a) Complex-**85**-CD_S and (b) dyed-NP_S (**86**).

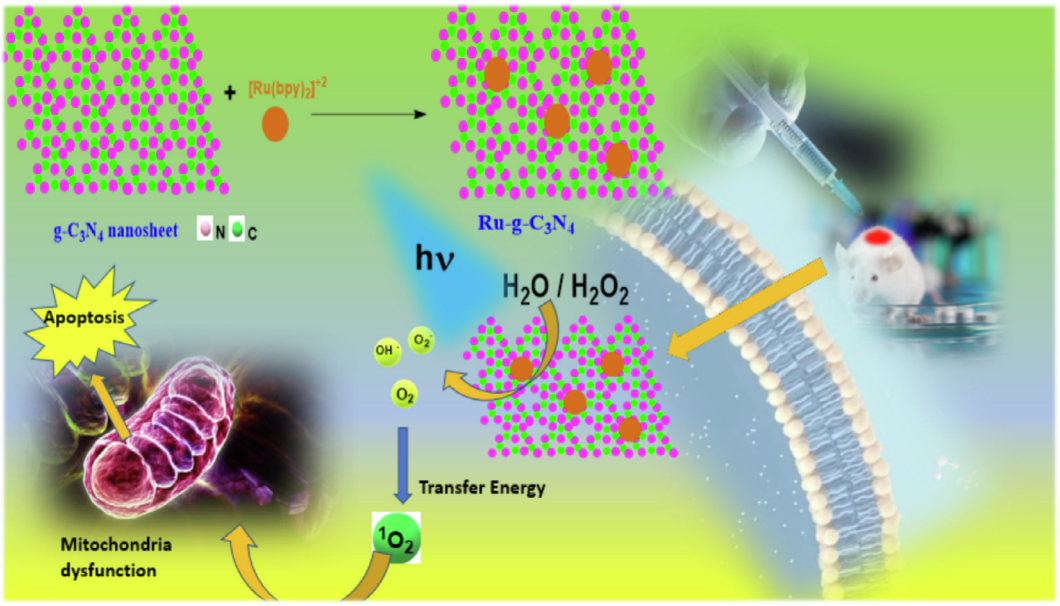

Fig. 62. Mitochondria targeted **Ru-g-C_3N_4** nano.

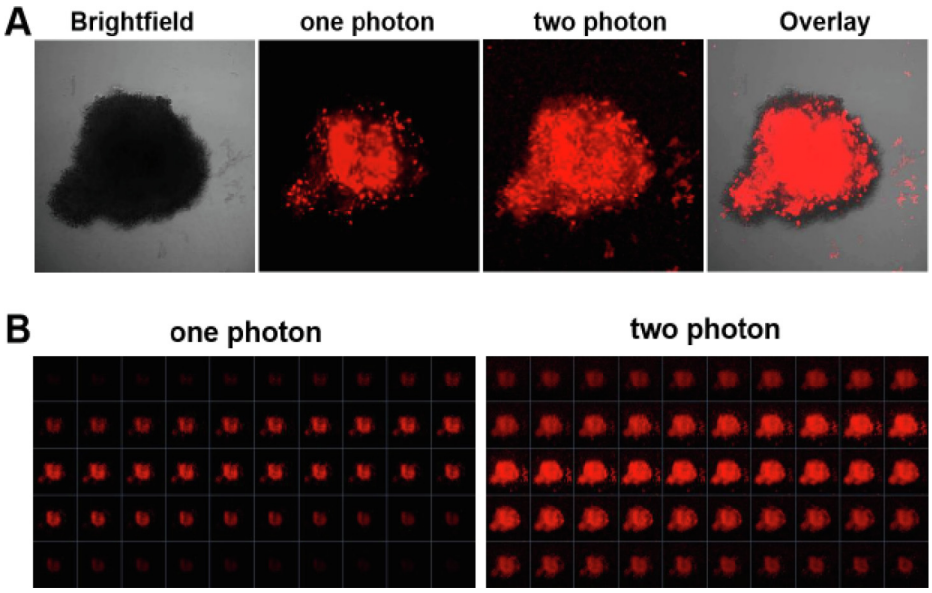

Fig. 63. (A) One Photon and Two Photon images of complex **88** (50 μM) after incubation with HeLa spheroids for 12 h. (B) Z-stack images of the same HeLa spheroids captured every 5 μm along the Z-axis. [Adopted from **ref. 122** with permission from Wiley-VCH].

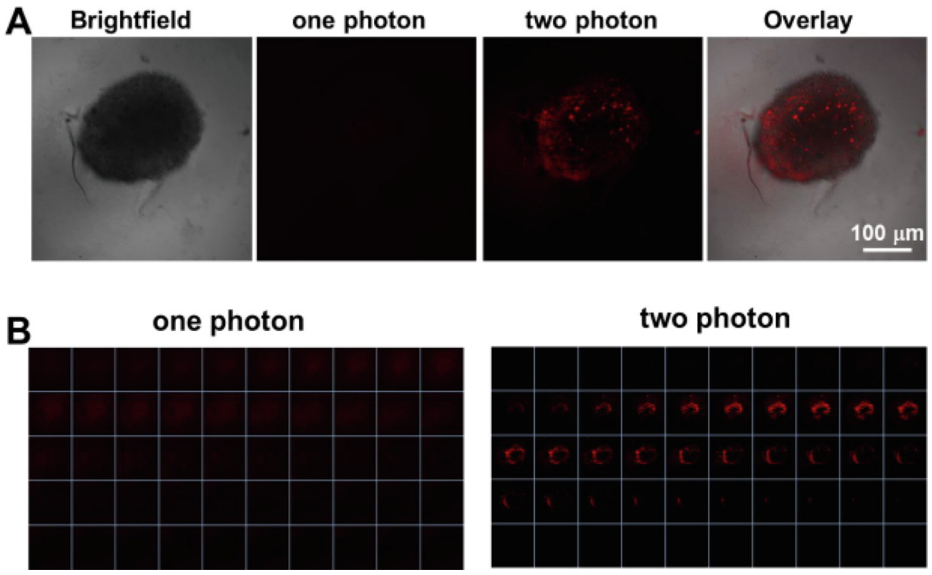

Fig. 64. (A) One Photon and Two Photonimages of complex **89** (50 μM) after incubation with HeLa spheroids for 12 h. (B) Z-stack images of the same HeLa spheroids captured every 5 μm along the Z-axis. [Adopted from **ref. 122** with permission from Wiley-VCH].

cantly higher phototoxicity in Hela cells under hypoxia than complex **92**. As in (Fig. 66b, c) under hypoxia, the percentages of apoptotic cells of each Ru (II) complex were calculated to be 2.83 % for complex **92** and 54.0 % for complex **93**. From the result authors came in conclusion that under hypoxia complex **93** demonstrated better PDT effect as a result of type-I photochemical process and there was direct charge transfer between the excited PS and an adjacent substrate which formed highly-oxidative hydroxyl radicals to damage tumor cells [124] (Figs. 67–69).

In case of two photon photodynamic therapy Zeng *et al.* synthesized GSH-activated dinuclear Ru(II) complex $[(DIP)_2Ru(azobpy)Ru(DIP)_2]Cl_4$ (**Ru-azo**) as aphotosensitizer for two-photon photodynamic therapy. The ligand 4, 4′-azobis (2, 2′-bipyridine) (azobpy) had strongly electron-withdrawing property and acted as a lock that was switched off the luminescence of the Ru(II) complex photosensitizer. GSH played an important role in that case. It could improve the optical properties of the photosensitizer by reducing the azo ligand and due to this the luminescence property of the Ru (II) complex was increased. The complex had a great ability to accumulate in the mitochondria of cancer cells and produced effectual photocytotoxicity under two-photon irradiation. The complex effectively inhibited the growth of cancer cell and killed cancer cells effectively [125].

Cyclometallated complexes also played an important role in the field of PDT. Two cyclometallated Ru complexes (**94, 95**) were synthesized and characterized by Palmer *et al.* 'phpy' presented in the complex which gave the red shift due to Ru → phen and Ru → bpy, metal-to-ligand charge transfer. As a result, light penetrated the

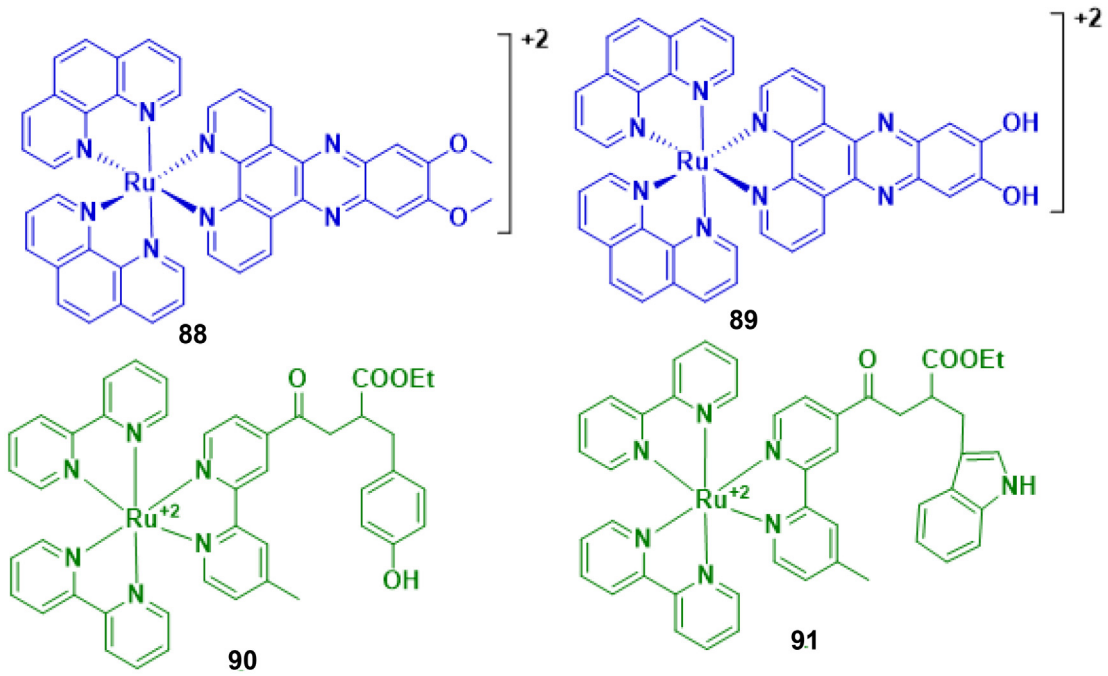

Fig. 65. Structure of complexes **88** and **89** are two $[Ru(phen)_2dppz]^{2+}$ derivatives and complexes **90** and **91** are two Ru (II)- polypyridyl complexes with two different amino acids.

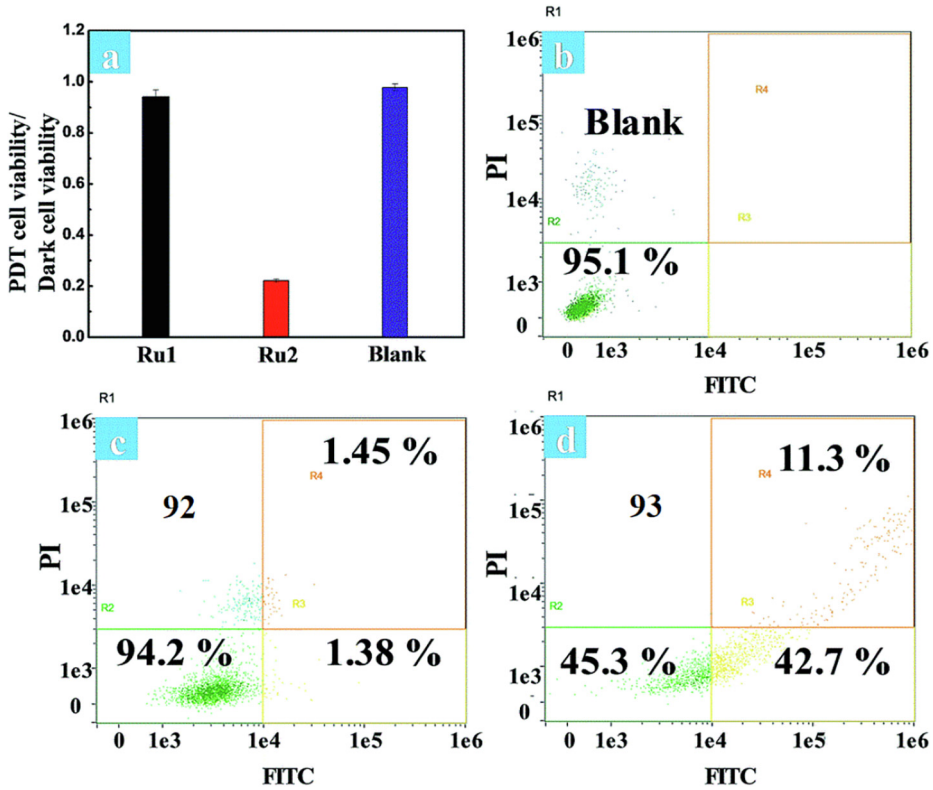

Fig. 66. (a) PDT cell viability and dark cell viability ratios underhypoxia condition. Flow cytometric analysis of cell death encouraged by (b) blank, (c) complex **92** and (d) complex **93** (5 μM) mediated PDT under hypoxia condition. [Adopted from **ref. 124** with permission from Royal Society of Chemistry].

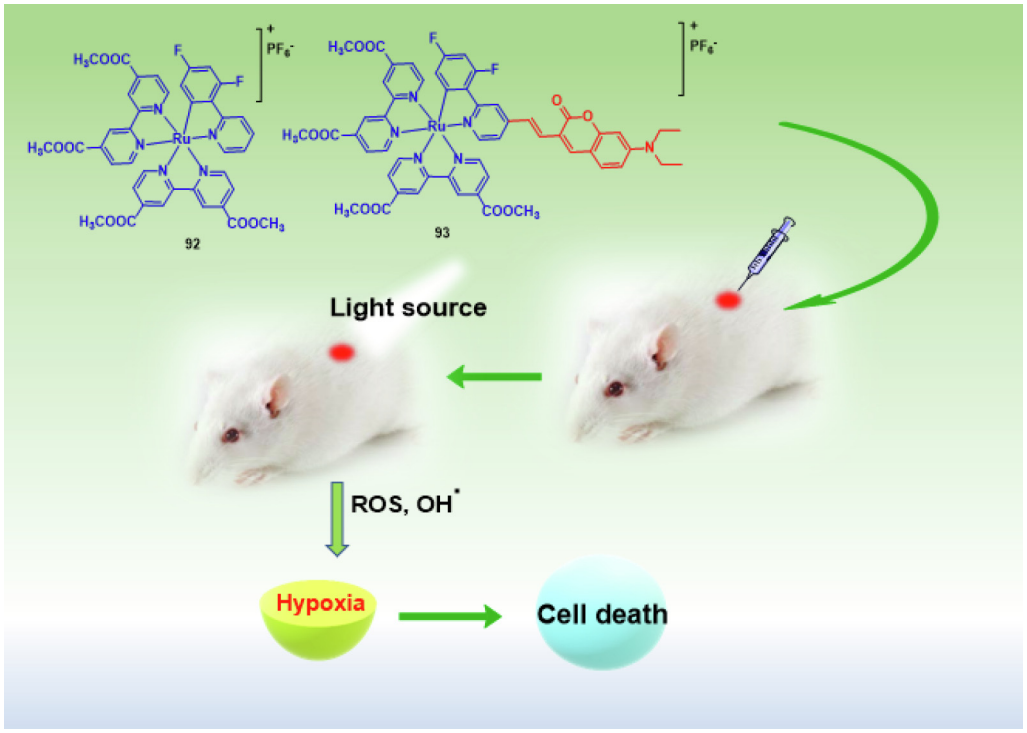

Fig. 67. Structure of complex **92** and complex **93** where complex **93** used as an efficient type I photosensitizer forphotodynamic therapy.

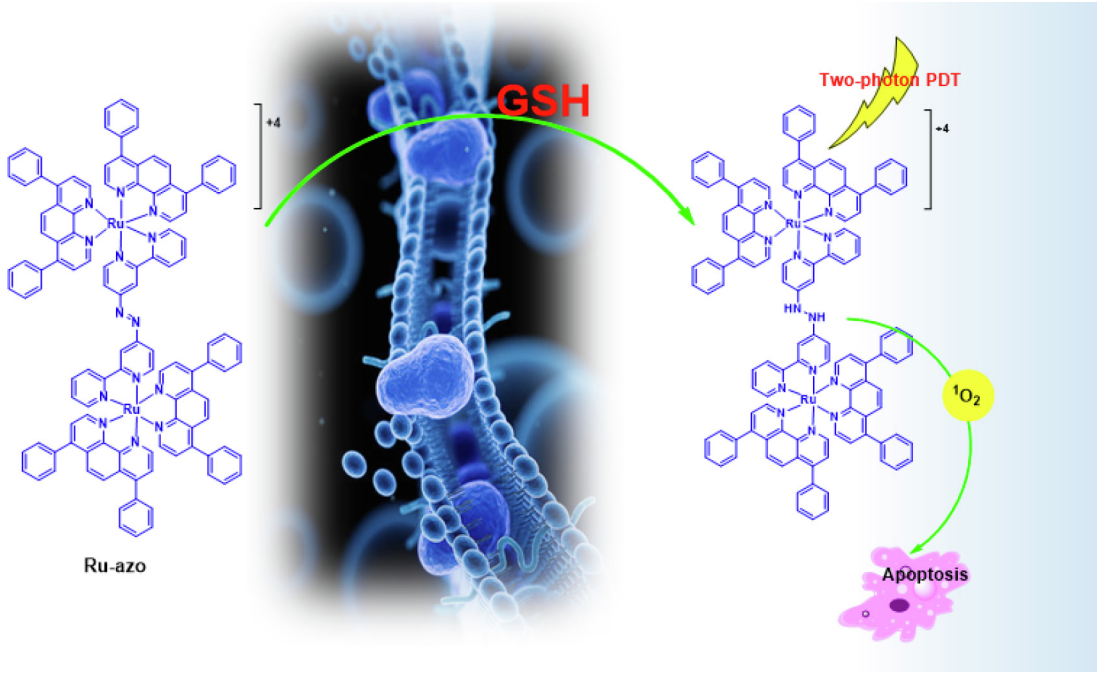

Fig. 68. GSH activation and phototoxicity of **Ru-azo** complex.

tissue more effectively while preserving the efficient photo-induced ligand exchange essential for DNA binding. Photo-aquation was responsible for the 14-fold increase in OVCAR-5 cell mortality that was occurred when cells were exposed to 690 nm light.The author also demonstrated that intracellular GSH might have a role in boosting ligand substitution in the dark and after implying the irradiation that increased the phototoxicity as a result of a combination of photo-induced ligand exchange and GSH reactivity [126].

7. Iridium based complex as a PDT agent

Because of distinct property of cyclometalated iridium (III) complexes like DNA binding, protein–protein interaction inhibition, catalytic oxidation, protein kinase activity inhibition etc., it gave a great impact in anticancer field [127–131]. Recently some complexes were investigated for damaging cancer cell through paraptotic, autophagy pathway. Here in this section, we have discussed some iridium-based PDT active anticancer complexes.

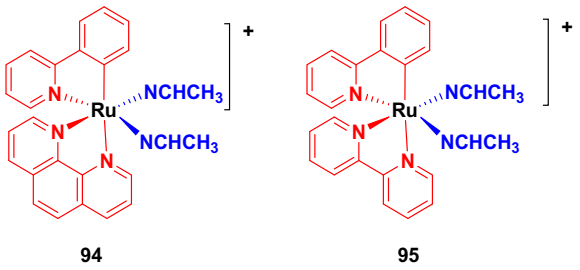

Fig. 69. Structure of complexes **94** and **95**.

Two photosensitizers based on iridium (III) complexes Ir-P(ph)$_3$ (**96**) and Ir-alkyl (**97**), were synthesized by Huang *et al.* These complexes targeted mitochondria and lysosomes respectively. Authors performed the colocalization experiment with the help of Mito-Tracker Green and Lyso Green. From this result they confirmed that complex **96** specifically targeted the mitochondria and complex **97** targeted the lysosomes. The luminescence intensity of complexes **96** and **97** were somewhat reduced after strong absorption at 488 nm light irradiation. The luminescence of MTG and LysoGreen, on the other hand, was virtually totally quenched confirming the better photostability of two complexes. Low concentration of oxygen level in cancer cell reduced the PDT effect. They observed the PDT effect of the complex under hypoxic condition because treatment with complex **96** resulted in relatively greater oxygen concentrations in the mitochondria. They used Annexin V-FITCand PI as an indicator for apoptotic and dead cells. They observed that the early apoptosis was stained with green luminescent Annexin V-FITC on cell membrane, on the other hand, cell was further stained with red luminescent of PI in the nucleus. This observation indicated the apoptosis and cell death. They investigated the PDT effect with the help of flow cytometry (Fig. 70). With increasing the irradiation time, the cell death was also increased. In comparison to irradiation in hypoxia, irradiation in normoxia resulted in a larger percentage of killed cells. When they treated the complex **96** with cell for 12 h at 475 nm irradiation under hypoxia condition for 15 min, they found 3.0 % death cell, but when they used complex **97**, the percentage was reduced to 0.15 %. At the end of their all experiments, they came to the conclusion that under hypoxia, the mitochondria-targeted complex **96** had a better PDT effect than the lysosome-specific complex **97**. With the help of MTT assay authors investigated the PDT effect of the complex (Fig. 71) under normoxia and hypoxia condition. Cell incubated with complex **96** maintained 87 % cell viability for 12 h and that was reduced to 7.6 % after light irradiation and again 2.3 % under normoxia condition. But 3.3 % cell viability was observed under hypoxia condition in presence of light irradiation. It was also observed that the cell viability of complex **97** and untreated cells remained in high percentage under both hypoxia and normoxia condition. Therefore, it can be depicted that mitochondria targeted complex **96** demonstrated good PDT effect under hypoxia condition [132] (See Fig. 72–75).

Mitochondria targeted another two complexes were synthesized and characterized by Yi Li *et al.* In this phosphorescent cyclometalated iridium (III) complexes (**98, 99**) having different bis (NHC) ligands (Fig. 73-a). Authors investigated intracellular distribution with the help of confocal microscopy. They co-stained A549 cell with the complexes and commercial mitochondrial specific dye MTDR (Fig. 73-b). The Pearson's coefficient was found to be 0.89 and 0.85 for complexes **98** and **99** respectively. From the

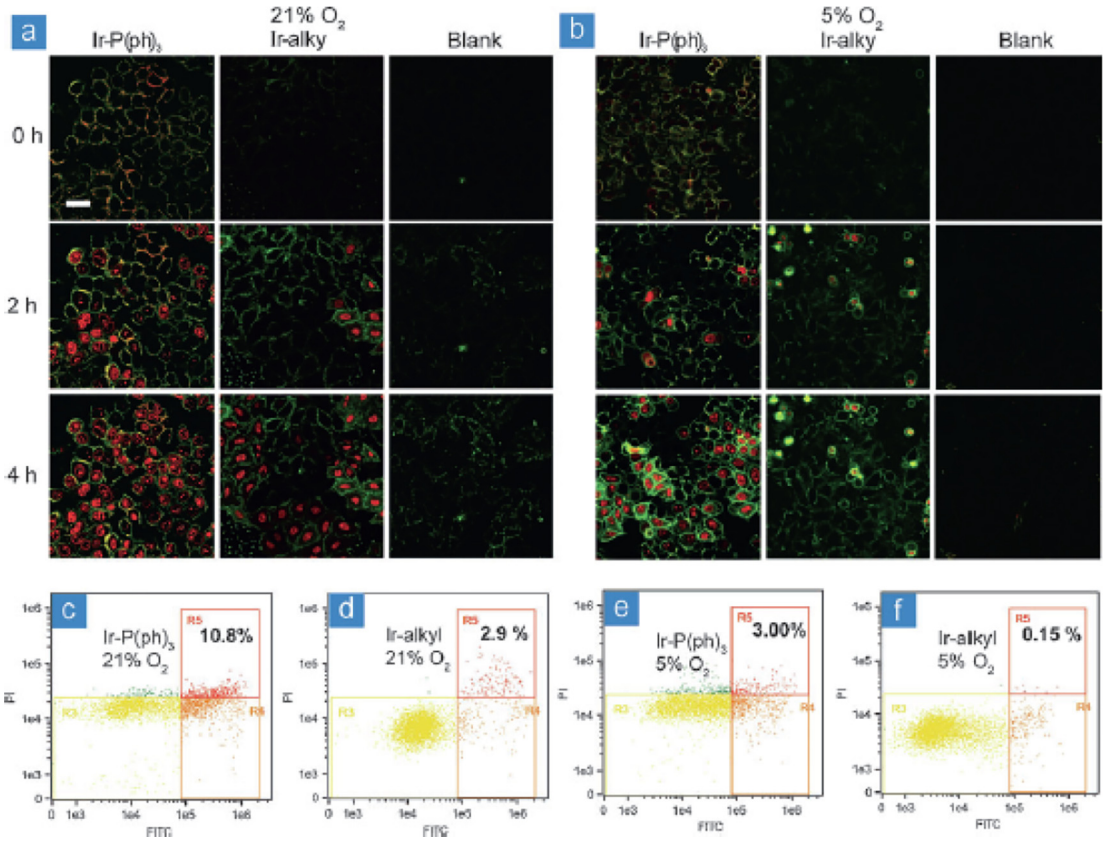

Fig. 70. Confocal microscopy images as well as flow cytometry quantificationof annexin V-FITC- and PI-labeled HeLa cells. [Adopted from **ref. 132** with permission from Wiley-VCH].

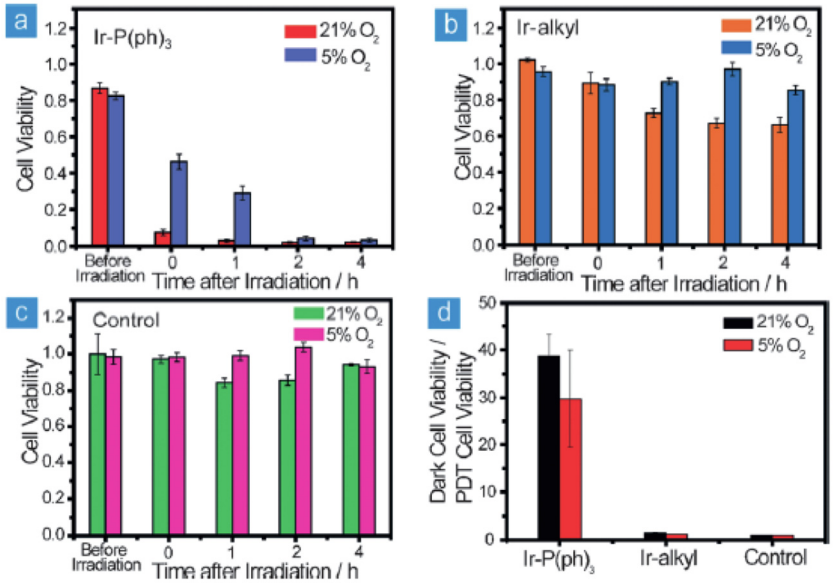

Fig. 71. HeLa cells *in vitro* viability [Adopted from **ref. 132** with permission from Wiley-VCH].

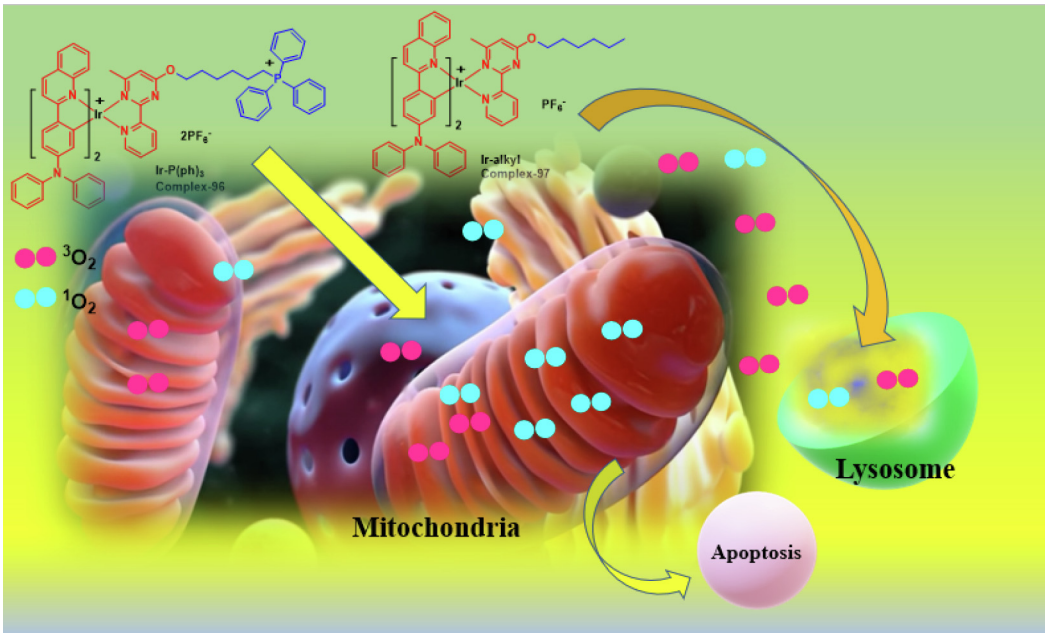

Fig. 72. Mitochondria and Lysosome targeted PDT effect of complexes **96** and **97**.

result they clearly understood that the complexes were localized mainly in mitochondria of A549 cell. From the ICP-MS study the author also confirmed the mitochondrial localization. Both the complexes enhanced intracellular ROS levels and exhibited strong absorption around 450 nm and weak absorption around 630 nm. The IC_{50} value was found to be 0.012 ± 0.004 and 0.037 ± 0.004 μ M in presence of light that was lower than the value in dark condition. They also obtained the PI values of 125, 531, 44 and 65, against A549, A549R, HeLa and U87 cells. As compared to the control and dark, the intracellular ROS level of complex **98**-treated A549 cells exhibited a considerable increase after irradiating at 630 nm for 10 min. Hence, from all studies it was understood that complex **98** acted as a potent PDT agent [133].

Three Ir (III) complexes (**100**, **101**, **102**) were synthesized by Sun *et al.* incorporating guanidinium groups as ligands (**Fig. 74a**). The

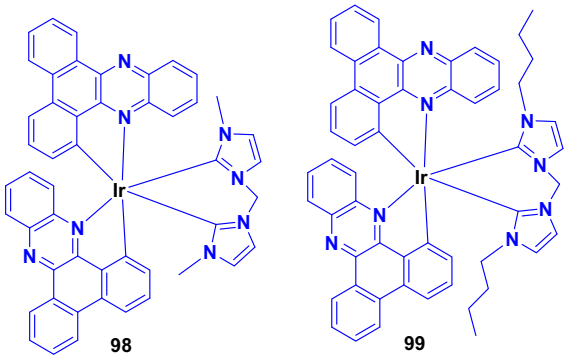

Fig. 73a. Chemical structure of complex-**98** and **99**.

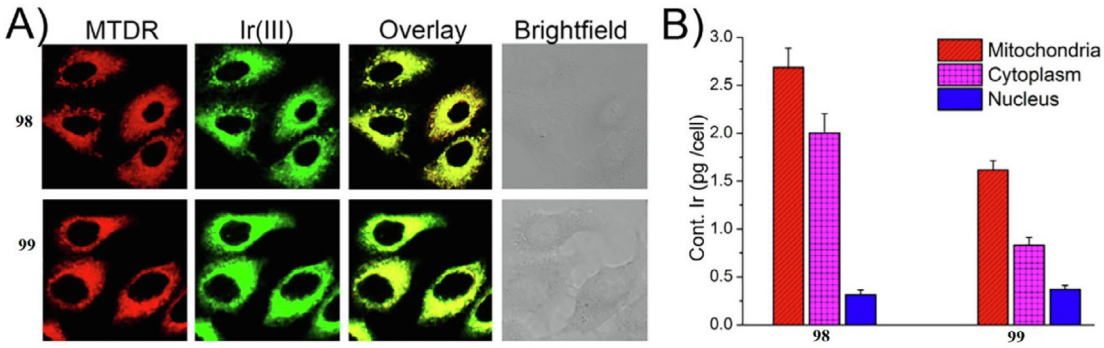

Fig. 73b. A) Intercellular localization of complexes **98** and **99** (10 μM) by confocal microscopy. B) By ICP-MS determination of complexes **98** and **99** in cellular compartments of A549 cells. [Adopted from **ref. 133** with permission from Elsevier].

singlet oxygen species is the most important factor in case of PDT. In presence of visible light at 425 nm the singlet oxygen quantum yield was found to be 0.68, 0.56 and 0.51 for complexes **100, 101, 102** respectively. From this result the authors depicted that all the complexes generated singlet oxygen under visible light condition. The phototoxicity test was performed with various cancer cell lines. Complex **100** exhibited high phototoxic index (PI) against HepG2 (425 nm) cells and the value was found to be >387. Authors also observed that among the three complexes, complex **100** demonstrated more significant and selective anticancer effect against various cancer cell lines. Flow cytometry and confocal imaging were used to confirm the mitochondrial localization of complex **100**. The decrease in red (JC-1 aggregates) to green (JC-1 monomers) fluorescence intensity ratio indicated the mitochondrial depolarization. When they tested the complex **100** in the cell under both light and dark conditions, a significant loss of MMP was found as indicated from the enormous shift in red to green fluorescence (**Fig. 74-b (A)**) and they also investigated the red to green fluorescence ratio with the help of flow cytometry (**Fig. 74b (B)**). Under dark condition the intensity ratio was found to be control: 40.6 ± 2.1, 20 μM complex **100**: 30.7 ± 1.3, 50 μM complex **100**: 22.8 ± 2.1, 100 μM complex **100**: 12.9 ± 0.8 and under light condition the value was control: 37.4 ± 1.9, 1 μM complex **100**: 30.5 ± 1.4, 2 μM complex **100**: 17.0 ± 0.8, 5 μM complex **100**: 6.9 ± 1.3. This result revealed that complex **100** affected the mitochondrial integrity in presence of light than in the dark condition [134].

Because of their advantageous photophysical characteristics, transition-metal complexes were capable of light-triggered toxicity had gotten a lot of attention in PDT research. In this regard Chao *et al.* synthesized mitochondria targeted Ir (III) cyclometalated co-drugs (**103**–**106**). In that study authors used $^1O_2$ scavenger 1, 3-diphenylisobenzofuran (DPBF) to determine the ability to generated ROS. The quantum yield was found to be 0.68, 0.74, 0.70 and 0.53 respectively. To investigate the intracellular distribution of the complexes, the authors performed the co-localization study by using MitoTracker green with the help of confocal laser scanning microscopy (CLSM) on HeLa cell. High colocalization coefficient ranging from 0.82 to 0.86 was observed from that experiment. For better investigation the author also performed the ICP-MS study under the same condition. From this both experiments the authors detected that the complexes were appeared to be able to traverse through mitochondria and assisted the transport of a DCA moiety to the organelles. So, form the overall observation based on all the complexes they came to conclude that complex **103** in particular showed the greatest efficacy in both monolayer cells and in hypoxic MCSs, making it a suitable candidate for cancer-specific TP PDT [135].

The use of two-photon at near-infrared light excitation in photodynamic treatment (PDT) is a very effective approach to avoid the use of shor twavelength UV or visible light, which cannot penetrate into biological tissues and is, therefore, detrimental to healthy cells. In this regard Gao *et al.* synthesized four cyclometalated Ir (III) complexes (**107**–**110**) (Fig. 76a) for two photon photodynamic therapy. Authors investigated the quantum yield of $^1O_2$ generation for all the complexes and they found that the quantum yield values of complexes **107** and **109** were 0.85 and 0.95 respectively. Due to the presence of electron withdrawing methoxy group present on the complex **109**, the quantum yield value was higher in case of this complex than complex **107**. Very low quantum yield

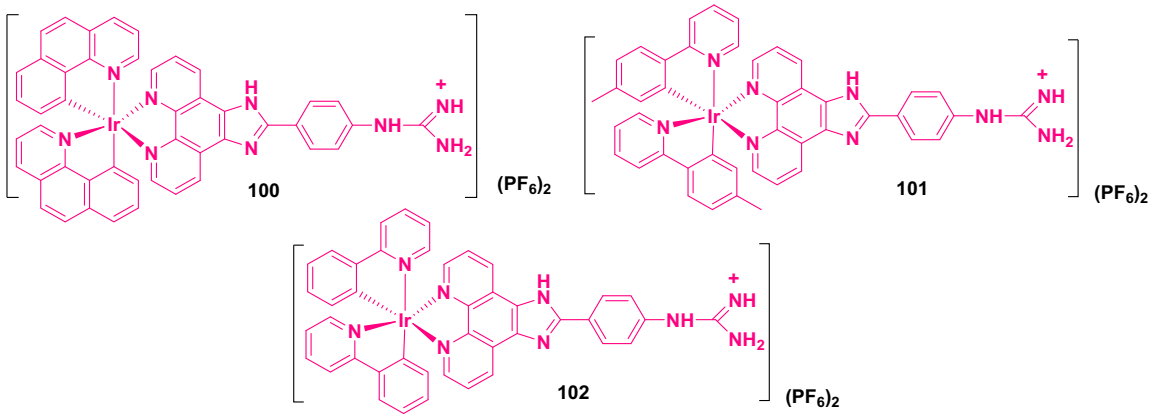

Fig. 74a. Structure of complexes **100**, **101**, and **102**.

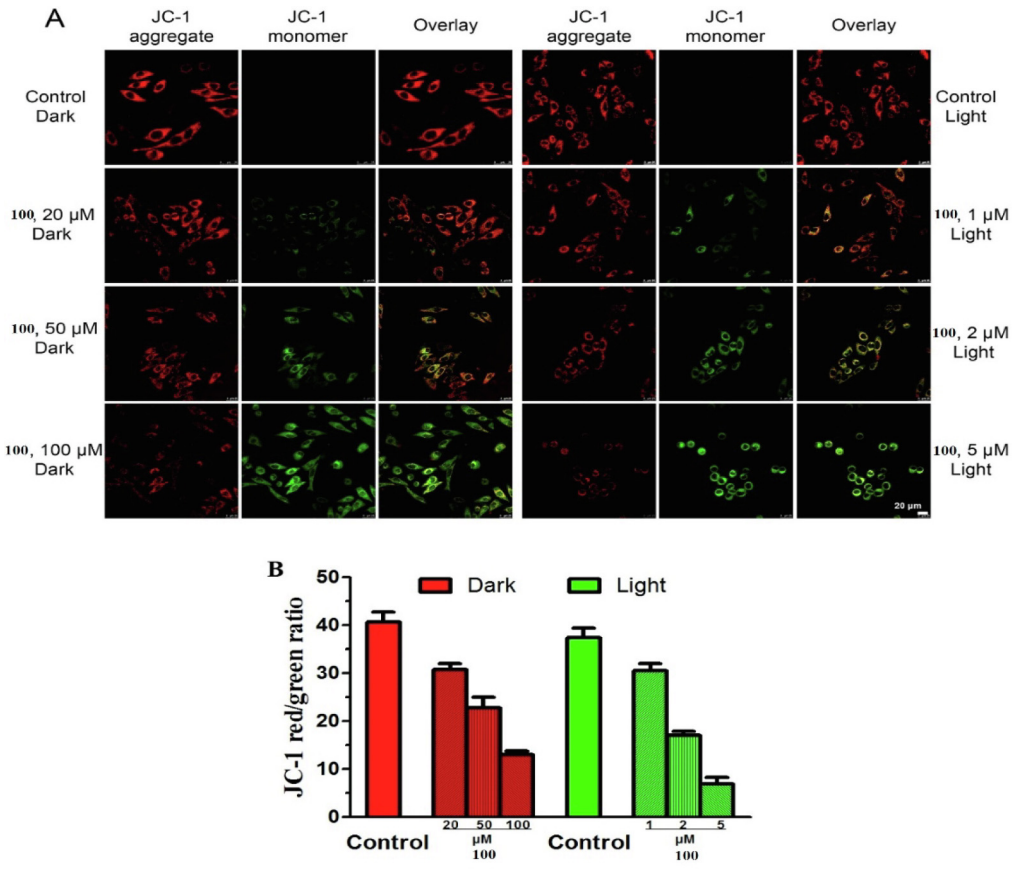

Fig. 74b. (A) Confocal microscopy for visualizing JC-1-stained cells. (B) Flow cytometry and JC-1 staining were used toinvestigated the role of complex **100** in MMP. HepG2 cells were treated with different concentrations of complex **100** for 6 h. 488 nm was the JC-1 excitation wavelength. [Adopted from **ref. 134** with permission from Elsevier].

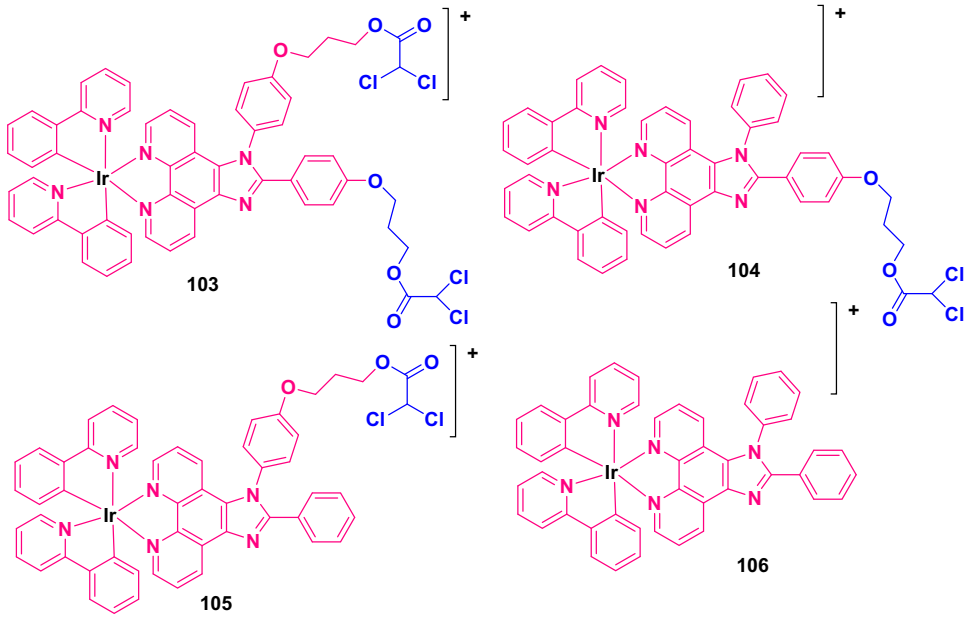

Fig. 75. Structure of complexes **103** to **106**.

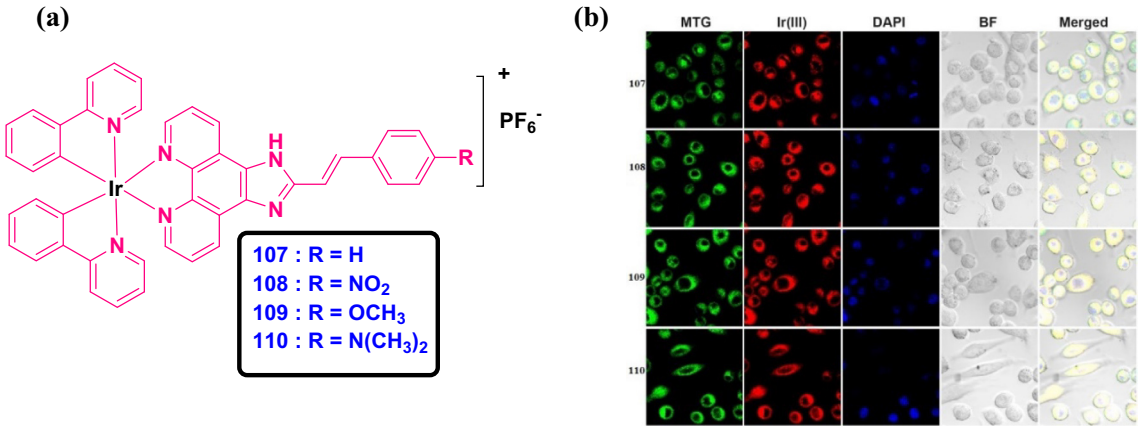

Fig. 76. (a) Structure of complexes **107** to **110** (b) Cellular localization of complexes **107–110** by two-photon confocal laser scanning microscopy on human cancer cells A549 in PBS containing 0.1 % (v/v) DMSO: MTG; Ir(III) complexes(**107–110**), red channel; DAPI, nucleus (DNA) dye,blue channel; BF, bright field; Merged, overlay of the four channels onthe left side. [Adopted from **ref. 136** with permission from American Chemical Society].

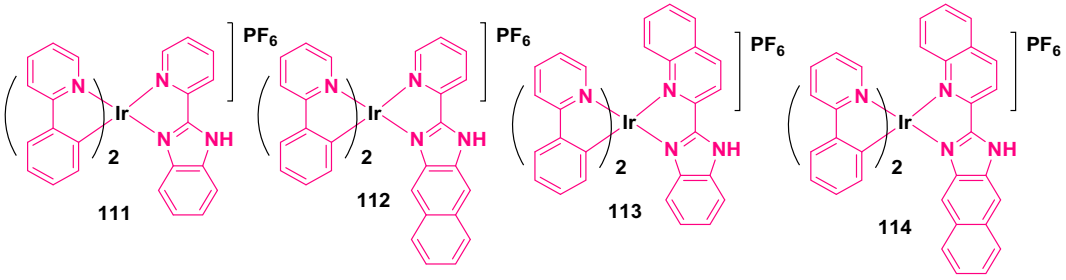

Fig. 77. Structure of complex from **111** to **114**.

value was found in case of complex **110** due to presence of electron donating group. This result indicated that singlet oxygen production could be modified by changing the substitution on ligand side and also the high quantum yield values of the complexes **107** and **109** made them good cell imaging as well as also PDT agent. Authors also used the RB as a standard for examined the two-photon absorption cross section. The two-photon absorption cross section was found to be 113–168 GM. They also investigated the cellular localization of the complexes on A549 cell with the help of confocal lasers canning microscopy (CLSM). All the complexes exhibited red luminescence in the cell under two-photon excitation (Fig. 76b). The signal from the complexes was well overlapped with the commercial mitochondrion-specific dye MTG. But when they used DAPI, poor correlation coefficient was found in such case. The research suggested that the complexes would be used as a mitochondrion-specific dye in cell biology and not only that they could be also used as a photosensitizer for TP-PDT in medicine [136] (See Fig 77).

In case of lysosomes damage Mao *et al.* designed and synthesized four cyclometalated Ir (III) complexes (**111 to 114**) with benzimidazolederivatives as ligands. Author investigated the cell apoptosis with the help of annexin V – fluoresceinisothiocyanate (FITC) assay. They incubated the HeLa cells with the four complexes for 24 h in presence of both light and dark condition. They observed that in dark condition small portion of complex-treated cells was annexin V positive but when they increased the light irradiation, the percentage of cells in apoptotic phase was increased (Fig. 78a). They also investigated the induced apoptosis through the lysosomal damage by the release of cathepsin B. The main function of cathepsin B was to cause apoptosis, when lysosomes were damaged through the release of cathepsin B and other hydrolases which triggered the release of cytosol. They detected cathepsin B by Magic Red MR-$(RR)_2$ staining. Also, they observed that after incubation with the complexes for 12 h in dark, the fluorescence of Magic Red MR-$(RR)_2$ was punctated in HeLa cells (Fig. 78b). But, upon irradiation of light, Magic Red MR-$(RR)_2$ exhibited dispersive pattern in cytoplasm. From the result authors confirmed that cathepsin B was released from lysosomes and after PDT treatment, lysosomal membrane permeabilization took place [137] (See Fig 79).

Mao *et al.* synthesized another lysosomes targeted four Ir(III) cyclometalated complexes (**115 to 118**) with β-carboline ligand. Authors investigated that in presence of visible light irradiation the complexes exhibited phototoxicity against cancer cell lines. Among all the complexes, comlex-**116** exhibited PI > 833 [425 nm LED light for 15 min (36 J cm^{-2})] against A549 cell. Author also demonstrated that through lysosomal destruction and the release of cathepsin B, 2-mediated PDT primarily promoted caspase- and ROS-dependent apoptotic cell death [138].

Another Ir (III) complex was synthesized by Yang *et al.* by incorporated the iridium center into donor-π-donor ligand (**119**). Author investigated the cytotoxicity of this complex by MTT assay with the help of HeLa cell. After incubation with different concentrations of the complex, no change in cell viability of HeLa cell was observed in Fig. 80a. Author used flow cytometry to quantify the endocytosis of complex by HeLa cells. From (Fig. 80b) it was indicated that>90 % of the HeLa cells incubated with 20 μM concentration for 2 h., which indicated significant uptake of complex by live cells. After that they incubated the HeLa cell with the complex for 2 h and then observed luminescence in cells (Fig. 80**c**) at 405 nm of excitation. From the overlay image in bright field and luminescence image, they confirmed that complex **119** was mostly found

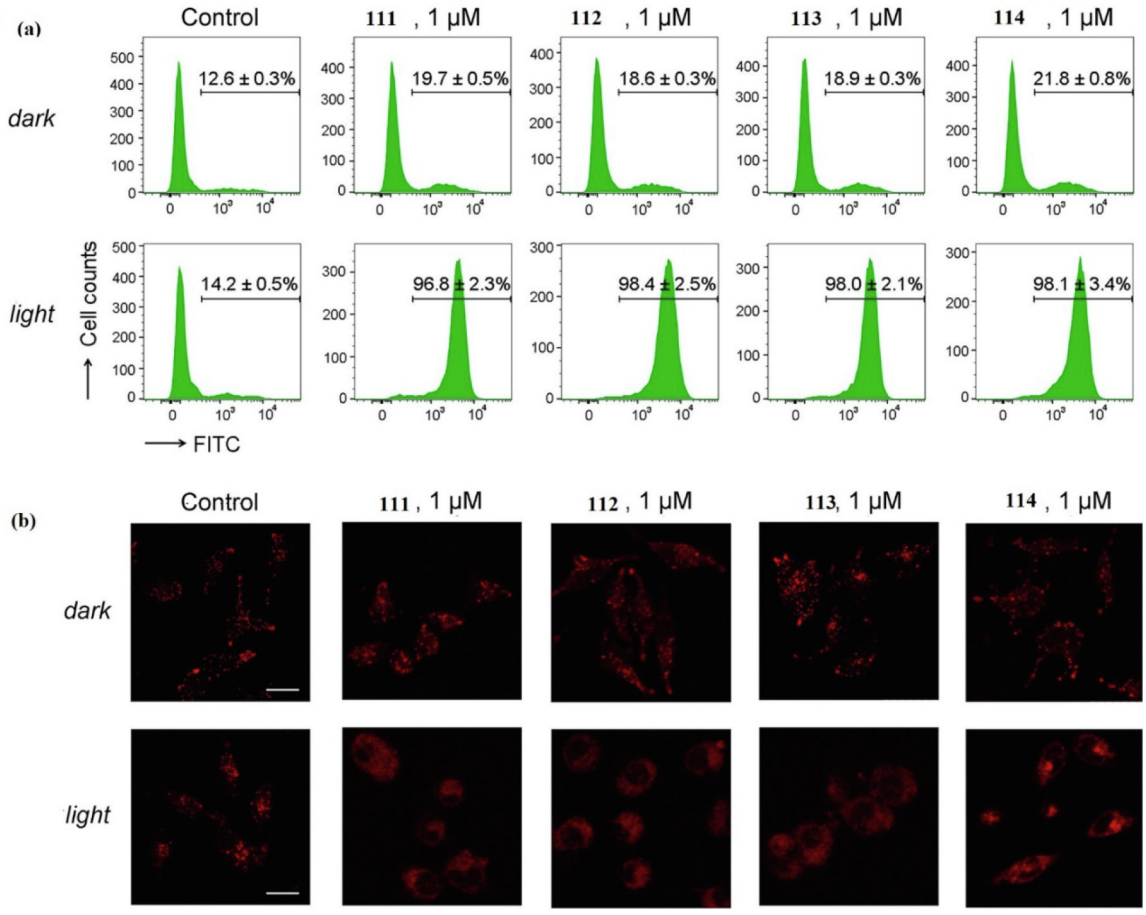

Fig. 78. (a) HeLa cells labeled with annexin V – FITC after incubation with complexes **111**–**114** (1 μM) for 24 h in both, absence or presence of light. (b) Changes in cathepsin B positionencouraged by complexes **111**–**114** (1 μM) for 12 h in both absence orpresence of light. Magic Red MR-$(RR)_2$ was excited at 543 nm, and the emission was noted at 630 ± 20 nm. Light condition: 425 nm LED lightarray, 1.2 J cm^{-2}. [Adopted from **ref. 137** with permission from American Chemical Society].

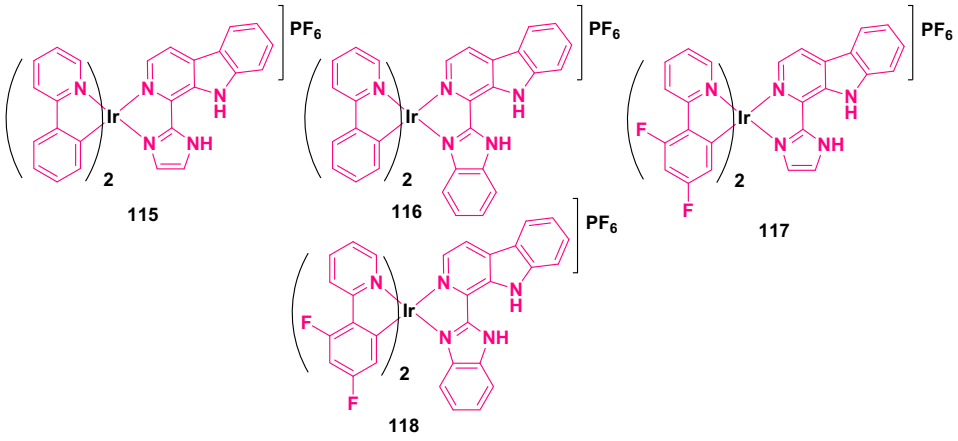

Fig. 79. Structure of complexes from **115** to **118**.

in the cytoplasm, with no evidence of nuclear uptake. After that author also intratumorally injected the complex on HeLa tumor bearing mice and irradiated by a 730 nm CW laser for 10 min in every 2 days interval for control experiment. After 14 days of this experiment, they used H&E staining for investigation of the affectedtumor tissues. From the result they found that high level of damaged tissues were found when the cell was treated with complex under incident of laser than the complex without incident of laser. At the end of experiment, they concluded that the complex damaged the cancer cell in presence of 730 nm CW laser [139] (See Figs. 81–84).

Mitochondria targeted another Ir(III) complex **NIR-Ir-XE** (**120**) was synthesized by Wong *et al.* In that case they conjugated the Ir-complex with xanthene dye. Author performed the cytotoxicity by MTT assay. Under the dark condition, not only the complex exhibited very low cytotoxicity towards MCF-7 cell, but also exhib-

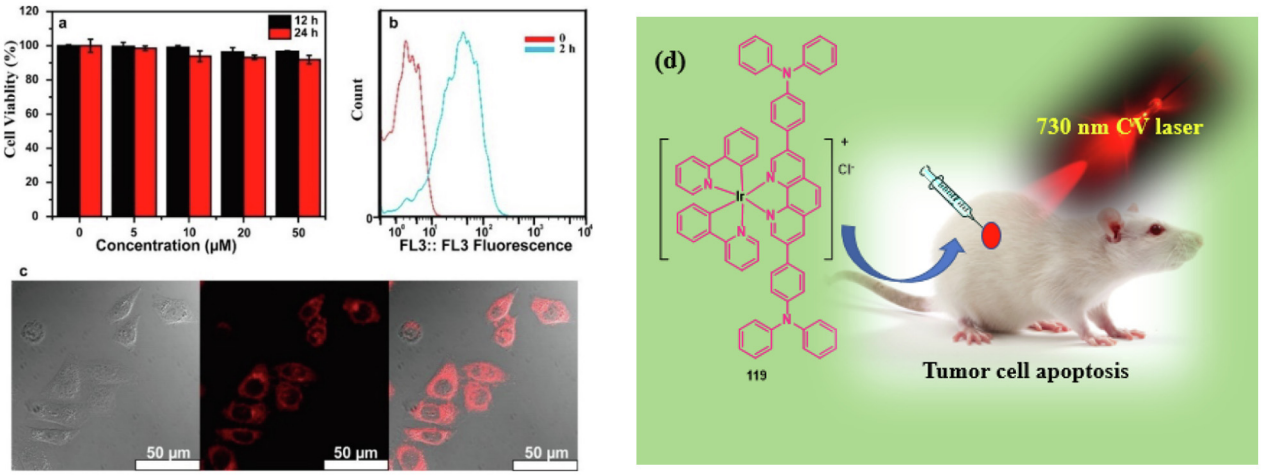

Fig. 80. (a) HeLa Cell viabilitymeasured using an MTT assay after the incubation of different concentrations of complex **119** for 12 and 24 h, respectively. (b) Flow cytometry study of HeLa cells incubated with complex **119** (20 μM) for 2 h. (c) Left indicated bright field, middle indicatedconfocal luminescenc, andright indicated overlayimages of HeLa cells incubated with complex **119** (20 μM) for 2 h. (d) pictorial representation of 730 nm CV laser on HeLa cell model. [Adopted from **ref. 139** with permission from American Chemical Society].

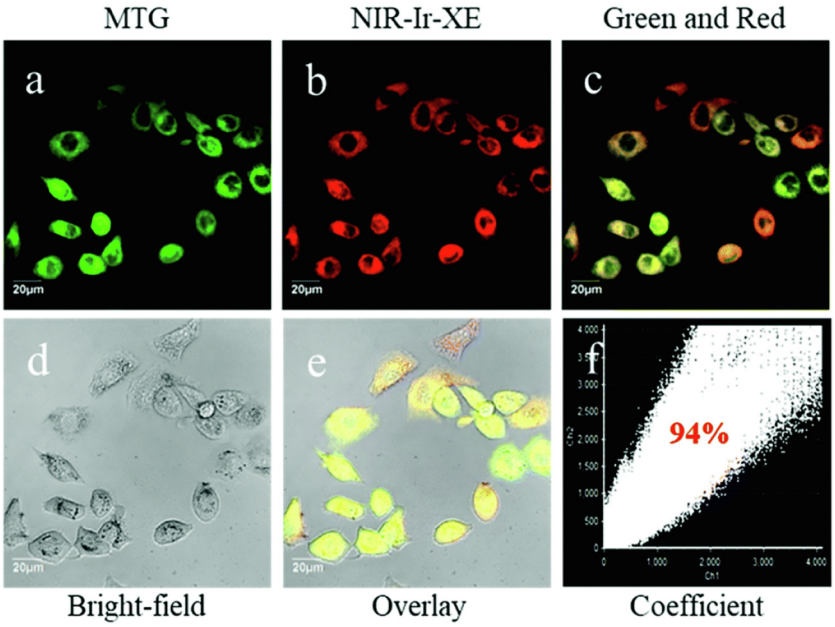

Fig. 81. Confocal images of MCF-7 cells incubatedwith complex **120** (5 μM) for 30 min followed by co-staining with Mito-TrackerGreen FM (a) green channel of MTG; (b) redchannel of **NIR-Ir-XE**; (c) overlaid green and red channels; (d) brightfield;(e) overlaid green, red, and bright-field channels; (f) Pearson's correlationcoefficients of green and red channels. [Adopted from **ref. 140** with permission from Royal Society of Chemistry].

ited dose dependent cytotoxicity under light irradiation. Author also investigated the intracellular localization of the complex and for this they used Mito-Tracker Green (MTG). Confocal microscopic image exhibited that most of the complexes were localized in the mitochondria. For better understanding, they observed the co-localization image between **NIR-Ir-XE** and MTG inMCF-7 cells. They clearly observed the red fluorescence of **NIR-Ir-XE** which was nicely overlapped with the green fluorescence of MTG and got the Pearson's correlation coefficient of 0.935. For detecting ROS as by-products of singlet oxygen generation, authors also used the indicator non-fluorescent agent dichlorofluorescein diacetate (DCF-DA). A strong fluorescence from the oxidized DCF-DA in the green channel was observed after addition of **NIR-Ir-XE** in presence of light irradiation. But when they used MCF-7 without **NIR-Ir-XE** as a control group, there was no discernible increase in fluorescence. This result specified that **NIR-Ir-XE** generated ROS in MCF-7 cell [140].

Another important organelle is endoplasmic Reticulum. Nam *et al.* presented four Ir(III) complexes (**121 to 124**) that were created using a logical technique to examine protein changes caused by ROS. Among the four complexes, **123** and **124** exhibited cytotoxic activity through ROS generation and localized in the ER in low concentration and weak energy condition. Authors also disclosed that by using two-photon irradiation, complex **123** was able to effectively trigger cancer cell death. They also described the routes of action for Ir (III) complexes for both protein cross-linking and protein oxidation by using MS. The considerable damage was mostly observed in proteins around the ER as well as in

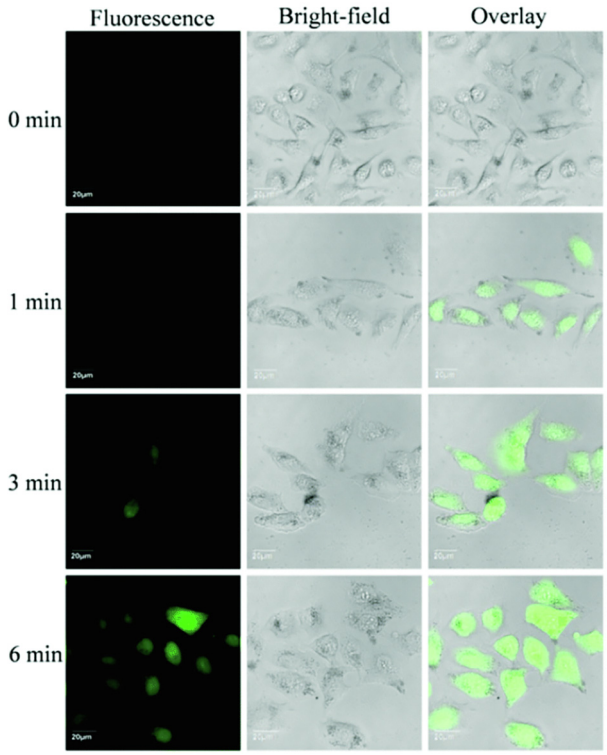

Fig. 82. Confocallaser scanning microscopy images indicated the ROS generation in MCF-7 cells with light irradiation (0, 1, 3, and 6 min) after treatment with DCF-DA. The green fluorescence came from DCF-DA. [Adopted from **ref. 140** with permission from Royal Society of Chemistry].

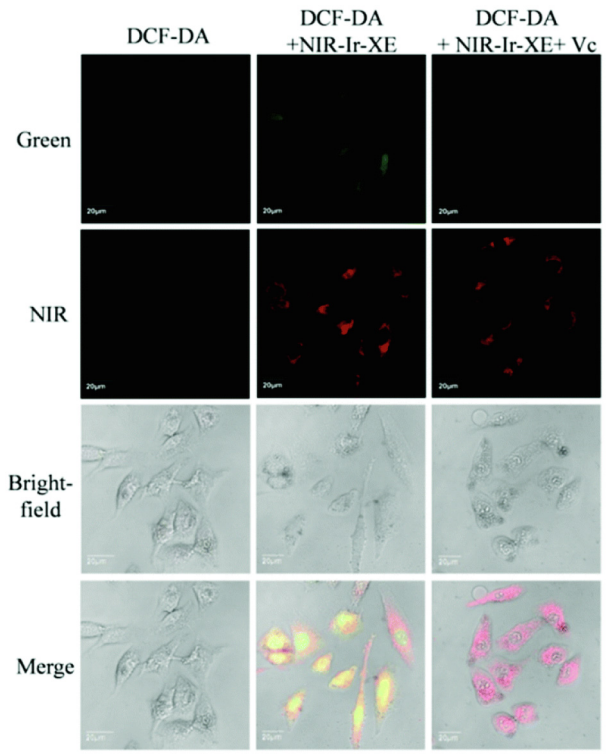

Fig. 83. Confocal images indicated the ROS generation in MCF-7 cellsin presence of light irradiation (100mW cm^{-2}, 5 min) after treatment with DCF-DA. The green fluorescence is from DCF-DA. [Adopted from **ref. 140** with permission from Royal Society of Chemistry].

mitochondria in live cells, with a strong linking to cell death pathways [141].

Mitochondria targeted one or two photon PDT activated iridium complexes were synthesized by Chao *et al.* In that case they represented the biological activity of three Ir complexes (**125**–**127**) as mitochondria targeted AIE-active TPA-PDT agents. Authors investigated intracellular distribution of all the complexes with the help of confocal laser scanningmicroscopy (CLSM) on HeLa cells and for this they used MitoTracker Green (MTG). From this result they confirmed that the complexes selectively accumulated in the mitochondria. The ICP-MS results also suggested that the concentration of Ir in mitochondria was extremely high, with mitochondria accounting for over 80 % of the complexes. To quantify TPA-induced ROS production by all the complexes, they utilized 2,7-dichlorofluorescein diacetate (DCFH-DA) as an *in vitro* ROS indicator.There was a significant increase in the intensity of fluorescence for cells treated with complex **125** after irradiation with a moderate light dose of two-photon laser but as the irradiation time increased, the intensity decreased. But other two complexes exhibited weak intensity of fluorescence. Author further investigated TPA phototherapy and due to this they co-stained HeLa cells with annexin V-FITC (AV)/propidium iodide (PI). After two photon irradiations, the most of the cells were treated with complex **125** which exhibited strong AV and PI signal. This specified that maximum cells were undergone in necrosis or late apoptosis. From their experiment, we understood that complex **125** was a real candidate for TPA-PDT since it displayed the largest TPA cross sections, highest ROS producing ability and most dramatic mortality at low concentration upon aggregated in mitochondria [142]. Chao group also synthesized another five mitochondria targeted Ir (III) complexes (**128**–**132**). Authors investigated singlet oxygen quantum yield with the help of methylene blue (MB) as the standard and they found the quantum yield values were 0.17, 0.21, 0.28, 0.51, 0.52, and 0.59 for complexes **128**, **130**, **129**, **131**, **MB**, and **132** respectively at 405 nm light irradiation. Colocalization study was also performed for all the complexes with MitoTrackerRed (MTR) in HeLa cells and this result demonstrated that the complexes were accumulated in mitochondria with high colocalizationcoefficients (Fig. 85a). The ICP-MS study confirmed that the most of the complexes were accumulated in mitochondria than in nucleus and in lysosomes (Fig. 85b). So, among all the complex, complex **132** demonstrated its potency. Author also inspected the change in mitochondrial membrane potential by using JC-1 as a probe with the help of fluorescence microscope. When they treated the HeLa cell with complex **132** in presence of light irradiation, red to green color change was found that indicated the loss of MMP (Fig. 85c). From all the experimental results authors concluded that complex **132** triggered apoptosis in HeLa cells through a mitochondrial-mediated mechanism [143] (See Fig 86).

Due to inhibitory potency and PDT activity of histone deacetylases (HDAC) Mao *et al.* synthesized theranostic **Ir (III)–HDAC** hybrid complexes with synergistic inhibition effects on cancercells. In this seris they synthesized four cyclometalated complexes (**133**–**136**). Author determined the singlet oxygen quantum yield with the help of methylene blue (**MB**) as a standard. Under UV light irradiation the quantum yield values were 0.21, 0.38, 0.45, 0.52 and 0.75 for complexes **135**, **134**, **133**, **MB**, and **136** respectively. The most important property of the complexes was that they all produced singlet oxygen under visible light irradiation. Author investigated the cytotoxicity towards HeLa, A549, A549R, and LO2 cell lines in presence and absence of visible light. They found that in dark condition all the complexes exhibited moderate cytotoxicity, but the cytotoxic activity increased under irradiation. Against HeLa cell, the PI was found to be 17.3, 16.2, 4.4, and 2.7 for complexes **133**, **134**, **135**, and **136** respectively. They also noted that negligible cytotoxicity was found against LO2 cell for all the complexes.

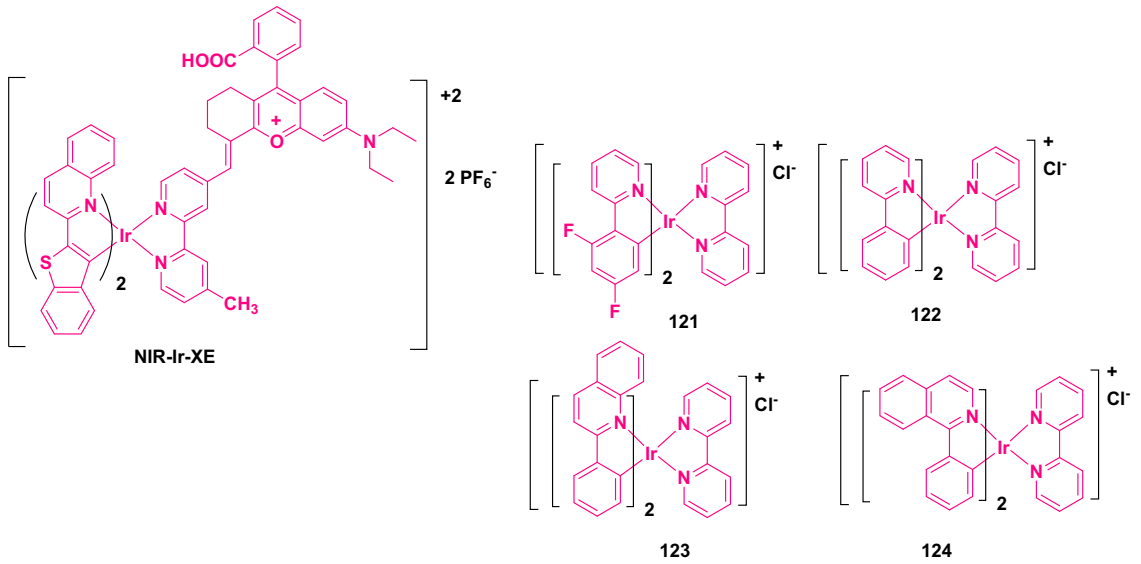

Fig. 84. Structure of NIR-Ir-XE and complexes from **121** to **124**.

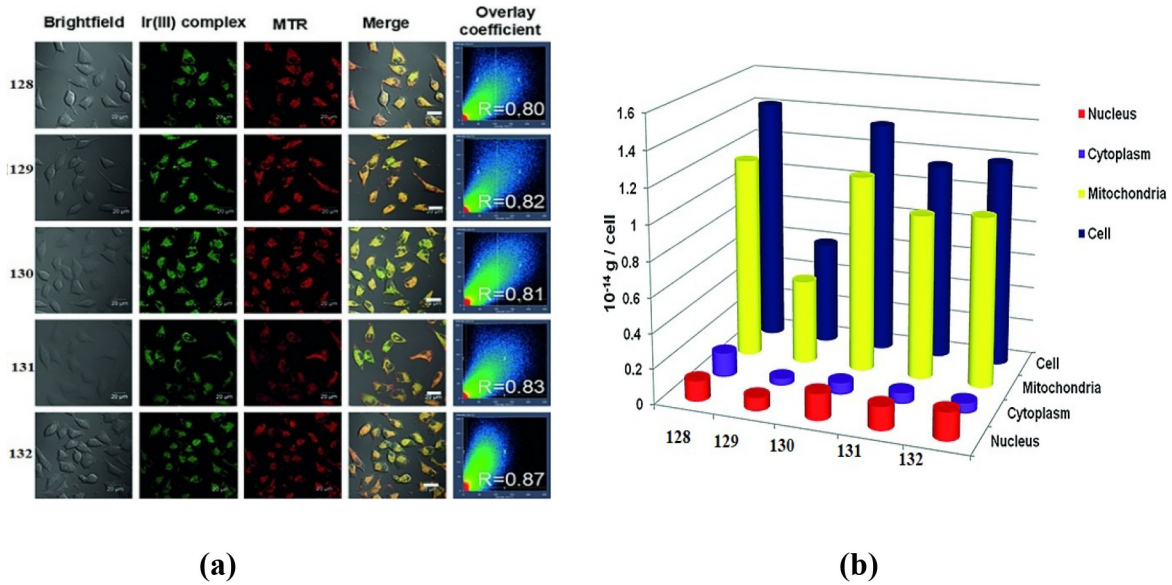

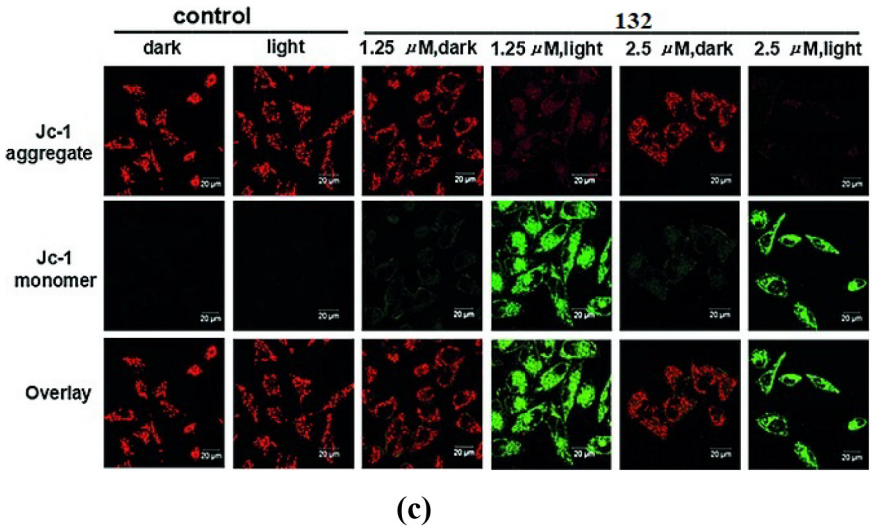

Fig. 85. (a) Colocalization images of Ir (III) complexes with MTR. (b) Distribution analysis of complexes **128**–**132** in HeLa cells with the help of ICP-MS. (c) Impression of complex **132** on mitochondrial integrity. [Adopted from **ref. 143** with permission from Wiley-VCH].

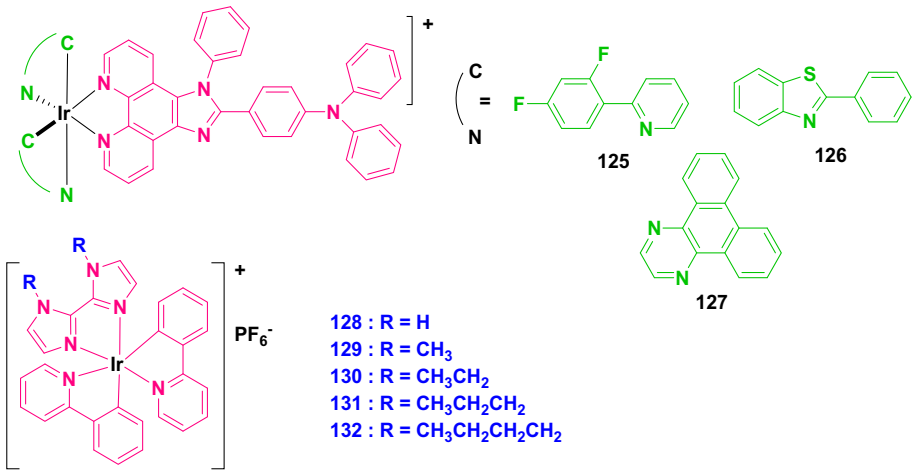

Fig. 86. Structure of mitochondria targeted complex from **125** to**132**.

Author also investigated the HDAC inhibitory activity of all the complexes. 134> SAHA>135>133>134 order was found in the case of inhibitory effects of compounds on HDAC activity [144]. Another cyclometalated Ir (III) complex (**137**) was designed and synthesized by Natrajan *et al.* At 740 nm, the 2PA cross-section was found to be 45 GM. In vitro tests with C6 Glioma cells demonstrated efficient cell damage when cells were treated with the complex and irradiated under two-photon with 740 nm fs pulsed light, but cells remained unaltered when they were irradiated without complex [145]. Other six cyclometalated Ir(III) complexes (**138**–**143**) were designed, synthesized and studied by Sun *et al.* Author calculated the EC_{50} value and PI value for all the complexes in both light

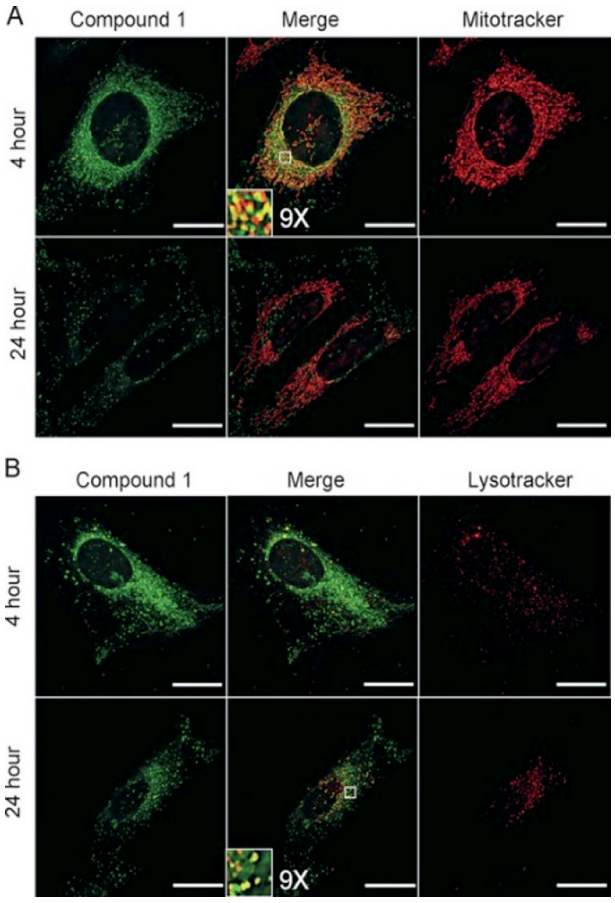

Fig. 87. Subcellular localisation of complex **146**. U2OS cells incubated with complex **146** (green) for 4 or 24 h, co-localised with: A) Mitotracker orange (red), B) Lysotracker (red). Zoomed sections has been shown as insets. Scale bars = 20 µm.

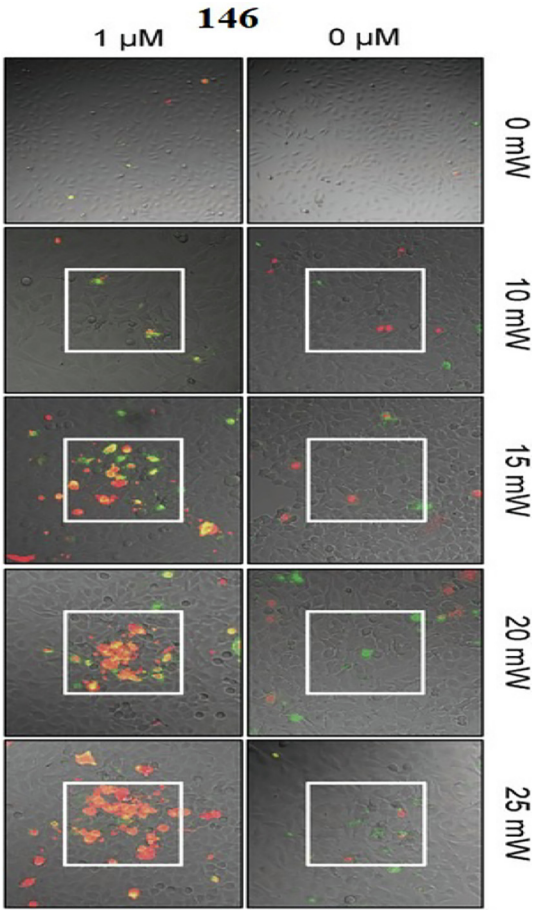

Fig. 88. PS activity of complex **146** generated by two photons. HeLa cells were treated with complex **146** or DMSO for 2 h before being irradiated with a 760 nm multiphoton laser on a central square. Apoptosis (Annexin V – red) and cell death (propidium iodide - green) markers were used to label cells after 24 h. [Adopted from **ref. 148** with permission from Wiley-VCH].

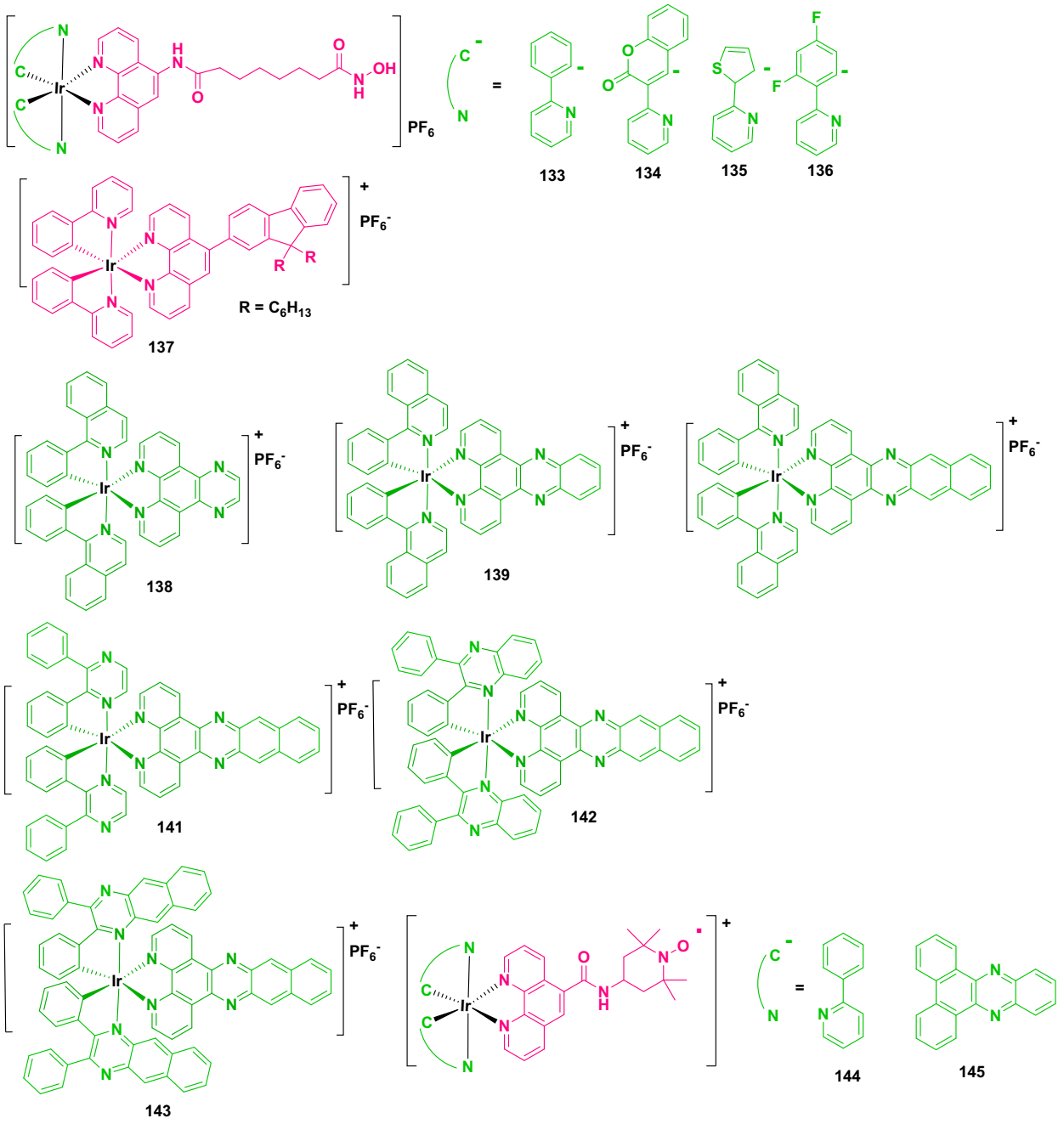

Fig. 89. Structure of complexes from **133** to **145**.

and dark condition towards SK-MEL-28 and HL60 cell lines. They also suggested that all the complexes demonstrated photodynamic therapeutic effect in presence of visible or red-light irradiation. Among all the complexes, complex **143** exhibited highest PI value in both the cell lines. The intense intracellular fluorescence of these Ir (III) complexes exhibited their potential as a significant theranostic agents [146]. Jing *et al.* designed and synthesized two mitochondria targeted Ir (III)–nitroxide conjugates as photosensitizers (**144, 145**). They investigated singlet oxygen quantum yield with the help of MB as a standard and the values were 0.25 and 0.50 for complex **144** and complex **145** respectively. The photo cytotoxicity of two complexes was examined towards HeLa, A549, A549R

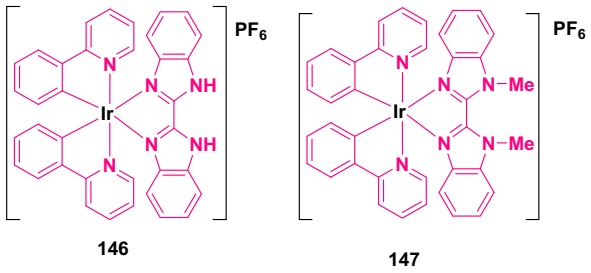

Fig. 90a. Structure of complex **146** and **147**.

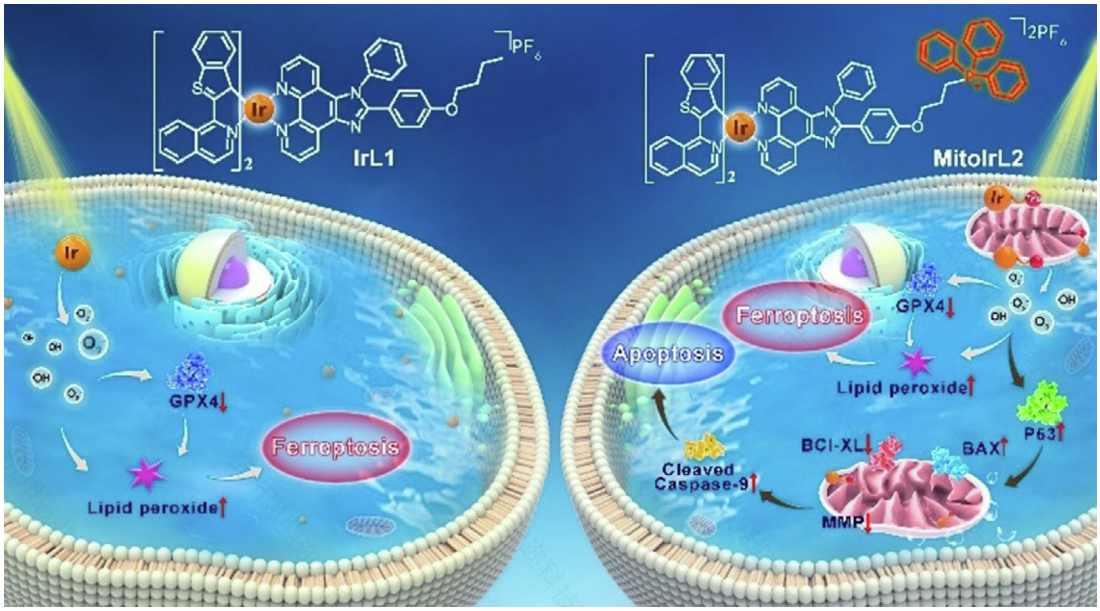

Fig. 90b. Chemical structures of complexes **IrL1** and **MitoIrL2**, and the illustration of cell death pathways induced by **IrL1** and **MitoIrL2** upon photoirradiation under hypoxia. [Adopted from **ref. 150b** with permission from Wiley-VCH].

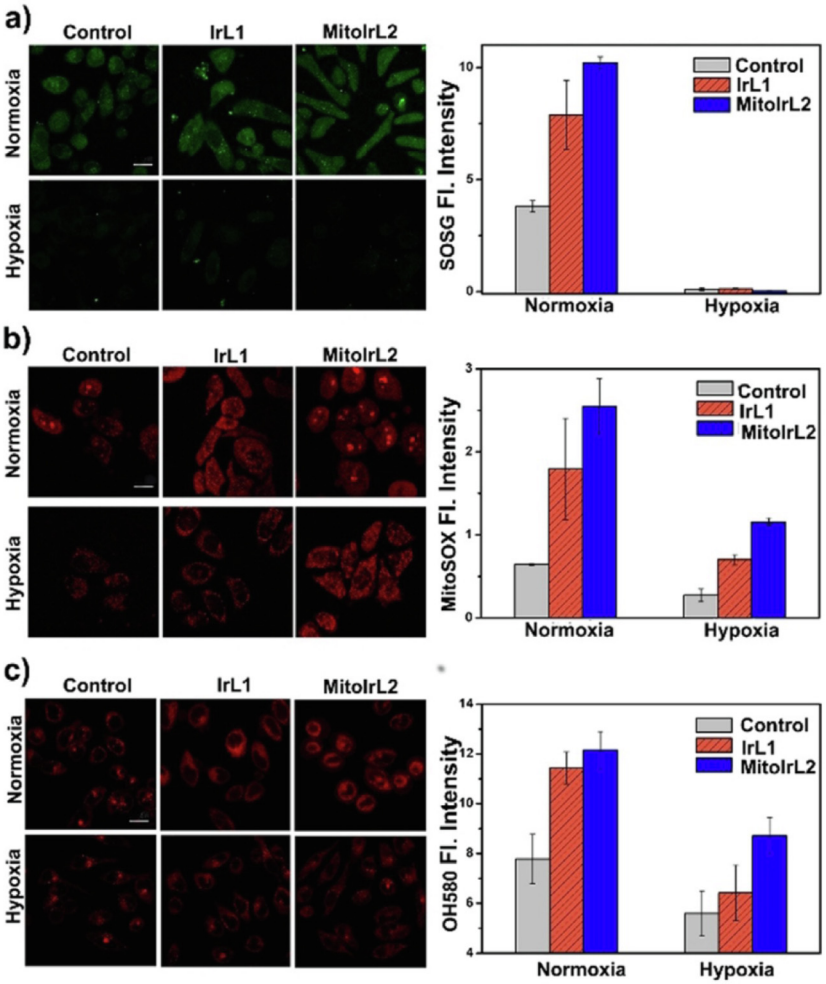

Fig. 90c. Confocal imaging of photoinduced ROS in MCF-7 cells incubated with **IrL1** and **MitoIrL2** (5 μM, 4 h, 37 ^{0}C in the dark) under normoxia (O_2 = 21 %) and hypoxia (O_2 < 0.1 %) using a) SOSG (bandpath 490–590 nm, 488 nm), b) MitoSOX (bandpath 550–600 nm, 488 nm), and c) OH580 (bandpath 545–645 nm, 488 nm) as fluorescence indicators for $^1O_2$, $\cdot O_2^-$ and $\cdot$OH, respectively. Photoirradiation was imposed with a laser (450 nm, 30 Jcm^{-2}, 5 min) after 4 h of complex incubation. Scale bar: 20 mm. [Adopted from **ref. 150b** with permission from Wiley-VCH].

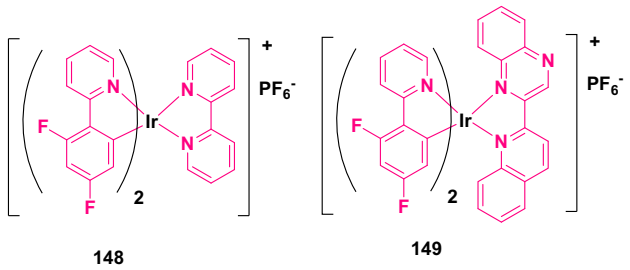

Fig. 91. Structure of complexes **148** and **149**.

and human normal liver LO2 cells. They observed that all the complexes exhibited moderate cytotoxicity for all the cell lines in dark condition, but in presence of irradiation cytotoxicity was increased. By using confocal microscopy authors also investigated the cellular uptake and distribution in presence of one and two photon. Effective penetration of A549 cell and specifically targeted mitochondria was observed by the experiment. They understood PDT efficacy of the complexes by phosphorescence intensities and lifetime distributions in cancer cells during PDT [147]. Lysosomes and mitochondria targeted two low molecular weight, photostable cyclometalated Ir(III) complexes (**146**, **147**) were synthesized by Bryant *et al.* Authors performed the co-localization experiment with the help of organelle specific fluorescent dyes which exhibited localization of mitochondria and lysosome. In (Fig. 87A) mitochondrial localization was observed with 0.547 Pearson's coefficient value. In (Fig. 87B), it was observed that by 24 h, lysosomal localization of complex **146** had taken over, with Pearson's coefficients 0.387 associated to 0.19 for mitochondrial staining. They also investigated the cytotoxicity in both light and dark condition. In the presence of HeLa cell **146** and **147** exhibited light cytotoxicity with LD_{50} value 0.3 and 0.5 μM. But in the case of dark cytotoxicity, **146** demonstrated very low dark cytotoxicity value with LD_{50}>100 μM whereas **147** exhibited high dark cytotoxicity value with EC_{50} 6.2 μM. They also observed PI value >333 (405 nm, 3.6 J cm^{-2}) of complex **146** and 12.4 for complex **147**. The lowest PI value of complex **147** was due to high dark cytotoxicity value. Under TPE with 760 nm light they also investigated the

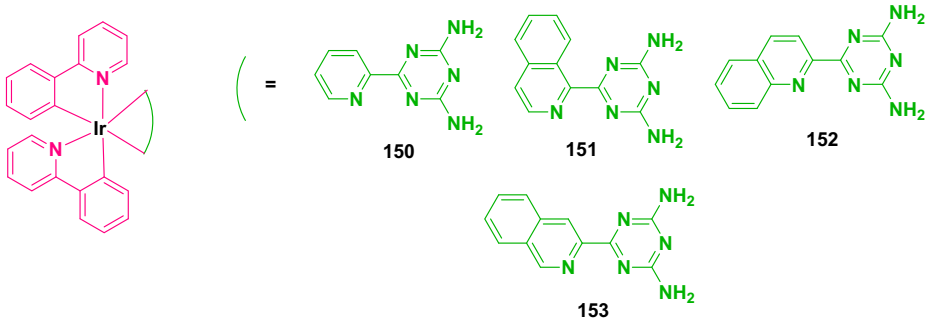

Fig. 92. Structure of complexes **150** to **153**.

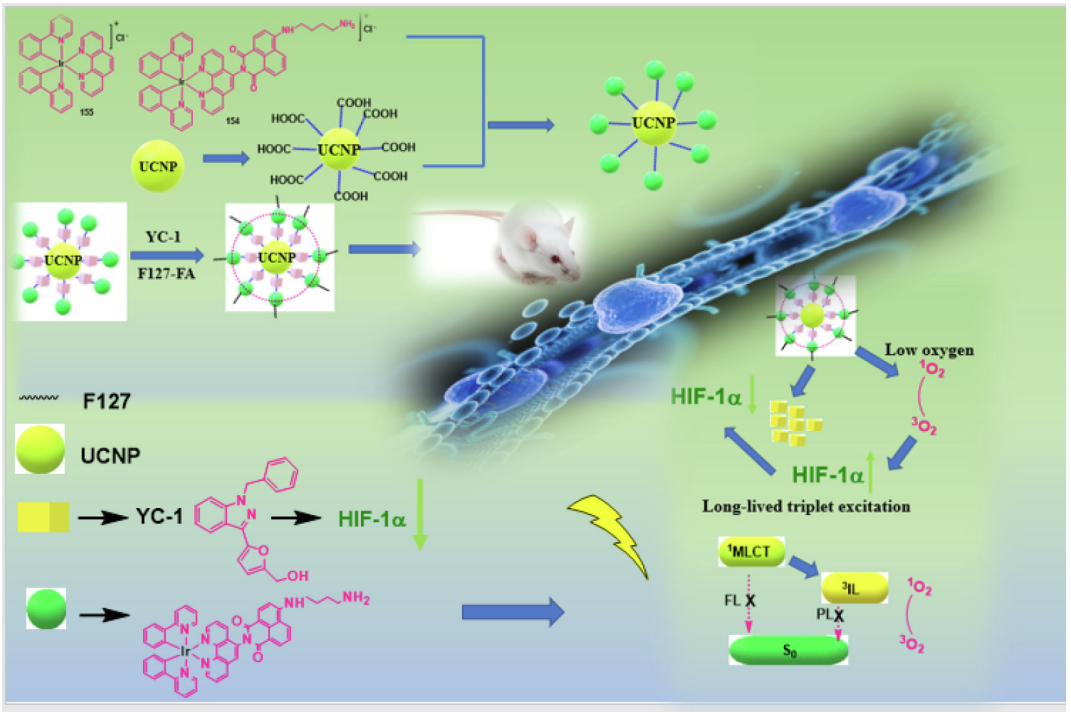

Fig. 93. Schematic representation of anticancer pattern of **UCNP@IrYCF127**.

photosensitizing activity of complex **146** (Fig. 88). Apoptosis with green and cell death with red was observed by TPE photosensitization. Apoptosis or cell death was clearly observed in complex **146** exposed cells within the irradiated area, but not in the surrounding non-irradiated cells. They also clearly explained that after light irradiation cell death was observed by localization of photosensitizer in lysosomes and mitochondria [148] (See Figs. 89–93).

Cyclometalated two Ir (III) complexes (**148, 149**) were introduced by Huang *et al.* Both the complexes demonstrated green and red photoluminescence with 0.90 and 1.10 μs emission lifetimes. The overlay of confocal luminescence and brightfield image exhibited that the luminescence was visible in the cytoplasm over the nucleus and membrane. This data explained that complexes internalized in to the cell. Due to their cell membrane permeability, moderate luminescence efficiencies in buffers solution gave the special advantage of the complexes as a phosphorescence bioimaging agents [149]. Mitochondria targeted four complexes (**150**–**153**) cyclometalated Ir (III) complexes were synthesized by Chao *et al.* Authors investigated the cytotoxicity of the complexes. Among the four complexes, complex **150** exhibited high phototoxicity with IC_{50} value 0.53 ± 0.04 and 0.83 ± 0.10 μM for A549 and A549R cell respectively and also 15.49 and 12.29 values of PI was found for A549 and A549R cell lines. They also noted that complex **150** separated the normal and cancer cell in dark and also in light condition. With the help of ICP-MS they observed the distribution of complex **150** against cancer cell. An outstanding superimposition pattern was observed between Mitotracker deep red, MDR and 150. With 0.87 correlation coefficient value a yellow phosphorescence was observed from complex **150** in mitochondria of living A549R cells. So, complex **150** was a good mitochondria targeted PDT agent [150a] Another two benzothiophenylisoquinoline (btiq)-derived cyclometalated Ir (III) complexes, **IrL1** and **MitoIrL2** were synthesized by Guo *et al.* for mitochondria accumulation (**Fig. 90b**). Under hypoxia, both complexes triggered photoinduced ferroptosis in tumor cells and exhibited a type I PDT mechanism. Confocal image revealed the fluorescence increases under normoxia condition, demonstrating the photoinduced intracellular singlet oxygen production capability of the two complexes. But both complexes produced very little intracellular singlet oxygen when exposed to light in a hypoxic environment. Confocal image also exhibited that after photoirradiation in normoxia, both complexes could effectively produced $^{\cdot}O_2^-$ in MCF-7 cells. Both complexes maintained their $^{\cdot}O_2^-$ production capacity under hypoxia, albeit at a lower rate. In

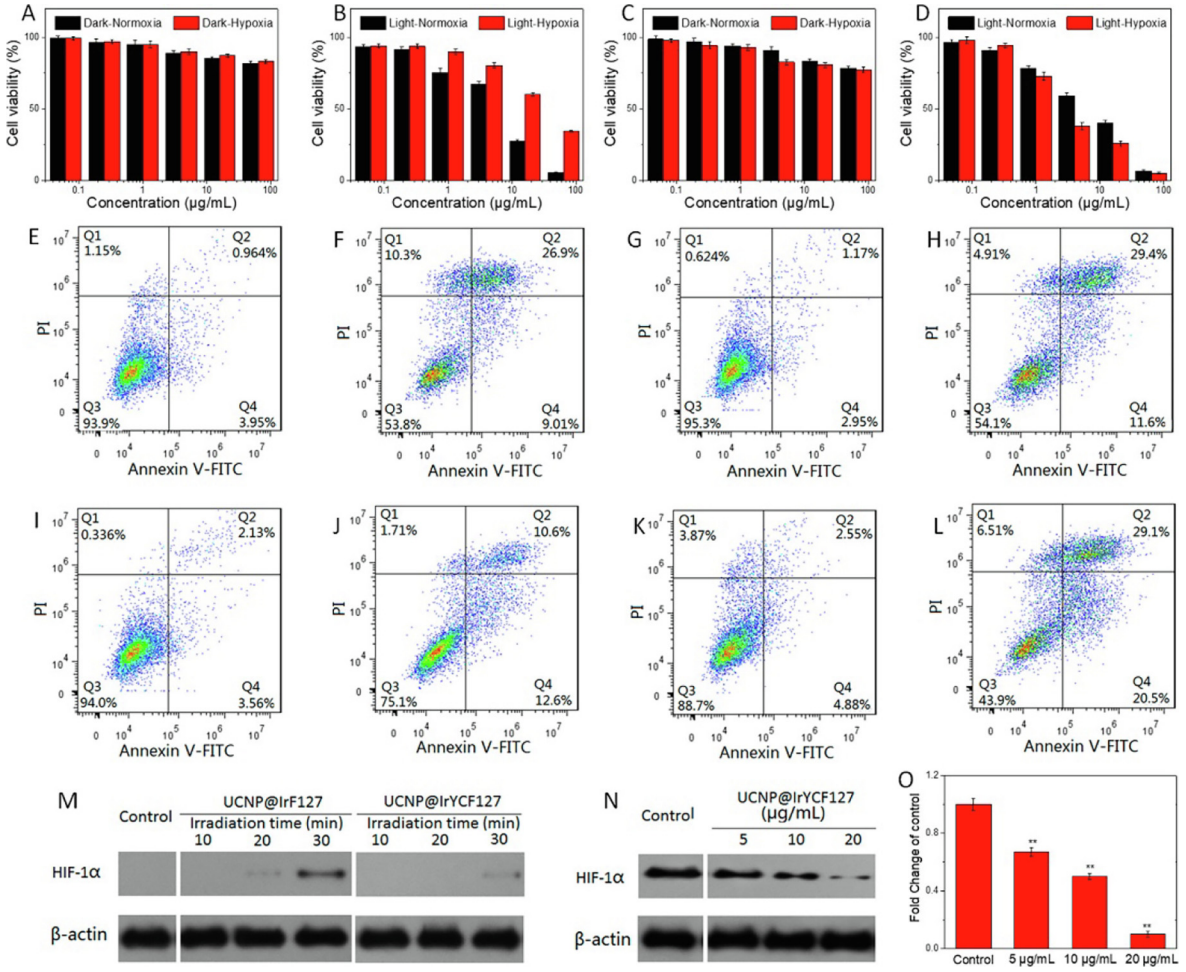

Fig. 94. MTT study of MBA-MD-231 cells exposed to (A) **UCNP@IrF127** missingof irradiation, (B) **UCNP@IrF127** in presence of laser irradiation (980 nm), (C) **UCNP@IrYCF127** missing of irradiation, and (D) **UCNP@IrYCF127** in presence of laser irradiation (980 nm). Apoptosis and necrosisanalysis of MBA-MD-231 cancer cells after various treatments: (E) **UCNP@IrF127** missing of irradiation (normoxia), (F) **UCNP@IrF127** in presence of laserirradiation (980 nm, normoxia), (G) **UCNP@IrYCF127** missing of irradiation (normoxia), (H) **UCNP@IrYCF127** in presence of irradiation (980 nm,normoxia), (I) **UCNP@IrF127** missing of irradiation (hypoxia), (J) **UCNP@IrF127** in presence of laser irradiation (980 nm, hypoxia), (K) **UCNP@IrYCF127** missing of irradiation (hypoxia) and (L) **UCNP@IrYCF127** in presence of laser irradiation (980 nm, hypoxia). HIF-1α protein levels as determinedby immunoblotting: (M) MBA-MD-231 cancer cells treated with **UCNP@IrF127** and **UCNP@IrYCF127** for different irradiation time periods, (N) MBA-MD-231 cancer cells treated with **UCNP@IrYCF127** under hypoxic conditions (1 % O2) for 12 h, (O) densitometric analysis of theexpression of HIF-1α proteins of (N). [Adapted from **ref. 158** with permission from American Chemical Society].

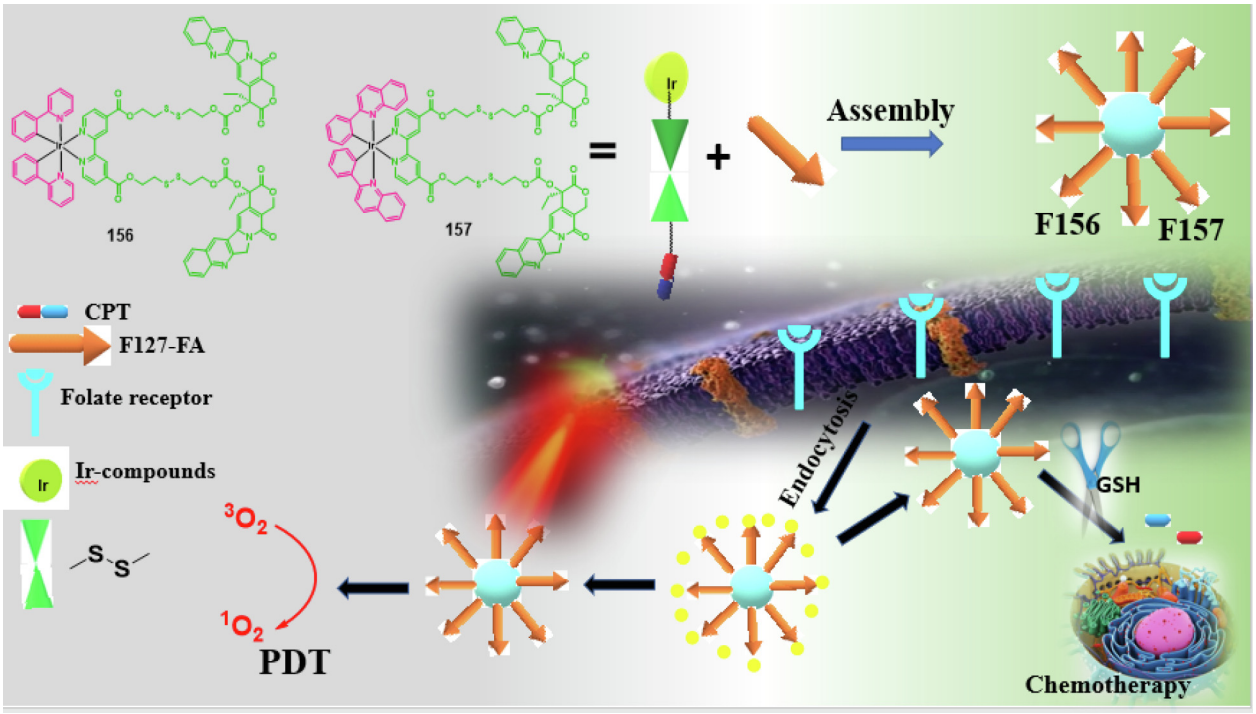

Fig. 95. Schematic Illustration of the ROS Generation upon Visible Light Illumination forPDT and Anticancer Drug Release Triggered by GSH for Chemotherapy in Tumor Cells.

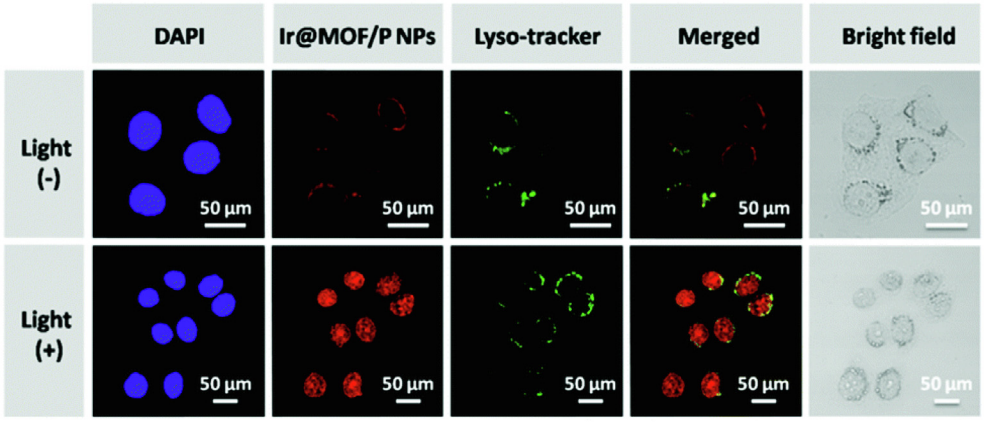

Fig. 96. CLSM was used to study the intracellular distribution of **Ir@MOF/P** NPs in HeLa cells in the absence and presence of daylight. Use of DAPI (blue) to staincell nucleus: lex = 402 nm and lem = 461 nm; Use of Lyso-tracker (green) to stain endo/lysosomes: lex = 504 nm and lem = 511 nm. Scale bars:50 mm. [Adapted from **ref. 167** with permission from Royal Society of Chemistry].

hypoxia condition the abiity of $^{\cdot}$**OH** generation ability was also conformed by stained the cell with help of mitochondrial hydroxyl radical probe OH580. From this author understood that both complexes facilitated type I photochemical processes in MCF-7 cells to produce $^{\cdot}O_2^-$ and $^{\cdot}$**OH** even in hypoxic conditions, despite the fact that type II photochemical processes to produce singlet oxygen were nearly completely prevented (**Fig. 90c**) [150b].

7.1. Iridium based nano complex act as PDT in cancer therapy:

In the field of nano conjugated Ir complex in cancer therapy, Gou *et al.* designed and synthesized iridium based photosensitizer (**154**) which exhibited high range singlet oxygen ($^1O_2$) generation at 460 nm irradiation than the model Ir (III) complex (**155**). Because of the weak absorption in the near-infrared range of iridium (III) complexes, which was known as the primary barrier, their utilization for treatment of tumor tissue in depth was limited [151]. An impressive property of Lanthanide-doped up conversion-nanoparticles (UCNPs) is conversion of NIR light to high energy visible light [152–157]. Due to this reason authors covalently conjugated the complex on the surface of UCNPs. Effective HIF-1α inhibitor, 1-benzyl-3-(5′-hydroxymethyl-2′-furyl) indazole (YC-1) was absorbed at surface of UCNPs into the hydrophobic layer. The preparation and application of the nano was very interesting. First, they conjugated complex **154** to the surface of **UCNP$_S$** named **UCNP@Ir**. After that the increase in biocompatibility of the nanoparticles, UCNP@ Ir was coated with F127 (biodegradable copolymer Pluronic) named **UCNP@IrF127**. For targeting the hypoxia tumor cells they also incorporated YC-1 in **UCNP@IrF127** and denoted as **UCNP@IrYCF127**. With the help of MTT assay authors investigated the photocytotoxicity against MBA-MD-231 cells under both normoxic and hypoxic conditions (Fig. 94A–D).

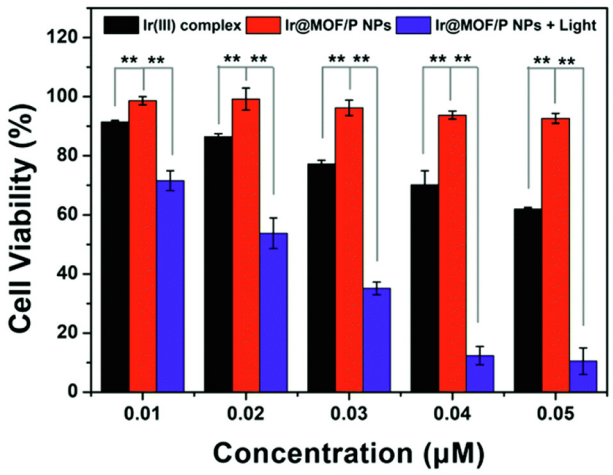

Fig. 97. HeLa cells treated with various concentrations of the Ir(III) complex in the dark and **Ir@MOF/P NPs** containing various concentrations of the Ir(III) complex in the dark and in the presence of daylight irradiation were analyzed for cytotoxicity. [Adopted from **ref. 167** with permission from Royal Society of Chemistry].

Very negligible cytotoxicity was found in normoxic and hypoxic conditions for both **UCNP@IrF127** and **UCNP@IrYCF127** under the absence of NIR irradiation but cytotoxicity was found with IC_{50} values of 7.23 and 6.77 μg/mL for **UCNP@IrF127** and **UCNP@IrYCF127** respectively at 980 nm laser irradiation under normoxia condition. They also observed **UCNP@IrF127** which revealed IC_{50} value of 31.63 μg/mL under hypoxia condition which was 4.4-fold higher than normoxic conditions. Very impressive phototoxicity was found in the case of **UCNP@IrYCF127** in hypoxia than normoxia conditions. From this result they confirmed that YC-1 gave an impressive impact to improve the PDT of **UCNP@IrF127** under hypoxia condition. From the flow cytometry study (Fig. 94E–L), it was clearly observed that without laser irradiation, **UCNP@IrF127** and **UCNP@IrYCF127** exhibited minimal cell death under normoxia condition. Under 980 laser irradiation the rate of cell death was induced to 46.2 % and 45.9 % for **UCNP@IrF127** and **UCNP@IrYCF127** respectively. But in hypoxia condition UCNP@IrF127 exhibited low rate of cell death (24.9 %) than the normoxia condition (46.2 %). High rate of cell death in hypoxia condition (56.1 %) was found in the case of **UCNP@IrYCF127** than the normoxia condition (45.9 %). This result also demonstrated that YC-1 increased the PDT effect of **UCNP@IrYCF127** in hypoxia condition. Authors also investigated the HIF-1α protein expression by Western blot analysis in MBA-MD-231 cell with **UCNP@IrF127** and **UCNP@IrYCF127** in different irradiation time period under slight hypoxia condition (10 % O_2). After 30 min irradiation HIF-1α was detected for **UCNP@IrF127** (Fig. 94 **M**). This suggested that PDT can aggravate hypoxia in tumors and, as a result, boosted HIF-1α expression. The expression of HIF-1α subsequently decreased with increasing nanoparticle concentration, as shown in (Fig. 94N, O) demonstrated that **UCNP@IrYCF127** could effectively block hypoxia or PDT-induced HIF-1α accumulated in MBA-MD-231 cells [158] (See Fig. 95).

As the concentration of glutathione (GSH) available in tumor cells is 100–1000 times higher than in the extracellular microenvironment, this reducing microenvironment gives a suitable chance to accomplish selective intracellular drug release in tumor cells [159–161]. Thus, it was highly desirable to improve the therapeutic efficacy and selectivity of anticancer medications by cleverly designing GSH-activatable prodrugs containing disulfide bond connections. In this regard, Xiang *et al.* reported two GSH activated Ir (III) complexes **156** and **157**. For organelle specific imaging, PDT, and chemotherapy they encapsulated amphiphilic surfactant (Pluronic F127-FA) micelles (**F156**, **F157**). Actually, GSH-responsive photosensitizers **156** and **157** were created by covalently conjugating the chemotherapeutic agent camptothecin (CPT) with Ir(III) complexes via disulfide linkers. Due to poor water solubility of Ir (III) complex in biological environment authors encapsulated the Ir(III) complex with Pluronic F127-FA which pro-

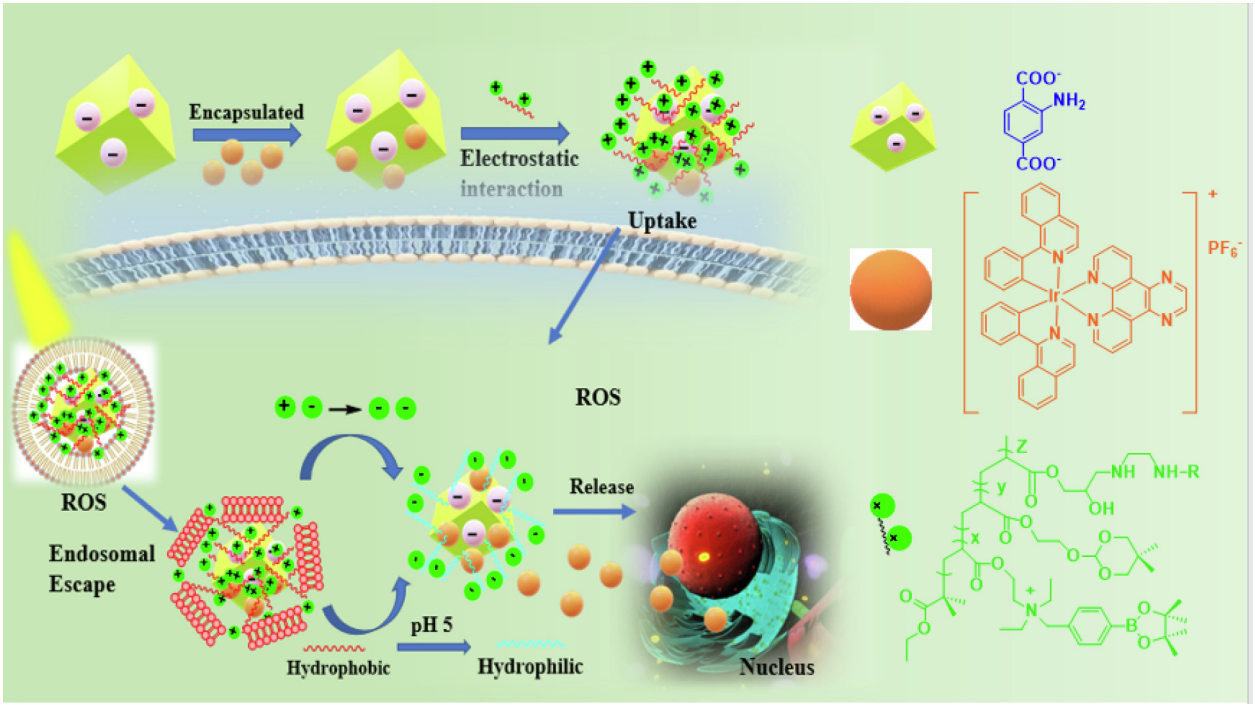

Fig. 98. Schematic representation of the assembly process of multifunctional **Ir@MOF/P** NPs and the putative mechanism for intracellularmetabolism and ROS-induced tumor inhibition processes.

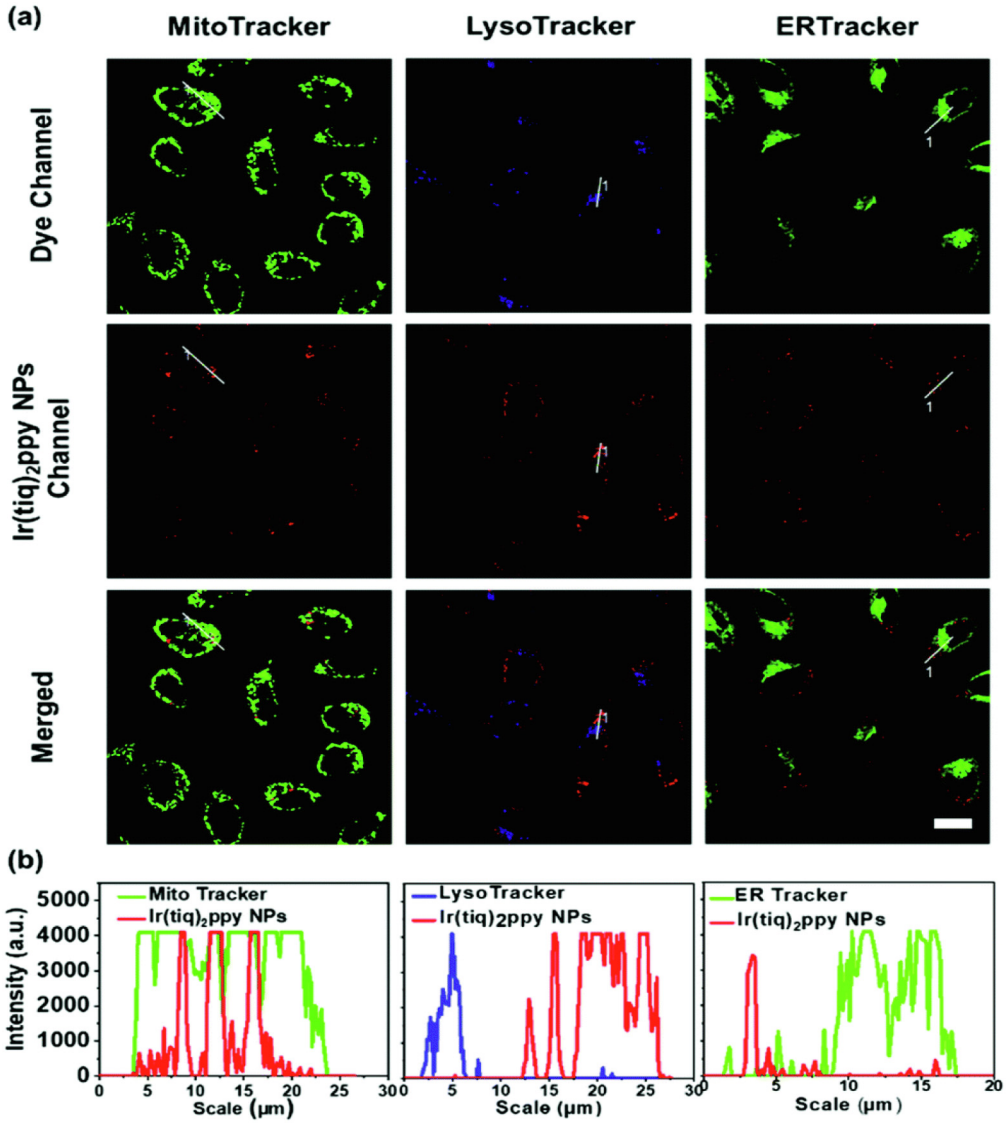

Fig. 99. (a) Co-localizing study after incubating MCF-7 cells with **Ir(tiq)2ppy** NPs for 24 h with MitoTracker, LysoTracker and ERTracker. Scale bar: 20 μm (b) Line series investigation of **Ir(tiq)2ppy** NPs with MitoTracker, LysoTracker and ERTracker. The colours exhibited in the images like red represents **Ir(tiq)2ppy** NPs, green represents MitoTracker and ERTracker, blue represents LysoTracker used to stain cells. [Adopted from **ref. 171** with permission from Royal Society of Chemistry].

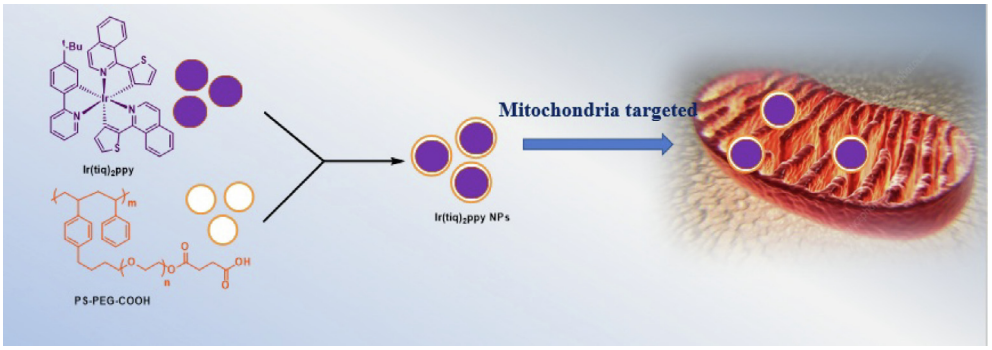

Fig. 100. Mitochondria targeted **Ir(tiq)$_2$ppy** NPs.

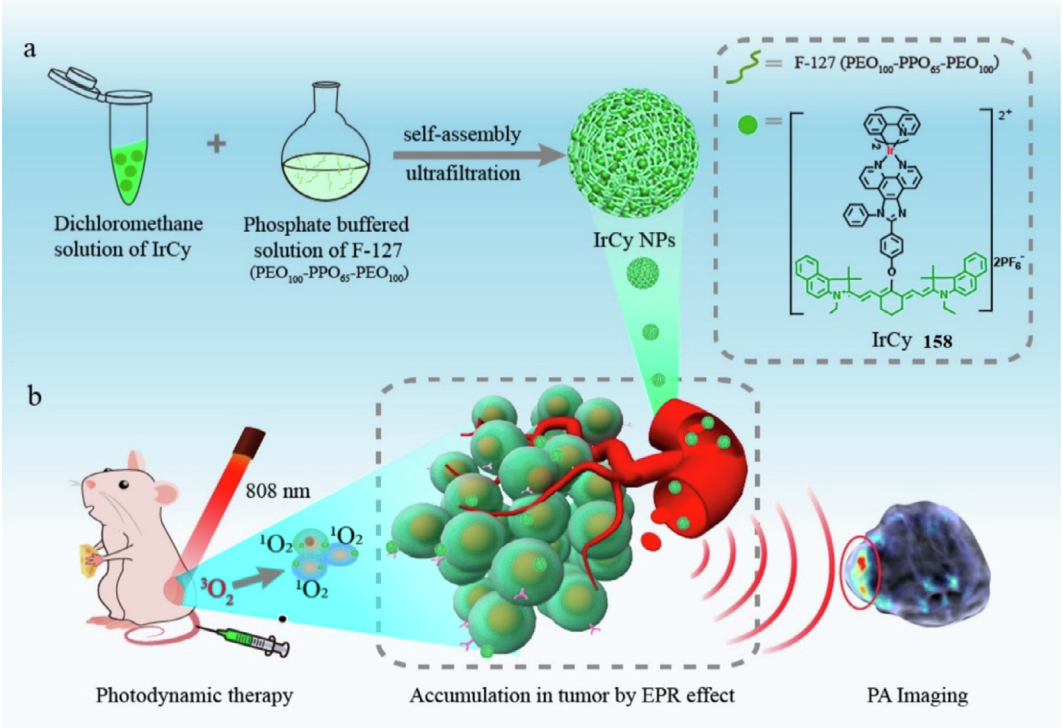

Fig. 101. (a) The Fabrication of **IrCy** NPs (**158**) (b) Application forin Vivo PA-Guided PhotodynamicTherapy [Adopted from **ref. 178** with permission from American Chemical Society].

duced useful micelles **F156** and **F157**. The release of the anticancer drug CPT in the tumor microenvironment by GSH–provoked and PDT under visible light gave an important impact in cancer therapy. Actually, high GSH concentration cleaved the disulfide bond and released the anticancer drug CPT. Additionally, as compared to normal cells, these micelles containing FA targeting ligands showed significantly greater cellular uptake in HeLa cells, resulting in a selective cancer cell killing action. Author also mentioned that micelles containing tailored combinational chemotherapy and PDT had greater potency and efficacy in killing tumor cells at low doses [162].

MOFs exhibited substantial potential in the domains of drug delivery and cancer treatment due to their enormous surface area, rich compositional variety, structural variation, and customizable pore diameters. Because of its excellent stability and low cytotoxicity, zirconium (Zr)-based MOF (UiO-66) has been widely used in biomedical research [163–166]. Keeping these in mind Gao *et al.* designed an antitumor delivery nanoplatform (**Ir@MOF/PNPs**) with Zr-MOF (UiO-66), a biscyclometalated Ir(III) complex and a dual-responsive **BP-PDM-PG** for PDT and cell imaging. Ir complex was released from **Ir@MOF/PNPs** in different pH values. They found that at pH 5.4 Ir complex released from **Ir@MOF/PNPs** than pH 7.4. Not only that they also observed that **Ir@MOF/PNPs** produced ROS after day light irradiation. From this observation they said that in day light condition and acidic condition was accelerated the released of Ir complex from **Ir@MOF/PNPs**. Authors measured the degree of co-localization between NPs (red) and endo/lysosomes (green) (Fig. 96) for investigated the escape ability of **Ir@MOF/P NPs**. Only when exposed to daylight could the isolated distribution of red and green fluorescence be identified, showing that **Ir@MOF/P** NPs successfully escaped from endo/lysosomes. A red fluorescence was observed in nucleus, these findings suggested that daylight-induced ROS generation could cause the endosomal membrane to break, allowing the endosome to escape. From the MTT assay (Fig. 97) they also observed that in absence of daylight **Ir@MOF/P NPs** exhibited very low cytotoxicity but, for 30 min of daylight exposure **Ir@MOF/P** NPs showed considerable ROS phototoxicity [167] (See Fig. 98).

Poly (ethylene glycol) (PEG) on cyclometalated Ir(III) complexes have been successfully employed as non-cytotoxic water-soluble bioimaging reagents as well as PDT agents. PEG chains on Ir(III) complexes can also improve the uptake property towards mitochondria, not only that also shield photosensitizers from nonspecific interactions with proteins [168–170]. For this reason, Yuguo Ma *et al.* selected polystyrene grafted with carboxyl terminated poly (ethylene glycol) (**PS-PEG-COOH**), as an amphiphilic polymer to prepare **Ir(tiq)$_2$ppy** NPs with the help of co-precipitation method. The **Ir(tiq)$_2$ppy** NPs were predominantly distributed in mitochondria after being encapsulated by **PS-PEG-COOH**, which increased their water solubility and photoluminescence in aqueous solution. Authors investigated the ROS generation ability of **Ir(tiq)$_2$ppy** NPs by 2′,7′-dichlorodihydrofluorescein diacetate (DCFH) probe in presence of white light irradiation. Actually, DCFH oxidized by ROS and product 2′,7′-dichlorofluorescein (DCF) exhibited strong fluorescence. They recorded the fluorescence intensity at 528 nm and observed that the intensity increased in **Ir(tiq)$_2$ppy** NPs than **Ir(tiq)$_2$ppy** and DCFH itself. This result indicated that nanoparticles had strong tendency to generate ROS. Authors also observed intracellular distribution and co-localization with the help of specific organelle dyes under confocal laser scanning microscope. From (Fig. 99a) it is clearly observed that **Ir(tiq)$_2$ppy** NPs overlapped with Mito tracker but not with LysoTracker or ERTracker. The observation revealed that **Ir(tiq)$_2$ppy** NPs specifically targeted mitochondria in MCF-7 cells, and this was due to presence of PEG units outside the NPs [171] (See Fig. 100 and 101).

As the capabilities of high spatial resolution ultrasound and high sensitivity optical imaging, photoacoustic (PA) imaging has gained considerable attention in the field of biological applications. The PA influence of endogenous or exogenous contrast agents is responsible for these benefits. From some literature [172–175].

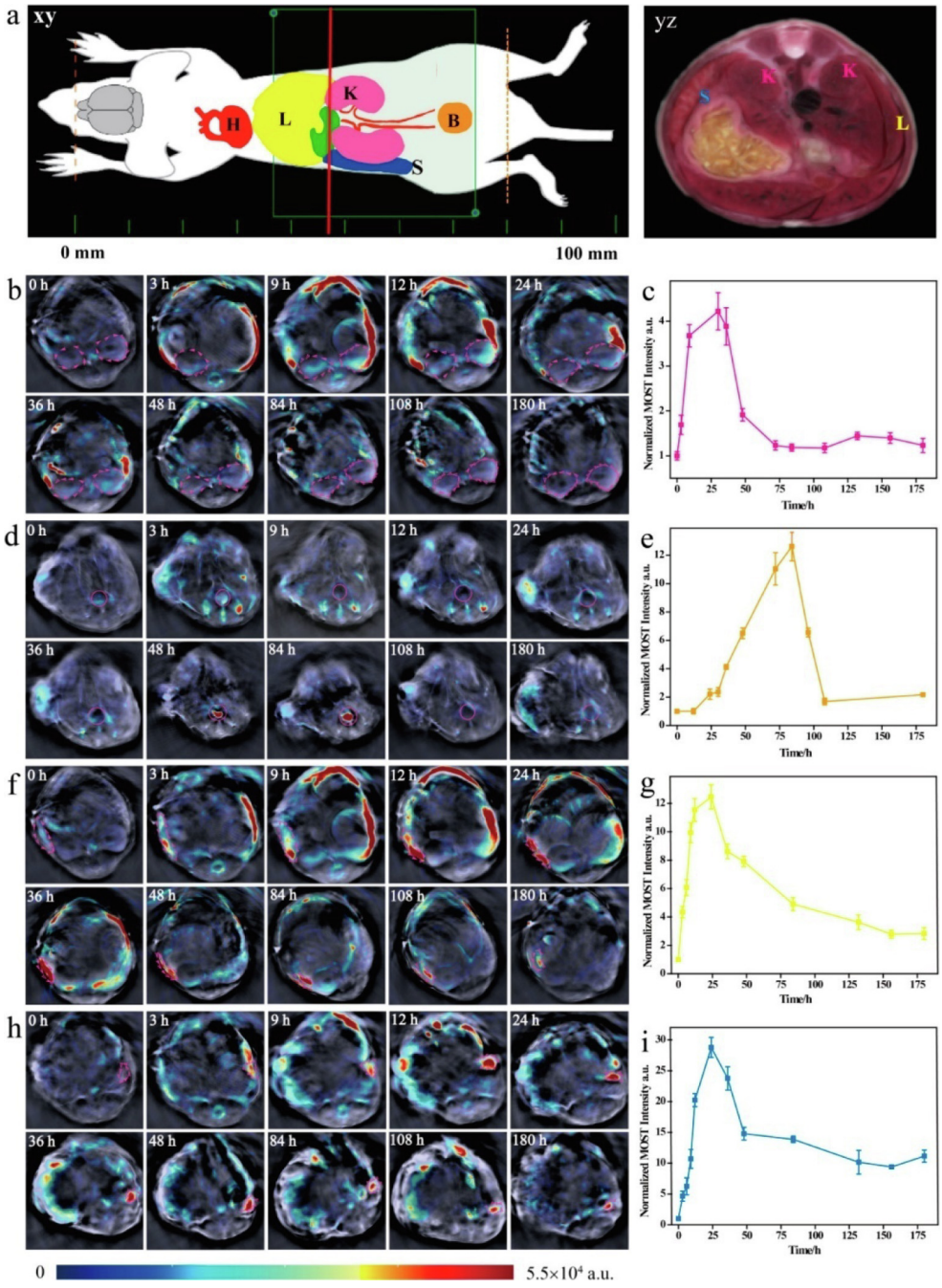

Fig. 102. (a) The diagonal (xy) and longitudinal view (yz) of the mouse for quantitative analysis of different organs. The letters of H, L, K, B, and S represented heart, liver, kidney, bladder, and spleen, respectively. The time-dependent change of the relative PAimaging signals in kidney (b), bladder (d) liver (f), and spleen (h) after injected of the complex (20 mg/kg IrCy) through the tail vein. In the ROIs drawn around the (c) kidney (pink line), (e) bladder (brown line), (g) liver (yellow line), and (i) spleen (blue line), the signal of **IrCy** NPs was measured as a function of time [Adopted from **ref. 178** with permission from American Chemical Society].

we found that, small molecule organic dyes, polymer-based nanomaterials, and metallic or semi metallic nanomaterials are the three types of exogenous PA contrast agents (CAs). Because ofstrong absorption in the near-infrared region, great biocompatibility, biodegradability, cyanine dyes are one of the most widely used small molecule PA probes [176,177]. Due to all the characteristics Yang *et al.* incorporated iridium center with cyanine dye and established Ir(III)-cyanine complex (**158**) with intense NIR absorption. They showed a significant PA signal due to the immense NIR absorption, which may be used to investigate the pharmacokinetics, tumor targeting, and biodistribution of **IrCy** NPs in real time, as well as the effective creation of singlet oxygen ($^1O_2$) for PDT of

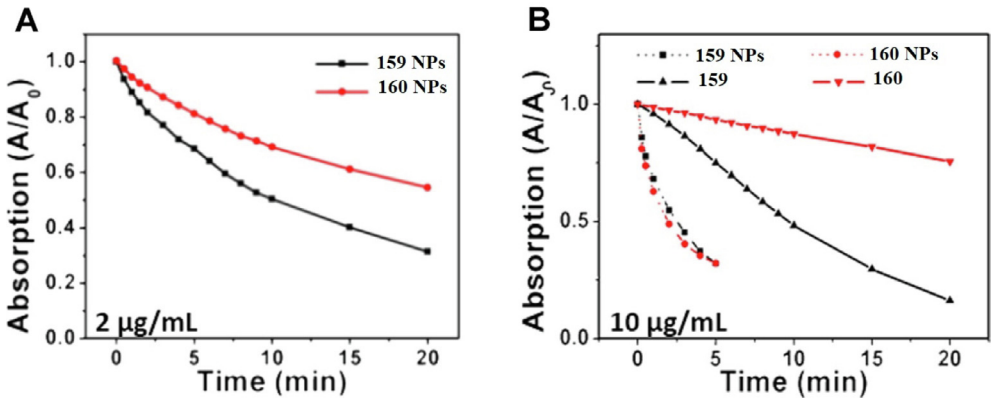

Fig. 103. (A) The effect of Photodynamic of **159** (black) and **160** (red) NPs at 2 μg·mL^{-1}. (B) The effect of Photodynamic of small molecules (10 μg·mL^{-1}) in DMF. [Adopted from **ref. 179a** with permission from American Chemical Society].

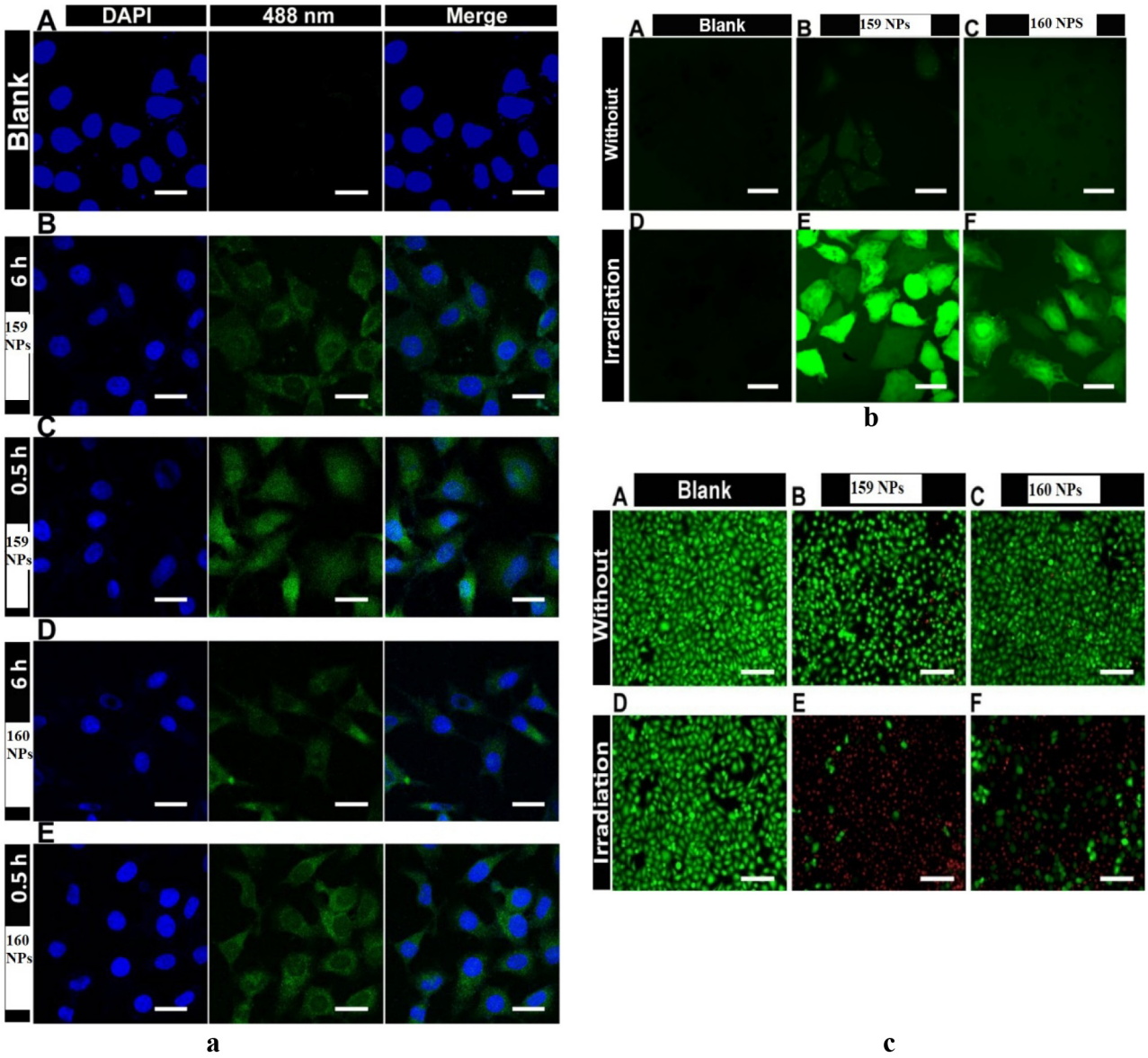

Fig. 104. (**a**). CLSM was used to quantify the endocytosis of NPs in HeLa cells. Control group (A), CLSM of HeLa cells treated with **159** NPs for 0.5 and 6 h (B, C), CLSM result for **160** NPs (D, E). (**b**) To detect ROS in cells, DCFH-DA probes were utilized. Control group (A, D), Treated with **159** NPs (B, E), Treated with **160** NPs (C, F), Light was used to irradiate the groups (D-F), Groups that was not exposed to light (A-C). (**c**) HeLa cell staining (live/dead) in various conditions. Control group (A, D), Treated with **159** NPs (B, E), Treated with **160** NPs (C, F), without light cultured (A-C), with irradiation (D-F). [Adopted from **ref. 179a** with permission from American Chemical Society].

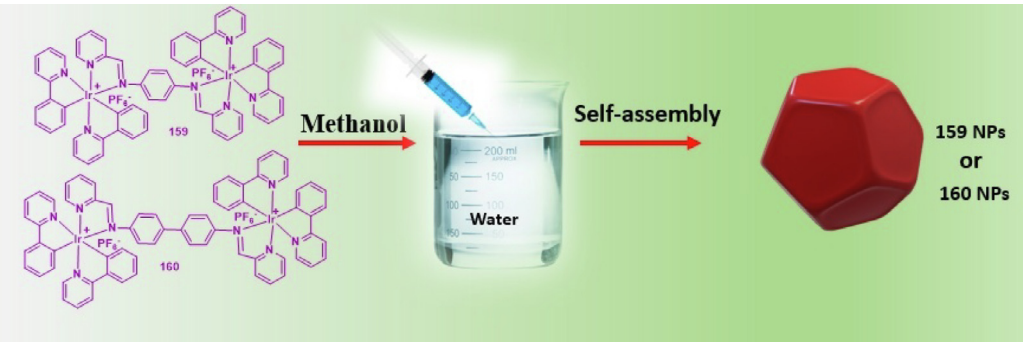

Fig. 105a. formation of 159 NP_S and 160 NP_S from 159 and 160.

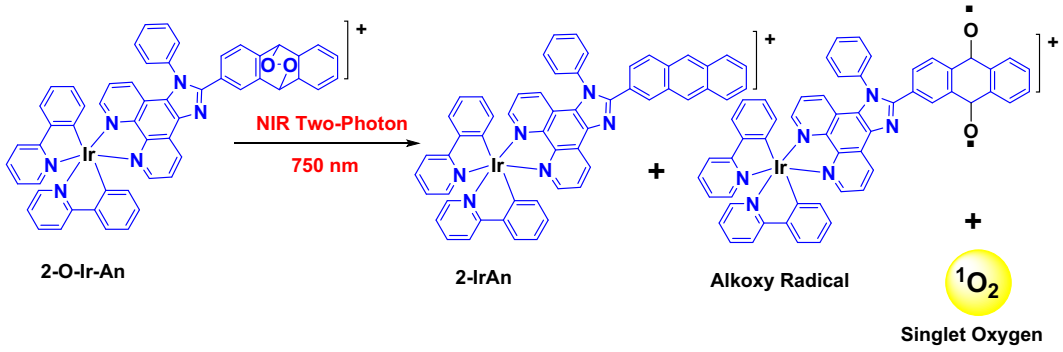

Fig. 105b. Mechanism of formation of **2-Ir-An**, alkoxy radical and singlet oxygen from **2-O-Ir-An**.

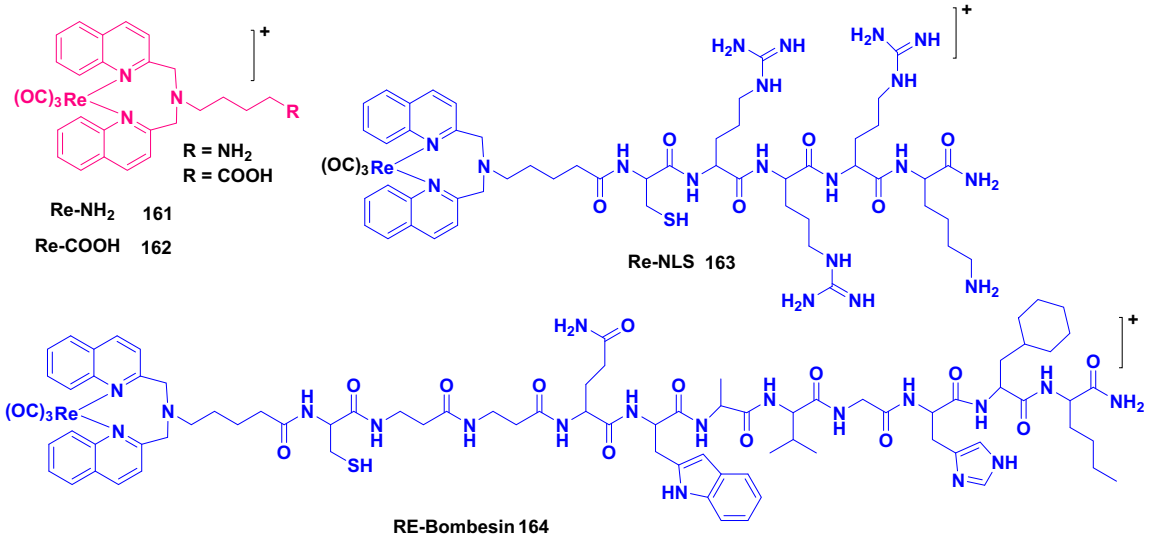

Fig. 106. Structure of **re-NH_2, re-COOH, re-NLS, re-Bombesin**.

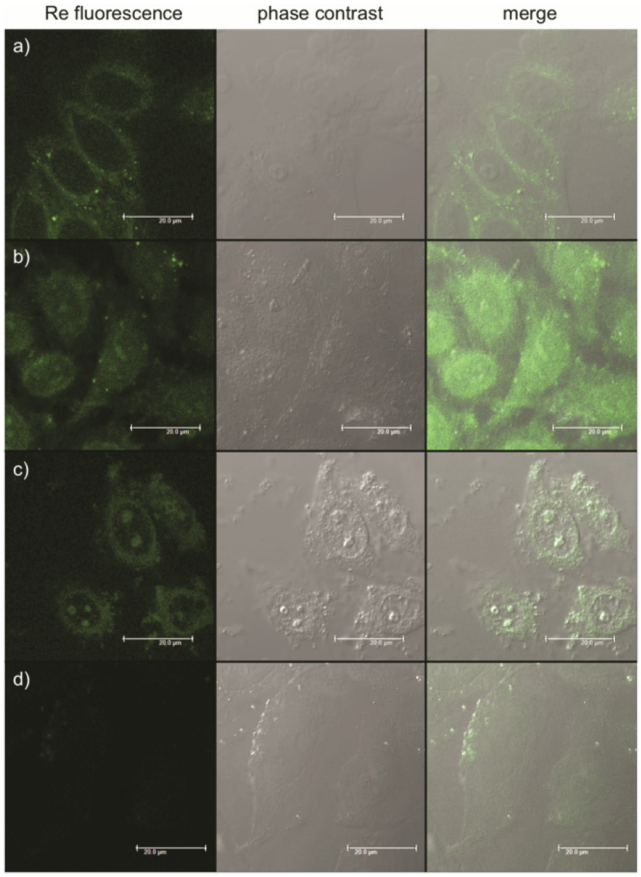

Fig. 107. Fluorescence microscopy images exhibited HeLa cells fixed after treatment with: (a) **Re–NH_2** 100 μM 2 h; (b) **Re–COOH** 2.5 μM 2 h; (c) **Re–NLS** 100 μM 1 h; (d) **Re–Bombesin** 50 μM 2 h. [Adopted from **ref. 180** with permission from Royal Society of Chemistry].

tumors using an 808 nm laser. The biodistribution in the 4 T1 xenograft model was rigorously investigated by the authors through real-time PA imaging following injection to study the clearance pathway of **IrCy** NPs *in vivo* (Fig. 102a). They observed that in the case of kidney the relative PA intensity was found to be around 4.1 at 30 h after injection and then it gradually declined to around 2.0 at 48 h after injection (Fig. 102b, c). Similarly, the relative PA intensity in the bladder at 84 h was nearly 12.6 times that of before injection (Fig. 102d, e). From this observation of PA signal change in the kidney and bladder they said that **IrCy** NPs should be eliminated partially from the urine system. Authors also observed that in the case of liver the relative PA intensity increased from 4.3 to 12.5 (Fig. 102f, g) and increased from 4.6 to 28.8 in the spleen from 3 to 24 h (Fig. 102h, i) but, the relative PA intensity of the liver and spleen diminished to 2.8 and 9.4 after 150 h. So, it was found that the partial hepatic metabolic pathway was highlighted by these biodistributions of **IrCy** NPs in the liver and spleen. The authors also reported that **IrCy** NPs had outstanding tumor ablation capabilities due to their effective creation of $^1O_2$ and targeting effect [178].

Xie *et al.* synthesized two Ir(III) complexes (**159, 160**) and this complexes formed nano (**159 NPs, 160 NPs**) by self-assemble in aqueous media. Authors investigated the photodynamic effect and due to this they dissolved the complex in DMF. They observed that at low concentration 159 NPs exhibited stronger photodynamic effect than **160 NPs** (**103, a**). But when they increased the concentration there was no difference found in photodynamic activity. In (Fig. 103b) it was clearly observed that **159 NPs**, **160 NPs** took 5 mints to reduce the absorption whereas complexes **159**, **160** took 20 mints. This was due to the self-assembly of molecules into NPs causes fluorescence self-quenching and light transfer energy to ROS. From this observation it was clear that nano exhibited good photodynamic activity than complexes **159**, **160** itself. Authors also investigated the cytotoxicity of nano particle toward HeLa and HepG2 cells. In (Fig. 104a) the time-dependent

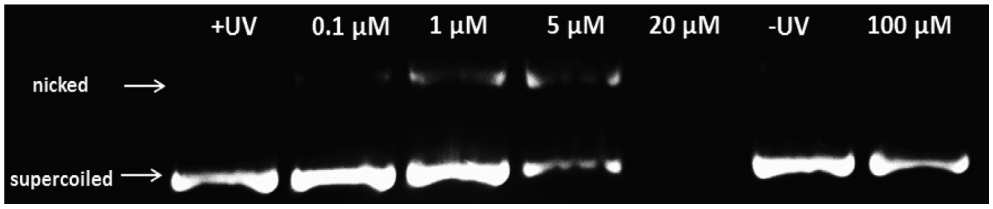

Fig. 108. DNA photo-cleavage by Electrophoresis experiment of pcDNA3 plasmid treated with various concentrations of the complex **Re–NLS**. [Adopted from **ref. 180** with permission from Royal Society of Chemistry].

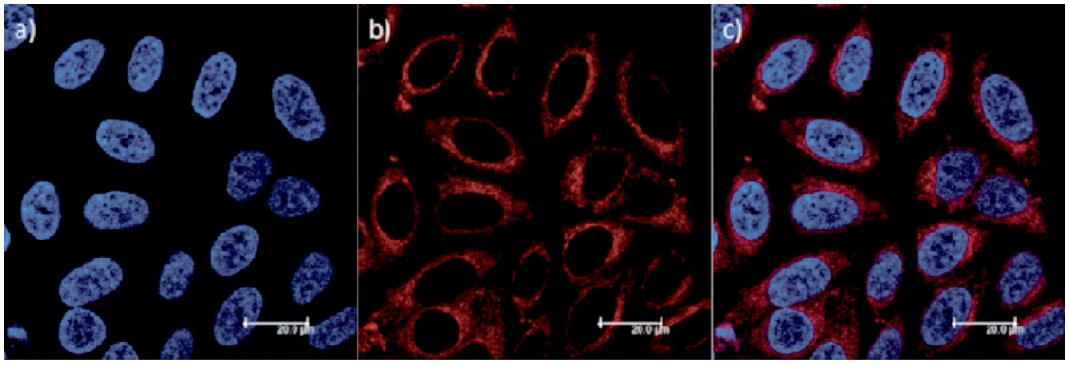

Fig. 109. Confocal microscopy images of HeLa cells incubated with complex **165** (20 mm) for 2 h: a. Staining of DAPI; b. cellular distribution of 165; c. overlay. [Adopted from **ref. 181** with permission from Wiley-VCH].

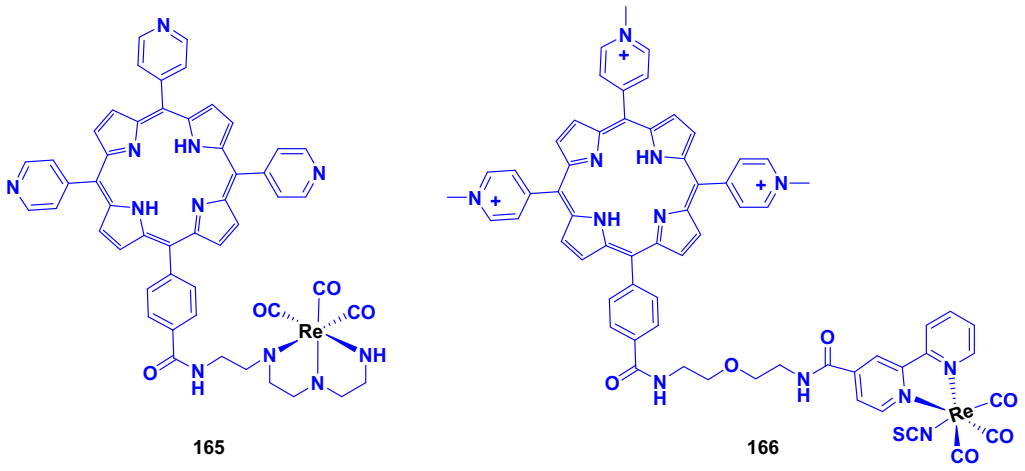

Fig. 110. Structure of complexes **165** and **166**.

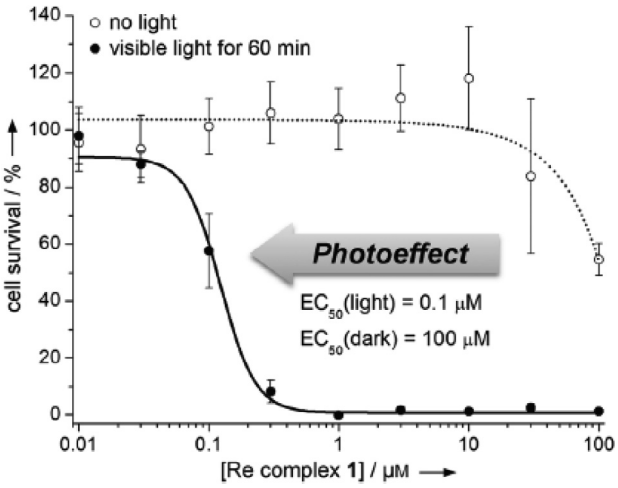

Fig. 111. Antiproliferative action against HeLa cells caused by visible light. MTT assay was used to assess cytotoxicity after an additional 22 h. The standard deviations are based on the results of two separate tests with a total of 18 data points for each component concentration. [Adopted from **ref. 182** with permission from Wiley-VCH].

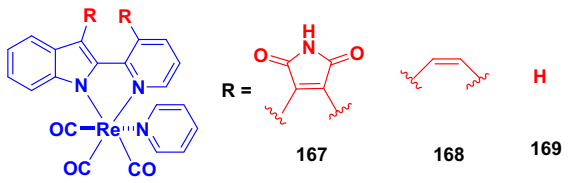

Fig. 112. Structure of complexes **167**, **168**, **169**.

internalisation of **159 NPs**, **160 NPs** was observed. They also used DCFH-DA as a ROS detector. As we know in presence of ROS, DCFH-DA changed to DCF. By CLSM image they observed that without light irradiation very less ROS generation observed but after irradiation ROS production was high (Fig. 104b). They also performed the MTT assay for scrutinized the PDT effects in different cancer cells. They detected that in presence of light irradiation most of all cells were died by 159 NPs but 160 NPs exhibited inferior toxicity under the same condition (Fig. 104c) [179a] (Figs. 105–106).

Very recent Chao *et al.* developed mitochondria localized Ir (III) endoperoxide prodrug **2-O-IrAn.** In presence of two photon irradiation in NIR region **2-O-IrAn** generated Ir (III) complex **2-IrAn** with high cytotoxic effect, an alkoxy radical, and singlet oxygen. Authors observed that in hypoxic tumor cells and multicellular tumor spheroids (MCTS), **2-O-IrAn** exhibited greate phototoxic effect. From detailed analysis of the mechanism of action authors understood that the complex mainly accumulated in the mitochondria, which results in the loss of the mitochondrial membrane potential. To improve the tumor selectivity uptake authors encapsulated the complex with biotin-functionalized phospholipid and finally formed **DSPE-PEG-Biotin@ 2-O-IrAn** nanoparticles**.** They observed that upon two-photon irradiation in the NIR region the nanoparticle entirely eliminated tumor inside the mouse model in just one treatment [179b].

8. Rhenium based complexes as a PDT agent

In comparison to other PSs, tricarbonyl rhenium complexes exhibited attractive and interesting property due to their exceptional photophysical and photochemical properties, less heavy metal toxicity, organelle targeting ability and so on. So, the tricarbonyl rhenium-based PSs came under profound research in order to be used in cancer therapy.

8.1. Tricarbonyl rhenium complexes with different conjugates:

In this regard, Gasser *et al.* developed two tricarbonyl rhenium (I) derivatives, re-NH_2 (**161**), re-COOH (**162**) as a PS in PDT. They observed that in lipophilic environment both the complexes produced singlet oxygen with about 75 % of quantum yield. To develop the selectivity of complex **162**, authors conjugated two types of peptides and produced **re-NLS** (**163**), **re-Bombesin** (**164**). From fluorescent microscopic image (Fig. 107) of HeLa cell, authors observed the improvement of cellular accumulation inside the cell nucleus, specifically in nucleoli. The complexes were not so much cytotoxic in dark, but in presence of light irradiation the complexes as well as the conjugates exhibited their keen cytotoxicity. After light irradiation 20-fold more cytotoxicity was found in case of re-Bombesin (**164**). Authors also investigated the DNA photocleavage with the help of closed circular plasmid DNA (pcDNA3)

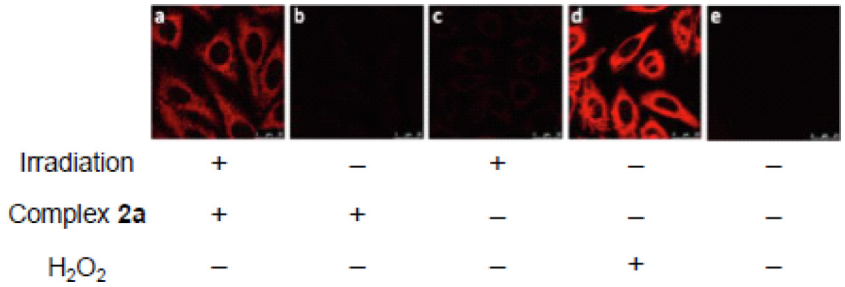

Fig. 113. Discovery of oxidative stress using CellROX™ Deep Red. (a) 365 nm irradiation (b) absence of irradiation at 365 nm (c) Irradiated at 365 nm in untreated HeLa cells were (d) As positive control HeLa cells were treatedwith H_2O_2 (e) As a negative control untreated HeLa cell without irradiation were used. [Adopted from **ref. 189** with permission from Wiley-VCH].

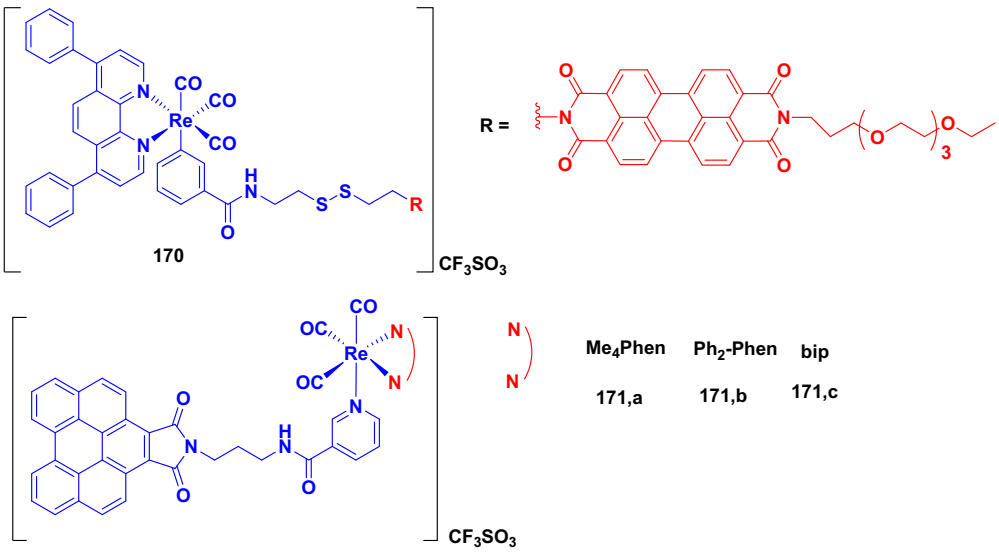

Fig. 114. Structure of complexes **170**, **171a**, **171b**, **171c**.

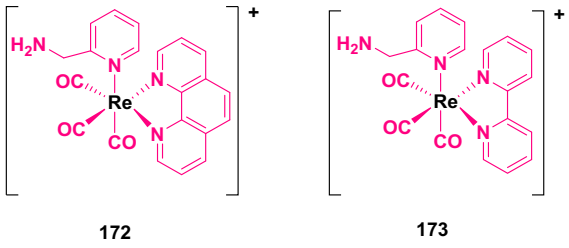

Fig. 115. Structure of complexes **172** and **173**.

(Fig. 108). They incubated pcDNA3 with different concentration of compounds and were irradiated by light. They observed all the compounds changes supercoiled DNA form to circular or nicked forms. In between all the complexes, complex **163** damaged DNA in very low concentration. But in presence of dark not a single compound exhibited this kind of effect [180].

Gianferrara *et al.* developed water-soluble porphyrin conjugated rhenium complexes with diethylenetriamine (**165**) and bipyridyl ligand (**166**). Authors investigated the cytotoxicity against HeLa cell and found the IC_{50} values were 1.9 μM and 4.0 μM for complex **165** and complex **166** respectively. But the negligible cytotoxicity was found in dark condition. They also found the singlet oxygen quantum yield 0.36 and 0.62 for complexes **165** and **166** respectively and it was quite similar with the parent porphyrin moiety indicating that rhenium complexes did not generate singlet oxygen, but its phototoxicity was increased after conjugation with porphyrin moiety. Authors also observed the cellular localization by confocal fluorescence microscopy in HeLa cells. It was clearly observed that complex **165** accumulated in the vicinity of nuclear membrane and exhibited cytoplasmic fluorescence with formation of a ring (Fig. 109b) like structure [181] (See Figs. 110–112).

8.2. Tri-carbonyl rhenium complex with N—N chelating ligand:

By increasing the light absorption profiles of the complexes, the phototoxicity and PDT effect of the rhenium complexes can be increased. Keeping this work in mind Meggers *et al.* developed tricarbonyl Re (I) indolato complexes (**167, 168, 169**). The potent complex **167** exhibited no phototoxicity under dark condition against HeLa cell but in presence of visible light irradiation it exhibited phototoxicity with IC_{50} value 0.1 μM. The more lipophilic, easy penetration property through cell membrane and high phototoxicity effect against HeLa cell of complex **167** was assumed

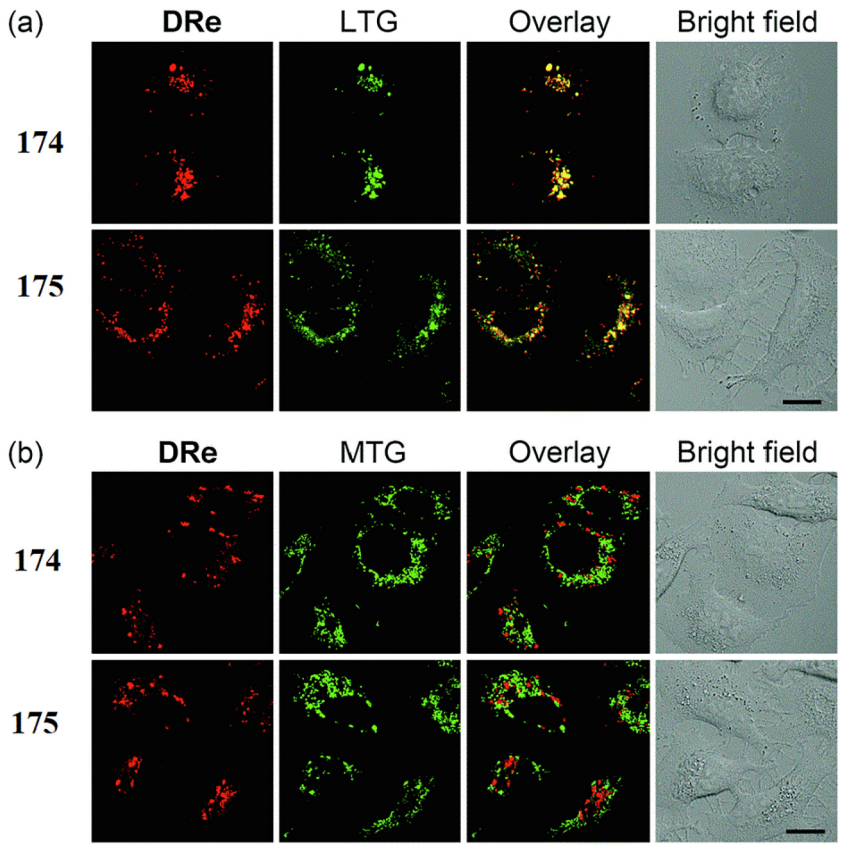

Fig. 116. (a) Confocal images of A549 cells co-localized with complex **174** (20 μM, 1 h), complex **175** (5 μM, 1 h) and LysoTracker Green DND-26 (LTG). (b) CLSM images of A549 cells co-labeled with **174** (20 μM, 1 h), **175**(5 μM, 1 h) and MitoTracker Green FM (MTG). All images in scale bar: 20 μm [Adopted from **ref. 194** with permission from Royal Society of Chemistry].

due to the oxygen and nitrogen substituted five-member ring [182].

perylene diimide (PDI) and benzoperylene monoimide (BPMI) exhibited their promising impact in case of supramolecular system. The fluorogenic responses of a PDI-polyetheramine molecule towards live cells had been discovered to be quite fascinating [183], also multi cationic fluorescent and amphiphilic PDI compound had also used as an imaging agent [184,185]. It was also found that water soluble PDI and BPMI complexes were also used for DNA intercalation [186]. Scientist modified the PDI with some metal center, which was exhibited photocytotoxicity and also acted as a photocatalyst for water oxidation [187–188]. Due to this property Alex *et al.* developed luminescent tricarbonyl Re(I) complexes with PDI (**170**) and BPMI (**171(a), 171(b)** **171(c)**). Authors investigated the phototoxicity of the complexes against HeLa cell in presence of 365 nm UV-A irradiation. They observed the IC_{50} values were 18.21 μM, 0.27 μM, 2.21 μM, and 1.51 μM for complexes **170**, **171(a)**, **171(b)**, **171(c)** respectively. Complex **171(a)** was found to be the most potent among the other four. Authors also investigated the photoinduced cell death (Fig. 113) by using CellROX^{TM} (Deep Red as an oxidative stress indicator) with the help of confocal imaging studies. The highest phototoxicity index (PI) 27.8 was found for the complex **171(a)** [189] (See Figs. 114 and 115).

Frin *et al.* synthesized two tricarbonyl rhenium(I) complexes fac-[Re(ampy)$(CO)_3$(NN)]PF_6 (Where, NN = 1,10-phenanthroline (phen), 2,2′-bipyridine (bpy), and ampy = 2-aminomethylpyridine) (**172, 173**). Authors exhibited two absorption band, one for IL (intraligand transition) and another for MLCT. Both the complexes generated singlet oxygen quantum yield with the range of 0.59 to 0.28 [190].

8.3. Di-nuclear rhenium complex

Like mono nuclear complexes, di nuclear complex also exhibited photodynamic therapy as well as organelle specificity. Many anticancer drugs, including cisplatin have been demonstrated to be resistant to lysosomes after investigation. Effective LMP (lysosomal membrane permeabilization) induction techniques can be employed for effective anticancer treatment [190–193]. Liang *et al.* developed two di-nuclear tricarbonyl rhenium complexes (**174**, **175**) and investigated their ROS production, cellular uptake property, lysosomes targeting ability and cell death outline. Authors studied the cytotoxicity towards different cell lines like A549, A549R, HeLa, and MCF-7. The IC_{50} values ranging from 2.2 to 15.8 μM was found in case of complexes **174** and **175** against different cancer cell lines and that was lower than the cisplatin value under the same condition against the same cancer cell lines.

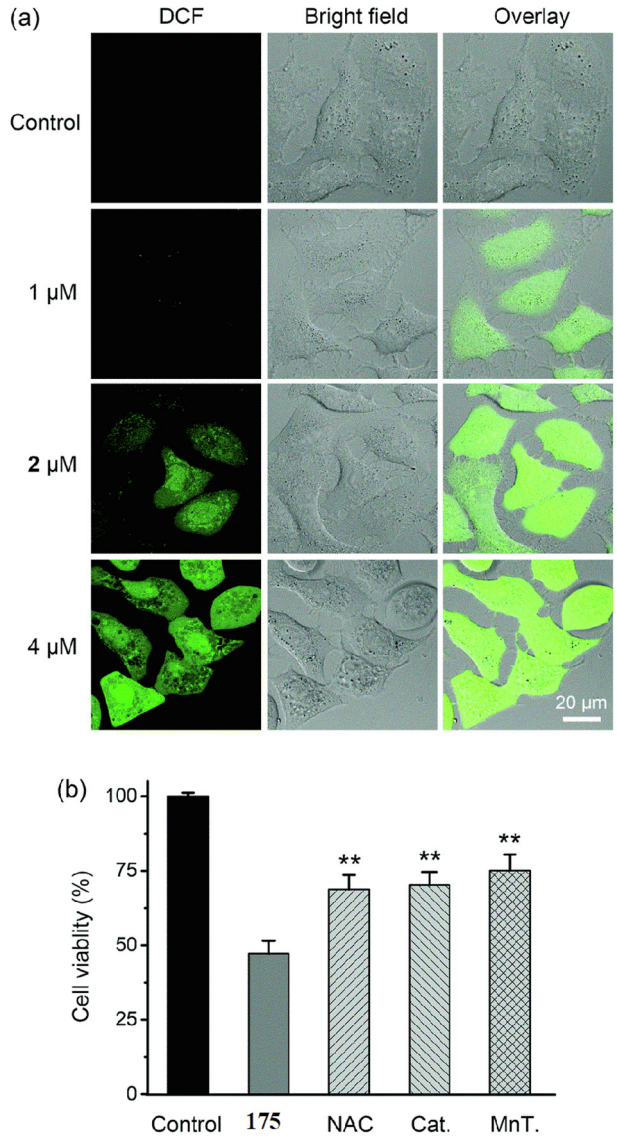

Fig. 117. (a) Intracellular ROS were detected using confocal microscopy and H_2DCF DA. A549 cells were incubated with different concentrations of complex **175** for 4 h. DCF: (green). All images in the same scale bar. (b) Cell viability after a 24-hour treatment with complex **175** (4 M) in the absence or presence of different ROS inhibitors in A549 cells. [Adopted from **ref. 194** with permission from Royal Society of Chemistry].

In case of A549, complex **175** showed 4 times more activity than cisplatin. They also observed the IC_{50} value of complex **175** which was lower than the complex**174**. Actually complex **175** exhibited 3.4 times more anticancer activity against A549 cell than complex **174**. Authors investigated the cellular uptake property by confocal laser scanning microscopy in A549 cell. In (Fig. 116) it was clearly observed that there was nice overlapped between the cellular fluorescence of complexes and LysoTracker Green, but very feeble overlapped was found in case of MitoTracker Green FM(MTG). To study the intracellular ROS levels in A549 cells after exposure of complex **175**, authors used ROS-sensitive fluorescent probe (H_2DCF-DA). H_2DCF-DA was oxidized by ROS to DCF with green fluorescence and it had been clearly observed in (Fig. 117a). So, complex **175** increased the intracellular ROS levels [194] (See Fig. 118).

8.4. Carbonic anhydrase IX (CAIX)-Anchored Rhenium(I) photosensitizer

Su *et al* had been designed a carbonic anhydrase IX (CAIX)-anchored rhenium(I) photosensitizer, named **CA-Re** (Fig. 119), that not only accomplishes type-I and type-II photodynamic therapy (PDT) with high efficiency under hypoxic environment (nanomolar-level phototoxicity), but also induces gasdermin D (GSDMD) mediated pyroptotic cell death to effectively stimulate tumor immunogenicity and it could also self-report the loss of membrane integrity simultaneously [195]. This promoted the maturation and antigen-presenting ability of dendritic cells (DCs), and fully activated T cells dependent adaptive immune response *in vivo*, eventually eliminating distant tumors at the same time as destroying primary tumors.

9. Conclusion

Coming to the brink of thorough discussion, it can be depicted that in current context photodynamic therapy (PDT) is very relevant and serves as a selective tool for cancer therapy where different types of ruthenium (II), iridium (III) and rhenium (I) complexes are very much susceptible to undergo PDT, acting as adroit photosensitizers and hence they are recently being well-studied by the scientists to be appeared as PDT active highly potent anticancer agents. As the PDT can be accomplished only under the irradiation of localised light at affected portion particularly, this therapy can be used safely in cancer-riddled patient without damaging the healthy cells. The detailed mechanism of PDT along with the notion of good photosensitizing agents will help to provide the knowledge of designing the ample PDT active molecules in near future. Not only that the concept of Förster resonance energy transfer (FRET), fluorescence resonance energy transfer (FRET), resonance energy transfer (RET) and electronic energytransfer (EET) will help to modify the absorption efficiency of the photosensitisers. It's a matter of great pleasure that we have been able to accumulate a galore of organelle specific PDT active ruthenium (II), iridium (III) and rhenium (I) complexes in this article mentioning their specific targets and mechanism of action as these complexes are really noticible to damage cancer cells selectively under PDT condition where it has been observed that these complexes are very much efficient to emerge the singlet oxygen or other reactive oxygen species (ROS) at particular organelle such as cell membrane, nucleus, mitochondria, lysosome, endoplasmic reticulum etc. upon irradiation with visible or NIR light and thereby exterminate the cancer cells in body. Moreover, the conjugation of these complexes with nanomaterials or peptides and the formation of molecular organic framework (MOF) are also very sensitive under irradiation of light and exhibit high phototoxicity selectively towards cancer cells. Although the ascending fame in extensive uses of PDT has drawn the attention of the researchers, several challenges with currently developed photosensitizers such as poor water solubility, synthetic and purification difficulties, very short life time of ROS, absence of tumour-targeting moiety, metal complexation in cavity are needed to be improved in near future so as to develop very effective and selective anticancer treatment strategy. Therefore, it can be evidently predicted that the pace of recent advancement of organelle specific ruthenium (II), iridium (III) and rhenium (I) complexes in photodynamic therapy for healing cancer may quench the thirst of the researchers or may open the new door of anticancer research in imminent future.

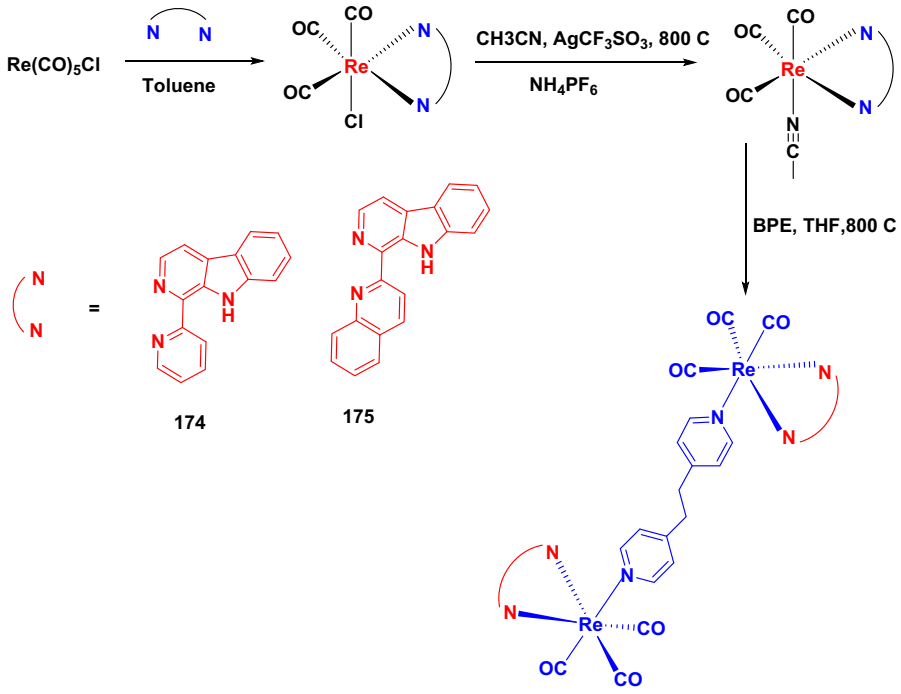

Fig. 118. Synthesis pathway of complexes **174**, **175**.

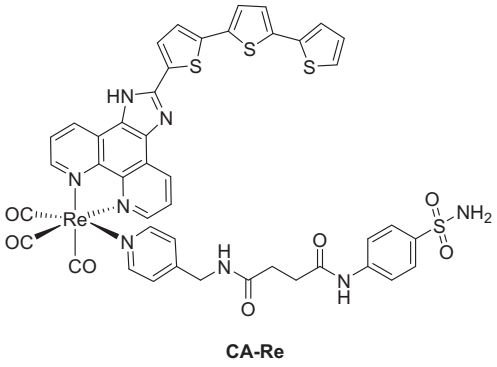

Fig. 119. Structure of **CA-Re**.

Data availability

No data was used for the research described in the article.

Declaration of Competing Interest

The authors declare that they have no known competing financial interests or personal relationships that could have appeared to influence the work reported in this paper.

Acknowledgements

The authors are grateful to VIT for 'VIT SEED GRANT'. We acknowledge DST, New Delhi, India for DST-FIST project. Authors are grateful to Department of Science and Technology, Government of India for supporting the work through the DST-SERB CRG project grant (CRG/2021/002267).

References

[1] (404) 320-3333 American Cancer Society, Inc., 250 Williams St., NW, Atlanta, GA 30303-1002, Global Facts and Figures 2007 Rev2P, 2007. http://www.cancer.org/acs/groups/content/@nho/documents/document/globalfactsandfigures2007rev2p.pdf.
[2] R.L. Siegel, K.D. Miller, H.E. Fuchs, A. Jemal, Cancer statistics, 2022, CA, Cancer J. Clin. 72 (2022) 7–33, https://doi.org/10.3322/caac.21708.
[3] S. Kim, T.Y. Ohulchanskyy, H.E. Pudavar, R.K. Pandey, P.N. Prasad, Organically modified silica nanoparticles co-encapsulating photosensitizing drug and aggregation-enhanced two-photon absorbing fluorescent dye aggregates for two-photon photodynamic therapy, J. Am. Chem. Soc. 129 (2007) 2669–2675, https://doi.org/10.1021/ja0680257.
[4] D. Phillips, The photochemistry of sensitisers for photodynamic therapy, Pure Appl. Chem. 67 (1995) 117–126, https://doi.org/10.1351/pac199567010117.
[5] P. Agostinis, K. Berg, K.A. Cengel, T.H. Foster, A.W. Girotti, S.O. Gollnick, S.M. Hahn, M.R. Hamblin, A. Juzeniene, D. Kessel, M. Korbelik, J. Moan, P. Mroz, D. Nowis, J. Piette, B.C. Wilson, J. Golab, Photodynamic therapy of cancer: an update, CA, Cancer J. Clin. 61 (2011) 250–281, https://doi.org/10.3322/caac.20114.
[6] B.W. Henderson, T.J. Dougherty, How does photodynamic therapy work?, Photochem Photobiol. 55 (1992) 145–157, https://doi.org/10.1111/j.1751-1097.1992.tb04222.x.
[7] P. Mroz, Y. Huang, A. Szokalska, T. Zhiyentayev, S. Janjua, A. Nifli, M.E. Sherwood, C. Ruzié, K.E. Borbas, D. Fan, M. Krayer, T. Balasubramanian, E. Yang, H.L. Kee, C. Kirmaier, J.R. Diers, D.F. Bocian, D. Holten, J.S. Lindsey, M.R. Hamblin, Stable synthetic bacteriochlorins overcome the resistance of melanoma to photodynamic therapy, FASEB J. 24 (2010) 3160–3170, https://doi.org/10.1096/fj.09-152587.
[8] P. Mroz, J. Bhaumik, D.K. Dogutan, Z. Aly, Z. Kamal, L. Khalid, H.L. Kee, D.F. Bocian, D. Holten, J.S. Lindsey, M.R. Hamblin, Imidazole metalloporphyrins as photosensitizers for photodynamic therapy: role of molecular charge, central metal and hydroxyl radical production, Cancer Lett. 282 (2009) 63–76, https://doi.org/10.1016/j.canlet.2009.02.054.
[9] P. Mroz, A. Pawlak, M. Satti, H. Lee, T. Wharton, H. Gali, T. Sarna, M.R. Hamblin, Functionalized fullerenes mediate photodynamic killing of cancer cells: type I versus Type II photochemical mechanism, Free Radic. Biol. Med. 43 (2007) 711–719, https://doi.org/10.1016/j.freeradbiomed.2007.05.005.
[10] P. Mroz, A. Szokalska, M.X. Wu, M.R. Hamblin, R.L. Mosley, Photodynamic therapy of tumors can lead to development of systemic antigen-specific immune response, PLoS One 5 (12) (2010) e15194.
[11] A.P. Castano, P. Mroz, M.R. Hamblin, Photodynamic therapy and anti-tumour immunity, Nat. Rev. Cancer. 6 (2006) 535–545, https://doi.org/10.1038/nrc1894.
[12] P. Mroz, J.T. Hashmi, Y.Y. Huang, N. Lange, M.R. Hamblin, Stimulation of anti-tumor immunity by photodynamic therapy, Expert Rev. Clin. Immunol. 7 (2011) 75–91, https://doi.org/10.1586/eci.10.81.

[13] E. Ruggiero, S. Alonso-De Castro, A. Habtemariam, L. Salassa, Upconverting nanoparticles for the near infrared photoactivation of transition metal complexes: new opportunities and challenges in medicinal inorganic photochemistry, Dalt. Trans. 45 (2016) 13012–13020, https://doi.org/10.1039/c6dt01428c.
[14] L.K. McKenzie, H.E. Bryant, J.A. Weinstein, Transition metal complexes as photosensitisers in one- and two-photon photodynamic therapy, Coord. Chem. Rev. 379 (2019) 2–29, https://doi.org/10.1016/j.ccr.2018.03.020.
[15] X. Zhao, J. Liu, J. Fan, H. Chao, X. Peng, Recent progress in photosensitizers for overcoming the challenges of photodynamic therapy: from molecular design to application, Chem. Soc. Rev. 50 (2021) 4185–4219, https://doi.org/10.1039/d0cs00173b.
[16] S.Q. Zhang, T.T. Meng, J. Li, F. Hong, J. Liu, Y. Wang, L.H. Gao, H. Zhao, K.Z. Wang, Near-IR/visible-emitting thiophenyl-based Ru(II) complexes: efficient photodynamic therapy, cellular uptake, and DNA binding, Inorg. Chem. 58 (2019) 14244–14259, https://doi.org/10.1021/acs.inorgchem.9b02420.
[17] U. Das, B. Kar, S. Pete, P. Paira, Ru(ii), Ir(iii), Re(i) and Rh(iii) based complexes as next generation anticancer metallopharmaceuticals, Dalt. Trans. 50 (2021) 11259–11290, https://doi.org/10.1039/d1dt01326b.
[18] J.F. Lovell, T.W.B. Liu, J. Chen, G. Zheng, Activatable photosensitizers for imaging and therapy, Chem. Rev. 110 (2010) 2839–2857, https://doi.org/10.1021/cr900236h.
[19] D.W. Felsher, Cancer revoked: oncogenes as therapeutic targets, Nat. Rev. Cancer. 3 (2003) 375–380, https://doi.org/10.1038/nrc1070.
[20] Y. Yuan, C.J. Zhang, M. Gao, R. Zhang, B.Z. Tang, B. Liu, Specific light-up bioprobe with aggregation-induced emission and activatable photoactivity for the targeted and image-guided photodynamic ablation of cancer cells, Angew. Chemie – Int. Ed. 54 (2015) 1780–1786, https://doi.org/10.1002/anie.201408476.
[21] M. Balaz, H.A. Collins, E. Dahlstedt, H.L. Anderson, Synthesis of hydrophilic conjugated porphyrin dimers for one-photon and two-photon photodynamic therapy at NIR wavelengths, Org. Biomol. Chem. 7 (2009) 874–888, https://doi.org/10.1039/b814789b.
[22] A. Kamkaew, S.H. Lim, H.B. Lee, L.V. Kiew, L.Y. Chung, K. Burgess, BODIPY dyes in photodynamic therapy, Chem. Soc. Rev. 42 (2013) 77–88, https://doi.org/10.1039/c2cs35216h.
[23] A.P. Castano, T.N. Demidova, M.R. Hamblin, Mechanisms in photodynamic therapy: part one – photosensitizers, photochemistry and cellular localization, Photodiagnosis Photodyn. Ther. 1 (2004) 279–293, https://doi.org/10.1016/S1572-1000(05)00007-4.
[24] T.J. Dougherty, An update on photodynamic therapy applications, J. Clin. Laser Med. Surg. 20 (2002) 3–7, https://doi.org/10.1089/104454702753474931.
[25] H.I. Pass, Photodynamic therapy in oncology: mechanisms and clinical use, J. Natl. Cancer Inst. 85 (1993) 443–456, https://doi.org/10.1093/jnci/85.6.443.
[26] N.L. Oleinick, H.H. Evans, The photobiology of photodynamic therapy: cellular targets and mechanisms, Radiat. Res. 150 (1998) 146–156, https://doi.org/10.2307/3579816.
[27] R. Bonnett, Photosensitizers of the porphyrin and phthalocyanine series for photodynamic therapy, Chem. Soc. Rev. 24 (1995) 19–33, https://doi.org/10.1039/CS9952400019.
[28] E.D. Sternberg, D. Dolphin, C. Brückner, Porphyrin-based photosensitizers for use in photodynamic therapy, Tetrahedron 54 (1998) 4151–4202, https://doi.org/10.1016/S0040-4020(98)00015-5.
[29] R. Ackroyd, C. Kelty, N. Brown, M. Reed, The history of photodetection and photodynamic therapy¶, Photochem. Photobiol. 74 (2001) 656, https://doi.org/10.1562/0031-8655(2001)074<0656:thopap>2.0.co;2.
[30] A. Bergamo, C. Gaiddon, J.H.M. Schellens, J.H. Beijnen, G. Sava, Approaching tumour therapy beyond platinum drugs: status of the art and perspectives of ruthenium drug candidates, J. Inorg. Biochem. 106 (2012) 90–99, https://doi.org/10.1016/j.jinorgbio.2011.09.030.
[31] N.L. Kilah, E. Meggers, Sixty Years young: the diverse biological activities of metal polypyridyl complexes pioneered by Francis P. Dwyer, Aust. J. Chem. 65 (9) (2012) 1325.
[32] (a) L. Salassa, Polypyridyl metal complexes with biological activity, Eur. J. Inorg. Chem. (2011) 4931–4947, https://doi.org/10.1002/ejic.201100376;
(b) Y. Wu, S. Li, Y. Chen, W. He, Z. Guo, Recent advances in noble metal complex based photodynamic therapy, Chem. Sci. (2022) 5085–5106. https://doi.org/10.1039/d1sc05478c.
[33] B. Sun, W. Li, N. Liu, Curative effect of the recent photofrin photodynamic adjuvant treatment on young patients with advanced colorectal cancer, Oncol. Lett. 11 (2016) 2071–2074, https://doi.org/10.3892/ol.2016.4179.
[34] S.S. Stylli, M. Howes, L. MacGregor, P. Rajendra, A.H. Kaye, Photodynamic therapy of brain tumours: evaluation of porphyrin uptake versus clinical outcome, J. Clin. Neurosci. 11 (2004) 584–596, https://doi.org/10.1016/j.jocn.2004.02.001.
[35] C. Tanielian, C. Schweitzer, R. Mechin, C. Wolff, Quantum yield of singlet oxygen production by monomeric and aggregated forms of hematoporphyrin derivative, Free Radic. Biol. Med. 30 (2001) 208–212, https://doi.org/10.1016/S0891-5849(00)00460-3.
[36] J. Kou, D. Dou, L. Yang, Porphyrin photosensitizers in photodynamic therapy and its applications, Oncotargetics 8 (2017) 81591–81603. https://doi.org/10.18632/oncotarget.20189.
[37] (a) D. Wöhrle, A. Hirth, T. Bogdahn-Rai, G. Schnurpfeil, M. Shopova, Photodynamic therapy of cancer: second and third generations of photosensitizers, Russ. Chem. Bull. 47 (1998) 807–816, https://doi.org/10.1007/BF02498146;
(b) R. Wang, X. Li, J. Yoon, Organelle-targeted photosensitizers for precision photodynamic therapy, ACS Appl. Mater. Interfaces. 13 (2021) 19543–19571. https://doi.org/10.1021/acsami.1c02019.
[38] A. Escudero, C. Carrillo-Carrión, M.C. Castillejos, E. Romero-Ben, C. Rosales-Barrios, N. Khiar, Photodynamic therapy: photosensitizers and nanostructures, Mater. Chem. Front. 5 (2021) 3788–3812, https://doi.org/10.1039/d0qm00922a.
[39] W. Fan, P. Huang, X. Chen, Overcoming the Achilles' heel of photodynamic therapy, Chem. Soc. Rev. 45 (2016) 6488–6519, https://doi.org/10.1039/c6cs00616g.
[40] C. Kojima, Y. Toi, A. Harada, K. Kono, Preparation of poly (ethylene glycol)-attached dendrimers encapsulating photosensitizers for application to photodynamic therapy, Bioconjug. Chem. 18 (2007) 663–670, https://doi.org/10.1021/bc060244u.
[41] X. Ma, Q. Qu, Y. Zhao, Targeted delivery of 5-aminolevulinic acid by multifunctional hollow mesoporous silica nanoparticles for photodynamic skin cancer therapy, ACS Appl. Mater. Interfaces 7 (2015) 10671–10676, https://doi.org/10.1021/acsami.5b03087.
[42] N. Lagopati, P.V. Kitsiou, A.I. Kontos, P. Venieratos, E. Kotsopoulou, A.G. Kontos, D.D. Dionysiou, S. Pispas, E.C. Tsilibary, P. Falaras, Photo-induced treatment of breast epithelial cancer cells using nanostructured titanium dioxide solution, J. Photochem. Photobiol. A Chem. 214 (2010) 215–223, https://doi.org/10.1016/j.jphotochem.2010.06.031.
[43] E.A. Rozhkova, I. Ulasov, B. Lai, N.M. Dimitrijevic, M.S. Lesniak, T. Rajh, A High-performance nanobio photocatalyst for targeted brain cancer therapy, Nano Lett. 9 (2009) 3337–3342, https://doi.org/10.1021/nl901610f.
[44] C. Wang, S. Cao, X. Tie, B. Qiu, A. Wu, Z. Zheng, Induction of cytotoxicity by photoexcitation of TiO2 can prolong survival in glioma-bearing mice, Mol. Biol. Rep. 38 (2011) 523–530, https://doi.org/10.1007/s11033-010-0136-9.
[45] R. Vankayala, A. Sagadevan, P. Vijayaraghavan, C.L. Kuo, K.C. Hwang, Metal nanoparticles sensitize the formation of singlet oxygen, Angew. Chemie - Int. Ed. 50 (2011) 10640–10644, https://doi.org/10.1002/anie.201105236.
[46] D.B. Nowak, A.J. Lawrence, E.J. Sánchez, Apertureless near-field/far-field CW two-photon microscope for biological and material imaging and spectroscopic applications, Appl. Opt. 49 (2010) 6766–6771, https://doi.org/10.1364/AO.49.006766.
[47] J. Yao, L.V. Wang, Photoacoustic microscopy, Laser Photon. Rev. 7 (2013) 758–778, https://doi.org/10.1002/lpor.201200060.
[48] Y. Aoyagi, R. Kawakami, H. Osanai, T. Hibi, T. Nemoto, A rapid optical clearing protocol using 2,2′-thiodiethanol for microscopic observation of fixed mouse brain, PLoS One 10 (2015) 1–13, https://doi.org/10.1371/journal.pone.0116280.
[49] S. Monro, K.L. Colón, H. Yin, J. Roque, P. Konda, S. Gujar, R.P. Thummel, L. Lilge, C.G. Cameron, S.A. McFarland, Transition metal complexes and photodynamic therapy from a tumor-centered approach: challenges, opportunities, and highlights from the development of TLD1433, Chem. Rev. 119 (2019) 797–828, https://doi.org/10.1021/acs.chemrev.8b00211.
[50] W.R. Dichtel, J.M. Serin, C. Edder, J.M.J. Fréchet, M. Matuszewski, L.S. Tan, T.Y. Ohulchanskyy, P.N. Prasad, Singlet oxygen generation via two-photon excited FRET, J. Am. Chem. Soc. 126 (2004) 5380–5381, https://doi.org/10.1021/ja031647x.
[51] M. Zhu, J. Zhang, Y. Zhou, P. Xing, L. Gong, C. Su, D. Qi, H. Du, Y. Bian, J. Jiang, Two-photon excited FRET dyads for lysosome-targeted imaging and photodynamic therapy, Inorg. Chem. 57 (2018) 11537–11542, https://doi.org/10.1021/acs.inorgchem.8b01581.
[52] Y. Zhao, Z. Zhang, Z. Lu, H. Wang, Y. Tang, Enhanced energy transfer in a donor-acceptor photosensitizer triggers efficient photodynamic therapy, ACS Appl. Mater. Interfaces. 11 (2019) 38467–38474, https://doi.org/10.1021/acsami.9b12375.
[53] J. Sun, Q. Xin, Y. Yang, H. Shah, H. Cao, Y. Qi, J.R. Gong, J. Li, Nitrogen-doped graphene quantum dots coupled with photosensitizers for one-/two-photon activated photodynamic therapy based on a FRET mechanism, Chem. Commun. 54 (2018) 715–718, https://doi.org/10.1039/c7cc08820e.
[54] J. Zou, Z. Yin, P. Wang, D. Chen, J. Shao, Q. Zhang, L. Sun, W. Huang, X. Dong, Photosensitizer synergistic effects: D-A-D structured organic molecule with enhanced fluorescence and singlet oxygen quantum yield for photodynamic therapy, Chem. Sci. 9 (2018) 2188–2194, https://doi.org/10.1039/c7sc04694d.
[55] Y. Tang, H. Chen, K. Chang, Z. Liu, Y. Wang, S. Qu, H. Xu, C. Wu, Photo-cross-linkable polymer dots with stable sensitizer loading and amplified singlet oxygen generation for photodynamic therapy, ACS Appl. Mater. Interfaces 9 (2017) 3419–3431, https://doi.org/10.1021/acsami.6b14325.
[56] L. Huang, Z. Li, Y. Zhao, J. Yang, Y. Yang, A.I. Pendharkar, Y. Zhang, S. Kelmar, L. Chen, W. Wu, J. Zhao, G. Han, Enhancing photodynamic therapy through resonance energy transfer constructed near-infrared photosensitized nanoparticles, Adv. Mater. 29 (2017) 1–7, https://doi.org/10.1002/adma.201604789.
[57] S. Fantacci, F. De Angelis, A computational approach to the electronic and optical properties of Ru(II) and Ir(III) polypyridyl complexes: applications to DSC, OLED and NLO, Coord. Chem. Rev. 255 (2011) 2704–2726, https://doi.org/10.1016/j.ccr.2011.03.008.
[58] C. Daniel, Photochemistry and photophysics of transition metal complexes: quantum chemistry, Coord. Chem. Rev. 282–283 (2015) 19–32, https://doi.org/10.1016/j.ccr.2014.05.023.
[59] V. Marin, E. Holder, R. Hoogenboom, U.S. Schubert, Functional ruthenium(ii)- and iridium(iii)-containing polymers for potential electro-optical

applications, Chem. Soc. Rev. 36 (2007) 618–635, https://doi.org/10.1039/b610016c.
[60] M. Abrahamsson, H. Wolpher, O. Johansson, J. Larsson, M. Kritikos, L. Eriksson, P.O. Norrby, J. Bergquist, L. Sun, B. Åkermark, L. Hammarström, A new strategy for the improvement of photophysical properties in ruthenium(II) polypyridyl complexes. Synthesis and photophysical and electrochemical characterization of six mononuclear ruthenium(II) bisterpyridine-type complexes, Inorg. Chem. 44 (2005) 3215–3225, https://doi.org/10.1021/ic048247a.
[61] L. Zayat, O. Filevich, L.M. Baraldo, R. Etchenique, Ruthenium polypyridyl phototriggers: from beginnings to perspectives, Philos. Trans. R. Soc. A Math. Phys. Eng. Sci. 371 (2013), https://doi.org/10.1098/rsta.2012.0330.
[62] J.X. Zhang, J.W. Zhou, C.F. Chan, T.C.K. Lau, D.W.J. Kwong, H.L. Tam, N.K. Mak, K.L. Wong, W.K. Wong, Comparative studies of the cellular uptake, subcellular localization, and cytotoxic and phototoxic antitumor properties of ruthenium (II)-porphyrin conjugates with different linkers, Bioconjug. Chem. 23 (2012) 1623–1638, https://doi.org/10.1021/bc300201h.
[63] J. Zhang, K.L. Wong, W.K. Wong, N.K. Mak, D.W.J. Kwong, H.L. Tam, Two-photon induced luminescence, singlet oxygen generation, cellular uptake and photocytotoxic properties of amphiphilic Ru(ii) polypyridyl-porphyrin conjugates as potential bifunctional photodynamic therapeutic agents, Org. Biomol. Chem. 9 (2011) 6004–6010, https://doi.org/10.1039/c1ob05415e.
[64] Y. Zhang, Q. Zhou, N. Tian, C. Li, X. Wang, Ru(II)-complex-based DNA photocleaver having intense absorption in the phototherapeutic window, Inorg. Chem. 56 (2017) 1865–1873, https://doi.org/10.1021/acs.inorgchem.6b02459.
[65] E. Wachter, D.K. Heidary, B.S. Howerton, S. Parkin, E.C. Glazer, Light-activated ruthenium complexes photobind DNA and are cytotoxic in the photodynamic therapy window, Chem. Commun. 48 (2012) 9649–9651, https://doi.org/10.1039/c2cc33359g.
[66] J. Yang, Q. Cao, W.L. Hu, R.R. Ye, L. He, L.N. Ji, P.Z. Qin, Z.W. Mao, Theranostic TEMPO-functionalized Ru(ii) complexes as photosensitizers and oxidative stress indicators, Dalt. Trans. 46 (2017) 445–454, https://doi.org/10.1039/c6dt04028d.
[67] Q.X. Zhou, W.H. Lei, C. Li, Y.J. Hou, X.S. Wang, B.W. Zhang, DNA photocleavage in anaerobic conditions by a Ru(ii) polypyridyl complex with long wavelength MLCT absorption, New J. Chem. 34 (2010) 137–140, https://doi.org/10.1039/b9nj00465c.
[68] V. Pierroz, R. Rubbiani, C. Gentili, M. Patra, C. Mari, G. Gasser, S. Ferrari, Dual mode of cell death upon the photo-irradiation of a RuII polypyridyl complex in interphase or mitosis, Chem. Sci. 7 (2016) 6115–6124, https://doi.org/10.1039/c6sc00387g.
[69] J. Liu, Y. Chen, G. Li, P. Zhang, C. Jin, L. Zeng, L. Ji, H. Chao, Ruthenium(II) polypyridyl complexes as mitochondria-targeted two-photon photodynamic anticancer agents, Biomaterials 56 (2015) 140–153, https://doi.org/10.1016/j.biomaterials.2015.04.002.
[70] H. Huang, B. Yu, P. Zhang, J. Huang, Y. Chen, G. Gasser, L. Ji, H. Chao, Highly charged ruthenium(II) polypyridyl complexes as lysosome-localized photosensitizers for two-photon photodynamic therapy, Angew. Chemie – Int. Ed. 54 (2015) 14049–14052, https://doi.org/10.1002/anie.201507800.
[71] L. Conti, A. Bencini, C. Ferrante, C. Gellini, P. Paoli, M. Parri, G. Pietraperzia, B. Valtancoli, C. Giorgi, Highly charged ruthenium(II) polypyridyl complexes as effective photosensitizer in photodynamic therapy, Chem. – A Eur. J. 25 (2019) 10606–10615, https://doi.org/10.1002/chem.201901570.
[72] J. Karges, J. Li, L. Zeng, H. Chao, G. Gasser, Polymeric encapsulation of a ruthenium polypyridine complex for tumor targeted one- and two-photon photodynamic therapy, ACS Appl. Mater. Interfaces 12 (2020) 54433–54444, https://doi.org/10.1021/acsami.0c16119.
[73] S. Roy, E. Colombo, R. Vinck, C. Mari, R. Rubbiani, M. Patra, G. Gasser, Increased lipophilicity of halogenated ruthenium(II) polypyridyl complexes leads to decreased phototoxicity in vitro when used as photosensitizers for photodynamic therapy, ChemBioChem 21 (2020) 2966–2973, https://doi.org/10.1002/cbic.202000289.
[74] X. Zhao, M. Li, W. Sun, J. Fan, J. Du, X. Peng, An estrogen receptor targeted ruthenium complex as a two-photon photodynamic therapy agent for breast cancer cells, Chem. Commun. 54 (2018) 7038–7041, https://doi.org/10.1039/c8cc03786h.
[75] J. Karges, F. Heinemann, F. Maschietto, M. Patra, O. Blacque, I. Ciofini, B. Spingler, G. Gasser, A Ru(II) polypyridyl complex bearing aldehyde functions as a versatile synthetic precursor for long-wavelength absorbing photodynamic therapy photosensitizers, Elsevier Ltd (2019), https://doi.org/10.1016/j.bmc.2019.05.011.
[76] J. Karges, M. Tharaud, G. Gasser, Polymeric encapsulation of a Ru(II)-based photosensitizer for folate-targeted photodynamic therapy of drug resistant cancers, J. Med. Chem. 64 (2021) 4612–4622, https://doi.org/10.1021/acs.jmedchem.0c02006.
[77] S. Rani-Beeram, K. Meyer, A. McCrate, Y. Hong, M. Nielsen, S. Swavey, A fluorinated ruthenium porphyrin as a potential photodynamic therapy agent: synthesis, characterization, DNA binding, and melanoma cell studies, Inorg. Chem. 47 (2008) 11278–11283, https://doi.org/10.1021/ic8015589.
[78] R.E. Goldbach, I. Rodriguez-Garcia, J.H. Van Lenthe, M.A. Siegler, S. Bonnet, N-acetylmethionine and biotin as photocleavable protective groups for ruthenium polypyridyl complexes, Chem. – A Eur. J. 17 (2011) 9924–9929, https://doi.org/10.1002/chem.201101541.
[79] B. Liu, Y. Gao, M.A. Jabed, S. Kilina, G. Liu, W. Sun, Lysosome targeting bis-terpyridine ruthenium(II) complexes: photophysical properties and in vitro photodynamic therapy, ACS Appl. Bio Mater. 3 (2020) 6025–6038, https://doi.org/10.1021/acsabm.0c00647.
[80] J. Chen, Q. Tao, J. Wu, M. Wang, Z. Su, Y. Qian, T. Yu, Y. Wang, X. Xue, H.K. Liu, A lysosome-targeted ruthenium(II) polypyridyl complex as photodynamic anticancer agent, J. Inorg. Biochem. 210 (2020), https://doi.org/10.1016/j.jinorgbio.2020.111132 111132.
[81] M. Samoc, J.P. Morrall, G.T. Dalton, M.P. Cifuentes, M.G. Humphrey, Two-photon and three-photon absorption in an organometallic dendrimer, Angew. Chemie – Int. Ed. 46 (2007) 731–733, https://doi.org/10.1002/anie.200602341.
[82] B.J. Coe, Switchable nonlinear optical metallochromophores with pyridinium electron acceptor groups, Acc. Chem. Res. 39 (2006) 383–393, https://doi.org/10.1021/ar050225k.
[83] Y. Zhu, T. Fei, Y. Ma, A highly efficient red-emitting ruthenium complex with 3,5-difluorophenyl substituents, Chemluschem 81 (2016) 73–79, https://doi.org/10.1002/cplu.201500346.
[84] F. Schmitt, P. Govindaswamy, O. Zava, G. Süss-Fink, L. Juillerat-Jeanneret, B. Therrien, Combined arene ruthenium porphyrins as chemotherapeutics and photosensitizers for cancer therapy, J. Biol. Inorg. Chem. 14 (2009) 101–109, https://doi.org/10.1007/s00775-008-0427-y.
[85] L.S. Rallidis, N.H. Papageorgakis, A.A. Megalou, N.J. Exadactylos, G.K. Tsitouris, E.G. Papasteriadis, High incidence of dyslipidaemia in the offspring of Greek men with premature coronary artery disease, Eur. Heart J. 19 (1998) 395–401, https://doi.org/10.1053/euhj.1997.0770.
[86] J.X. Zhang, M. Pan, C.Y. Su, Synthesis, photophysical properties and: in vitro evaluation of a chlorambucil conjugated ruthenium(II) complex for combined chemo-photodynamic therapy against HeLa cells, J. Mater. Chem. B 5 (2017) 4623–4632, https://doi.org/10.1039/c7tb00702g.
[87] F. Zhao, W. Wang, W. Wu, A novel ruthenium polypyridyl complex for the selective imaging and photodynamic targeting of the Golgi apparatus, Dalt. Trans. 50 (2021) 3536–3541, https://doi.org/10.1039/d1dt00216c.
[88] G. Bianchini, J.M. Balko, I.A. Mayer, M.E. Sanders, L. Gianni, Triple-negative breast cancer: challenges and opportunities of a heterogeneous disease, Nat. Rev. Clin. Oncol. 13 (2016) 674–690, https://doi.org/10.1038/nrclinonc.2016.66.
[89] H. Wang, D.J. Mooney, Metabolic glycan labelling for cancer-targeted therapy, Nat. Chem. 12 (2020) 1102–1114, https://doi.org/10.1038/s41557-020-00587-w.
[90] L. Shen, L. Shen, K. Cai, J. Yu, J. Cheng, Facile click-mediated cell imaging strategy of liposomal azido mannosamine lipids via metabolic or nonmetabolic glycoengineering, ACS Omega. 5 (2020) 14111–14115, https://doi.org/10.1021/acsomega.0c01644.
[91] S.H. Park, H. Jung, H. Lee, T.M. Kim, J.W. Cho, W.D. Jang, J.Y. Hyun, I. Shin, Cancer cell death using metabolic glycan labelling techniques, Chem. Commun. 56 (2020) 10650–10653, https://doi.org/10.1039/d0cc04474a.
[92] H. Wang, Y. Bo, Y. Liu, M. Xu, K. Cai, R. Wang, J. Cheng, In vivo cancer targeting via glycopolyester nanoparticle mediated metabolic cell labeling followed by click reaction, Biomaterials 218 (2019), https://doi.org/10.1016/j.biomaterials.2019.119305 119305.
[93] H. Wang, R. Wang, K. Cai, H. He, Y. Liu, J. Yen, Z. Wang, M. Xu, Y. Sun, X. Zhou, Q. Yin, L. Tang, I.T. Dobrucki, L.W. Dobrucki, E.J. Chaney, S.A. Boppart, T.M. Fan, S. Lezmi, X. Chen, L. Yin, J. Cheng, Selective in vivo metabolic cell-labeling-mediated cancer targeting, Nat. Chem. Biol. 13 (2017) 415–424, https://doi.org/10.1038/nchembio.2297.
[94] C. Agatemor, M.J. Buettner, R. Ariss, K. Muthiah, C.T. Saeui, K.J. Yarema, Exploiting metabolic glycoengineering to advance healthcare, Nat. Rev. Chem. 3 (2019) 605–620, https://doi.org/10.1038/s41570-019-0126-y.
[95] M. Lin, S. Zou, X. Liao, Y. Chen, D. Luo, L. Ji, H. Chao, Ruthenium(ii) complexes as bioorthogonal two-photon photosensitizers for tumour-specific photodynamic therapy against triple-negative breast cancer cells, Chem. Commun. 57 (2021) 4408–4411, https://doi.org/10.1039/d1cc00661d.
[96] Y. Chen, W. Lei, G. Jiang, Q. Zhou, Y. Hou, C. Li, B. Zhang, X. Wang, A ruthenium (ii) arene complex showing emission enhancement and photocleavage activity towards DNA from singlet and triplet excited states respectively, Dalt. Trans. 42 (2013) 5924–5931, https://doi.org/10.1039/c3dt33090g.
[97] C. Mari, V. Pierroz, R. Rubbiani, M. Patra, J. Hess, B. Spingler, L. Oehninger, J. Schur, I. Ott, L. Salassa, S. Ferrari, G. Gasser, DNA intercalating RuII polypyridyl complexes as effective photosensitizers in photodynamic therapy, Chem. – A Eur. J. 20 (2014) 14421–14436, https://doi.org/10.1002/chem.201402796.
[98] H. Ke, H. Wang, W.K. Wong, N.K. Mak, D.W.J. Kwong, K.L. Wong, H.L. Tam, Responsive and mitochondria-specific ruthenium(ii) complex for dual in vitro applications: two-photon (near-infrared) induced imaging and regioselective cell killing, Chem. Commun. 46 (2010) 6678–6680, https://doi.org/10.1039/c0cc01848a.
[99] L.N. Lameijer, S.L. Hopkins, T.G. Brevé, S.H.C. Askes, S. Bonnet, d- Versus l-Glucose conjugation: mitochondrial targeting of a light-activated dual-mode-of-action ruthenium-based anticancer prodrug, Chem. – A Eur. J. 22 (2016) 18484–18491, https://doi.org/10.1002/chem.201603066.
[100] H. Huang, P. Zhang, B. Yu, C. Jin, L. Ji, H. Chao, Synthesis, characterization and biological evaluation of mixed-ligand ruthenium(II) complexes for photodynamic therapy, Dalt. Trans. 44 (2015) 17335–17345, https://doi.org/10.1039/c5dt02081f.
[101] R. Kikkeri, I. García-Rubio, P.H. Seeberger, Ru(II)-carbohydrate dendrimers as photoinduced electron transfer lectin biosensors, Chem. Commun. (2009) 235–237, https://doi.org/10.1039/b814146k.

[102] C. Hartinger, A. Nazarov, S. Ashraf, P. Dyson, B. Keppler, Carbohydrate-metal complexes and their potential as anticancer agents, Curr. Med. Chem. 15 (2008) 2574–2591, https://doi.org/10.2174/092986708785908978.
[103] M. Gottschaldt, U.S. Schubert, Prospects of metal complexes peripherally substituted with sugars in biomedicinal applications, Chem. - A Eur. J. 15 (2009) 1548–1557, https://doi.org/10.1002/chem.200802013.
[104] M. Gottschaldt, U.S. Schubert, S. Rau, S. Yano, J.G. Vos, T. Kroll, J. Clement, I. Hilger, Sugar-selective enrichment of a D-glucose-substituted ruthenium bipyridyl complex inside HepG2 cancer cells, ChemBioChem. 11 (2010) 649–652, https://doi.org/10.1002/cbic.200900769.
[105] S. Chakrabortty, B.K. Agrawalla, A. Stumper, N.M. Vegi, S. Fischer, C. Reichardt, M. Kögler, B. Dietzek, M. Feuring-Buske, C. Buske, S. Rau, T. Weil, Mitochondria targeted protein-ruthenium photosensitizer for efficient photodynamic applications, J. Am. Chem. Soc. 139 (2017) 2512–2519, https://doi.org/10.1021/jacs.6b13399.
[106] F. Paquin, J. Rivnay, A. Salleo, N. Stingelin, C. Silva, Multi-phase semicrystalline microstructures drive exciton dissociation in neat plastic semiconductors, J. Mater. Chem. C. 3 (2015) 10715–10722, https://doi.org/10.1039/b000000x.
[107] L. Blackmore, R. Moriarty, C. Dolan, K. Adamson, R.J. Forster, M. Devocelle, T.E. Keyes, Peptide directed transmembrane transport and nuclear localization of Ru(II) polypyridyl complexes in mammalian cells, Chem. Commun. 49 (2013) 2658–2660, https://doi.org/10.1039/c3cc40453f.
[108] L. Marcélis, S. Kajouj, J. Ghesquière, G. Fettweis, I. Coupienne, R. Lartia, M. Surin, E. Defrancq, J. Piette, C. Moucheron, A. Kirsch-De Mesmaeker, Highly DNA-photoreactive ruthenium 1,4,5,8-tetraazaphenanthrene complex conjugated to the TAT peptide: efficient vectorization inside HeLa Cells without Phototoxicity – The Importance of Cellular Distribution, Eur. J. Inorg. Chem. (2016 (2016)) 2902–2911, https://doi.org/10.1002/ejic.201600278.
[109] A. Martin, A. Byrne, C.S. Burke, R.J. Forster, T.E. Keyes, Peptide-bridged dinuclear Ru(II) complex for mitochondrial targeted monitoring of dynamic changes to oxygen concentration and ROS generation in live mammalian cells, J. Am. Chem. Soc. 136 (2014) 15300–15309, https://doi.org/10.1021/ja508043q.
[110] W. Xu, J. Zuo, L. Wang, L. Ji, H. Chao, Dinuclear ruthenium(II) polypyridyl complexes as single and two-photon luminescence cellular imaging probes, Chem. Commun. 50 (2014) 2123–2125, https://doi.org/10.1039/c3cc48916g.
[111] M.R. Gill, D. Cecchin, M.G. Walker, R.S. Mulla, G. Battaglia, C. Smythe, J.A. Thomas, Targeting the endoplasmic reticulum with a membrane-interactive luminescent ruthenium(ii) polypyridyl complex, Chem. Sci. 4 (2013) 4512–4519, https://doi.org/10.1039/c3sc51725j.
[112] R. Chakrabarty, P.S. Mukherjee, P.J. Stang, Supramolecular coordination: self-assembly of finite two- and three-dimensional ensembles, Chem. Rev. 111 (2011) 6810–6918, https://doi.org/10.1021/cr200077m.
[113] M. Fujita, M. Tominaga, A. Hori, B. Therrien, Coordination assemblies from a Pd(II)-cornered square complex, Acc. Chem. Res. 38 (2005) 369–378, https://doi.org/10.1021/ar040153h.
[114] G. of food science and nutrition/University of L. Williamson, U. of S. Clifford, M.N. (School of Bioscience and Medicine, Version : accepted Version Article :, Biochem Pharmacol. 139 (2017) 24–39. https://doi.org/10.1002/chem.200)).
[115] A. Wragg, M.R. Gill, L. McKenzie, C. Glover, R. Mowll, J.A. Weinstein, X. Su, C. Smythe, J.A. Thomas, Serum albumin binding inhibits nuclear uptake of luminescent metal-complex-based DNA IMAGING PROBEs, Chem. - A Eur. J. 21 (2015) 11865–11871, https://doi.org/10.1002/chem.201501675.
[116] W.A. Wani, S. Prashar, S. Shreaz, S. Gómez-Ruiz, Nanostructured materials functionalized with metal complexes: in search of alternatives for administering anticancer metallodrugs, Coord. Chem. Rev. 312 (2016) 67–98, https://doi.org/10.1016/j.ccr.2016.01.001.
[117] C. Li, J. Wang, Y. Wang, H. Gao, G. Wei, Y. Huang, H. Yu, Y. Gan, Y. Wang, L. Mei, H. Chen, H. Hu, Z. Zhang, Y. Jin, Recent progress in drug delivery, Acta Pharm. Sin. B 9 (2019) 1145–1162, https://doi.org/10.1016/j.apsb.2019.08.003.
[118] J. Karges, D. Díaz-García, S. Prashar, S. Gómez-Ruiz, G. Gasser, Ru(II) polypyridine complex-functionalized mesoporous silica nanoparticles as photosensitizers for cancer targeted photodynamic therapy, ACS Appl. Bio Mater. 4 (2021) 4394–4405, https://doi.org/10.1021/acsabm.1c00151.
[119] D.Y. Zhang, Y. Zheng, H. Zhang, L. He, C.P. Tan, J.H. Sun, W. Zhang, X. Peng, Q. Zhan, L.N. Ji, Z.W. Mao, Ruthenium complex-modified carbon nanodots for lysosome-targeted one- and two-photon imaging and photodynamic therapy, Nanoscale 9 (2017) 18966–18976, https://doi.org/10.1039/c7nr05349e.
[120] M.H. Sakr, N.M. Halabi, L.N. Kalash, S.I. Al-Ghadban, M.K. Rammah, M.E. El Sabban, K.H. Bouhadir, T.H. Ghaddar, Synthesis and: in vitro cytotoxicity evaluation of ruthenium polypyridyl-sensitized paramagnetic titania nanoparticles for photodynamic therapy, RSC Adv. 6 (2016) 47520–47529, https://doi.org/10.1039/c6ra09696d.
[121] F. Wei, S. Kuang, T.W. Rees, X. Liao, J. Liu, D. Luo, J. Wang, X. Zhang, L. Ji, H. Chao, Ruthenium(II) complexes coordinated to graphitic carbon nitride: oxygen self-sufficient photosensitizers which produce multiple ROS for photodynamic therapy in hypoxia, Biomaterials 276 (2021), https://doi.org/10.1016/j.biomaterials.2021.121064 121064.
[122] J. Hess, H. Huang, A. Kaiser, V. Pierroz, O. Blacque, H. Chao, G. Gasser, Evaluation of the medicinal potential of two ruthenium(II) polypyridine complexes as one- and two-photon photodynamic therapy photosensitizers, Chem. - A Eur. J. 23 (2017) 9888–9896, https://doi.org/10.1002/chem.201701392.
[123] V. Ramu, S. Aute, N. Taye, R. Guha, M.G. Walker, D. Mogare, A. Parulekar, J.A. Thomas, S. Chattopadhyay, A. Das, Photo-induced cytotoxicity and anti-metastatic activity of ruthenium(II)-polypyridyl complexes functionalized with tyrosine or tryptophan, Dalt. Trans. 46 (2017) 6634–6644, https://doi.org/10.1039/c7dt00670e.
[124] Z. Lv, H. Wei, Q. Li, X. Su, S. Liu, K.Y. Zhang, W. Lv, Q. Zhao, X. Li, W. Huang, Achieving efficient photodynamic therapy under both normoxia and hypoxia using cyclometalated Ru(II) photosensitizer through type i photochemical process, Chem. Sci. 9 (2018) 502–512, https://doi.org/10.1039/c7sc03765a.
[125] L. Zeng, S. Kuang, G. Li, C. Jin, L. Ji, H. Chao, A GSH-activatable ruthenium(ii)-azo photosensitizer for two-photon photodynamic therapy, Chem. Commun. 53 (2017) 1977–1980, https://doi.org/10.1039/c6cc10330h.
[126] A.M. Palmer, B. Peña, R.B. Sears, O. Chen, M. El Ojaimi, R.R. Thummel, K.R. Dunbar, C. Turro, Cytotoxicity of cyclometallated ruthenium complexes: the role of ligand exchange on the activity, Philos. Trans. R. Soc. A Math. Phys. Eng. Sci. 371 (2013), https://doi.org/10.1098/rsta.2012.0135.
[127] Z. Liu, A. Habtemariam, A.M. Pizarro, S.A. Fletcher, A. Kisova, O. Vrana, L. Salassa, P.C.A. Bruijnincx, G.J. Clarkson, V. Brabec, P.J. Sadler, Organometallic half-sandwich iridium anticancer complexes, J. Med. Chem. 54 (2011) 3011–3026, https://doi.org/10.1021/jm2000932.
[128] A. Wilbuer, D.H. Vlecken, D.J. Schmitz, K. Kräling, K. Harms, C.P. Bagowski, E. Meggers, Iridium complex with antiangiogenic properties, Angew. Chemie - Int. Ed. 49 (2010) 3839–3842, https://doi.org/10.1002/anie.201000682.
[129] R. Pettinari, F. Marchetti, C. Pettinari, F. Condello, A. Petrini, R. Scopelliti, T. Riedel, P.J. Dyson, Organometallic rhodium(III) and iridium(III) cyclopentadienyl complexes with curcumin and bisdemethoxycurcumin co-ligands, Dalt. Trans. 44 (2015) 20523–20531, https://doi.org/10.1039/c5dt03037d.
[130] L. Tabrizi, H. Chiniforoshan, Designing new iridium(iii) arene complexes of naphthoquinone derivatives as anticancer agents: a structure-activity relationship study, 2017. https://doi.org/10.1039/C6DT04339A.
[131] C.H. Leung, H.J. Zhong, D.S.H. Chan, D.L. Ma, Bioactive iridium and rhodium complexes as therapeutic agents, Coord. Chem. Rev. 257 (2013) 1764–1776, https://doi.org/10.1016/j.ccr.2013.01.034.
[132] W. Lv, Z. Zhang, K.Y. Zhang, H. Yang, S. Liu, A. Xu, S. Guo, Q. Zhao, W. Huang, A Mitochondria-targeted photosensitizer showing improved photodynamic therapy effects under hypoxia, Angew. Chemie - Int. Ed. 55 (2016) 9947–9951, https://doi.org/10.1002/anie.201604130.
[133] Y. Li, K.N. Wang, L. He, L.N. Ji, Z.W. Mao, Synthesis, photophysical and anticancer properties of mitochondria-targeted phosphorescent cyclometalated iridium(III) N-heterocyclic carbene complexes, J. Inorg. Biochem. 205 (2020), https://doi.org/10.1016/j.jinorgbio.2019.110976.
[134] X.D. Song, B.B. Chen, S.F. He, N.L. Pan, J.X. Liao, J.X. Chen, G.H. Wang, J. Sun, Guanidine-modified cyclometalated iridium(III) complexes for mitochondria-targeted imaging and photodynamic therapy, Eur. J. Med. Chem. 179 (2019) 26–37, https://doi.org/10.1016/j.ejmech.2019.06.045.
[135] J. Liu, C. Jin, B. Yuan, Y. Chen, X. Liu, L. Ji, H. Chao, Enhanced cancer therapy by the marriage of metabolic alteration and mitochondrial-targeted photodynamic therapy using cyclometalated Ir(III) complexes, Chem. Commun. 53 (2017) 9878–9881, https://doi.org/10.1039/c7cc05518h.
[136] X.D. Bi, R. Yang, Y.C. Zhou, D. Chen, G.K. Li, Y.X. Guo, M.F. Wang, D. Liu, F. Gao, Cyclometalated iridium(III) complexes as high-sensitivity two-photon excited mitochondria dyes and near-infrared photodynamic therapy agents, Inorg. Chem. 59 (2020) 14920–14931, https://doi.org/10.1021/acs.inorgchem.0c01509.
[137] F.X. Wang, M.H. Chen, Y.N. Lin, H. Zhang, C.P. Tan, L.N. Ji, Z.W. Mao, Dual functions of cyclometalated iridium(III) complexes: anti-metastasis and lysosome-damaged photodynamic therapy, ACS Appl. Mater. Interfaces 9 (2017) 42471–42481, https://doi.org/10.1021/acsami.7b10258.
[138] L. He, Y. Li, C.P. Tan, R.R. Ye, M.H. Chen, J.J. Cao, L.N. Ji, Z.W. Mao, Cyclometalated iridium(III) complexes as lysosome-targeted photodynamic anticancer and real-time tracking agents, Chem. Sci. 6 (2015) 5409–5418, https://doi.org/10.1039/c5sc01955a.
[139] F. Xue, Y. Lu, Z. Zhou, M. Shi, Y. Yan, H. Yang, S. Yang, Two in one: luminescence imaging and 730 nm continuous wave laser driven photodynamic therapy of iridium complexes, Organometallics 34 (2015) 73–77, https://doi.org/10.1021/om500895y.
[140] Y. Wu, J. Wu, W.Y. Wong, A new near-infrared phosphorescent iridium(iii) complex conjugated to a xanthene dye for mitochondria-Targeted photodynamic therapy, Biomater. Sci. 9 (2021) 4843–4853, https://doi.org/10.1039/d1bm00128k.
[141] J.S. Nam, M.G. Kang, J. Kang, S.Y. Park, S.J.C. Lee, H.T. Kim, J.K. Seo, O.H. Kwon, M.H. Lim, H.W. Rhee, T.H. Kwon, Endoplasmic reticulum-localized iridium (III) complexes as efficient photodynamic therapy agents via protein modifications, J. Am. Chem. Soc. 138 (2016) 10968–10977, https://doi.org/10.1021/jacs.6b05302.
[142] J. Liu, C. Jin, B. Yuan, X. Liu, Y. Chen, L. Ji, H. Chao, Selectively lighting up two-photon photodynamic activity in mitochondria with AIE-active iridium(iii) complexes, Chem. Commun. 53 (2017) 2052–2055, https://doi.org/10.1039/c6cc10015e.
[143] Y. Wang, H. Fan, G. Zhao, D. Liu, L. Du, Z. Wang, Accepted Article, (2012). https://doi.org/10.1111/febs.12037.
[144] R.R. Ye, C.P. Tan, L. He, M.H. Chen, L.N. Ji, Z.W. Mao, Cyclometalated ir(iii) complexes as targeted theranostic anticancer therapeutics: combining hdac inhibition with photodynamic therapy, Chem. Commun. 50 (2014) 10945–10948, https://doi.org/10.1039/c4cc05215c.

[145] E.M. Boreham, L. Jones, A.N. Swinburne, M. Blanchard-Desce, V. Hugues, C. Terryn, F. Miomandre, G. Lemercier, L.S. Natrajan, A cyclometallated fluorenyl Ir(iii) complex as a potential sensitiser for two-photon excited photodynamic therapy (2PE-PDT), Dalt. Trans. 44 (2015) 16127–16135, https://doi.org/10.1039/c5dt01855b.
[146] C. Wang, L. Lystrom, H. Yin, M. Hetu, S. Kilina, S.A. McFarland, W. Sun, Increasing the triplet lifetime and extending the ground-state absorption of biscyclometalated Ir(III) complexes for reverse saturable absorption and photodynamic therapy applications, Dalt. Trans. 45 (2016) 16366–16378, https://doi.org/10.1039/c6dt02416e.
[147] Y. Jing, Q. Cao, L. Hao, G.G. Yang, W.L. Hu, L.N. Ji, Z.W. Mao, A self-assessed photosensitizer: inducing and dual-modal phosphorescence imaging of mitochondria oxidative stress, Chem. Commun. 54 (2018) 271–274, https://doi.org/10.1039/c7cc07797a.
[148] M. Bonneau, V. Guerchais, G. Williams, Accepted article, J. Subst. Abuse Treat. 13 (1996) 287–288, https://doi.org/10.1016/s0740-5472(96)90021-5.
[149] M. Yu, Q. Zhao, L. Shi, F. Li, Z. Zhou, H. Yang, T. Yi, C. Huang, Cationic iridium (III) complexes for phosphorescence staining in the cytoplasm of living cells, Chem. Commun. (2008) 2115–2117, https://doi.org/10.1039/b800939b.
[150] (a) K. Xiong, Y. Zhou, X. Lin, J. Kou, M. Lin, R. Guan, Y. Chen, L. Ji, H. Chao, Cyclometalated Iridium(III) Complexes as Mitochondria-targeting Photosensitizers against Cisplatin-resistant Cells†, Photochem. Photobiol. 98 (2022) 85–91, https://doi.org/10.1111/php.13404;
(b) H. Yuan, Z. Han, Y. Chen, F. Qi, H. Fang, Z. Guo, S. Zhang, W. He, Ferroptosis Photoinduced by New Cyclometalated Iridium(III) Complexes and Its Synergism with Apoptosis in Tumor Cell Inhibition, Angew, Chemie. 133 (2021) 8255–8262. https://doi.org/10.1002/ange.202014959.
[151] X. Zheng, J. Ge, J. Wu, W. Liu, L. Guo, Q. Jia, Y. Ding, H. Zhang, P. Wang, Biodegradable hypocrellin derivative nanovesicle as a near-infrared light-driven theranostic for dually photoactive cancer imaging and therapy, Biomaterials 185 (2018) 133–141, https://doi.org/10.1016/j.biomaterials.2018.09.021.
[152] H. Zhao, W. Hu, H. Ma, R. Jiang, Y. Tang, Y. Ji, X. Lu, B. Hou, W. Deng, W. Huang, Q. Fan, Photo-induced charge-variable conjugated polyelectrolyte brushes encapsulating upconversion nanoparticles for promoted siRNA release and collaborative photodynamic therapy under NIR light irradiation, Adv. Funct. Mater. 27 (2017) 1–14, https://doi.org/10.1002/adfm.201702592.
[153] J. Xu, L. Xu, C. Wang, R. Yang, Q. Zhuang, X. Han, Z. Dong, W. Zhu, R. Peng, Z. Liu, Near-infrared-triggered photodynamic therapy with multitasking upconversion nanoparticles in combination with checkpoint blockade for immunotherapy of colorectal cancer, ACS Nano. 11 (2017) 4463–4474, https://doi.org/10.1021/acsnano.7b00715.
[154] G. Chen, R. Jaskula-Sztul, C.R. Esquibel, I. Lou, Q. Zheng, A. Dammalapati, A. Harrison, K.W. Eliceiri, W. Tang, H. Chen, S. Gong, Neuroendocrine tumor-targeted upconversion nanoparticle-based micelles for simultaneous NIR-controlled combination chemotherapy and photodynamic therapy, and fluorescence imaging, Adv. Funct. Mater. 27 (2017) 1–13, https://doi.org/10.1002/adfm.201604671.
[155] J. Xu, W. Han, Z. Cheng, P. Yang, H. Bi, D. Yang, N. Niu, F. He, S. Gai, J. Lin, Bioresponsive and near infrared photon co-enhanced cancer theranostic based on upconversion nanocapsules, Chem. Sci. 9 (2018) 3233–3247, https://doi.org/10.1039/c7sc05414a.
[156] H. Li, W. Lei, J. Wu, S. Li, G. Zhou, D. Liu, X. Yang, S. Wang, Z. Li, J. Zhang, An upconverting nanotheranostic agent activated by hypoxia combined with NIR irradiation for selective hypoxia imaging and tumour therapy, J. Mater. Chem. B 6 (2018) 2747–2757, https://doi.org/10.1039/c8tb00637g.
[157] K. Liu, X. Liu, Q. Zeng, Y. Zhang, L. Tu, T. Liu, X. Kong, Y. Wang, F. Cao, S.A.G. Lambrechts, M.C.G. Aalders, H. Zhang, Covalently assembled NIR nanoplatform for simultaneous fluorescence imaging and photodynamic therapy of cancer cells, ACS Nano. 6 (2012) 4054–4062, https://doi.org/10.1021/nn300436b.
[158] J. Zhao, S. Sun, X. Li, W. Zhang, S. Gou, Enhancing photodynamic therapy efficacy of upconversion-based nanoparticles conjugated with a long-lived triplet excited state Iridium(III)-naphthalimide complex: toward highly enhanced hypoxia-inducible factor-1, ACS Appl. Bio Mater. 3 (2020) 252–262, https://doi.org/10.1021/acsabm.9b00774.
[159] H. Chen, H.P. Tham, C.Y. Ang, Q. Qu, L. Zhao, P. Xing, L. Bai, S.Y. Tan, Y. Zhao, Responsive prodrug self-assembled vesicles for targeted chemotherapy in combination with intracellular imaging, ACS Appl. Mater. Interfaces. 8 (2016) 24319–24324, https://doi.org/10.1021/acsami.6b08044.
[160] Y. Wang, L. Zhu, Y. Wang, L. Li, Y. Lu, L. Shen, L.W. Zhang, Ultrasensitive GSH-responsive ditelluride-containing poly(ether-urethane) nanoparticles for controlled drug release, ACS Appl. Mater. Interfaces. 8 (2016) 35106–35113, https://doi.org/10.1021/acsami.6b14639.
[161] X. Wu, X. Sun, Z. Guo, J. Tang, Y. Shen, T.D. James, H. Tian, W. Zhu, In vivo and in situ tracking cancer chemotherapy by highly photostable NIR fluorescent theranostic prodrug, J. Am. Chem. Soc. 136 (2014) 3579–3588, https://doi.org/10.1021/ja412380j.
[162] H. Xiang, H. Chen, H.P. Tham, S.Z.F. Phua, J.G. Liu, Y. Zhao, Cyclometalated Iridium(III)-complex-based micelles for glutathione-responsive targeted chemotherapy and photodynamic therapy, ACS Appl. Mater. Interfaces. 9 (2017) 27553–27562, https://doi.org/10.1021/acsami.7b09506.
[163] S. Dong, Q. Chen, W. Li, Z. Jiang, J. Ma, H. Gao, A dendritic catiomer with an MOF motif for the construction of safe and efficient gene delivery systems, J. Mater. Chem. B 5 (2017) 8322–8329, https://doi.org/10.1039/c7tb01966a.
[164] K. Zhang, X. Meng, Y. Cao, Z. Yang, H. Dong, Y. Zhang, H. Lu, Z. Shi, X. Zhang, Metal-Organic Framework Nanoshuttle for Synergistic Photodynamic and Low-Temperature Photothermal Therapy, Adv. Funct. Mater. 28 (2018) 1–10, https://doi.org/10.1002/adfm.201804634.
[165] J.S. Kahn, L. Freage, N. Enkin, M.A.A. Garcia, I. Willner, Stimuli-responsive dna-functionalized metal-organic frameworks (MOFs), Adv. Mater. 29 (2017) 1–6, https://doi.org/10.1002/adma.201602782.
[166] Z. Dong, Y. Sun, J. Chu, X. Zhang, H. Deng, Multivariate metal-organic frameworks for dialing-in the binding and programming the release of drug molecules, J. Am. Chem. Soc. 139 (2017) 14209–14216, https://doi.org/10.1021/jacs.7b07392.
[167] Y. Zhang, H. Fu, S. Chen, B. Liu, W. Sun, H. Gao, Construction of an iridium(iii)-complex-loaded MOF nanoplatform mediated with a dual-responsive polycationic polymer for photodynamic therapy and cell imaging, Chem. Commun. 56 (2020) 762–765, https://doi.org/10.1039/c9cc09357e.
[168] H. Huang, S. Banerjee, P.J. Sadler, Recent advances in the design of targeted iridium(III) photosensitizers for photodynamic therapy, ChemBioChem. 19 (2018) 1574–1589, https://doi.org/10.1002/cbic.201800182.
[169] S.P.Y. Li, H.W. Liu, K.Y. Zhang, K.K.W. Lo, Modification of luminescent iridium (III) polypyridine complexes with discrete polyethylene glycol (PEG) pendants: synthesis, emissive behavior, intracellular uptake, and PEGylation properties, Chem. – A Eur. J. 16 (2010) 8329–8339, https://doi.org/10.1002/chem.201000474.
[170] S.P.Y. Li, C.T.S. Lau, M.W. Louie, Y.W. Lam, S.H. Cheng, K.K.W. Lo, Mitochondria-targeting cyclometalated iridium(III)-PEG complexes with tunable photodynamic activity, Biomaterials 34 (2013) 7519–7532, https://doi.org/10.1016/j.biomaterials.2013.06.028.
[171] H. Lu, X. Jiang, Y. Chen, K. Peng, Y. Huang, H. Zhao, Q. Chen, F. Lv, L. Liu, S. Wang, Y. Ma, Cyclometalated iridium(iii) complex nanoparticles for mitochondria-targeted photodynamic therapy, Nanoscale 12 (2020) 14061–14067, https://doi.org/10.1039/d0nr03398g.
[172] Q. Chen, X. Liu, J. Zeng, Z. Cheng, Z. Liu, Albumin-NIR dye self-assembled nanoparticles for photoacoustic pH imaging and pH-responsive photothermal therapy effective for large tumors, Biomaterials 98 (2016) 23–30, https://doi.org/10.1016/j.biomaterials.2016.04.041.
[173] J. Li, K. Pu, Development of organic semiconducting materials for deep-tissue optical imaging, phototherapy and photoactivation, Chem. Soc. Rev. 48 (2019) 38–71, https://doi.org/10.1039/c8cs00001h.
[174] K. Pu, J. Mei, J.V. Jokerst, G. Hong, A.L. Antaris, N. Chattopadhyay, A.J. Shuhendler, T. Kurosawa, Y. Zhou, S.S. Gambhir, Z. Bao, J. Rao, Diketopyrrolopyrrole-based semiconducting polymer nanoparticles for in vivo photoacoustic imaging, Adv. Mater. 27 (2015) 5184–5190, https://doi.org/10.1002/adma.201502285.
[175] H.W. Yang, H.L. Liu, M.L. Li, I.W. Hsi, C.T. Fan, C.Y. Huang, Y.J. Lu, M.Y. Hua, H. Y. Chou, J.W. Liaw, C.C.M. Ma, K.C. Wei, Magnetic gold-nanorod/ PNIPAAmMA nanoparticles for dual magnetic resonance and photoacoustic imaging and targeted photothermal therapy, Biomaterials 34 (2013) 5651–5660, https://doi.org/10.1016/j.biomaterials.2013.03.085.
[176] T. Temma, S. Onoe, K. Kanazaki, M. Ono, H. Saji, Preclinical evaluation of a novel cyanine dye for tumor imaging with in vivo photoacoustic imaging, J. Biomed. Opt. 19 (2014), https://doi.org/10.1117/1.jbo.19.9.090501 090501.
[177] S. Onoe, T. Temma, K. Kanazaki, M. Ono, H. Saji, Development of photostabilized asymmetrical cyanine dyes for in vivo photoacoustic imaging of tumors, J. Biomed. Opt. 20 (2015), https://doi.org/10.1117/1.jbo.20.9.096006 096006.
[178] Q. Yang, H. Jin, Y. Gao, J. Lin, H. Yang, S. Yang, Photostable iridium(III)-cyanine complex nanoparticles for photoacoustic imaging guided near-infrared photodynamic therapy in vivo, ACS Appl. Mater. Interfaces. 11 (2019) 15417–15425, https://doi.org/10.1021/acsami.9b04098.
[179] (a) Y. Liu, D. Zhu, Z. Xie, Ir(III) complex dimer nanoparticles for photodynamic therapy, ACS Med. Chem. Lett. 12 (2021) 1374–1379, https://doi.org/10.1021/acsmedchemlett.1c00362;
(b) S. Kuang, F. Wei, J. Karges, L. Ke, K. Xiong, X. Liao, G. Gasser, L. Ji, H. Chao, Photodecaging of a mitochondria-localized iridium(iii) endoperoxide complex for two-photon photoactivated therapy under hypoxia, J. Am. Chem. Soc. 144 (2022) 4091–4101. https://doi.org/10.1021/jacs.1c13137.
[180] A. Leonidova, V. Pierroz, R. Rubbiani, J. Heier, S. Ferrari, G. Gasser, Towards cancer cell-specific phototoxic organometallic rhenium(i) complexes, Dalt. Trans. 43 (2014) 4287–4294, https://doi.org/10.1039/c3dt51817e.
[181] T. Gianferrara, C. Spagnul, R. Alberto, G. Gasser, S. Ferrari, V. Pierroz, A. Bergamo, E. Alessio, Towards matched pairs of porphyrin-ReI/99mTc I conjugates that combine photodynamic activity with fluorescence and radio imaging, ChemMedChem 9 (2014) 1231–1237, https://doi.org/10.1002/cmdc.201300501.
[182] A. Kastl, S. Dieckmann, K. Wähler, T. Völker, L. Kastl, A.L. Merkel, A. Vultur, B. Shannan, K. Harms, M. Ocker, W.J. Parak, M. Herlyn, E. Meggers, Rhenium complexes with visible-light-induced anticancer activity, ChemMedChem 8 (2013) 924–927, https://doi.org/10.1002/cmdc.201300060.
[183] M. Montalti, G. Battistelli, A. Cantelli, D. Genovese, Photo-tunable multicolour fluorescence imaging based on self-assembled fluorogenic nanoparticles, Chem. Commun. 50 (2014) 5326–5329, https://doi.org/10.1039/c3cc48464e.
[184] J. Zhou, J. Zhang, Y. Lai, Z. Zhou, Y. Zhao, H. Wang, Z. Wang, Guanidinium-dendronized perylene bisimides as stable, water-soluble fluorophores for live-cell imaging, New J. Chem. 37 (2013) 2983–2986, https://doi.org/10.1039/c3nj00876b.

[185] T. Heek, J. Nikolaus, R. Schwarzer, C. Fasting, P. Welker, K. Licha, A. Herrmann, R. Haag, An amphiphilic perylene imido diester for selective cellular imaging, Bioconjug. Chem. 24 (2013) 153–158, https://doi.org/10.1021/bc3005655.
[186] Z. Xu, K. Guo, J. Yu, H. Sun, J. Tang, J. Shen, K. Müllen, W. Yang, M. Yin, A unique perylene-based DNA intercalator: localization in cell nuclei and inhibition of cancer cells and tumors, Small 10 (2014) 4087–4092, https://doi.org/10.1002/smll.201401262.
[187] M. Schulze, A. Steffen, F. Würthner, Near-IR phosphorescent ruthenium(II) and iridium(III) perylene bisimide metal complexes, Angew. Chemie – Int. Ed. 54 (2015) 1570–1573, https://doi.org/10.1002/anie.201410437.
[188] M.T. Vagnini, A.L. Smeigh, J.D. Blakemore, S.W. Eaton, N.D. Schley, F. D'Souza, R.H. Crabtree, G.W. Brudvig, D.T. Co, M.R. Wasielewski, Ultrafast photodriven intramolecular electron transfer from an iridium-based water-oxidation catalyst to perylene diimide derivatives, Proc. Natl. Acad. Sci. U. S. A. 109 (2012) 15651–15656, https://doi.org/10.1073/pnas.1202075109.
[189] A.M.H. Yip, J. Shum, H.W. Liu, H. Zhou, M. Jia, N. Niu, Y. Li, C. Yu, K.K.W. Lo, Luminescent Rhenium(I)–polypyridine complexes appended with a perylene diimide or benzoperylene monoimide moiety: photophysics, intracellular sensing, and photocytotoxic activity, Chem. – A Eur. J. 25 (2019) 8970–8974, https://doi.org/10.1002/chem.201900345.
[190] L.D. Ramos, H.M. Da Cruz, K.P. Morelli Frin, Photophysical properties of rhenium(i) complexes and photosensitized generation of singlet oxygen, Photochem. Photobiol. Sci. 16 (2017) 459–466. https://doi.org/10.1039/c6pp00364h.
[191] P. Boya, G. Kroemer, Lysosomal membrane permeabilization in cell death, Oncogene 27 (2008) 6434–6451, https://doi.org/10.1038/onc.2008.310.
[192] L. Groth-Pedersen, M. Jäättelä, Combating apoptosis and multidrug resistant cancers by targeting lysosomes, Cancer Lett. 332 (2013) 265–274, https://doi.org/10.1016/j.canlet.2010.05.021.
[193] B. Zhitomirsky, Y.G. Assaraf, Lysosomes as mediators of drug resistance in cancer, Drug Resist. Updat. 24 (2016) 23–33, https://doi.org/10.1016/j.drup.2015.11.004.
[194] Z.Y. Pan, D.H. Cai, L. He, Dinuclear phosphorescent rhenium(i) complexes as potential anticancer and photodynamic therapy agents, Dalt. Trans. 49 (2020) 11583–11590, https://doi.org/10.1039/d0dt02424d.
[195] X. Su, W.-J. Wang, Q. Cao, H. Zhang, B. Liu, Y. Ling, X. Zhou, Z.-W. Mao, A Carbonic anhydrase IX (CAIX)-anchored rhenium(I) photosensitizer evokes pyroptosis for enhanced anti-tumor immunity, Angew. Chem. Int. Ed. 61 (2022) e202115800.